# Properties of Star Clusters

A Thesis presented for the degree of
Doctor of Philosophy in Physics


Centre of Astrophysics and Planetary Science
University of Kent

Author
Anne Buckner

Primary Supervisor
Dr. Dirk Froebrich

Secondary Supervisor
Professor Michael Smith

# Abstract

Star clusters are tracers of both stellar and Galactic evolution. As such it is essential to analyse their properties and distribution in the Galaxy. Ideally clusters' fundamental properties (distance, reddening, age, metallicity) should be derived homogeneously, so that their uncertainties are systematic and any global trends identified can be trusted. With the increase of newly discovered, purely photometric, large cluster samples from infrared surveys such as 2MASS, WISE, UKIDSS-GPS and VISTA-VVV, new methods to reliably derive these properties are required.

This Thesis presents novel methods to homogeneously derive the distances, extinctions, ages and scale height measurements of cluster samples. Distances and extinctions are derived from photometry alone, without the use of isochrone fitting, and cluster distances can be estimated with a better than 40% accuracy. Cluster ages are derived using a pipeline which is designed to consistently determine the values of clusters' fundamental properties. Novel scale height measurements are established with a 25% uncertainty for a sample size of 38.

Using these methods, the FSR List cluster catalogue is found to be biased towards a distance of 3 kpc and modal age of 400 Myr. A dependence between the interstellar absorption value and Galactic longitude is found, characterised by $A_H(l)[mag/kpc] = 0.10 + 0.001 \times |l - 180°|/°$ for regions more than 60° from the Galactic Centre.

The temporal scale height evolution of clusters is accurately traced for the first time. A linear relationship between cluster scale height and log(age/yr) is found which is significantly different from the stellar component of the Galactic Disk. There is also a weak age-independent trend between cluster scale height and Galactocentric distance. No significant temporal or spatial variations of the cluster distribution vertical zero point are found. The Sun's vertical displacement from the Galactic Plane is measured to be $Z_\odot = 18.5 \pm 1.2$ pc.

Plan purposely,
Prepare prayerfully,
Proceed positively,
Pursue persistently.

– *William Arthur Ward*

# Contents

# List of Acronyms

| | |
|---|---|
| **2MASS** | Two Micron All-Sky Survey |
| **2sKST** | 2 sample Kolmogorov- Smirnov Test |
| **ASCC-2.5** | All-Sky Compiled Catalogue of 2.5 million stars |
| **BGM** | Besançon Galaxy Model |
| **CCM** | Colour Colour Magnitude |
| **CCS 1** | Cluster Calibration Sample 1 |
| **CCS 2** | Cluster Calibration Sample 2 |
| **CDF** | Cumulative Distribution Function |
| **CMD** | Colour Magnitude Diagram |
| **CS 1** | Cluster Sample 1 |
| **CS 2** | Cluster Sample 2 |
| **CS 3** | Cluster Sample 3 |
| **CS 4** | Cluster Sample 4 |
| **DAML02** | Dias, Alessi, Moitinho and Lepine 2002 (cluster catalogue) |
| **DENIS** | DEep Near-Infrared Survey |
| **FSR List** | Froebrich, Scholz and Raftery List (cluster catalogue) |
| **Gaia-ESO** | Gaia-European South Observatory (spectroscopic survey) |
| **GC** | Galactic Centre |
| **GlC** | Globular Cluster |
| **GD** | Galactic Disk |
| **GLIMPSE** | Galactic Legacy Infrared Midplane Survey Extraordinaire |
| **GMC** | Giant Molecular Cloud |
| **GP** | Galactic Plane |
| **HIPPARCOS** | HIgh Precision PARallax COllecting Satellite |
| **HVC** | High Velocity Cloud |

| | |
|---|---|
| **IR** | InfaRed |
| **IRAS** | InfraRed Astronomical Satellite |
| **KS-statistic** | Kolmogorov- Smirnov statistic |
| **MIR** | Mid-InfraRed |
| **MPI** | Membership Probability Index |
| **MS** | Main Sequence |
| **MWSC** | Milky Way Star Cluster (catalogue) |
| **OC** | Open Cluster |
| **NIR** | Near-InfraRed |
| **NTT** | New Technology Telescope (European South Observatory) |
| **PDT** | Photometric Decontamination Technique |
| **PMS** | Pre-Main Sequence |
| **PPMXL** | Positions and Proper Motions eXtended cataLogue |
| **Qflag** | Quality flag (2MASS Survey) |
| **RGC** | Red Giant Clump |
| **S : N** | Signal-to-Noise ratio |
| **TRILEGAL** | TRIdimensional modeL of thE GALaxy |
| **UKDISS-GPS** | UKIRT Infrared Deep Sky Survey |
| **UKIRT** | United Kingdom Infra-Red Telescope |
| **VISTA-VVV** | Visible and Infrared Survey Telescope for Astronomy - Vista Variables in the Via lactea survey |
| **WEBDA** | WEb version of the database known as Base Données Amas (cluster catalogue) |
| **WISE** | Wide-field Infrared Survey Explorer |
| **YSO** | Young Stellar Object |

# Part I

# Background

# Chapter 1

# Introduction

Star clusters are tracers of both stellar and Galactic evolution. Individually they act as laboratories, demonstrating how stellar systems comprised of various masses work and interact as member stars share similar properties (distance, age, reddening and metallicity). Collectively clusters provide insight into the chemical and structural evolution of the Galaxy.

Open clusters are loosely and mutually gravitationally bound groups of stars which are the building blocks of the Galaxy. Unlike globular clusters, open clusters are an integral part of the active star formation process, with the majority of stars in the Galaxy forming within these clustered environments in Giant Molecular Clouds (GMCs) (Carpenter (2000), Lada and Lada (2003), Porras et al. (2003), Allen et al. (2007)). Open clusters will remain embedded in their parental clouds for up to 10 Myr during which time radiative pressure from stellar feedback (stellar winds, supernovae, outflows, jets), will expel gas left-over from star formation. This gas removal process is violent and few clusters meet the physical conditions necessary to emerge as a bound open cluster. To survive, a cluster needs to have high enough star formation efficiency, begin the process in a subvirial state and the rate of gas expulsion needs to not be too high (Hills (1980), Geyer and Burkert (2001), Baumgardt and Kroupa (2008), Lada (2010), Bastian (2011), Pelupessy and Portegies Zwart (2012)). Ultimately, only 4-7% of embedded clusters emerge as bound open clusters (Lada and Lada, 2003).

Both physical processes and observational effects contribute to difficulties in locating bound open clusters. Physically, the main causes of bound cluster disruption include stellar evolution and gravitational interactions with e.g. GMCs and tidal forces (Lamers et al. (2005), Gieles et al. (2006), Gieles (2009), Bastian (2011) etc.). Whilst exact disruption time-scales

are dependent on Galactocentric distance, relatively few clusters survive for more than a gigayear and typical disruption time-scales for clusters with low initial densities are less than 50 Myr. It has also been shown that older clusters typically have a wider spatial distribution perpendicular to the Galactic Plane (i.e. scale height) than their younger counterparts, which coupled with their large angular extensions, means it is reasonable to expect the number of observed open clusters to decrease with age (Moitinho (2010), Buckner and Froebrich (2014)). Yet, even after taking the disruption time scales and observational biases into account, there is still a distinct lack of known clusters older than 1 Gyr within about 1 kpc of the Sun despite targeted searches (Kharchenko et al. (2013), Schmeja et al. (2014)). It should be noted that detection difficulties are not, however, limited to older clusters. For instance, younger clusters are typically associated with an obscuring parental cloud, whilst observations of intermediate aged clusters can be affected by large scale foreground extinction. It is also difficult to distinguish clusters in a high star density field such as towards the Galactic Centre (GC), where potential obscuring by the central Bulge and/or Bar is an additional concern. Subsequently, to date only about 3% of the $10^5$ predicated bound open clusters have actually been observed and confirmed (Piskunov et al. (2006), Kharchenko et al. (2013)). Cluster detection remains one of the ongoing challenges in this field of research.

The majority of bound open clusters have been discovered as apparent stellar overdensities on the background star field. Until fairly recently, searches for these overdensities primarily utilised Visual band photometry from a wide range and variety of telescopes. The rate of cluster discovery was low, with only ∼1200 candidates listed in composite literature catalogues by the mid-1990s (Alter et al. (1970), Janes and Adler (1982), Lynga (1995)). Over the last decade, technological advancements have enabled the focus of the community to switch from primarily using Visual to InfraRed (IR) band photometry to search for clusters. The IR bands are more suited for the search, as the longer wavelengths make an ideal tool to penetrate the dust veil of the Galaxy to greater distances and deeper magnitudes than is possible with the Visual bands. The launch of multiple large scale Near-IR (NIR) and Mid-IR (MIR) surveys such as DENIS (Epchtein et al., 1997), GLIMPSE (Benjamin et al., 2003), 2MASS (Skrutskie et al., 2006), UKIDSS-GPS (Lucas et al., 2008), VISTA-VVV (Minniti et al., 2010) and WISE (Wright et al., 2010), has resulted in a dramatic increase in the number of clusters discovered (see Dutra and Bica (2001), Reylé and Robin (2002), Dutra et al. (2003), Mercer et al. (2005), Froebrich et al. (2007), Glushkova et al. (2010), Borissova et al. (2011), Solin et al. (2012), Chené et al. (2013), Majaess (2013), Schmeja et al. (2014), Borissova et al. (2014), Camargo et al. (2015), Barbá et al. (2015) etc.). At the time of writing, composite literature catalogues contain ∼4000 cluster candidates (Dias et al. (2002), Kharchenko et al. (2013), Morales et al.

(2013) etc.).

Overdensities found using IR photometry are typically identified using an automated procedure, manual inspection, or some combination of the two. The benefit of automated search methods is that they make it possible to query large survey areas with minimal effort and time expended, however they are not infallible and often miss less pronounced overdensities. Therefore authors regularly augment their automated searches with a manual inspection and consult multiple surveys/photometric bands (e.g. Borissova et al. (2003), Mercer et al. (2005), Froebrich et al. (2007)). Regions with a high field star density (e.g. towards the GC), are particularly problematic, as here the stellar density peaks are less prominent on the background field. As such, there is relative lack of known cluster candidates towards the GC, and those which have been discovered near the GC are compact and associated with another identifying feature e.g. bright and dark nebulosity, IR and Radio sources, methanol maser emission, Galactic bubbles and hot molecular cores (Froebrich et al. (2007), Borissova et al. (2011), Barbá et al. (2015)).

Although searches for clusters as overdensities have been successful, it is not their sole identifying feature and numerous cluster candidates have been discovered using alternative methods. Several searches have focused on the similar age and chemical composition of clusters' stellar members. For example, a sample of embedded clusters were serendipitously found through identification of their young stellar populations during a search for Young Stellar Objects (YSOs) (Majaess, 2013), and a cluster with a Pre-Main Sequence (PMS) population in the $\eta$ Cha region was found through the emissions of its X-ray luminous members (Mamajek et al., 1999). Unfortunately, the nature of the searches is such that they are time expensive and not very fruitful, so are not conducive with the discovery of large cluster samples.

A number of searches have attempted to identify clusters from their stellar members' common kinematic data, querying astrometric catalogues such as HIPPARCOS (Perryman et al., 1997), TYCHO-2 (Høg et al., 2000), ASCC-2.5 (Kharchenko, 2001) and PPMXL (Roeser et al., 2010). The nature of this type of search is such that the discovered sample is dominated by nearby clusters with bright high proper motion members, positioned in the Galactic mid-plane (e.g. Platais et al. (1998), Alessi et al. (2003), Kharchenko et al. (2005), Scholz et al. (2015)). Nonetheless, this method simultaneously finds cluster candidates and confirms them as real, which is desirable. In contrast, photometrically sourced cluster samples can potentially consist of a large number of asterisms resulting from random field star density fluctuations or differential reddening in the observer's line of sight, rather the presence of a real cluster. The FSR List catalogue (Froebrich et al., 2007) is a good example of this, as

it contains more than 1000 cluster candidates discovered as projected NIR overdensities, but spatial analyses have indicated that only about 50% are real clusters (Froebrich et al. (2007), Bica et al. (2008), Camargo et al. (2010)).

The importance of verifying whether a discovered overdensity is a real cluster or an asterism is obvious, but as their fields are contaminated by interloping foreground and background stars, this is a difficult task. Various methods can be employed to distinguish cluster members from interloping stars and verify the true nature of a candidate. The most direct approaches identify members through their shared properties using e.g. spectroscopy (comparing spectra to stellar standards; H$\alpha$, Li, Na absorption features), astrometry (radial and proper motion measurements) and/or X-ray emissions (Hanson (1975), Marschall et al. (1982), Prosser (1992), Montes et al. (2001), Martín et al. (2000), Meibom et al. (2002), Kenyon et al. (2005), Fang et al. (2012), Majaess (2013) etc.). Unfortunately, this data is not available for the vast majority of overdensties as they are neither positioned within the ranges of relevant surveys, nor have been previously studied on an individual basis. Gathering and processing this data is too time intensive to be practical for large samples containing a few thousand objects, so alternative methods of member identification need to be employed.

In principle stellar members can be statistically identified from their positional data as it is reasonable to expect there to be less contamination from interlopers towards a cluster's centre, so the likelihood that a star is a member of the cluster increases with decreasing radial distance (Dias et al. (2012), Krone-Martins and Moitinho (2014)). Membership probabilities derived in this way should be treated with caution, however, as they can be unreliable for clusters which are: (i) dense, as stellar crowding in their central regions will make accurate membership determination difficult; (ii) projected onto high density stellar field, as they are not clearly distinguished from the field and a significant proportion of true members may be outside the determined cluster radius; (iii) young, as these clusters may not necessarily be circular in projection and have substructure (e.g. Sánchez and Alfaro (2009), Gregorio-Hetem et al. (2015)). Ideally, members should be identified through their stellar colours when only photometry is available using a process known as *photometric decontamination*. Numerous realisations of this process can be found in the literature, and of these the two most popular (and relevant to this work) identify potential members using modelled cluster sequences or through an analysis of their stellar colours.

The former approach involves plotting all stars within the candidate cluster's field on Colour Colour Magnitude (CCM) diagrams, and fitting a modelled cluster sequence isochrone to the photometry. Membership probabilities are derived as a function of stars' colour dis-

tances from the fitted isochrone, such that those exhibiting the largest scatter are assumed interlopers (see e.g. Claria and Lapasset (1986), Jeffries et al. (2001), Naylor and Jeffries (2006), Glushkova et al. (2010), Piatti et al. (2010)). Beneficially, this approach allows for the distance, reddening and age of a cluster to be derived simultaneously, but there are some fallibility issues. Firstly, as cluster metallicities are unknown they are usually assumed Solar for the purpose of fitting the isochrone. Although this is a statistically reasonable assumption (Buckner and Froebrich, 2014), it will result in incorrect property derivations for all non-Solar metallicity clusters. Secondly, members which are intrinsically red/blue, binary, variable or near completeness limits of the photometry (e.g. YSOs, blue stragglers, Cepheids, late type dwarfs), will naturally exhibit a larger scatter about the cluster sequence, and consequently may be misidentified as interlopers. Similarly, bright interlopers have the potential to be misinterpreted as early-type members. Cluster properties derived using this approach are subsequently subjective to authors' (individual or software related) interpretation, which can vary significantly as the parameters (distance, reddening, age, metallicity) are free. This is particularly an issue for clusters that are sparsely populated, are less well defined on the field and/or lacking prominent features such as a strong Main Sequence (MS), giants etc. For example, despite Froebrich et al. (2010) and Bonatto and Bica (2008b) both fitting Solar metallicity isochrones to the CCM diagrams of FSR1716, they determined it to be an open cluster of 7.0kpc/2Gyr and 0.8kpc/7Gyr respectively. It could be argued that incongruity between individual cluster properties is not problematic, so long as the reliability of the methods used to derived them is considered, i.e. when multiple property values are available for a single cluster, the most accurate is selected or an average is taken (e.g. Netopil et al. (2015)). This is impractical for the compilation of a large cluster sample, and ultimately the results of any global analyses undertaken therewith would be unreliable due to its heterogeneous nature. Attempts have been made by the community to statistically address this issue by developing methodologies that homogeneously derive the properties of cluster samples, but as these rely on modelled cluster sequences and/or positional data, the accuracy of individual cluster property values remains questionable (Monteiro et al. (2010), Kharchenko et al. (2012), Perren et al. (2015)).

The latter approach identifies members by comparing the colours of stars in the candidate cluster field and a specified offset control field. In principle the members of a cluster are at the same Solar distance and have a similar reddening so will appear clumped on a Colour Magnitude Diagram (CMD); whereas interlopers and stars in the control field are homogeneously distributed, as they have variable Solar distances and reddenings. Members are therefore identified by measuring and comparing star colour distances on a CMD (see e.g. Bonatto

and Bica (2007b), Carraro and Costa (2007), Froebrich et al. (2010), Maia et al. (2010), Pavani et al. (2011)). An arbitrary combination of colours can be used to construct the required CMD, but JHK photometry provides the most variance between cluster sequences of different ages (Bonatto and Bica, 2007b). Arguably, this approach is the more versatile, as it relies solely on photometric data to verify the nature of an overdensity, and to identify a cluster's members. As such there should be comparatively little disagreement between authors' implementations. Conversely, this approach does not simultaneously derive cluster properties which can only be derived through fitting modelled sequences to their decontaminated CCM diagrams, but (as discussed) this has the potential to produce values that vary between authors due to the initial free parameters. Evidently there is a need for a purely photometric method to constrain distances and reddenings of clusters independent of isochrone fitting.

The FSR List catalogue by Froebrich et al. (2007) is one of many NIR cluster catalogues which would benefit from the development of a purely photometric method to derive cluster distances and reddenings. Like most large samples, it is expected to contain objects of interest such as clusters with a large population of PMS stars, massive clusters and old clusters near the GC, but a lack of available data means few have been confirmed. To date, the vast majority of the 1788 overdensities discovered remain unstudied, and only a small number have been investigated on an individual basis (Bonatto and Bica (2007a), Bica et al. (2008), Bonatto and Bica (2008a), Momany et al. (2008), Froebrich et al. (2008), Camargo et al. (2009), Camargo et al. (2010), Glushkova et al. (2010), Camargo et al. (2012), Camargo et al. (2013)). The largest study of the catalogue so far has been provided by Froebrich et al. (2010) who characterised 203 open clusters by fitting modelled cluster sequence isochrones to their CCM diagrams, using the colour position of their red giant star clumps as a marker. The authors focused on clusters they suspected as 'old' ($\geq 1$ Gyr) primarily because, in the absence of red giant members, the catalogues remaining (younger) clusters typically lack other prominent features on the CCM diagrams, which makes an accurate isochrone fit nearly impossible. Clearly further investigation is needed to ascertain the prevalence of objects of interest in the full catalogue, and to study them in-depth. Perhaps the most exciting avenue of research that a large cluster sample presents, is the ability to explore the structure and chemical enrichment of the Galactic Plane (GP) through analyses of cluster distributions. Although these analyses can be undertaken with any cluster sample (regardless of the nature of their properties), subsequent global trends identified can only be trusted if the properties are derived homogeneously, as their uncertainties are systematic.

Numerous works have used spatial analyses of cluster samples to probe Disk structure, trace

star formation regions and measure the Solar position (Vogt and Moffat (1975), Janes and Adler (1982), Moitinho (2002), Dias and Lépine (2005), Piskunov et al. (2006),Vázquez et al. (2008), Moitinho (2010), Carraro (2014), Junqueira et al. (2015) etc.). However, it is not yet fully understood how gravitational interactions, with e.g. GMCs and the Galactic tidal force, temporally and spatially affect clusters. It is well documented that these interactions are a primary source for cluster disruption (e.g. Lamers et al. (2005), Gieles et al. (2006), Lamers and Gieles (2006), Gieles et al. (2008), Gieles (2009)), which coupled with the discussed observational limitations, means that the number of clusters observed in the Solar Neighbourhood decreases with increasing cluster age. Put in perspective, although almost 4000 cluster candidates have been discovered, only ∼3000 have been confirmed and of these, about 30% are within the completeness limit of the sample, i.e. less than 1000 clusters can be used for spatial scale analyses (Kharchenko et al. (2013), Buckner and Froebrich (2014)). Subsequently, it has not been possible to observationally track in detail the evolution of cluster scale height as (due to their constraints) established methods cannot be applied to small sample sizes. Previous studies have determined cluster scale heights of 48 pc (<200 Myr), 150 pc (200 Myr to 1 Gyr) and 375 pc (>1 Gyr) respectively, though it has been argued that it is not possible to make a measurement for old clusters due to the flattering of their vertical distribution (Janes and Phelps (1994), Bonatto et al. (2006), Froebrich et al. (2010), Moitinho (2010)). Still, these results imply that some evolution of cluster scale height occurs, but with only three data points and no numerical simulations available, it remains unclear what form (if any) the function will take. It is therefore desirable to have a reliable, robust method which allows for a determination of the scale height of small distributions. Again, it is preferable for cluster samples to have homogeneously derived properties (particularly distances and ages), so that uncertainties are systematic.

Analyses of cluster reddening distributions present the opportunity to constrain extinction laws. Properly constrained extinction laws are essential for the generation of synthetic star fields with Galaxy models (e.g. Robin et al. (2003), Girardi et al. (2012)) as if an incorrect interstellar absorption value is assumed the density of field stars will be over or under estimated. In the literature, interstellar absorption is typically assumed to be constant per unit distance in all lines of sight and is measured as the average observed in the Solar Neighbourhood with a canonical value of 0.7 mag/kpc in the optical V-band, although values are derived as high as 1.5 mag/kpc depending on the nature of the objects and methods used to make the measurement (e.g. Lynga (1979), Milne and Aller (1980), Vergely et al. (1997), Froebrich et al. (2010)). Using a sample of clusters with a latitude of $|b| \leq 5°$, Joshi (2005) showed that interstellar absorption varies sinusoidally as a function of Galactic longitude, effectively

demonstrating that the canonical value should not be adopted. There are, however, some issues with the author's methodology. The sample is heterogeneous in nature as extinction and distance values were taken from the DAML02 catalogue (Dias et al., 2002), which is compiled from a variety of literature sources. Clusters with a Solar distance of 15 kpc were included, despite the sample only being complete up to 2−3 kpc, thus introducing a potential reddening and/or distance bias. To derive interstellar absorption values, the authors divided the sample into 10° longitude bins and measured the average extinction per unit distance of the clusters in each bin. Consequently the bins are of unequal sizing, with as few as 3 clusters per bin, and have a maximum distance that ranges between <4 kpc to >12 kpc. Obviously it is impossible to make an accurate statement about interstellar absorption from bins whose maximum distances differ so dramatically and contain clusters outside the completeness limit of a sample. It is also not advisable to trust absorption values that are derived from bins which contain only a few clusters as their properties are not necessarily typical of that particular longitude, particularly as a potential reddening and/or distance bias has been identified in the sample. Therefore further analysis is needed to verify, refine and explore the findings and implications of the Joshi (2005) study, using a consistent, unbiased approach with a cluster sample whose properties have been derived homogeneously.

The focus of this Thesis is the properties of open clusters, and its aims are to address the issues identified here. Specifically, novel methods will be presented to: (i) homogeneously and photometrically determine cluster distances and extinctions without isochrone fitting; (ii) systematically derive cluster ages; (iii) measure scale height for small sample sizes. Using these novel methods, an analysis of the full FSR List catalogue will be undertaken for the first time. The Galactic spatial evolution of clusters will be traced in detail, and the implications of any relationship between scale height, Galactocentric distance and age that is identified will be explored.

This Thesis is structured as follows. Chapter 2 introduces the four cluster samples that will be used in this work. Chapter 3 details the methodology that will be used to identify stellar cluster members. In Chapters 4-7 methods to determine cluster distance, reddening, age and scale height are presented. An analysis of the FSR List catalogue is presented in Chapter 8. The Galactic extinction law is refined in Chapter 9. The scale height evolution of clusters is traced in Chapter 10 and the relationship between cluster scale height, Galactocentric distance and age is explored. Conclusions are presented in Part IV.

# Chapter 2

# Cluster Samples

This Thesis aims to explore the individual and global properties of open clusters. This will be partially achieved through analyses of multiple observed cluster samples, as it is necessary to compare, verify and evaluate any discrepancies in the results of said analyses that may arise from using the different samples. Ideally each sample should contain a large number of clusters whose fundamental properties (such as distance, extinction, age) have wide distributions, and were derived homogeneously (so that the uncertainties in analyses are systematic).

Four suitable cluster catalogues have been selected: The MWSC catalogue by Kharchenko et al. (2013); the DAML02 catalogue by Dias et al. (2002); the WEBDA catalogue by Mermilliod (1995); the FSR List catalogue by Froebrich et al. (2007). This Chapter provides an introduction and discussion of these catalogues. The reader is encouraged to use this Chapter as a reference for the remainder of this Thesis.

## 2.1 CS 1: The MWSC Catalogue

The Milky Way Star Cluster (MWSC) catalogue by Kharchenko et al. (2013) is a compilation catalogue which, at the time it was created, contained all known cluster candidates. There are 3784 cluster candidates listed in the catalogue, of which 3006 were confirmed to be real objects and the remainder were either flagged as not real or duplicate entries. Objects confirmed as real were sub-categorised as either: 'Open Clusters', 'Nebulous', 'Remnants', 'Globular Clusters', 'Associations' or 'Moving Groups'. The category naming conventions

were chosen to be self explanatory, with the 'Nebulous' and 'Remnants' flags denoting that an object is a cluster associated with nebulosity or is a cluster remnant, respectively.

The catalogue has a deficit of open clusters older than $log(age/yr) > 9.2$, within 1 kpc of the Sun (Kharchenko et al., 2013). A study by Schmeja et al. (2014) attempted to search for these 'missing' clusters, but ultimately exacerbated the deficit. The cause of the deficit has not yet been corroborated in the literature, but it is reasonable to expect that a significant number of clusters older than 1 Gyr may be located at vertical distances above the GP of greater than 1 kpc, as old open clusters have a scale height larger than their younger counterparts (Moitinho (2010), Buckner and Froebrich (2014)). Additional observational considerations are the large angular extension of old clusters (comparative to their younger counterparts), which can reduce their prominence against the field and make them undetectable at small distances (i.e. $<1$ kpc). It should be noted, however, that there may be a physical effect contributing to the deficit, the nature of which is not yet clear.

The authors homogeneously re−/determined the distance, reddening, age, metallicity and radius of each object in the catalogue using their data-processing pipeline. As such the MWSC catalogue is the largest in the literature with homogeneously derived fundamental properties. The authors' data-processing pipeline utilises data from the PPMXL and 2MASS surveys to blindly fit modelled cluster sequence isochrones to the candidates' CCM diagrams. As the identity of the candidates is unknown when the isochrones are fitted, the derived properties of a number of candidates significantly vary from accepted literature values. For example, a detailed study by Davies et al. (2007) found Stephenson 2 to have an age of 12 – 17 Myr and distance of $5.8^{+1.9}_{-0.8}$ kpc, whereas MWSC catalogue lists the cluster to be of age 1 Myr at a distance of 1.1 kpc. Stephenson 2 is a young massive cluster with 26 red supergiants, whose CCM diagrams can be easily be misinterpreted unless its status as a young massive cluster is already known, as it was not in the MWSC catalogue pipeline. However, as the properties of *all* the MWSC catalogue cluster candidates were derived in the same way (i.e. homogeneously), so were their uncertainties and thus any trends identified through large scale analyses using the sample will not be significantly affected by the property peculiarities of individual objects (such as Stephenson 2).

To create Cluster Sample 1 (CS 1), objects flagged as 'Open Clusters', 'Nebulous' or 'Remnants' were selected. Objects flagged as 'Globular Clusters', 'Associations' or 'Moving Groups' were excluded as a sample of bound open clusters is required and although associations and moving groups are part of cluster evolution, neither of these are sufficiently bound to warrant inclusion. Objects flagged as 'Nebulous' or 'Remnants' were included as these flags suggest

that the objects are either very young or old open clusters, respectively.

To determine the completeness limit of the selected clusters, a plot of their surface density projected onto the GP, $\sum_{XY}$, against their distance from the Sun, $d_{XY}$, was made (Figure 2.1). Taking the old cluster deficit into consideration, the selected clusters are complete (i.e. have an approximately constant surface density) in the range $0.8\,\mathrm{kpc} \leq d_{XY} \leq 1.8\,\mathrm{kpc}$ for $|b| \leq 90^\circ$ with an average surface density of $115\,\mathrm{clusters}\,/\,\mathrm{kpc}^2$. A selection of clusters which have a distance within the determined completeness limit was made. This final selection leaves 960 clusters in CS 1.

Figure 2.3 shows the age distribution of CS 1 to steeply decrease with age, as expected with a homogeneous completeness limit. CS 1 contains a sufficient number of objects to contain a sizeable number of clusters between 1-4 Gyr, which is useful for investigating old open cluster behaviours.

## 2.2 CS 2: The DAML02 Catalogue

The DAML02[1] catalogue by Dias et al. (2002) is an online database compiled from all known cluster/candidates in the literature which is regularly updated as new data becomes available. At the time of writing it contains 2174 objects. The fundamental properties for each object (distance, reddening, age etc.) are taken from the literature so have been derived using methodologies with varying degrees of accuracy i.e. the database's properties are heterogeneous in nature.

DAML02 pre-dates, and was the primary data source for, the MWSC catalogue. Many objects are in both the DAML02 and MWSC catalogues, but have listed property values which are not in agreement. Thus the two catalogues provide an opportunity to study the impact of using cluster samples with homogeneous and heterogeneous derived properties in large scale analyses.

To create Cluster Sample 2 (CS 2), DAML02 objects with distance, reddening and age values are selected. To determine the completeness limit of this selection, a plot of the objects' surface density projected onto the GP, $\sum_{XY}$, against their distance from the Sun, $d_{XY}$, was made (Figure 2.1). The selected objects are complete within the range $0\,\mathrm{kpc} \leq d_{XY} \leq 1.0\,\mathrm{kpc}$ for $|b| \leq 90^\circ$, with an average surface density of $110\,\mathrm{clusters}\,/\,\mathrm{kpc}^2$. A selection of objects

[1] http://www.astro.iag.usp.br/ocdb/

which have a distance within the determined completeness limit was made.

Unlike the MWSC catalogue, there is no deficit of old open clusters ($> 1$ Gyr). This is most likely due to the reduced completeness limit of the DAML02 catalogue, i.e. the deficit is observed in the MWSC catalogue when the surface density for clusters at distances $< 1$ kpc is compared to that of clusters at distances $> 1$ kpc, but the DAML02 catalogue is only complete for clusters with distances up to 1 kpc. Thus, the DAML02 catalogue is *relatively* complete for old open clusters, and the average surface density of clusters within the completeness limit is comparable to the MWSC catalogue. The final selection leaves 389 clusters in CS 2.

Figure 2.3 shows the age distribution of CS 2 to steeply decrease with age, as expected with a homogeneous completeness limit. CS 2 contains less objects than CS 1, but has a sufficient number of clusters with ages of 1-2 Gyr, which is useful for analysing the 'younger' old open cluster behaviours.

## 2.3 CS 3: The WEBDA Catalogue

The WEBDA[2] catalogue by Mermilliod (1995) is an online interactive database, comprised of Galactic open clusters which have been confirmed as real and have high accuracy measurements. Thus, WEBDA contains less objects than DAML02. At the date of writing it contains 1755 open clusters.

To create Cluster Sample 3 (CS 3), all clusters in the WEBDA catalogue are selected. To determine the completeness limit of the selection, a plot of the clusters' surface density projected onto the GP, $\sum_{XY}$, against their distance from the Sun, $d_{XY}$, was made (Figure 2.2). The clusters are complete within the range $0\,\mathrm{kpc} \leq d_{XY} \leq 1.0\,\mathrm{kpc}$ for $|b| \leq 90°$, with an average surface density of 98 clusters / kpc$^2$. A selection of clusters which have a distance within the determined completeness limit was made. This final selection leaves 358 clusters in CS 3.

Figure 2.4 shows the age distribution of CS 3 to steeply decrease with age, as expected with a homogeneous completeness limit. CS 3 contains a number of objects comparable to CS 2, but the majority of the CS 3 clusters are in the age range 10 Myr-1 Gyr, with only a few clusters older than this. Thus CS 3 is a good sample to investigate young-intermediate aged clusters.

[2] http://www.univie.ac.at/webda/

## 2.4 CS 4: The FSR List Catalogue

To date, the FSR List catalogue by Froebrich et al. (2007) is one of the largest homogeneously sourced cluster catalogues with 1788 objects, of which 1021 were previously undiscovered 'new' open cluster candidates, 680 are known open clusters and 87 are globular clusters. The authors searched the GP within $|b| \leq 20°$ using 2MASS star density maps and identified each object as a projected stellar overdensity on the background field. Only a small number of the new cluster candidates have been studied in the literature on an individual basis (e.g. Bonatto and Bica (2007a), Bica et al. (2008), Camargo et al. (2009), Froebrich et al. (2010), Camargo et al. (2012), Camargo et al. (2013)). The majority of the catalogue remains unstudied primarily due to the lack of additional data available (e.g. spectroscopy, astrometry), which has made an accurate, homogeneous derivation of their properties difficult.

To create Cluster Sample 4 (CS 4) all open cluster/candidates are selected and their distance, extinction and age values were determined using the methods outlined in Chapter 4, 5 and 6 respectively. All three properties were successfully determined for 298 objects, of which 82 previously undiscovered cluster candidates were confirmed as real clusters (see Chapter 8 for details). To determine the completeness limit of the remaining clusters, a plot of their surface density projected onto the GP, $\sum_{XY}$, against their distance from the Sun, $d_{XY}$, was made (Figure 2.2). The clusters are complete within the range $1.5\,\mathrm{kpc} \leq d_{XY} \leq 2.1\,\mathrm{kpc}$ for $|b| \leq 20°$, with an average surface density of $15\,\mathrm{clusters}\,/\,\mathrm{kpc}^2$. A selection of clusters which have a distance within the determined completeness limit was made. This final selection leaves 95 clusters in CS 4.

Figure 2.4 shows that the age distribution of CS 4 does not steeply decrease with age, but becomes flat between 0.5 and 2.0 Gyr, thus indicating that the sample has an age bias towards older clusters. This bias could have been caused by several factors. Observationally younger clusters are typically concentrated in the Galactic mid-plane comparative to their older counterparts (Buckner and Froebrich, 2014), where large scale foreground extinction is more likely to occlude them from detection, i.e. younger clusters are not present in the FSR List catalogue. The methodology used to derive the clusters' distance and extinction values (see Chapter 4 and 5 for details) require them to have at least 30 stars within one core radius, i.e. clusters with a high amount of foreground extinction (typically younger) were less likely to fulfil this requirement and to have been excluded from the sample. Cluster ages were derived using a pipeline which fitted modelled cluster sequence isochrones (see Chapter 6 for details) which favours older clusters as they typically have prominent markers on their CCM

diagrams (well defined MS/turn-off, giants) comparative to their younger counterparts which would have been more likely to be excluded from the sample due to an inability to accurately fit an isochrone to their CCM diagrams and derive their ages.

Although CS 4 is significantly smaller than the other cluster samples, it is homogeneously complete at a slightly greater distance, and contains a higher fraction of older clusters. Thus, CS 4 is a good sample to investigate old clusters at (relatively) large distances.

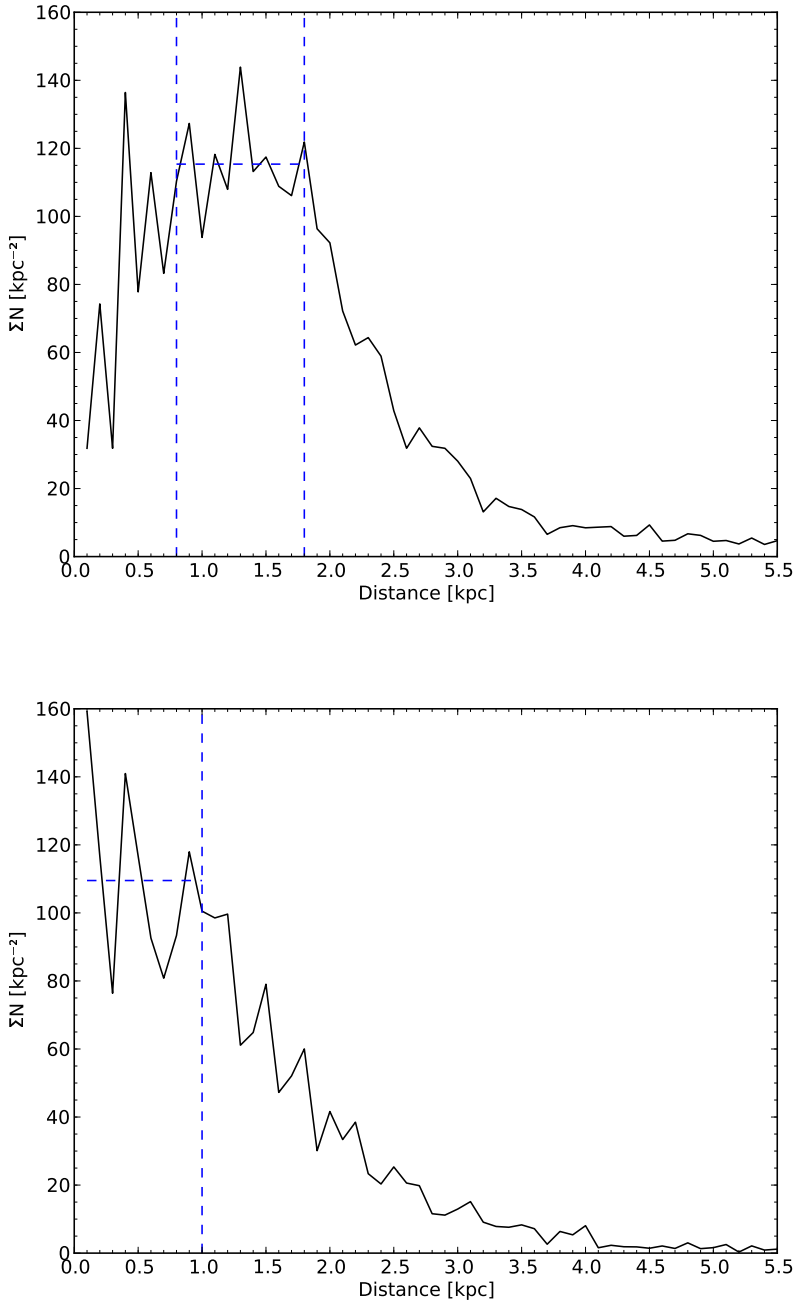


Figure 2.1: Plots of surface density distribution of selected (*Top*) MWSC and (*Bottom*) DAML02 catalogue clusters, as a function of distance. Vertical dashed lines represent the minimum and maximum completeness distance, and the horizontal dashed lines show the average surface density of 115 clusters / $\mathrm{kpc}^2$ for CS 1 and 110 clusters / $\mathrm{kpc}^2$ for CS 2.

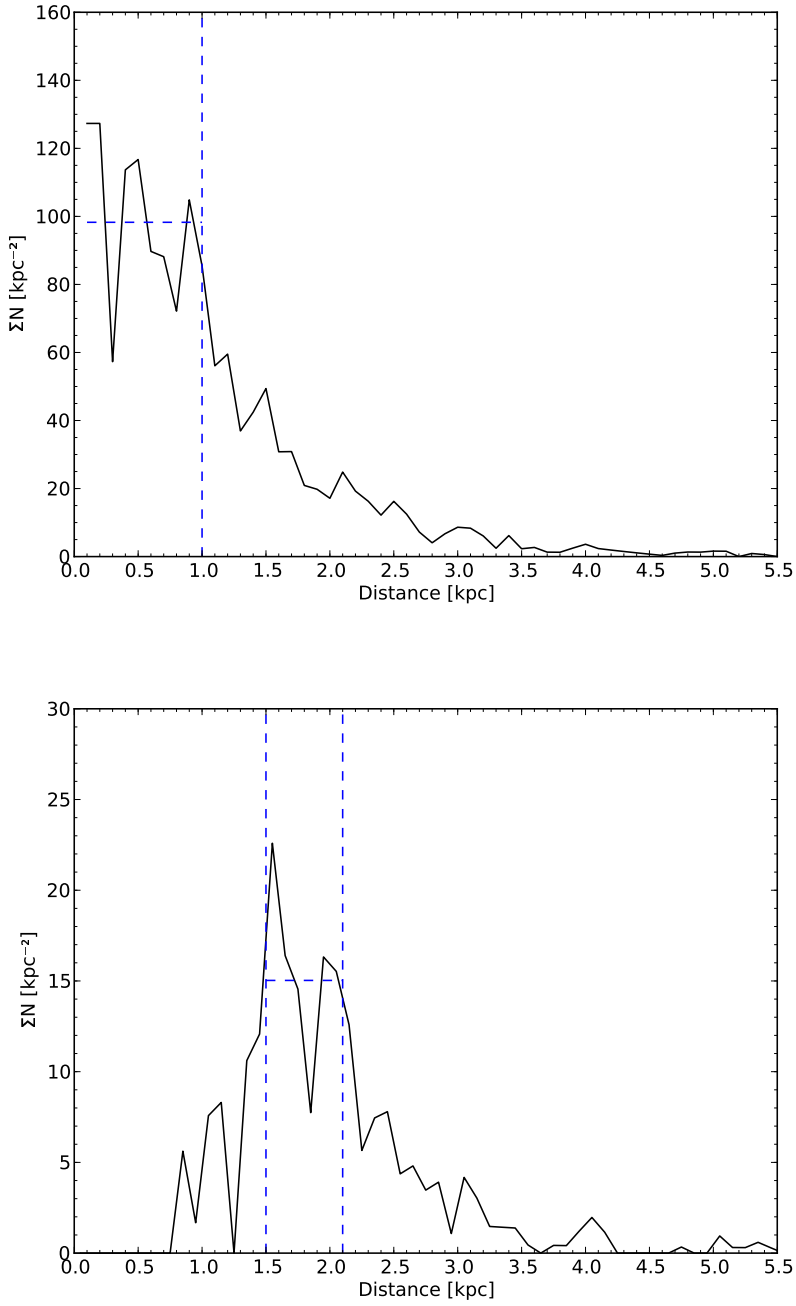


Figure 2.2: Plots of surface density distribution of selected (*Top*) WEBDA and (*Bottom*) FSR List catalogue clusters, as a function of distance. Vertical dashed lines represent the minimum and maximum completeness distance, and the horizontal dashed lines show the average surface density of 98 clusters / kpc$^2$ for CS 3 and 15 clusters / kpc$^2$ for CS 4.

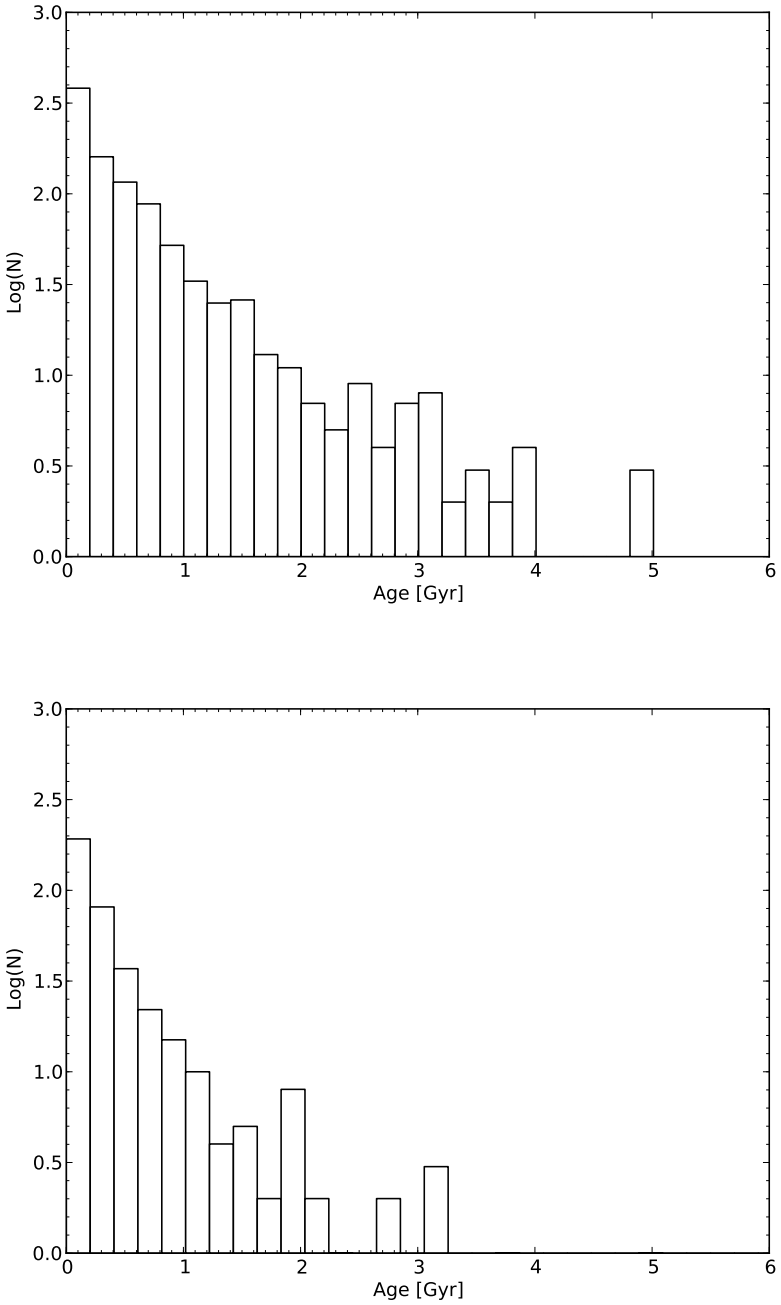


Figure 2.3: Histograms of the age distribution of (*Top*) CS 1 and (*Bottom*) CS 2.

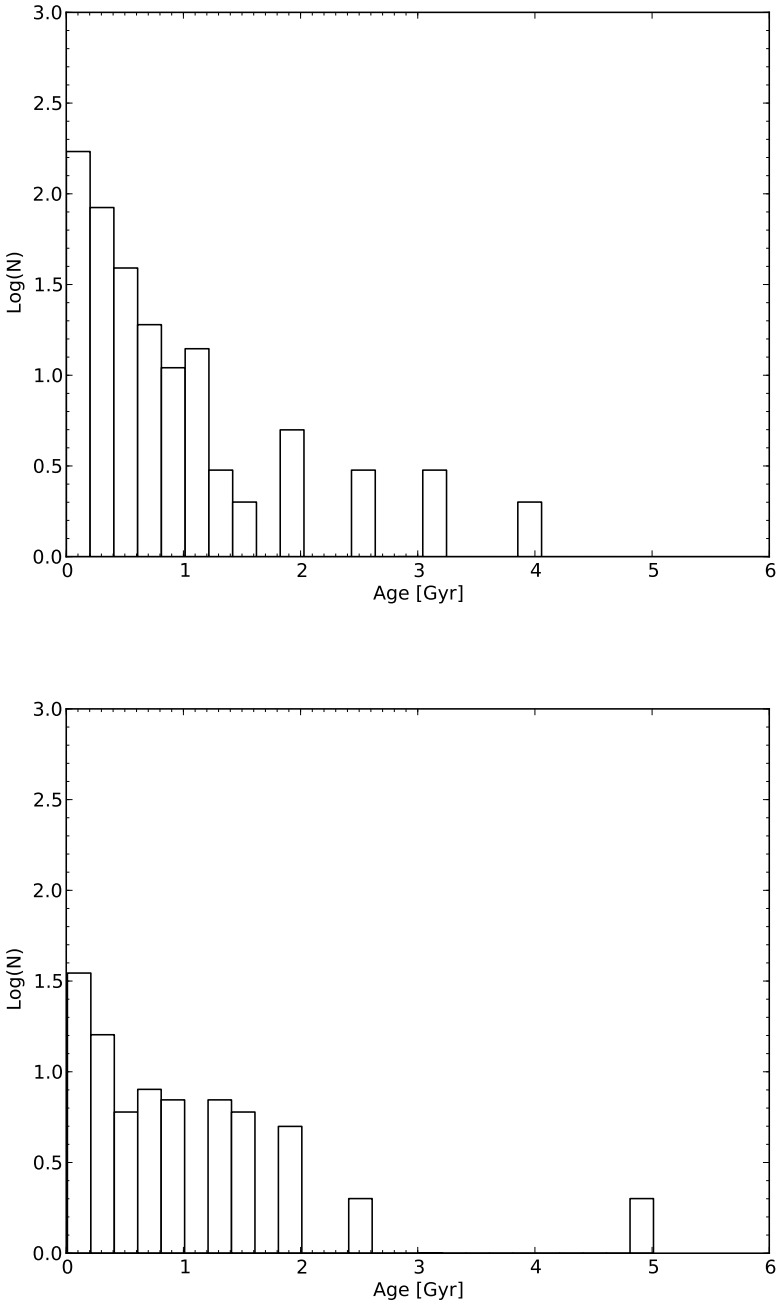


Figure 2.4: Histograms of the age distribution of (*Top*) CS 3 and (*Bottom*) CS 4.

# Part II

# Methods

# Chapter 3

# Identifying Cluster Members

The foundation of any method which derives cluster's fundamental properties (such as distance, extinction, age), is dependent on an accurate and reliable identification of their members. When only photometry is available for clusters this poses a significant problem as, in the absence of spectrometry, astrometry and/or X-ray emissions, distinguishing cluster members from interloping field stars becomes an arduous task. When clusters are sparsely populated, projected onto the Galactic mid-plane and/or regions with a high field star density such as towards the GC where field star contamination is high (e.g. Bica et al. (2008)), identifying true members from photometry alone can be near impossible.

In principle, members can be spatially identified from their apparent position with respect to a cluster's centre, i.e. the closer a star is to the central density peak, the more likely that it is a member (Dias et al. (2012), Krone-Martins and Moitinho (2014)). However, this approach is unreliable for clusters which are dense (stellar crowding), projected onto a high density stellar field (difficult to distinguish from the field population) and/or young (typically non-circular in projection, multiple density peaks), see Froebrich et al. (2010), Buckner and Froebrich (2013).

Alternatively, members can be identified from their stellar colours using a process known as *photometric decontamination*, for which there are many realisations in the literature (Jeffries et al. (2001), Naylor and Jeffries (2006), Piatti et al. (2010), Maia et al. (2010), Pavani et al. (2011) etc.). This Thesis uses an approach that is based on the works of Bonatto and Bica (2007b) and Froebrich et al. (2010), known as the Photometric Decontamination Technique

(PDT). The PDT is the approach of choice as it determines the likelihood that a star projected onto a cluster is a member from photometry alone, without the need to fit modelled cluster sequence isochrones to the cluster's CCM diagrams, and can derive properties for a single cluster that vary significantly between authors (see Chapter 1, Chapter 6, Sect. 8.4).

## 3.1 The Photometric Decontamination Technique

As true members of a cluster are at the same Solar distance and have a similar reddening, they will appear clumped on a Colour Magnitude Diagram (CMD), whereas interlopers have variable Solar distances and reddenings so will appear homogeneously distributed on a CMD. Using this principle, the PDT identifies cluster members through a 4-step process, detailed below.

### 3.1.1 STEP 1: Define the Areas for Photometric Decontamination

First, the core radius of a cluster, $r_{cor}$, is determined from a radial star density profile fit of the form:

$$\rho(r) = \rho_{bg} + \rho_{cen}\left[1 + \left(\frac{r}{r_{cor}}\right)^2\right]^{-1} \tag{3.1}$$

Where $r$ is the distance from the cluster centre; $\rho(r)$ the projected radial star density; $\rho_{bg}$ is the projected background star density which is assumed constant; and $\rho_{cen}$ the central star density above the background of the cluster.

The *cluster area*, $A_{cl}$, is then defined as a circular area around the centre of the cluster within which the majority of members are expected to be contained, typically 1, 2 or $3 \times r_{cor}$. The *control area*, $A_{con}$, is defined as an annulus around the centre of the cluster within which all stars are expected to belong to the field population, typically $> 5 \times r_{cor}$ (see e.g. Buckner and Froebrich (2013)).

### 3.1.2 STEP 2: Measure CCM Distances in the Cluster Area

The second stage is to determine the Colour Colour Magnitude (CCM) distance between star $i$ and every other star $j$ ($i \neq j$) in the cluster area. To do this a small ellipsoid in the CCM space is defined:

$$r_{ccm}^{cl} = \sqrt{e\,(J_i - J_j)^2 + (JK_i - JK_j)^2 + (JH_i - JH_j)^2} \quad \text{for } j{=}1, 2, 3...\text{N} \qquad (3.2)$$

where $r_{ccm}^{cl}$ is the CCM distance between star $i$ and $j$ in the cluster area; and $e$ is the shape factor of the ellipsoid whose value ($0 < e \leq 1.0$) determines whether it is prolate, oblate or degenerate. J, H and K are the NIR magnitudes of the stars and $JK = [J - K]$, $JH = [J - H]$. Different colour/magnitude combinations can be used in Eq. 3.2 if desired, however Bonatto and Bica (2007b) showed that using this particular combination of colours provides the maximum variance among CCM sequences for open clusters of different ages.

The *Nearest Neighbour number*, $N$, defines the resolution at which potential cluster members are separated from field stars in CCM space. It is the number of stars nearest to star $i$ for which a CCM distance is measured. For example if $N = 10$, the CCM distance between star $i$ and the 10 nearest stars in the CCM space is determined; if $N = 20$, the CCM distance between star $i$ and the 20 nearest stars in the CCM space is determined; if $N = 30$, the CCM distance between star $i$ and the 30 nearest stars in the CCM space is determined, etc. Low values of $N$ increase the resolution, high values of $N$ decrease the resolution.

### 3.1.3 STEP 3: Measure CCM Distances in the Control Area

The third stage is to determine the CCM distance between star $i$ in the cluster area and every other star $j$ in the control area. As in Eq. 3.2, a small ellipsoid in the CCM space is defined:

$$r_{ccm}^{con} = \sqrt{e\,(J_i - J_j)^2 + (JK_i - JK_j)^2 + (JH_i - JH_j)^2} \quad \text{for } j{=}1, 2, 3...\text{N} \qquad (3.3)$$

Where $r_{ccm}^{con}$ is the CCM distance between star $i$ in the cluster area and $j$ in the control area.

### 3.1.4 STEP 4: Calculate Membership Probability

The final stage is to determine the probability that star $i$ is a member of the cluster. The CCM distance of stars in the cluster and control areas to star $i$ are compared. The number of stars, $N_{ccm}^{con}$, in the control area which have a smaller CCM distance than stars in the cluster area to star $i$ are counted i.e. where $r_{ccm}^{cl} > r_{ccm}^{con}$.

The probability star $i$ is a member of the cluster is then given by:

$$P_{cl}^{i} = 1.0 - \frac{N_{ccm}^{con}}{N}\frac{A_{cl}}{A_{con}}. \tag{3.4}$$

Where $P_{cl}^{i}$ is the *Membership Probability Index* (MPI) of star $i$. In principle, $P_{cl}^{i}$ can have a negative value due to statistical fluctuations in the number of field stars in the control and cluster area, and thus it is not in fact a true probability so has been named an index. As a negative value simply means that a star is very unlikely to be a member of the cluster, all negative $P_{cl}^{i}$ values are set to zero.

### 3.1.5 An Example: FSR0233 (LK 10)

The PDT is applied to the open cluster FSR0233 to identify its most probable members. Figure 3.1 and 3.2 show that the MS and some giants are clearly identified, which suggests that it is quite old and perhaps massive. Indeed, fitting modelled cluster sequence isochrones to the cluster's CCM diagrams gives an age of 1 Gyr which is consistent with the age derived by Bonatto and Bica (2009), whilst a search of the literature confirms that the cluster is relatively massive. Figure 3.3 shows some structure/clumping amongst the most likely cluster members of FSR0233 at coordinates ($l = 79.84°, b = -0.92°$) which is not present amongst the homogeneously distributed least likely cluster members, suggesting this is the cluster's centre.

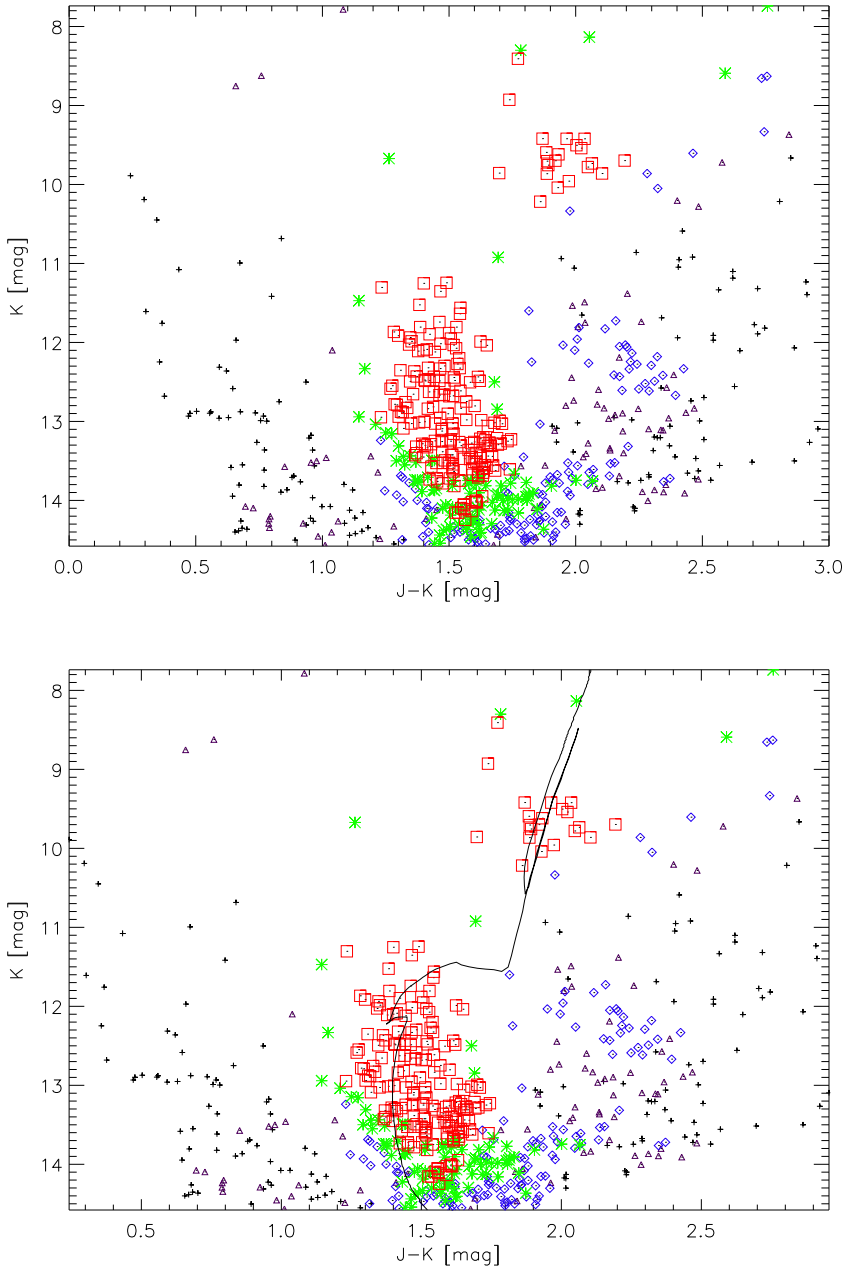


Figure 3.1: Colour-Magnitude plots of **FSR0233**. The size of the cluster area was $2 \times r_{cor}$, the Nearest Neighbour number chosen was $N = 15$ and all stars have a 2MASS quality flag of "AAA". Photometric membership probabilities are represented as follows: $P^i_{cl} \geq 80\%$ red squares; $60 \leq P^i_{cl} < 80\%$ green stars; $40 \leq P^i_{cl} < 60\%$ blue diamonds; $20 \leq P^i_{cl} < 40\%$ purple triangles; $P^i_{cl} < 20\%$ black plus signs. The MS/turn-off and a number of giants of have been clearly identified, as demonstrated by the Solar metallicity modelled cluster sequence isochrone which has been overplotted on the (*Bottom*) plot. The isochrone's parameters are: distance $d = 1.6$ kpc, H-band extinction $A_H = 1.3$ mag and $log(age/yr) = 9$.

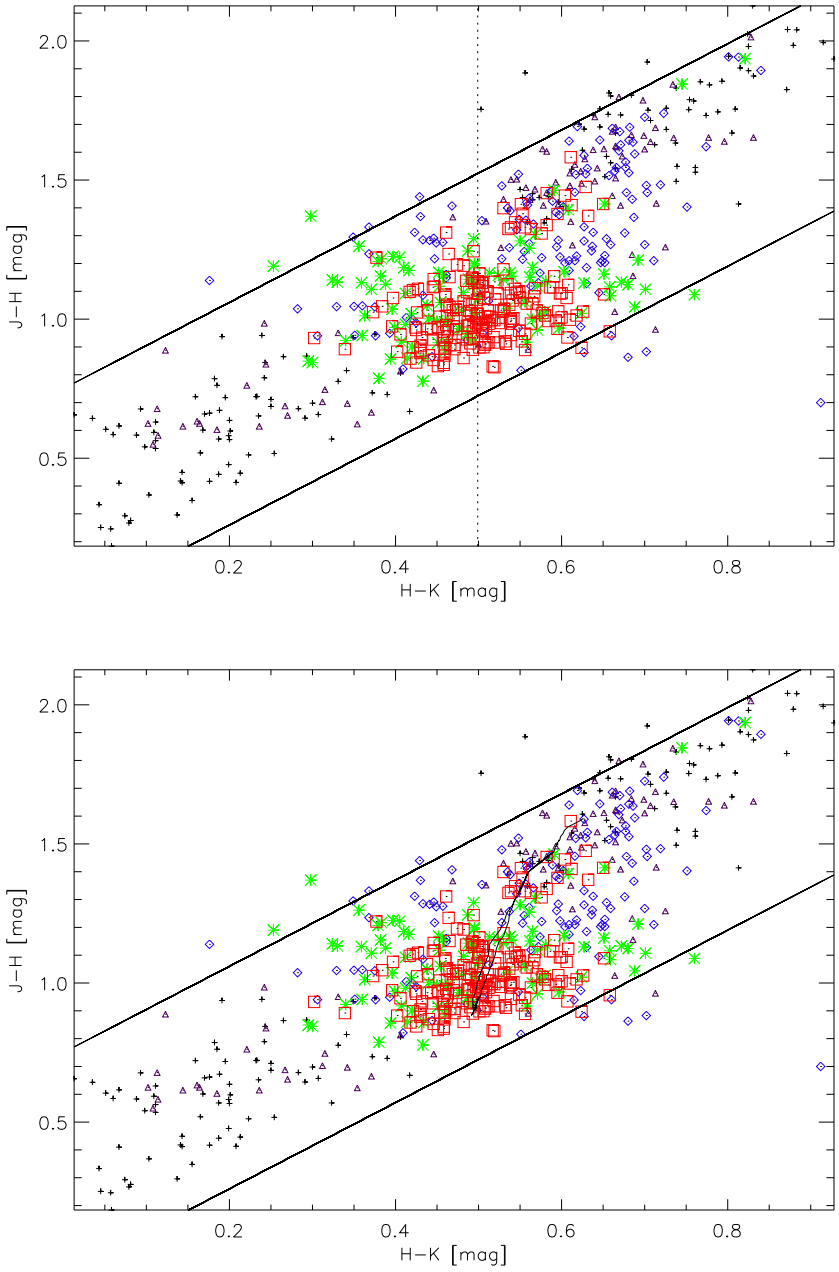


Figure 3.2: Colour-Colour plots of **FSR0233**. The size of the cluster area was $2 \times r_{cor}$, the Nearest Neighbour number chosen was $N = 15$ and all stars have a 2MASS quality flag of "AAA". Photometric membership probabilities are represented as follows: $P^i_{cl} \geq 80\%$ red squares; $60 \leq P^i_{cl} < 80\%$ green stars; $40 \leq P^i_{cl} < 60\%$ blue diamonds; $20 \leq P^i_{cl} < 40\%$ purple triangles; $P^i_{cl} < 20\%$ black plus signs. (*Top*) The dashed black line represents the measured median [H-K] colour of FSR0233 – see Section 4.2.2.1. (*Bottom*) The solid line represents the fitted modelled cluster sequence isochrone as for Figure 3.1.

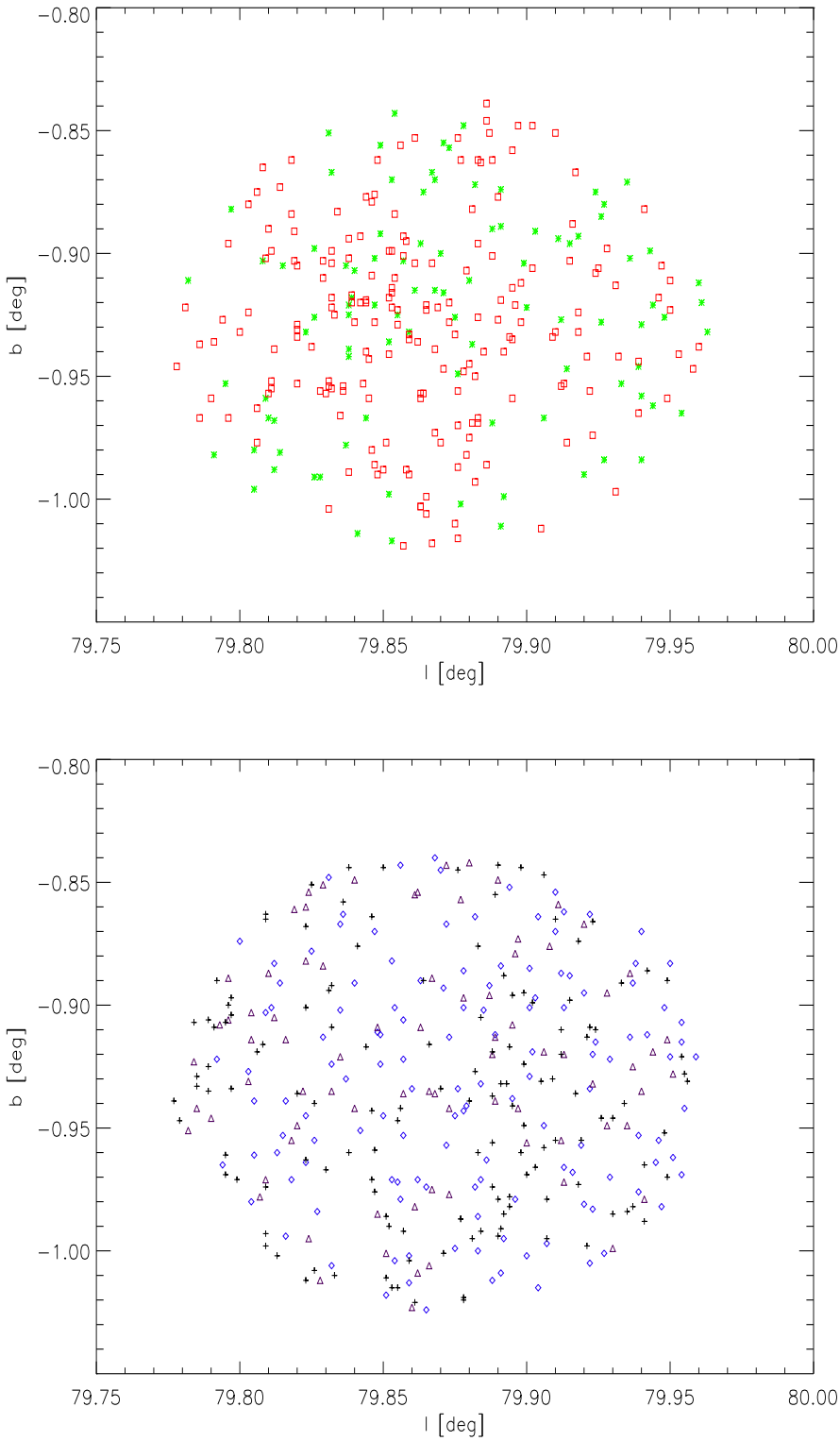


Figure 3.3: Plots of $(l, b)$ positions of stars for **FSR0233** that have a 2MASS quality flag of "AAA", are within 2 $\times$ $r_{cor}$ with and a MPI (*Top*) greater than 60 % (*Bottom*) less than 60 %. The Nearest Neighbour number chosen was $N = 15$. Photometric membership probabilities are represented as follows: $P^i_{cl} \geq 80\%$ red squares; $60 \leq P^i_{cl} < 80\%$ green stars; $40 \leq P^i_{cl} < 60\%$ blue diamonds; $20 \leq P^i_{cl} < 40\%$ purple triangles; $P^i_{cl} < 20\%$ black plus signs.

### 3.1.6 Photometric Decontamination Shape

Equations 3.2 and 3.3 follow the work of Froebrich et al. (2010) by selecting a small *prolate ellipsoid* in the CCM space with an elongation of $e = 0.5$. In contrast, the original authors (Bonatto and Bica, 2007b) selected a small *cuboid* in the CCM space, whose J-band magnitude side length was larger than the side length of the JK and JH colours. This Thesis will use small prolate ellipsoid ($e = 0.5$) instead of a cuboid as it is computationally less time expensive.

However it should be noted that there are a near infinite number of shapes that could be used to make the selection in the CCM space, as the distance of star $i$ from every other star $j$ in the CCM space is not dependent on (and thus membership probabilities do not vary significantly with) the shape of the selection area. To demonstrate this, membership probabilities are determined and summed to determine the total number of members in FSR0233. Prolate, oblate and degenerate ellipsoids are used to make the selection in the CCM space, achieved by varying the shape factor (Eq. 3.2, 3.3) between $0 < e \leq 1.0$ in increments of 0.1. As shown by Figure 3.4 there is no significant variation in the total number of cluster members identified for FSR0233 with shape. Obviously this test is in no way extensive, but simply intended as an example for the reader.

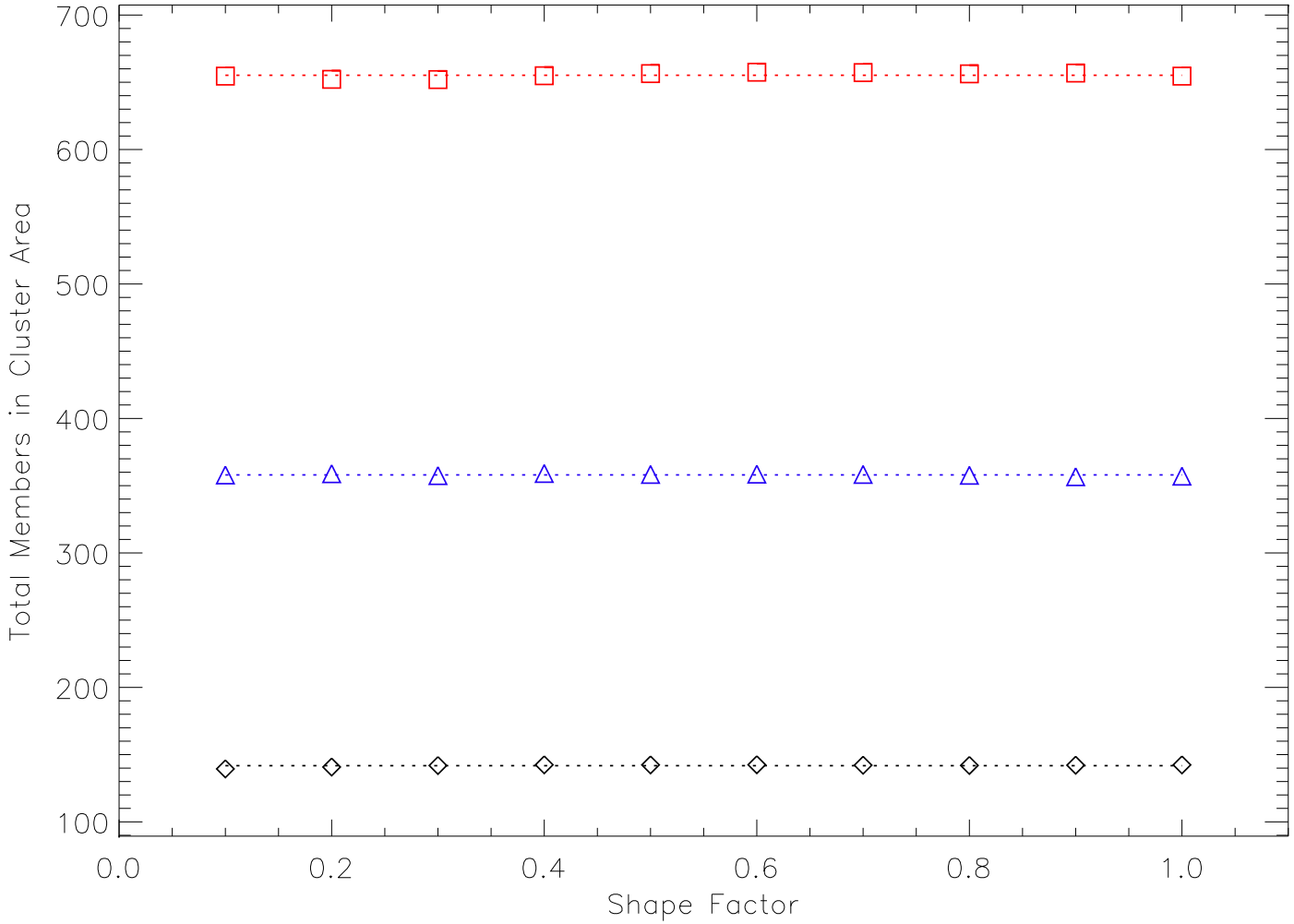


Figure 3.4: Plot of the total number of members of **FSR0233** that have a 2MASS quality flag of "AAA" and are within $1\times$ (black diamonds), $2\times$ (blue triangles) and $3\times$ (red squares) the cluster's core radius. The overplotted lines represent the mean number of cluster members. Membership probabilities were calculated using Eq. 3.2, 3.3 and 3.4 with a Nearest Neighbour number of $N = 10$. The shape factor was varied between 0.1 and 1.0 (see text for details). The total number of cluster members is determined through summation of the stars membership probabilities, and for each of the three radii the *root-mean-square-error* was $< 1\%$.

# Chapter 4

# Distance Determination

Over the past decade the focus of the star cluster community has notably shifted from the Optical to the NIR in an effort to uncover a fraction of the estimated 97 % of open clusters which have so far evaded detection [1]. This shift has been facilitated by technological advancements and subsequent NIR data releases (2MASS, VISTA-VVV, UKIDSS-GPS, to name a few). As a result, large NIR cluster candidate samples have started to become available (e.g. Froebrich et al. (2007), Borissova et al. (2011)).

Unfortunately with the number of discovered clusters growing, a new problem has emerged: how can the distances to these clusters be derived? For the majority of objects only photometry is available and in the absence of spectrometry, astrometry and/or X-ray emissions, established methods of distance determination are not viable. Determination of star cluster distances is essential to analyse both their Galactic distribution and individual properties, which subsequently provide insights into the past and present evolution of the Galaxy through e.g. an analysis of the relationship between cluster scale height and age. Thus, there is a real need for an reliable, automatic, robust, purely photometric method to estimate distances for the current and forthcoming large NIR cluster candidate samples. This Chapter establishes that method.

[1] Based on the 2808 confirmed open clusters listed in the MWSC catalogue and the estimated $10^5$ clusters in the Galactic Disk (Piskunov et al., 2006).

## 4.1 Current Limitations

In recent years large samples of clusters have been discovered in the NIR (e.g. Froebrich et al. (2007), Borissova et al. (2011)). Consequently, the fundamental properties of these clusters (distance, extinction, age, metallicity) are unknown. Furthermore, as there is *only* photometry available for the clusters, established methods of distance determination are not viable (see Chapter 1).

Attempts have been made to establish distances for such clusters through fitting modelled cluster sequence isochrones to their CCM diagrams, in the absence of additional data such as spectrometry and astrometry (e.g. Bonatto and Bica (2007a), Bonatto and Bica (2008b), Camargo et al. (2010), Froebrich et al. (2010), Güneş et al. (2012)). The advantage of isochrone fitting is that a cluster's distance, extinction and age are derived simultaneously. The disadvantage of isochrone fitting is that: (i) clusters' fundamental properties are 'free', so a number of isochrones with different property value combinations can provide equally good fits for a single cluster sequence. Cluster metallicities are typically assumed to be Solar, so derived properties will be incorrect for non-Solar metallicity clusters; (ii) members may be misidentified as interlopers if they are intrinsically blue/red, variable, binary or near completeness limits of the photometry; (iii) bright interlopers may be misinterpreted as early type members. Thus the reliability of their derived values is questionable and inevitably vary from author to author, sometimes significantly. For example, Solar metallicity isochrones were fitted to FSR1716 by both Froebrich et al. (2010) and Bonatto and Bica (2008b). Froebrich et al. (2010) found FSR1716 to be an open cluster with a distance/age of 7.0 kpc/ 2 Gyr, whereas Bonatto and Bica (2008b) determined it to be either an open cluster of 0.8 kpc/7 Gyr or a globular cluster of 2.3 kpc/12 Gyr. The differences in the derived properties of FSR1716 was due to the two authors having different interpretations of which isochrone was the best fit for the cluster. Additional examples can be found in Sect. 8.4. Properties values show the most variability between authors for clusters which are less well defined on the field, sparsely populated and/or lack prominent features (e.g. giants, a clearly defined MS/turn-off etc.). Clearly, an alternative to isochrone fitting is needed for clusters which only have photometry available.

In principle it should be possible to derive cluster distances from foreground star counts and photometry alone, as the number of stars foreground to an object is proportional to its distance. Indeed, this approach has been successfully applied and calibrated to estimate distances to dark clouds with maser sources (Foster et al., 2012), and with jets and outflows

(Ioannidis and Froebrich, 2012). Unfortunately, the application of the approach to clusters is infinitely more complex. Clusters are typically not associated with dark clouds and thus accurately distinguishing between foreground stars, cluster members and other field stars with only photometry available is a difficult task, one which is further compounded by astrophysical effects such as stellar crowding and large scale foreground extinction.

Therefore until now foreground star counts have not been used to estimate cluster distances. Instead, the community has been content to wait for additional data (e.g. spectrometry, astrometry) to become available before analysing clusters. With the advent of large NIR cluster samples becoming available and forthcoming ones expected from e.g. the VISTA-VVV and UKIDSS-GPS surveys, there is a real need to have a reliable, purely photometric method to homogeneously derive cluster distances which are independent of their other properties (extinction, age, metallicity) and isochrone fits.

## 4.2 Method

The number of foreground stars between an observer and an object in the Galaxy is intrinsically linked with distance. If the stars in the Galaxy are assumed to have a smooth radial distribution, then the projected number of stars foreground to an object are proportional to its distance. It is on this principal this method of deriving cluster distances, utilising only photometry, is founded.

The method consists of three main steps:

- Point source and cluster radii selections
- Identification of cluster members and stars foreground to the cluster
- Derivation of cluster distance

Below, each step is explained in detail.

### 4.2.1 STEP 1: Point Source, Radii Selections and Cluster Requirements

The reader should be aware that this method was originally developed to establish distances for the FSR List catalogue. Due to the FSR List clusters wide range of Galactic positions, and

the currently restrictive longitude/latitude ranges of the available NIR surveys, 2MASS was the highest resolution survey that could provide photometry for every cluster in the catalogue. As such, this method uses 2MASS photometry to derive cluster distances. However, the choice of survey is arbitrary and the method can be adapted and implemented with data from any available photometric survey.

#### 4.2.1.1 Point Source Selections

JHK photometry is extracted from the 2MASS NIR point source catalogue in a circular 0.5° area around the centre of each cluster [2] whose distance is to be determined. FSR List clusters' central coordinates are taken from Froebrich et al. (2007).

Typically, between 50 % and 70 % of all stars in the 2MASS catalogue have a Quality flag (Qflag) better than "CCC" i.e. are detected in the JHK bands with a Signal-to-Noise ratio (S : N) of greater than 5, with corrected photometric uncertainties of less than 0.22 mag. About 35 % to 45 % of all stars are of the highest photometric quality with a Qflag of "AAA", i.e. detected in the JHK bands with a S : N of greater than 10 and corrected photometric uncertainties of less than 0.11 mag.

Two cluster samples are created to test the effect of photometric quality and reduced/increased point source availability on the accuracy of the method:

- **The C-sample:** All stars within the circular area with quality flag better than "CCC", for every cluster.
- **The A-sample:** All stars within the circular area with quality flag better than "AAA", for every cluster.

As is shown in Figure 4.1 the C-sample contains on average about 1.5 times as many stars as the A-sample.

[2] Froebrich et al. (2010) found an apparent core radii bias for the old FSR List catalogue clusters of 0.01°, thus an area of 0.5° should satisfactorily encompass the members of all clusters in the catalogue.

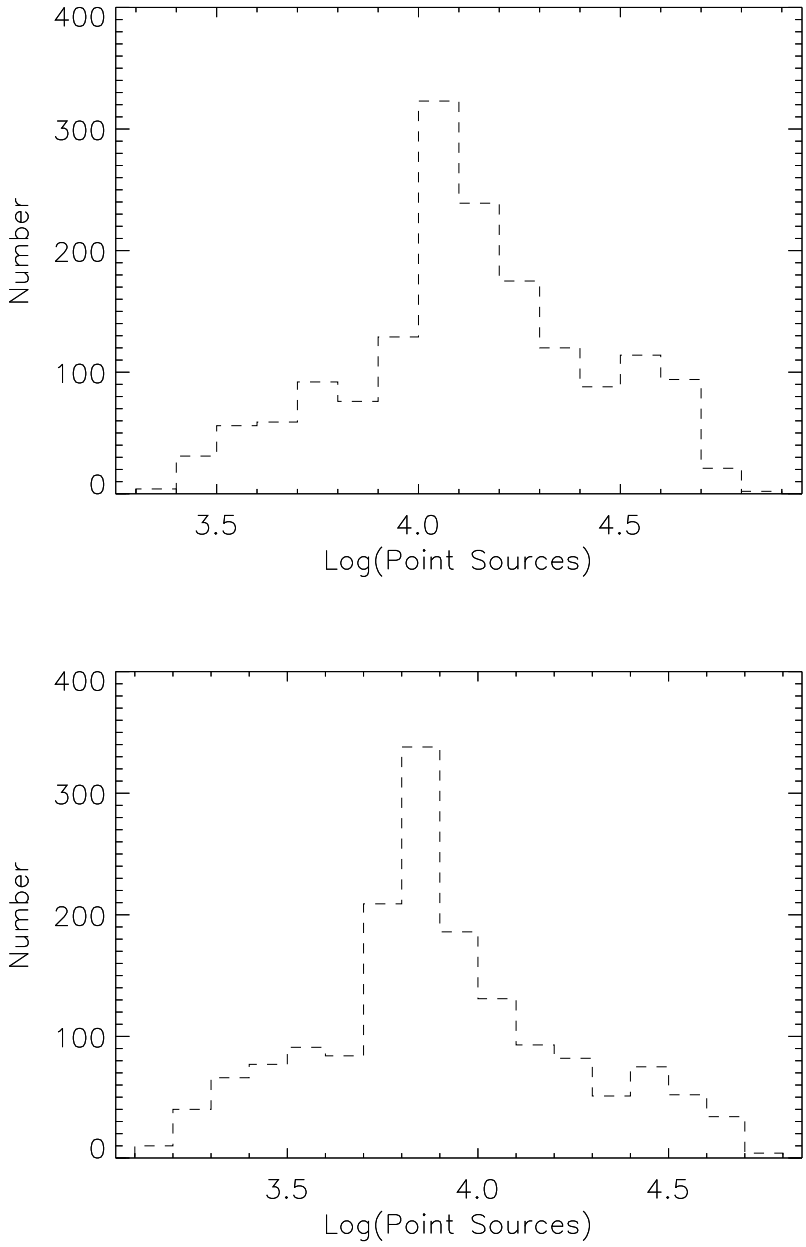


Figure 4.1: Histograms of point sources in a circular 0.5° area around the centre of each open cluster in the FSR List catalogue which has a core radius radius of $< 0.05°$ for (*Top*) C-sample and (*Bottom*) A-sample.

#### 4.2.1.2 Radii Selections

The *cluster area* is defined as a circular area around a cluster's centre which encompasses everything within $F$ times the cluster core radius, expressed as:

$$A_{cl} = \pi \left(F \times r_{cor}\right)^2 \tag{4.1}$$

Where $A_{cl}$ is the cluster area; $r_{cor}$ is the cluster's core radius; and $F$ is a integer factor which will be varied between $1 \leq F \leq 3$.

The *control area* is defined as an annulus area around a cluster's centre, which encompasses everything outside the inner radius $5 \times r_{cor}$ to a maximum outer radius of $r_{max}$, expressed as:

$$A_{con} = \pi \left(r_{max}^2 - (5 \times r_{cor})^2\right) \tag{4.2}$$

Where $A_{con}$ is the control area; and $r_{max}$ is a constant with value of $r_{max} = 0.5°$.

To determine the core radius of each cluster a radial star density profile fit is performed using the C-sample data, of the form:

$$\rho(r) = \rho_{bg} + \rho_{cen}\left[1 + \left(\frac{r}{r_{cor}}\right)^2\right]^{-1} \tag{4.3}$$

Where $\rho(r)$ the star density as a function of distance $r$ from the cluster centre; $\rho_{bg}$ the constant background star density; $\rho_{cen}$ the central star density above the background of the cluster; and $r_{cor}$ is the cluster core radius.

Theoretically Eq. 4.3 allows for an infinite number of cluster stars, as there is no defined tidal radius. However, it is reasonable to assume that there are no member stars in the control field (i.e. $r > 5 \times r_{cor}$), so about 70 % of all cluster members should be contained within $3 \times r_{cor}$ (Buckner and Froebrich, 2013).

#### 4.2.1.3 Cluster Requirements

Clusters whose distance is to be determined using this method must meet the following conditions:

- **Not be a globular cluster**
  As this method is designed to derive distances for open clusters only.
- **Have 30 or more stars with 2MASS Qflag "AAA" within one core radius**
  A cluster is defined as having *at least* 30 stars within one core radius.
- **Have 30 or more stars with 2MASS Qflag "AAA" in the control field**
  The control and cluster areas must have same minimum star count to identify cluster members (Chapter 3).
- **Have a core radius smaller than 0.05°**
  To ensure that the control field consists only of field stars, as 2MASS photometry has been extracted for a circular 0.5° area around the centre of the cluster.

### 4.2.2 STEP 2: Membership Identification

The second step is to distinguish between member stars and field interlopers in the cluster area. To do this, a photometric *Membership Probability Index* (MPI) is calculated for each star in the cluster area using the PDT as described in Chapter 3.

In principle, stars' MPI can be augmented with spatially derived membership probabilities i.e. stars toward the centre of the cluster have a higher likelihood of being a cluster member, and stars on the outer limits of cluster area have a lower likelihood of being a cluster member (see e.g. Dias et al. (2012), Krone-Martins and Moitinho (2014)). However following the work of Froebrich et al. (2010) and Buckner and Froebrich (2013), only the MPIs will be used to identify cluster members as spatial probabilities are unreliable for clusters which are:

- **Dense**, as they suffer from stellar crowding i.e. it is (observationally) difficult to resolve individual stars, especially using low resolution NIR surveys e.g. 2MASS.
- **Projected onto a high background density**, as it difficult to distinguish the cluster from the field and subsequently spatial membership probabilities tend to be very low.

- **Young**, as they may not appear circular in projection and have substructure (Sánchez and Alfaro (2009), Gregorio-Hetem et al. (2015)) i.e. spatially derived membership probabilities assume that clusters have a single central stellar density peak, from which the stellar density radially decreases until it becomes equal to the field.

.

#### 4.2.2.1 Identification of Foreground Stars

In principle, an object's apparent colour is an indicator of its distance as interstellar reddening material is accumulated in its line of sight i.e. an object's apparent colour becomes redder the more distant it is from the observer. Thus by measuring a cluster's median colour, stars which are bluer than this value can be identified as foreground to the cluster.

Obviously, this principle will fail in certain situations. Blue stragglers, blue super giants and other intrinsically hot/blue stars which are members of the cluster will be incorrectly identified as foreground to the cluster. Highly reddened clusters, such as those with a large proportion of red giants, associated clouds (embedded) or with foreground GMCs observationally in their line of sight, will have a relatively large proportion of member stars incorrectly identified as foreground to the cluster. It is also difficult to accurately measure the median colour of young clusters that contain a large proportion of members below the photometric detection limit (of e.g. 2MASS) as in these cases a measurement has to be made from visible members whose colour may not be typically representative of the entire cluster. These issues are addressed and statistically corrected for by the calibration procedure in Sect. 4.3.

An accurate measurement of clusters' median colour(s) is essential, as even a small inaccuracy can cause a significant over/under estimation of the number of stars foreground to a cluster and subsequently its distance estimate. Ideally it should be measured in the colour which has the smallest spread amongst the spectral types and luminosity classes, as any reddening can then be attributed to interstellar extinction. The colour $[H-4.5]$ has a well defined zero point as it measures the slope of the spectral energy distribution in the Rayleigh-Jeans part of the spectrum and is mostly independent of spectral type and/or luminosity class (Majewski et al., 2011). Unfortunately, the 4.5$\mu$m band magnitude is not available in 2MASS and has to be sourced from the WISE survey, whose lower resolutions means only $\sim$ 50 % of 2MASS point sources with a Qflag of "AAA" in the cluster area of any given cluster can be matched with WISE. Thus, the benefits of using the $[H-4.5]$ colour are negated by a lack of photometry

and the median cluster colour is instead measured in the 2MASS $[H-K]$ colour.

A cluster's median $[H-K]$ colour is measured as follows:

1. **The most likely members of the cluster are identified.**

   The MPIs of the stars in the cluster area are ordered highest to lowest. This is to facilitate measuring the median colour of the cluster from the its most likely members.

2. **The median $[H-K]$ colour of the top 25 %-45 % of the most likely cluster members is measured in 5 % increments.**

   As the MPIs form a continuous spectrum range, it is not possible to set a cut off for which a star is 'definitely a member' and 'definitely not a member'. The only conclusion that can be made is that a star with a very low MPI (e.g. $< 0.10$) is *most likely* not to be a cluster member. Similarly, a star with a very high MPI ($> 0.90$) is *most likely* to be a cluster member. Furthermore the range of MPI values per cluster will depend on both the number of stars in the cluster area and the individual cluster conditions and will therefore be different for every cluster. For example, a cluster may have stars in its cluster area with MPI values ranging between 0.10 and 1.00, whilst another cluster may have stars in its cluster area with MPI values ranging between 0.70 and 0.90.

   It is ideal for the distance method to be automated to facilitate establishing a large number of cluster distances in a short period of time and to minimise uncertainties introduced by human error. The most statistically fair way of determining the median colour of a cluster is to therefore not to select an arbitrary cut-off index value for the most likely cluster members (e.g. MPI$> 0.50$) but to measure the clusters median colour from various quantities of the most likely members i.e. the top 25 %, 30 %, 35 %, 40 % and 45 % of stars with the highest MPI values. In total five measurements are made of a cluster's median $[H-K]$ colour.

3. **The average median $[H-K]$ colour of the cluster, $HK_{med}$, is derived from the five $[H-K]$ measurements made in the previous step.**

   If the majority of stars in the cluster area have a high MPI value (e.g. 75 % of stars), the five measured median cluster colours will not significantly differ. If the minority of stars in the cluster area have a high MPI value (e.g. 20 % of stars), the process of averaging the five measured cluster colours will ensure the averaged measured median cluster colours should not (statistically) differ significantly from the clusters actual median colour.

From the median $[H-K]$ colour of the cluster, $HK_{med}$, the projected number density of stars foreground to a cluster, $\rho_{fg}^{cl}$, is defined as:

$$\rho_{fg}^{cl} = \frac{1}{A_{cl}} \sum^{i,blue} P_{field}^{i} \tag{4.4}$$

Where $A_{cl}$ is the cluster area in $sq/^{\circ}$; 'blue' denotes that only stars with a $[H-K]$ bluer than the median cluster colour (i.e. foreground) are included in the calculation; and $P_{field}^{i}$ is the probability that star $i$ is a field star, defined as:

$$P_{field}^{i} = 1.0 - P_{cl}^{i} \tag{4.5}$$

where $P_{cl}^{i}$ is the MPI for star $i$.

### 4.2.3 STEP 3: Deriving Distance

A Galactic model is used to derive cluster distances. The calibration procedure (Sect. 4.3) removes any model dependency on the method, rendering the choice of model arbitrary (as demonstrated in Sect. 4.4.2.5). The model of choice is the Besançon Galaxy Model (BGM) by Robin et al. (2003) which is dynamically self-consistent and uses the population synthesis approach to describe a smooth Galaxy with no spiral arms. Four stellar populations are described by the BGM: thin and thick Disk, stellar Halo, the outer Bulge; but white dwarfs are considered separately. Interstellar reddening material is modelled latitudinally as a double exponential and small scale variations are not described.

It is important to instruct the chosen model to generate an output which could have reasonably been detected by 2MASS. The completeness limit and photometric uncertainties in the 2MASS JHK filters are measured for each cluster position so that they can be included in the model input. Here, the completeness limit is defined as the magnitude depth at which the source count for each of the 2MASS JHK filter's begins to decline, and is measured by plotting each filters magnitude band against their respective source counts. The filters photometric uncertainties were determined as a function of brightness. The completeness limits and photometric uncertainties were measured for the control field of A-sample and C-sample, as the quality of point sources used in each sample translates to a difference in the magnitude

depth limit at which source counts begin to decline.

Next, the form of the model's extinction law is defined. A mean diffuse absorption value is adopted for all cluster positions, set as the average interstellar absorption in the Solar Neighbourhood which has a canonical value of 0.7 mag/kpc in the Optical V-band (see e.g. Froebrich et al. (2010)). As this method for deriving cluster distances is designed to be both automated and applicable to large cluster samples (i.e. for clusters at varying Galactic positions and local conditions) no position dependant discrete clouds are included in the simulations. Instead, the effects of large foreground extinction are considered and corrected for in Sect. 4.2.4.

A cluster's distance is derived as following:

1. **Instruct model to simulate 5000 stars**

   An area which contains 5000 simulated stars, centred around the cluster's central co-ordinates, is generated. Testing showed that 5000 simulated stars is sufficiently great to ensure that the uncertainties of the inferred cluster distances are not dominated by small number statistics of the random nature of the model output. For each simulated star the BGM provides data on its distance, Galactic position (l, b), age, mass, metallicity, luminosity, extinction, absolute and apparent magnitudes (U, B, V, I, K).

2. **Sort the model's simulated star distances in ascending order**

   The model simulates a field of 5000 stars using the Monte-Carlo method. The simulated stars are then placed in order of least to most distant.

3. **Infer cluster distance**

   In principle, any two objects at the same Galactic position, which are the same distance from an observer, will have an identical projected number density of stars foreground to them. Thus the cluster will have the same distance as the simulated star which is at the same Galactic position and that has the same projected number density of foreground stars.

   For each simulated star, a projected number density of foreground stars is calculated using:

$$\rho_{fg}^{model} = \frac{N_i}{A_{model}} \tag{4.6}$$

where $\rho_{fg}^{model}$ is the projected number density of star foreground to star $i$; $A_{model}$ is the size of the area simulated by the model in $sq/^{\circ}$; and $N_i$ is the position of star $i$ in the list e.g. if star $i$ is the $5^{th}$, $8^{th}$ or $10^{th}$ closest star, $N_i = 5, 8$ and 10 respectively.

The projected number density of stars foreground to the cluster is compared to that of each of the 5000 simulated stars. The cluster's distance, $d_{model}$, is equal to the distance of the simulated star with the same projected number density of foreground stars. For example, a cluster has $\rho_{fg}^{cl} = 10$ stars per $sq/^{\circ}$ and the simulated star with $\rho_{fg}^{model} = 10$ stars per $sq/^{\circ}$ has a distance of $d_{star} = 5\,\mathrm{kpc}$; therefore the cluster's distance is $d_{model} = 5\,\mathrm{kpc}$.

### 4.2.4 Stellar Crowding and Foreground Extinction

The density of stars foreground to a cluster is intrinsically linked to its distance. In Sect. 4.2.3 a method to infer a cluster's distance from its measured foreground star density was described. For this method to produce an accurate distance estimate, it is imperative the clusters measured foreground star density values are also accurate. Unfortunately, there are several astrophysical effects which affect the measured foreground star densities. These are described and corrected for below.

#### 4.2.4.1 Corrections to the Foreground Star Density

In principle the field star density of the Galactic model output ($\rho_{model}$) should be identical to the measured star density of a cluster's control field ($\rho_{con}$). However, in practise this is not always true.

Large scale foreground extinction (from e.g. GMCs) reduces the number of stars detected by 2MASS, which in turn reduces $\rho_{con}$. As the presence of clouds is not considered by the Galactic model (Sect. 4.2.3), the value of $\rho_{model}$ will be larger than $\rho_{con}$.

Similarly, it becomes difficult to resolve individual stars in regions which have a high projected field star density such as towards the GC, especially using lower resolution surveys such as 2MASS. This stellar 'crowding' will also cause the value of $\rho_{model}$ to be larger than $\rho_{con}$.

Both large scale foreground extinction and stellar crowding in the cluster control field can be corrected for by the factor:

$$X_1 = \frac{\rho_{model}}{\rho_{con}} \tag{4.7}$$

where $\rho_{model}$ is the field star density as predicted by the Galactic model; and $\rho_{con}$ is the measured star density in the cluster control field. Essentially Eq. 4.7 compares the measured density of field stars in the cluster control field with that predicted by the Galactic model output.

In the absence of stellar crowding, the density of field stars in the cluster area and control field should be identical. Thus further consideration of the affects of additional crowding in the cluster area is required. A correction is made with the factor:

$$X_2 = \frac{\rho_{con} \times A_{cl}}{\sum_i P^i_{field}} \tag{4.8}$$

where $P^i_{field}$ is the probability a star in the cluster area is a field star (Eq. 4.5); and $A_{cl}$ is the cluster area in $sq/^\circ$ (Eq.4.1). Essentially Eq. 4.8 compares the number density of field stars in the cluster area and the control field.

Applying these two factors, a cluster's foreground star density is re-determined as:

$$\rho^{cl,cor}_{fg} = X_1 \times X_2 \times \rho^{cl}_{fg} = \frac{\rho_{model} \times A_{cl}}{\sum_i P^i_{field}} \times \rho^{cl}_{fg} \tag{4.9}$$

where $\rho^{cl,cor}_{fg}$ is the clusters corrected foreground star density.

## 4.3 Calibration

Despite the above corrections, the inferred cluster distances are not necessarily precise. To ascertain how well the method estimates the cluster distances and make any further corrections, a comparison and subsequent analysis is needed of cluster samples inferred and literature distances.

### 4.3.1 Cluster Calibration Samples

It is necessary that the calibrating cluster sample has properties (distances, extinctions, ages) that are already known and, ideally, whose clusters are of a similar nature to the target clusters whose distances are to be determined. Additionally, it is important to accurately establish both the uncertainty on the method and to ascertain how it varies when different calibration samples are used. In principle, the value of the methods uncertainty should be higher when the calibrating cluster sample's properties have been derived heterogeneously (instead of homogeneously) as, by nature, additional scatter will be introduced (Buckner and Froebrich, 2013).

An obvious first step therefore is to determine the extent to which the choice of the calibrating cluster sample affects the uncertainty on the method. This is achieved by selecting and performing the calibration using two cluster samples: one with homogeneously, and the other with heterogeneously, derived properties. The obvious sources for the two calibration samples are the four cluster catalogues introduced in Chapter 2. Below, the merits of creating a calibration sample from each of the catalogues are discussed.

#### 4.3.1.1 Calibration Sample with Homogeneously Derived Properties

**Option 1: The FSR List Catalogue**

Although the method described by this Chapter can be used to determine distances for *any* photometric cluster sample, the original motivation behind its development was to establish distances for the FSR List catalogue (Sect. 2.4) clusters. As such, an obvious choice of calibration sample would be one which specifically includes FSR List catalogue clusters.

Froebrich et al. (2010) investigated the old (>1 Gyr) clusters of the FSR List catalogue using isochrone fitting and homogeneously derived the properties for a sub-sample of 269 objects of which 174 were open clusters, 63 globular clusters and 32 cluster candidates that were subsequently confirmed as real open clusters. Clusters from the sub-sample were selected which met the cluster requirements (Sect. 4.2.1.3).

These selections leave 115 clusters in Cluster Calibration Sample 1 (CCS 1). The majority of the sample have an age of about 1 Gyr, although a few clusters are significantly younger than this (Fig. 4.2). Most clusters have a distance of 1-4 kpc and few have a distance of more than 8 kpc (Fig. 4.3). The sample is biased towards low $A_V$ values. Figure 4.4 shows there is a

steep decline in the number of clusters with increasing $A_V$ and very few have a $A_V > 4$ mag.

**Option 2: The Milky Way Star Cluster Catalogue**

Another option for the calibration sample with homogeneously derived properties is the MWSC catalogue (Sect. 2.1). Unfortunately, when this methodology was developed in 2011 the catalogue was not yet published. There is no added value in having two homogeneous samples, and as only one is required, this option is not pursued.

#### 4.3.1.2 Calibration Sample with Heterogeneously Derived Properties

**Option 1: The WEBDA Catalogue**

The WEBDA catalogue (Sect. 2.3) is an ideal choice for the calibration sample with heterogeneously derived properties, as it contains only confirmed open clusters with high precision measurements.

To ensure that the WEBDA objects selected are of a similar nature to the FSR List catalogue clusters (i.e. CCS 1), the two catalogues were cross matched to identify WEBDA clusters which had a counterpart with the FSR List catalogue. WEBDA clusters were cross-matched and selected which met the cluster requirements (Sect. 4.2.1.3) and:

- **Had a FSR List catalogue counterpart within 7.5'**
- **Did not have two or more FSR List catalogue counterparts within 7.5'**

These selections leave 241 clusters in Cluster Calibration Sample 2 (CCS 2). The sample is biased towards younger ages and the majority of clusters are distributed between 10 Myr an a few Gyr, although a few are older than this (Fig. 4.2). The majority of clusters have a distance less than 3 kpc and few are more than 5 kpc distant (Fig. 4.3). The sample is biased towards low $A_V$ values, few clusters have a $A_V > 3$ mag (Fig. 4.4).

**Option 2: The DAML02 Catalogue**

Another option for the calibration sample with heterogeneously derived properties is the DAML02 catalogue (Sect. 2.2). DAML02 is compiled from the literature, with new clusters added as they become available. This means that, unlike WEBDA, the DAML02 catalogue includes objects with both high and low precision measurements. As it is desirable to have

a calibration sample with properties determined to similar levels of precision (to reduce the introduction of additional uncertainties), and there is no added value in having two samples with heterogeneously derived properties, it is favourable to form the second calibration sample from the WEBDA catalogue. Thus this option is not pursued.

### 4.3.2 Quantifying Calibration Accuracy

To measure how well the method estimates cluster distances, a logarithmic ratio of the estimated and literature distance for each cluster in the calibration samples is defined:

$$R = \log_{10}\left(\frac{d_{lit}}{d_{model}}\right) \tag{4.10}$$

where $R$ is the logarithmic distance ratio; $d_{lit}$ is the cluster's literature distance; and $d_{model}$ is the cluster's distance as estimated by the method. If the value of $R$ is positive the method has underestimated cluster distance. If $R$ is negative the method has overestimated cluster distance.

The uncertainty, S, is defined as the $root - mean - square$ $(rms)$ of each calibration samples distribution of $R$ values:

$$S = (10^{rms} - 1) \tag{4.11}$$

### 4.3.3 Additional Corrections

A comparison of cluster properties and the logarithmic distance ratio was made.

No correlation was found between $R$ and clusters':

- **Apparent radius**

  The method works by inferring distance from the projected number *density* $(sq/^{\circ})$ of stars foreground to the clusters i.e. is independent of clusters' apparent size and radius. Thus, as expected, there is no correlation between cluster apparent radius and $R$.

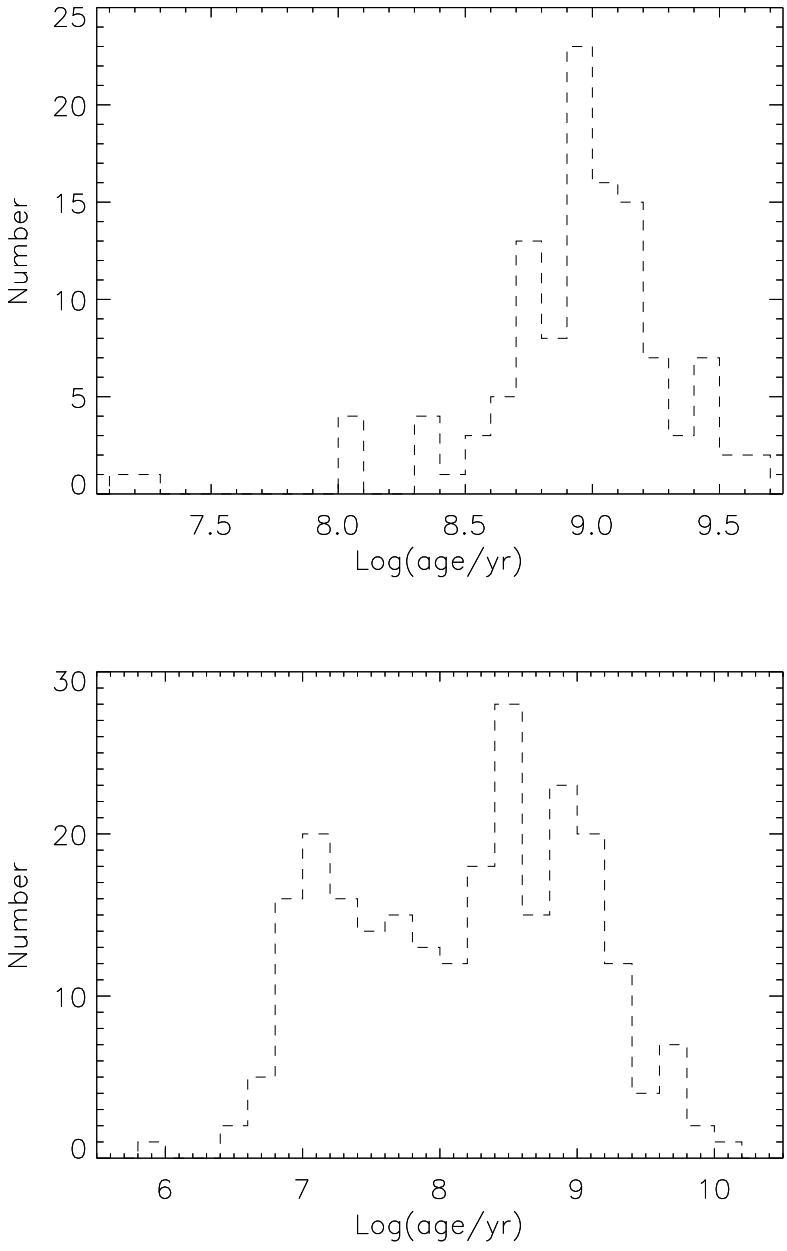


Figure 4.2: Histograms of the age distributions of (*Top*) CCS 1; and (*Bottom*) CCS 2.

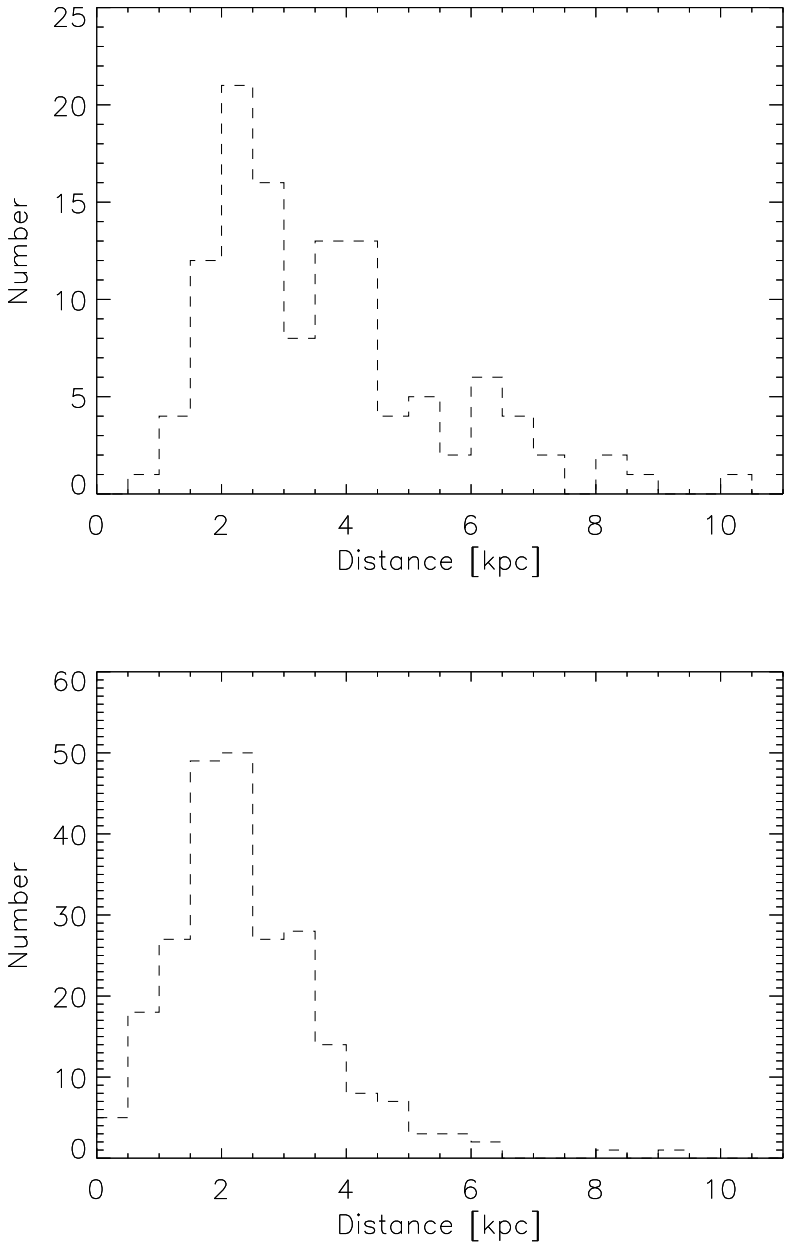


Figure 4.3: Histograms of the distance distributions of (*Top*) CCS 1; and (*Bottom*) CCS 2.

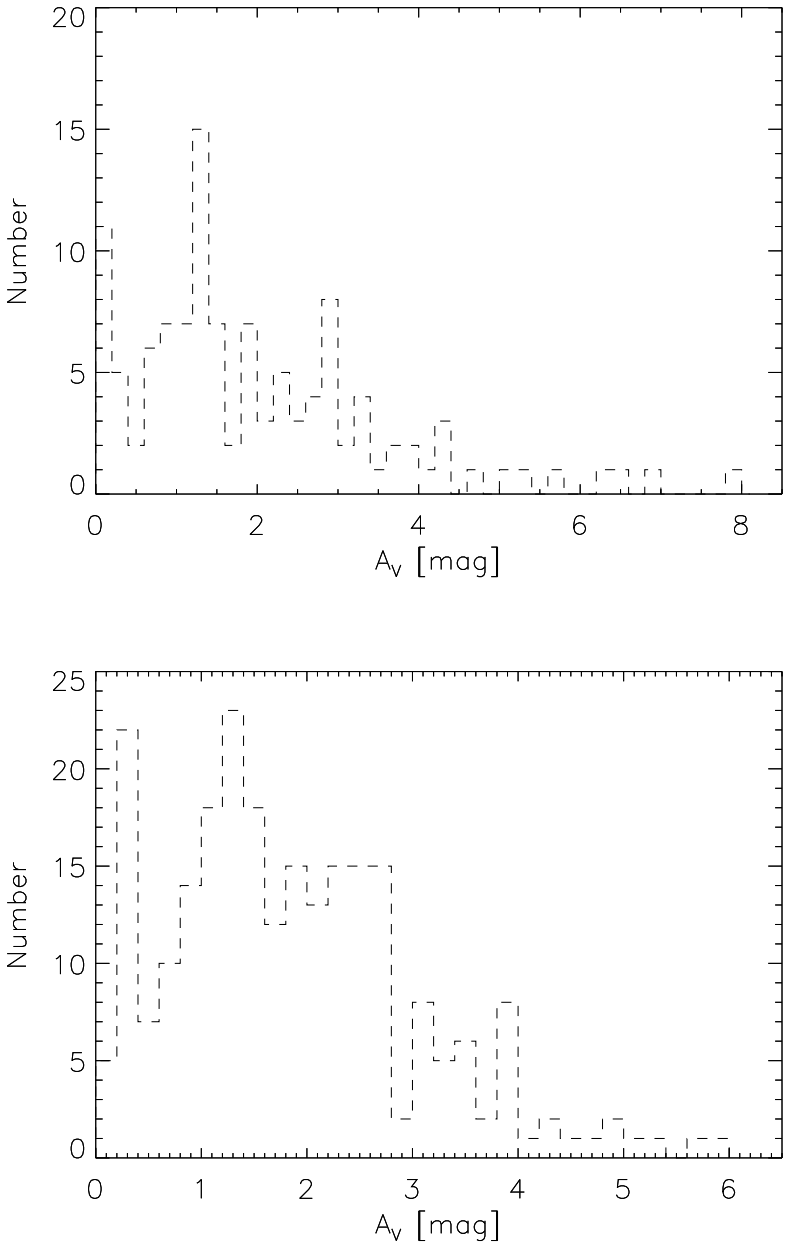


Figure 4.4: Histogram of the V-band extinction ($A_V$) distributions of (*Top*) CCS 1; and (*Bottom*) CCS 2.

- **Reddening**

  The effects of large scale foreground extinction on the measured projected number density of stars foreground to the clusters is corrected for in Sect. 4.2.4. Thus, any dependence between the cluster reddening and $R$ has been removed.

- **Galactic latitude**

  The method assumes that the density of field stars in any given line of sight is constant per unit distance, hence the projected number density of stars that are foreground to a cluster is proportional to the cluster's distance. At high Galactic latitudes (e.g. $|b| = 90°$) it is reasonable to expect the density of field stars per unit distance to not be statistically constant and to decrease with increasing distance from the GP. However, as clusters' projected foreground star number densities are corrected through a comparison to simulated star densities at the same position (Eq. 4.7 and 4.9), the accuracy of clusters' inferred distances is not dependant on Galactic latitude.

#### 4.3.3.1 Position Dependent Correction

A prominent correlation was found between $R$ and clusters' Galactic longitude. Figure 4.5 and 4.6 clearly show cluster distances are underestimated towards the Galactic Anticentre, and overestimated towards the GC. This is caused by an incorrect assumption in the extinction law of the model, where a mean diffuse absorption value of 0.7 mag/kpc for all cluster positions was adopted (Sect. 4.2.3). Joshi (2005) showed that the value of interstellar absorption is not constant and varies with Galactic longitude i.e. the mean value adopted in the model is too high towards the Galactic Anticentre and too low towards the GC. Unfortunately, the findings of Joshi (2005) require further investigation and refinement (Chapter 1), so it was necessary to adopt the mean absorption value. The variation of interstellar absorption with Galactic longitude is analysed in Chapter 9, and the impact of those results on the correlation between $R$ and cluster Galactic longitude are discussed in Sect. 9.4.

The correlation between $R$ and cluster Galactic longitude can be fitted with a $3^{rd}$ order polynomial of the form:

$$R = C_1 + C_2 \times |l - 180°| + C_3 \times |l - 180°|^2 + C_4 \times |l - 180°|^3 \tag{4.12}$$

where $l$ is cluster Galactic longitude; $R$ is the logarithmic distance ratio; and $C_{1-4}$ are

constants. The term $|l - 180°|$ ensures that the polynomial is symmetric at $l = 0°$ and $l = 360°$ (i.e. $R(0) \equiv R(360)$). The polynomial regression uses $3\sigma$ clipping to remove obvious outliers. Letting $L = |l - 180°|$, Eq.4.12 is simplified to:

$$R = C_1 + C_2 \times L + C_3 \times L^2 + C_4 \times L^3 \tag{4.13}$$

The method distance, $d_{model}$, is calibrated by rearranging Eq.4.13, such that:

$$d_{cal} = d_{model} \times 10^{C_1 + C_2 \times L + C_3 \times L^2 + C_4 \times L^3} \tag{4.14}$$

where $d_{cal}$ is the position calibrated method distances.

## 4.4 Uncertainty and Optimisation

### 4.4.1 Measuring Uncertainty

To quantify the accuracy of the calibrations procedure (Sect. 4.3), the logarithmic distance ratio is redefined for each cluster in the calibration samples as:

$$R_{cal} = \log_{10}\left(\frac{d_{lit}}{d_{cal}}\right) \tag{4.15}$$

where $R_{cal}$ is the calibrated logarithmic distance ratio; $d_{lit}$ is cluster's literature distance; and $d_{cal}$ is cluster's calibrated distance estimate.

The uncertainty, $S_{cal}$, of the method is defined as the $rms$ of each calibration samples distribution of $R_{cal}$ values:

$$S_{cal} = (10^{rms} - 1) \tag{4.16}$$

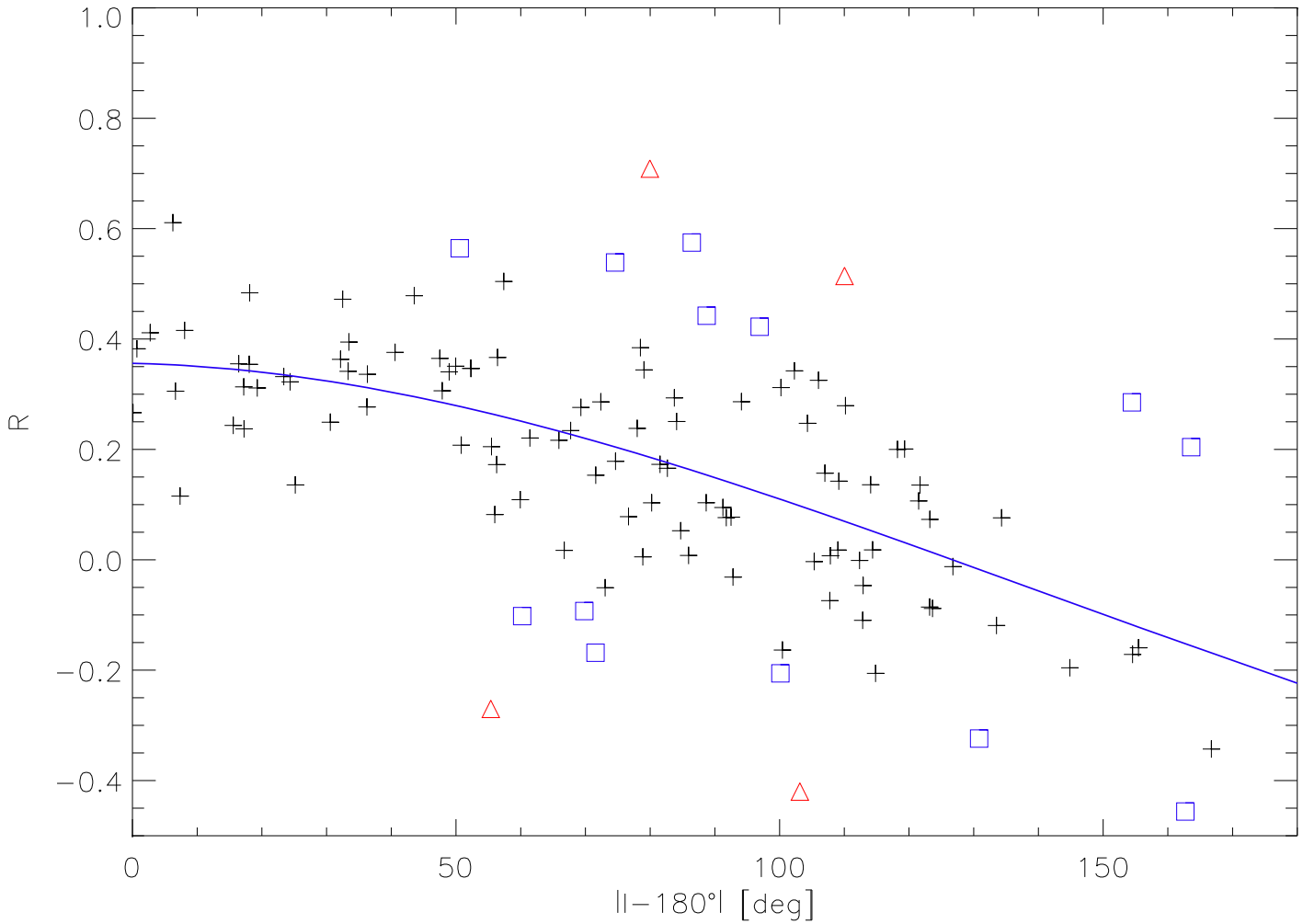


Figure 4.5: Plot of $R$ against $|l - 180°|$ for the A-sample CCS 1 objects with a cluster radius of $1 \times r_{cor}$. The solid blue line represents the $3^{rd}$ order polynomial fit with $2\sigma$ clipping. Black crosses represent clusters that were included in the fit. Blue squares represent clusters that were excluded at the $2\sigma$ level. Red triangles represent clusters excluded at the $3\sigma$ level. Cluster members were identified using the PDT and a Nearest Neighbour number of $N = 25$.

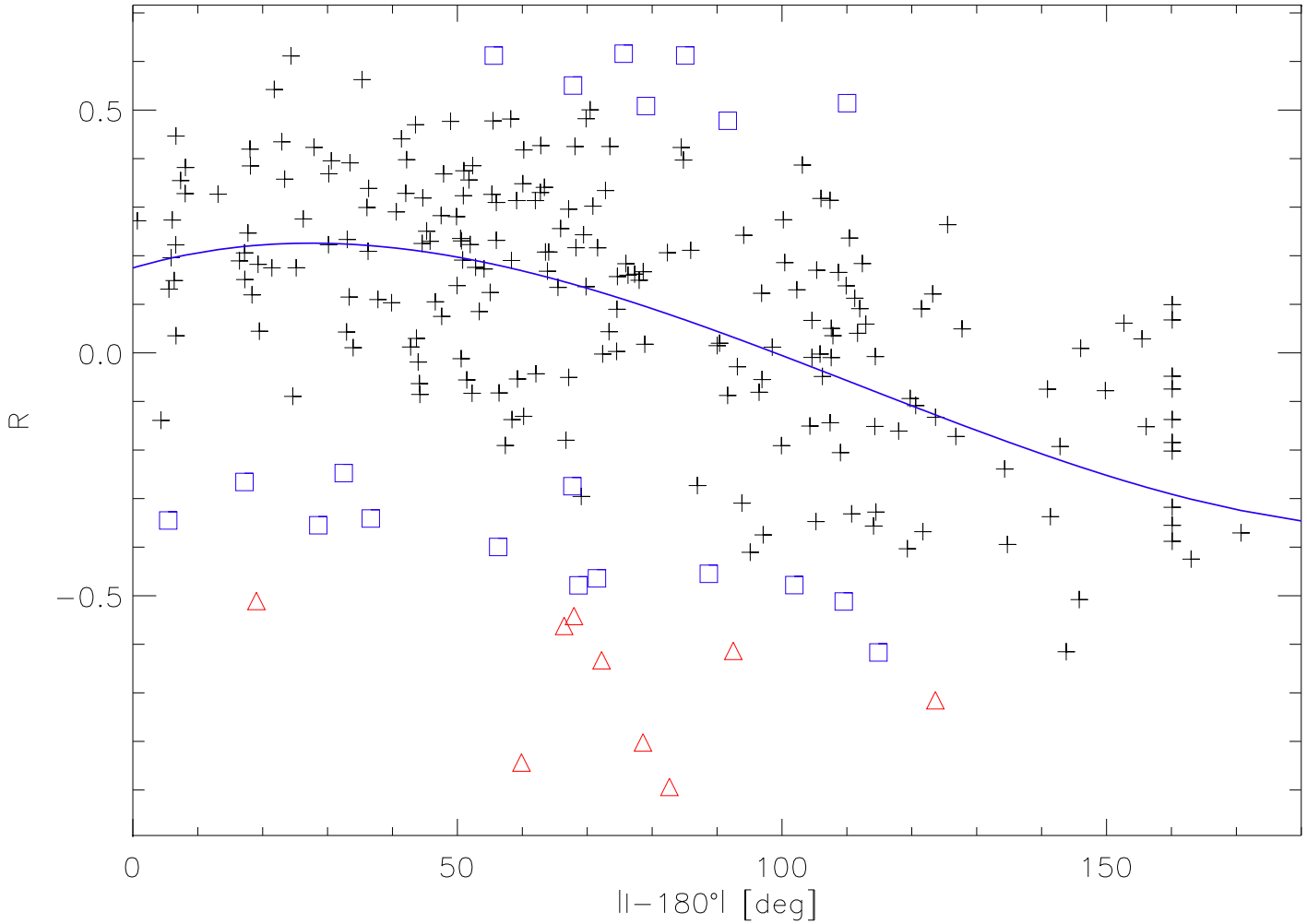


Figure 4.6: Plot of $R$ against $|l - 180°|$ for the A-sample CCS 2 objects with a cluster radius of $1 \times r_{cor}$. The solid blue line represents the $3^{rd}$ order polynomial fit with $2\sigma$ clipping. Black crosses represent clusters that were included in the fit. Blue squares represent clusters that were excluded at the $2\sigma$ level. Red triangles represent clusters excluded at the $3\sigma$ level. Cluster members were identified using the PDT and a Nearest Neighbour number of $N = 25$.

Table 4.1: Gives the method uncertainty, $S_{cal}$, for the best four sets of free variable value combinations. All calculations are done with the A-sample of stars. *Radius* represents the radius of the cluster area, and $N$ the Nearest Neighbour number used in the PDT. Note, CCS 1 has an intrinsic scatter of 30 %.

| | $N$ | *Radius* $[r_{cor}]$ | $S_{cal}$ (CCS 1) [%] | $S_{cal}$ (CCS 2) [%] |
|---|---|---|---|---|
| **Set 1** | 15 | 1 | 36 | 54 |
| **Set 2** | 25 | 1 | 37 | 50 |
| **Set 3** | 15 | 2 | 40 | 55 |
| **Set 4** | 25 | 2 | 46 | 56 |

### 4.4.2 Optimisation

The method employs a number of free variables and as a result the uncertainty on the distance estimates are dependant on the variable values. It is desirable, therefore, to identify the combination of variable values which result in the smallest uncertainty on the distance estimates. Here, the effect of each free variable is discussed and the optimum value combination selected. Table 4.1 provides a summary for the readers reference.

#### 4.4.2.1 Cluster Area

The cluster area was defined in Sect. 4.2.1.2 as a circular area around the centre of a cluster which encompasses all stars within a multiple of the cluster's core radius, either 1, 2 or 3 $\times$ $r_{cor}$. Clusters' core radii are determined using star density profiles i.e. the majority of cluster members will be concentrated within 1 $\times$ $r_{cor}$. Additional stars between 1 and 2 $\times$ $r_{cor}$ will mostly be cluster members with some field stars. Enlarging the cluster area from 2 to 3 $\times$ $r_{cor}$ will increase the number of field stars in the cluster area as additional stars will be field stars with few cluster members.

Testing showed that the size of the cluster area did not significantly affect the method uncertainty. This is because members and stars foreground to clusters were identified using their stellar colours alone. Therefore, as spatial positions are ignored, the additional field stars between 2 and 3 $\times$ $r_{cor}$ will not change the number density of stars identified as foreground to the cluster i.e. distance estimates are independent of the size of the cluster area. However, as the majority of the additional stars between 2 and 3 $\times$ $r_{cor}$ belong to the field, only 1 $\times$ $r_{cor}$

and $2 \times r_{cor}$ will be used in the distance calculation and calibration.

#### 4.4.2.2 Photometric Decontamination

Cluster members were identified from their stellar colours alone using the PDT as described by Chapter 3. The technique assigns a MPI to each star in the cluster area by measuring its distance from its $N^{th}$ nearest neighbours in CCM space. Bonatto and Bica (2007b) and Froebrich et al. (2010) used a Nearest Neighbour number of $N = 10$, but it had not been formally established in the literature whether the choice of $N$ affected the accuracy of membership identification. It is important to identify any correlation or trend between the value of $N$ and the MPI values, as this would cause a discrepancy in the measurements of the density of stars foreground a cluster (and thus conflicting distance estimates) for different values of $N$.

Essentially, the value of $N$ defines the resolution in CCM space at which potential cluster members can be separated from field stars and the S : N ratio of stars assigned MPI values. Increasing the value of $N$ decreases the resolution and increases the S : N ratio. Decreasing the value of $N$ increases the resolution, and decreases the S : N ratio. Therefore as $N$ has no influence on the stellar colours on it is expected that its value would not affect the MPIs. Testing confirmed that there is no correlation between value of $N$ (in the range $10 \leq N \leq 30$) and the method uncertainty i.e. the cluster distance estimates. However, the uncertainty does randomly fluctuate by a few percent at the edges of the parameter space ($N = 10, 30$), but this is negligible in comparison to the variations caused by the other free variables. Nevertheless, to avoid these random fluctuations two values of $N$ are chosen ($N = 15$ and $N = 25$) for the distance calculation and calibration.

The reader should note that the typical number of stars in the CCS 1 and CCS 2 cluster areas is between 100 to 300, and as a result the resolution only varies by a factor of $\sim 1.5$ over the range of $N$ values tested. If there were typically a large number of stars in the cluster area (e.g. 5000), it is expected that the uncertainty of the method would vary with the value of $N$. In this case, further testing would be needed to establish the exact nature of the correlation between the value of $N$ and the uncertainty.

#### 4.4.2.3 Cluster Calibration Samples

It is important to establish how the uncertainty on the distance estimates varies with the mean age of the calibration samples.

CCS 2 is divided into two sub-samples:

- $CCS\,2_o$ – The 'old' sub-sample comprising of clusters with an age of $log(age/yr) > 8.5$
- $CCS\,2_y$ – The 'young' sub-sample comprising of clusters with an age of $log(age/yr) < 8.5$

It was found that the uncertainty on the distance estimates produced by $CCS\,2_y$ was significantly higher than for $CCS\,2_o$. The uncertainty on the distance estimates produced by $CCS\,2_o$ did not differ with any statistical significance from that of the full CCS 2 sample. A possible explanation is that young clusters typically contain a higher fraction of K-band excess objects (e.g. YSOs), which will redden their median $[H-K]$ colour, $HK_{med}$. Furthermore, a large proportion of members in young clusters associated with clouds may fall below the 2MASS detection limit and thus the colours of the members used to measure $HK_{med}$ may not be typically representative of the cluster. As the method identifies foreground stars as those which are 'bluer' than the clusters measured $HK_{med}$, young clusters distance estimates are prone to inaccuracy.

Therefore the lowest uncertainty is achieved for calibration samples which comprise of either old clusters or have a large age range. Distances obtained for samples containing a large proportion of young clusters should be treated with care. Unfortunately, as CCS 1 is comprised primarily of older clusters ($log(age/yr) > 8.5$), it is not possible to compare how the uncertainty varies with the mean age of calibration samples that have homogeneously and heterogeneously derived properties. However, from the results of Table 4.1 it is reasonable to expect that a young sample with homogeneously derived properties would produce a higher uncertainty than an old sample with homogeneously derived properties, but a lower uncertainty than a young sample with heterogeneously derived properties.

#### 4.4.2.4 Photometric Samples

Distances were determined for the A-sample and C-sample of each calibration sample (see Sect. 4.2.1.1). For CCS 1 the A-sample produced a significantly lower uncertainty on the

distance estimates than the C-sample, the exact value of which was dependant on the combination of the other free variable values. For CCS 2 there was no statistically significant difference between the A- and C-sample for all combinations of free variable values. This could be because the literature distances of CCS 2 were determined by many different authors using various techniques, whereas the literature distances of CCS 1 were determined by a single author and technique. As such, it is reasonable to expect that the intrinsic scatter of the CCS 2 literature distances is significantly higher than that of CCS 1 (which is 30 %) and is large enough to cause there to be no significant difference in the uncertainty produced by the A- and C-sample of CCS 2.

In summary, the uncertainty is affected by the quality of the photometry for calibration samples with homogeneously derived properties, but not for calibration samples with heterogeneously derived properties. Therefore it is optimal to use only use the A-sample for all calibration samples (regardless of how their properties were derived).

#### 4.4.2.5 Galactic Model

Cluster distances are estimated through a comparison of their foreground star density to the field star density simulated by a Galactic model at the same coordinates (Sect. 4.2.3). Corrections are then made to clusters' foreground star and control field densities by comparing them to the models of field star density (Sect. 4.2.4).

Uncalibrated cluster distance estimates will vary between Galactic models due to systematic differences in the models field star densities. However, the calibrated cluster distance estimates are independent of the specific Galactic model used. This is demonstrated through a comparison of cluster distances obtained for CCS 1 from the (i) BGM and (ii) TRILEGAL (Girardi et al., 2012) Galactic models. Figure 4.7 shows that there is a clear linear correlation i.e. TRILEGAL distances are systematically a factor of $\approx 1.3$ larger than those given by the BGM, with a scatter of $\sim 5.5\,\%$ (much less than the optimised uncertainty − see Table 4.1). Thus, the BGM and TRILEGAL distance estimates for CCS 1 show the same polynomial correlation between $R$ and Galactic longitude. Therefore the calibration of Sect. 4.3.3.1 will remove the difference in the distances for CCS 1 given by the two models, albeit with a sightly different value for the $C_1$ parameter in Eq. 4.12. Since every other model will behave in a similar way, the calibration procedure removes any systematic dependence on the specific Galactic model used.

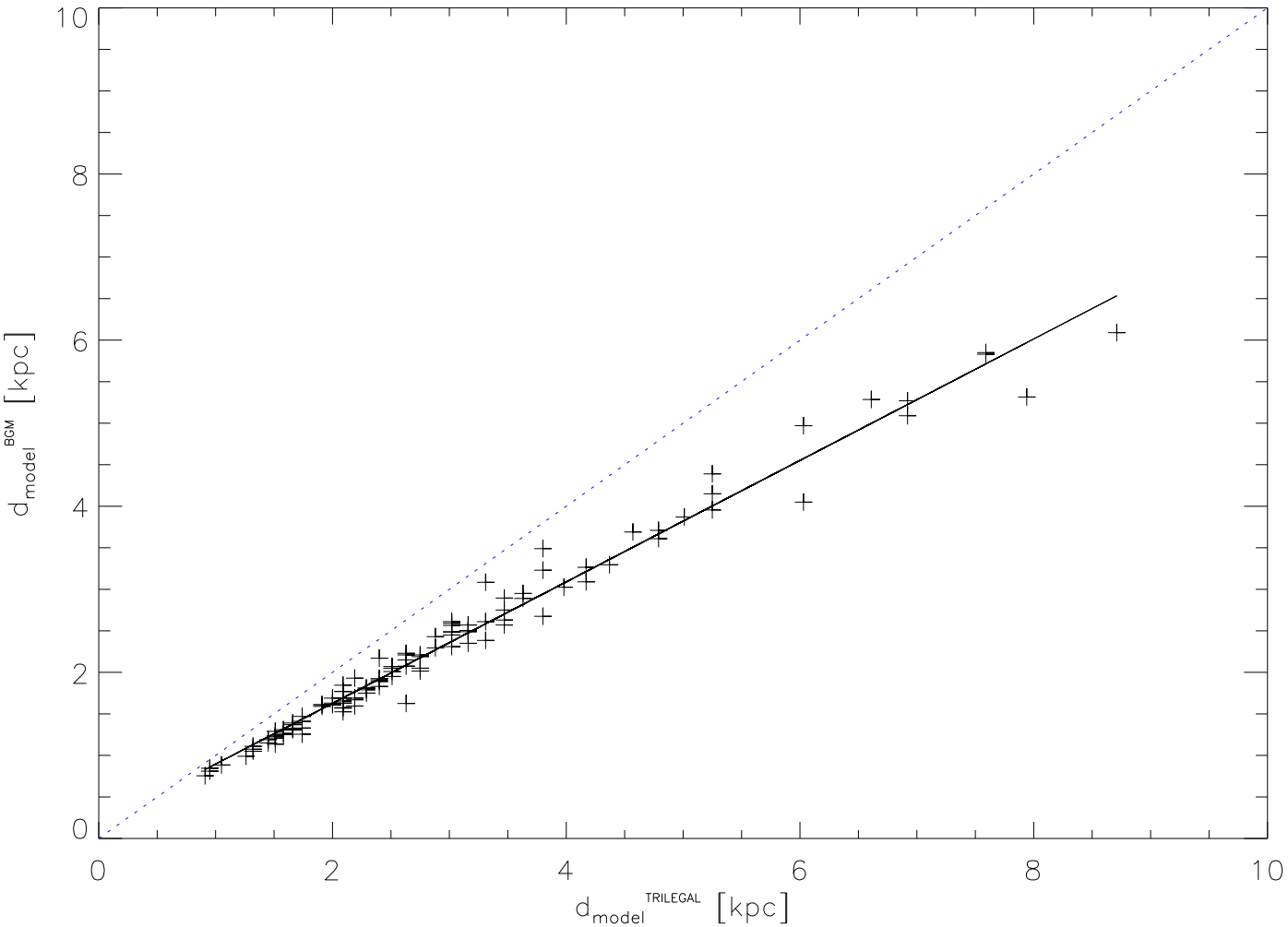


Figure 4.7: Plot shows the comparison of distances obtained for the A-sample CCS 1 objects with a cluster radius of $1 \times r_{cor}$ from the Besançon Galaxy Model and the TRILEGAL Galactic model. Cluster members were identified using the PDT and a Nearest Neighbour number of $N = 25$. Black crosses represent clusters. The solid black line is linear fitted to the data, with a gradient of 1.3 and scatter of 5.5 %. The dotted blue line represents a 1:1 relationship.

### 4.4.3 Method Uncertainty

To summarise, the smallest uncertainty on the distance estimates given by the method is achieved with the A-sample of a calibration sample whose properties have been homogeneously derived. The radius of the cluster area and Nearest Neighbour number in the PDT has no significant influence on the uncertainty. Table 4.1 gives the optimised uncertainty on the distance estimates, as achieved from the best four free variable value combinations.

### 4.4.4 Final Distance Estimate

The final distance for a cluster is determined as the median calibrated distance estimate, $d_{cal}$, obtained from variable Sets 1-4 defined in Table 4.1. Cluster distances are most accurately measured when a sample with homogeneously derived properties is used to calibrate the method. Distances can be determined with a better than 40 % accuracy when calibrated with a sample which has an intrinsic scatter of 30 %.

## 4.5 Potential Improvements

The method to obtain distance estimates for clusters presented in this Chapter has been calibrated and optimised to achieve the highest possible accuracy. To this end, the best combination of free variable values were selected and corrections were made for the effects of stellar crowding, large scale foreground extinction and cluster position. All possible variable selections and corrections which could improve the accuracy of the distance estimates have been considered.

However, there are potentially two ways to further improve accuracy. Firstly, if deeper (than 2MASS) photometry was available for all objects in the calibration samples, faint cluster members that are undetected by 2MASS would be included. These additional members would increase the accuracy of clusters' measured median colour. Subsequently, the accuracy of clusters' foreground star counts (and thus distance estimates) would be increased.

Secondly, if the intrinsic scatter of the calibration samples was lower, there would be a reduction on the uncertainty of the distance estimates i.e. CCS 1 has an intrinsic scatter of 30 % (Froebrich et al., 2010), but with which cluster distances can be estimated with a better than 40 % accuracy. This was demonstrated by Ioannidis and Froebrich (2012) who

determined the distance to dark clouds with jets and outflows using a similar approach, which once calibrated gave an uncertainty for the distances that resembled the intrinsic scatter of their calibration sample. Realistically, it is much simpler to identify stars which are foreground to dark clouds than those which are foreground to clusters and therefore the uncertainty on the cluster distance estimates will be higher than the intrinsic scatter of the calibration sample. However, it is reasonable to expect that a lower uncertainty on the cluster distance estimates would be achieved if the calibration sample had a lower intrinsic scatter.

## 4.6 Summary

This Chapter has presented a method to estimate cluster distances from photometric data alone. The founding principle of the method is the assumption that stars in the Galaxy have smooth radial distribution, so that the projected number of stars foreground to a cluster in the GP is proportional to its distance.

To begin, members of a cluster were distinguished from field stars in the cluster area using the Photometric Decontamination Technique described in Chapter 3. All stars in the cluster area that were bluer than the measured median colour of the cluster were identified as foreground. Next, the density of stars foreground to the cluster was calculated and compared to a Galactic model to infer the cluster's distance. It was shown that the method is independent of specific Galactic model used.

The method was calibrated with two samples of clusters with known distances. The first was a selection of 206 FSR List catalogue clusters whose distances were homogeneously derived by Froebrich et al. (2010) from fitting modelled cluster sequence isochrones to their CCM diagrams. The second was a selection of 241 clusters from the WEBDA catalogue, whose distances were determined by various authors and methods (i.e. are heterogeneous by nature). It was shown that the method overestimated cluster distances towards the GC and underestimated towards the Anticentre. After corrections for stellar crowding, large scale foreground extinction and Galactic position were made, it was shown that the method estimates clusters distances with a better than 40 % accuracy when calibrated with a cluster sample which has an intrinsic scatter of 30 %.

# Chapter 5

# Extinction Determination

It is essential that the fundamental properties of clusters (such as extinction) are determined homogeneously and accurately. Individually, cluster properties can be indicative of certain physical properties. For example, a high extinction value can indicate a cluster is very young (i.e. still strongly associated with dust and gas), is at a large distance, in the line of sight of a GMC, or some combination of all three. Collectively, clusters are a useful tool for investigating Galactic structure. For example, cluster samples' extinction and distance values can be used to investigate how interstellar absorption varies as a function of Galactic longitude.

This Chapter presents a method to homogeneously derive extinction estimates for cluster samples for which only photometry is available, independent of their other fundamental properties (distance, age, metallicity).

## 5.1 Current Limitations

In the absence of spectrometry, cluster extinctions are normally derived by fitting modelled cluster sequence isochrones to their CCM diagrams (e.g. Ann et al. (2002), Carraro et al. (2007), Bonatto and Bica (2007a), Bonatto et al. (2010), Froebrich et al. (2010), Kharchenko et al. (2012), Güneş et al. (2012) etc.). However, as previously discussed, the values of cluster properties derived from isochrone fitting are subjective to individuals' interpretations of a cluster's CCM diagrams and thus many discrepancies in the literature exist. For example, in the literature there are discrepancies for FSR0828 and FSR1716 of $\Delta A_H = 0.54$ mag and

0.37 mag respectively (Koposov et al. (2008), Kharchenko et al. (2013), Bonatto and Bica (2008b), Froebrich et al. (2010)).

An apparent good alternative to isochrone fitting are 3-D extinction maps, as they give the total extinction in the cluster's line of sight which can then be scaled by a factor of $1-e^{d\,sin|b|/h_0}$ to derive its extinction, where $d$ and $b$ are the distance and latitude of the cluster respectively and $h_0$ is the dust scale height (e.g. Akkaya et al. (2010), Clem et al. (2011)). However, cluster extinctions derived in this way are, again, not independent of clusters' other fundamental properties, i.e. the method is reliant on (accurately) knowing a cluster's distance to (accurately) derive its extinction. Furthermore, there are well-documented problems associated with extinction maps. For example, the most used extinction maps in the literature are, arguably, by Schlegel et al. (1998) which have been shown to be inaccurate in high extinction regions. These maps were calibrated from the measured $\langle\, B-V \,\rangle$ colour excess of elliptical galaxies which typically had a low reddening value ($\langle\, B-V \,\rangle\, < 0.1$ mag), and consequently there was an inaccurate conversion between dust column and reddening for Galactic regions with $A_V > 0.5$ mag (Arce and Goodman, 1999). Another example are the maps by Dobashi et al. (2005) which were developed using a star counting technique. Unfortunately, due to the technique's low resolution and limit ($A_V < 5$ mag), these maps fail to detect small scale structure and trace high extinction regions. For a full discussion of the above map sets see e.g. Schlegel et al. (1998), Arce and Goodman (1999), Dobashi et al. (2005) and Rowles and Froebrich (2009).

It is ideal therefore to employ a method to derive cluster extinction values homogeneously, without the use of isochrone fitting or extinction maps, which is independent of a cluster's distance and age.

## 5.2 Derivation of Cluster Extinction

### 5.2.1 Colour Excess Measurement

In principle, any colour excess can be used to determine cluster extinction (e.g. $\langle J-K \rangle$, $\langle H-K \rangle$ etc.). Ideally a colour excess should be chosen that has little to no change over stellar spectral types and luminosities, such that any cluster reddening can be attributed to interstellar extinction. It is also desirable that two (or more) colour excesses are utilised so that the derived extinction values can be verified against each other, and the reliability of

the method evaluated. Furthermore, it is advantageous to choose colour excesses for which an extinction can be derived in the same band (e.g. $A_H$), i.e. the extinctions can be directly compared without the need for conversion to a different magnitude band.

For these reasons the two colour excesses chosen for this method are:

- $\langle H - 4.5 \rangle$

  The preferred choice as it has a well defined zero point because it measures the slope of the spectral energy distribution in the Rayleigh-Jeans part of the spectrum. Thus the colour is almost independent of spectral type and/or luminosity class (Majewski et al., 2011). Unfortunately, the 4.5$\mu$m band magnitude is not available in the 2MASS catalogue, so photometry in this magnitude has to be drawn from the WISE catalogue (which has a lower spatial resolution). A cross-comparison of WISE point sources and the highest quality 2MASS point sources (Qflag "AAA") shows that only $\sim$ 50 % of 2MASS point sources have a counterpart in WISE. Essentially, WISE detects only the brightest (reddest) 2MASS point sources. Therefore, clusters' $\langle H - 4.5 \rangle$ values will be measured from their reddest members, i.e. their derived extinctions will be redder than the true value.

- $\langle H - K \rangle$

  The less desirable choice as this colour intrinsically depends on stellar spectral type and luminosity class, varying between $0.0 < [H - K] < 0.4$ mag for A-type stars to the latest spectral types (excluding L, T and Y dwarfs, Koornneef (1983)). However, a clear advantage of using this colour (instead of $[H - 4.5]$) is that its value can be derived from twice as many cluster members, as both the $H-$ and $K-$ band photometry is available from 2MASS.

### 5.2.2 Median Colour Measurement

Clusters' median $[H-4.5]$ colour, $H45_{med}$, and median $[H-K]$ colour, $HK_{med}$, are measured using the method outlined in Sect. 4.2.2.1.

### 5.2.3 Extinction Calculation

The $H-$band extinction of a cluster is derived from $H45_{med}$ using:

$$A_H^{H45} = \frac{A_H}{A_H - A_{45}} \times \langle H - 4.5 \rangle \tag{5.1}$$

where $A_H$ and $A_{45}$ are the $H-$ and 4.5$\mu$m band extinction respectively, and $\langle H - 4.5 \rangle$ is the colour excess defined as:

$$\langle H - 4.5 \rangle = H45_{med} - [H - 4.5]_0 \tag{5.2}$$

where $[H - 4.5]_0$ is the $[H - 4.5]$ zero point, and

$$\frac{A_{45}}{A_H} = 0.28 \quad \text{(Indebetouw et al., 2005)} \tag{5.3}$$

For MS stars (expected to form the majority of cluster members) $[H - 4.5]_0 = 0.03\,\text{mag}$ (Majewski et al., 2011).

The $H-$band extinction of a cluster is derived from $HK_{med}$ using:

$$A_H^{HK} = \frac{A_H}{A_H - A_K} \times \langle H - K \rangle \tag{5.4}$$

where $A_H$ and $A_K$ are the $H-$ and $K-$ band extinction respectively, and

$$\langle H - K \rangle = HK_{med} - [H - K]_0 \tag{5.5}$$

where $[H - K]_0$ is the $[H - K]$ zero point, and

$$\frac{A_K}{A_H} = 0.65 \quad \text{(Indebetouw et al., 2005)} \tag{5.6}$$

The value for $[H - K]_0$ is determined in Sect. 5.2.4.

### 5.2.4 Measuring $[H-K]_0$

The $[H-K]$ colour intrinsically depends on stellar spectral type and luminosity class, typically ranging between $0.0 - 0.4$ mag from early to late type stars (Koornneef, 1983). As such its zero point does not have a well defined value in the literature.

Using the above methodology, the $A_H^{H45}$ and $HK_{med}$ value of each cluster in the FSR List catalogue was determined, provided that the cluster:

- **Is not a globular cluster**

  As this method is designed to derive extinctions for open clusters only.

- **Has 30 or more stars with 2MASS Qflag "AAA" within one core radius**

  A cluster is defined as having *at least* 30 stars within one core radius.

- **Has 30 or more stars with 2MASS Qflag "AAA" in the control field**

  The control and cluster areas must have same minimum star count to identify cluster members (Chapter 3).

- **Has a core radius smaller than 0.05°**

  To ensure that the control field consists only of field stars, as 2MASS photometry has been extracted for a circular 0.5° area around the centre of the cluster.

In total, extinction estimates were derived for 775 clusters. The clusters' YSO fractions were calculated (Sect. 5.3) and those with a high YSO fraction ($> 10\,\%$) were removed, as the $K$-band excess produced by these objects will affect the accuracy of their measured $HK_{med}$ values and hence $[H-K]_0$. Clusters' with a high extinction value ($A_H^{H45} > 1$ mag) were also removed. These selections leave 601 clusters in the sample.

To establish the zero point, a plot of $A_H^{H45}$ and $HK_{med}$ was made for the sample (Fig. 5.1) which shows a good linear relationship between $A_H^{H45}$ and $HK_{med}$. A linear regression was made of the form:

$$HK_{med} = m \cdot A_H^{H45} + [H-K]_0 \tag{5.7}$$

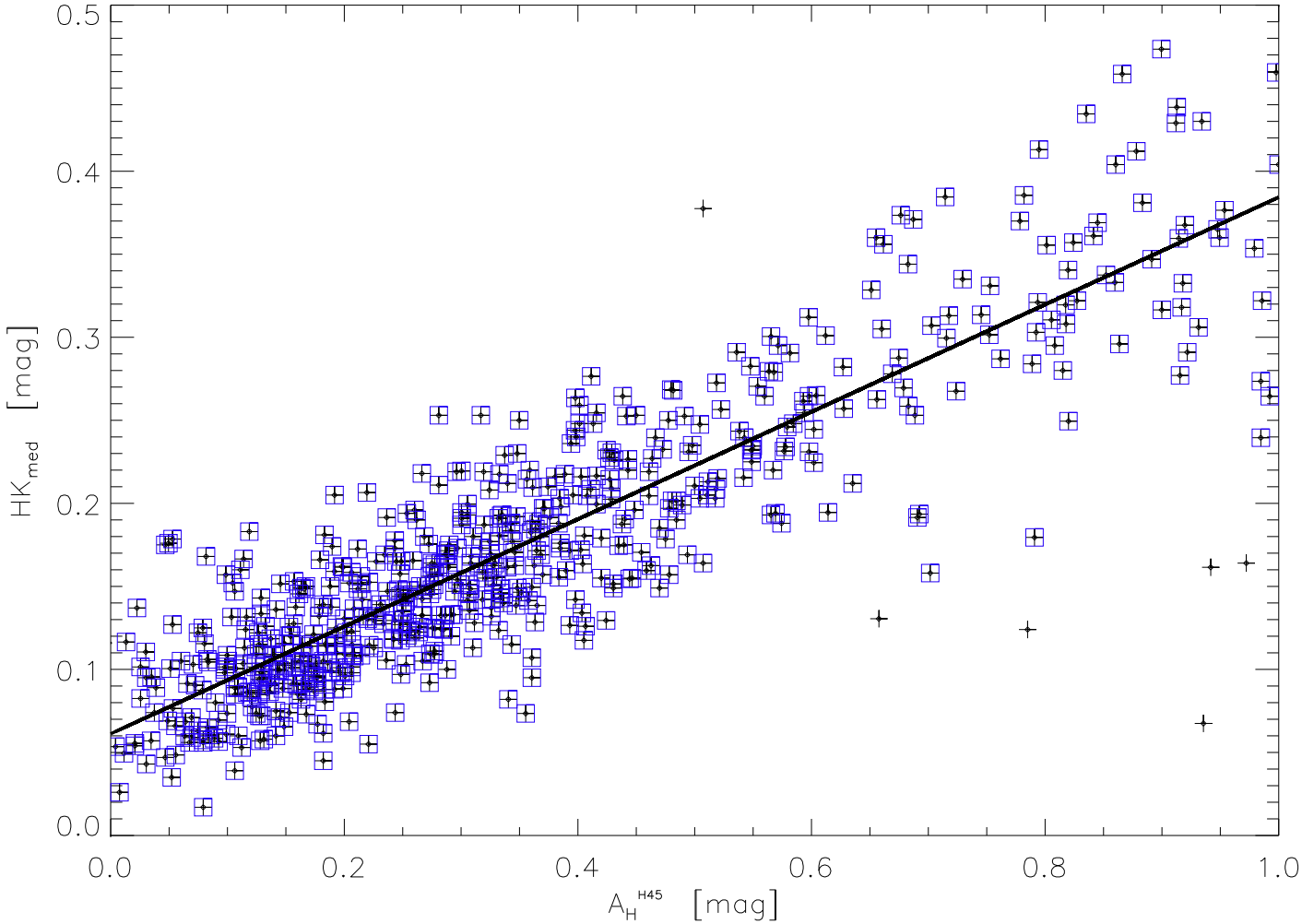


Figure 5.1: Plot of the $H-$band extinction determined from $H45_{med}$ ($A_H^{H45}$) against $HK_{med}$ for the sample (see text for details). Black crosses represent clusters. Clusters with a high YSO fraction ($> 10\,\%$) and/or have a high extinction value ($A_H^{H45} > 1\,\mathrm{mag}$) have been removed. The solid line has been linearly fitted to the data at the $3\sigma$ level, clusters included in the fit are marked with blue squares.

where the values of the gradient, $m$, and intercept, $[H-K]_0$, of the linear fit were measured to be:

$$m = 0.32 \tag{5.8}$$

and

$$[H-K]_0 = 0.06 \text{ mag} \tag{5.9}$$

## 5.3 Identification of Young Stellar Objects

Young Stellar Objects (YSOs) are an important aspect of cluster evolution and can serve as an age indicator. Young and embedded clusters contain a high fraction of YSOs as the majority of their low and intermediate mass stars have not had sufficient time to evolve onto the MS. In contrast, older clusters contain a very low to zero fraction of YSOs, as their low and intermediate mass stars have had sufficient time to evolve onto the MS and beyond.

YSOs have a $K$-band excess caused by warm dust in their disks (e.g Greene and Young (1992), Kaas (1999)). It is important to identify clusters with a high fraction of YSOs, as their $K-$band excess can affect the cluster's measured $HK_{med}$ and thus derived extinction value. If a sample contains embedded clusters, these should be removed from further analyses, such as e.g. investigating the variation of interstellar absorption with Galactic longitude. Any remaining clusters which are identified as having a large fraction of YSOs should then be removed also. Note, the FSR List catalogue contains no embedded clusters.

### 5.3.1 Reddening Limit

To determine a cluster's YSO fraction, the reddening limit is defined as:

$$Q = JH - (X \cdot HK) \tag{5.10}$$

where

$$\begin{aligned} JH &= [J-H] \\ HK &= [H-K] \end{aligned} \tag{5.11}$$

and

$$X = \frac{\langle J-H \rangle}{\langle H-K \rangle} = 1.55 \quad \text{(Mathis, 1990)} \tag{5.12}$$

where $Q$ is the reddening limit of the cluster; J, H and K are the observed 2MASS magnitudes with $\langle J-H \rangle$ and $\langle H-K \rangle$ representative of their respective colour excesses. A value of $Q \leq -0.05$ mag (by more than $1\sigma$, estimated from the photometric uncertainties) denotes a YSO.

The $Q$ parameter is calculated for each of the top 25 %, 30 %, 35 %, 40 % and 45 % of high probability member stars in the cluster, i.e. five sets of $Q$ values are generated for a cluster as demonstrated in Figure 5.2.

### 5.3.2 YSO Fraction

In principle the fraction of YSOs in a cluster, $Y_{frac}$, is the ratio of the number of identified YSOs and the total number of cluster members. For intrinsically red clusters (e.g. where the foreground extinction is high), the accuracy of $Y_{frac}$ will be diminished as these conditions affect the determined YSO reddening limit for a cluster, i.e. the $Q$ parameter. To compensate for this, $Y_{frac}$, is defined as:

$$Y_{frac} = \frac{N_{YSO} - \sqrt{N_{YSO}}}{N_{cl}} \tag{5.13}$$

where $N_{cl}$ is the number of cluster members,

$$N_{cl} = \sum^{N} P_{cl}^{i} \tag{5.14}$$

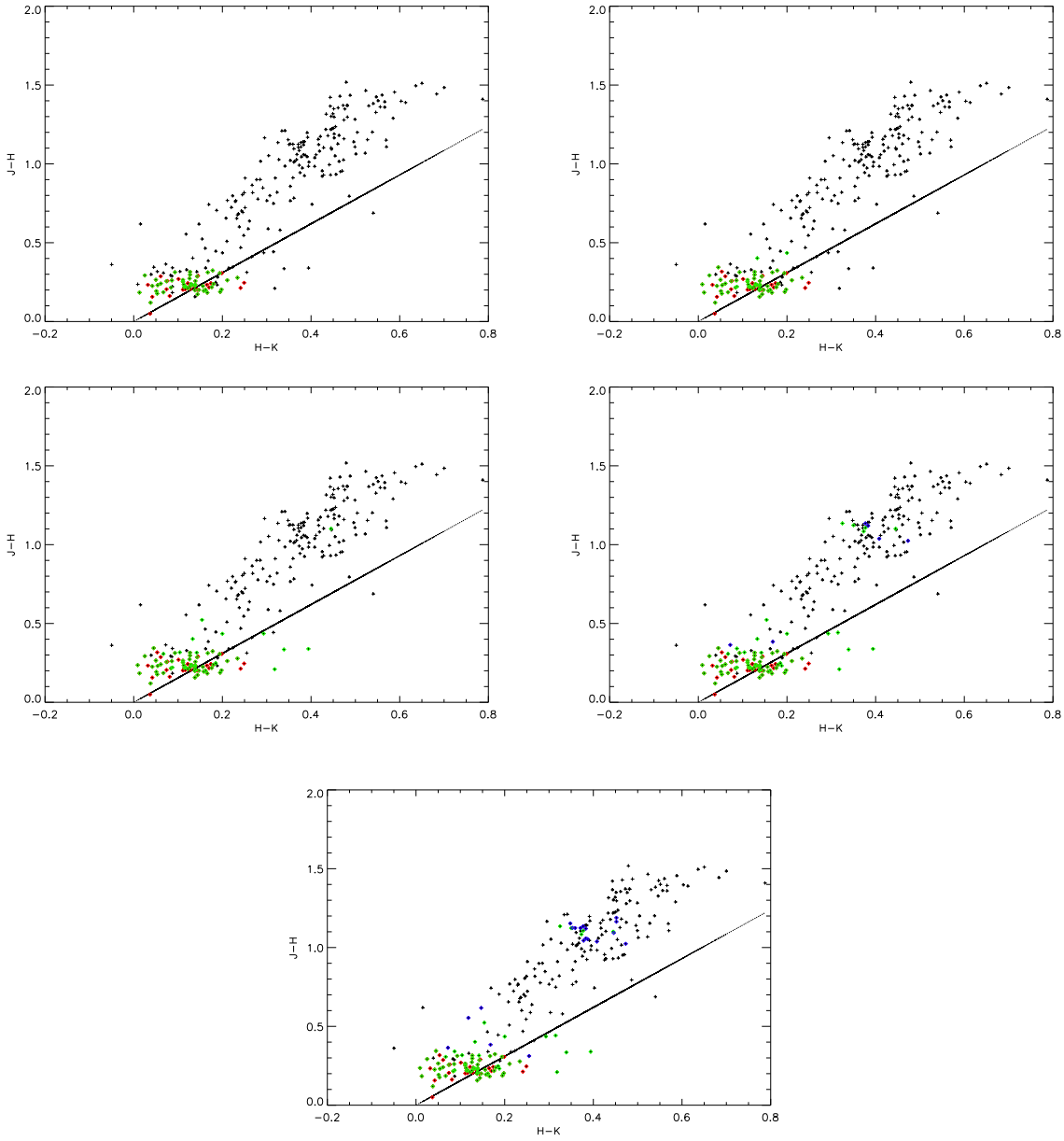


Figure 5.2: Colour-Colour plots of all stars (black crosses) in $2 \times r_{cor}$ of **FSR0045**. Coloured diamonds represent the stars' membership probabilities: $P^i_{cl} \geq 80\,\%$ red; $60\% < P^i_{cl} < 80\,\%$ green ; $40\% < P^i_{cl} < 60\,\%$ blue; $20\% < P^i_{cl} < 40\,\%$ purple ; $P^i_{cl} < 20\,\%$ black. The top (*Top Left*) 25 %; (*Top Right*) 30 %; (*Middle Left*) 35 %; (*Middle Right*) 40 %; (*Bottom*) 45 %; of high probability member stars are plotted. The solid line represents the reddening band ($Q = -0.05$ mag), such that all stars plotted below this line are considered YSOs.

$N_{YSO}$ is the number of YSOs in the cluster,

$$N_{YSO} = \sum_{i,Q \leq -0.05mag}^{N} P_{cl}^{i} \tag{5.15}$$

and $P_{cl}^{i}$ is the probability star $i$ is a member of the cluster (Eq. 3.4). If $Y_{frac}$ is negative ($N_{YSO} < 1$), its value is set to zero. The $N$ term is the number of stars in the top 25 %, 30 %, 35 %, 40 % and 45 % of high probability member stars, such that five sets of $Y_{frac}$ values are determined (i.e. one for each of the five $Q$ values). Essentially Eq. 5.14 calculates the total number of members of a cluster by summing the membership probabilities of high probability member stars. Similarly, Eq. 5.15 calculates the total number of YSOs in a cluster by summing the membership probabilities of high probability member stars that fall below the cluster's reddening limit.

The final YSO fraction for a cluster is determined as the median of the five $Y_{frac}$ values.

## 5.4 Potential Improvements

The method presented in this Chapter to measure cluster $H-$band extinctions could be improved by increasing the accuracy of the i) median cluster colours and ii) $[H - K]$ zero point measurements.

Cluster members are identified statistically using the PDT, which assigns membership probabilities based on stellar colours and has been shown to identify members with good accuracy (e.g. Bonatto and Bica (2007b), Buckner and Froebrich (2013), Chapter 3). However, difficulties arise when discerning true members from interloping field stars which have similar colours, particularly for clusters that: (i) are projected onto a high star density field (e.g. towards the GC); (ii) that are partially occluded e.g. by a GMC (so only the brightest/reddest members are identifiable); (iii) have a large proportion of intrinsically red members (e.g. YSOs); (iv) have blue straggler members. As this method measures a cluster's $H-$band extinction value from the median colours of its highest probability members ($HK_{med}$ and $H45_{med}$ − Sect. 5.2.3), it is reliant on the accurate identification of cluster members. Hence, although the PDT is a reliable technique to statistically identify cluster members, it is ideal to confirm stars membership using e.g. spectroscopy, astrometry, X-ray emissions. Unfortunately, at present the majority of new candidates in samples which have been discovered

as projected overdensities on the field only have photometry available (e.g. the FSR List catalogue).

The accuracy with which clusters' $HK_{med}$ and $H45_{med}$ values can be measured is also reliant on the resolution of the photometry used. Cross-matching 2MASS and WISE photometry showed that only approximately 50 % of the 2MASS high quality photometry stars (Qflag "AAA"), are detected by WISE within 1 to 3 times clusters' core radii. This is because WISE only detects the brightest (reddest) cluster members, i.e. the value of $H45_{med}$ will be redder than clusters' true values. Thus, although in principle $A_H^{H45}$ should be more accurate than $A_H^{HK}$ (as, unlike $[H-K]$, the $[H-4.5]$ colour is almost independent of luminosity and spectral class), its measured value will be redder than is true for the cluster. Consequently, it is also reasonable to expect that the measured $[H-K]$ zero point is smaller, and $A_H^{HK}$ will be systematically larger (redder), than their true values as well (Fig. 5.1, Eq. 5.4). Hence use of deeper, high resolution photometry (when available) will improve the accuracy of the measured $[H-K]$ zero point value, and clusters' $A_H^{HK}$, $A_H^{H45}$ values.

The addition of deeper high resolution photometry, spectrometry, astrometry and/or X-ray emissions for cluster samples will also improve the accuracy of their measured YSO fractions. Better photometry will refine clusters' measured reddening band (i.e. the $Q$ parameter − Eq. 5.10), and hence the identification of YSOs. Furthermore, the correction to clusters' measured YSO fraction (Sect. 5.3.2) was necessary as members were identified statistically, but confirmation of stars' membership (from e.g. astrometry) would render this correction obsolete.

## 5.5 Summary

This Chapter has presented methods to homogeneously measure cluster $H-$band extinctions and YSO fractions using photometry only. The $[H-K]$ zero point was also measured.

Two $H-$band extinction values are determined for clusters from their measured median $[H-K]$ and $[H-4.5]$ colours ($A_H^{HK}$ and $A_H^{H45}$ respectively). It is preferable to measure cluster extinction values from their median $[H-4.5]$ colours, as it has a well defined zero point and is almost independent of spectral type and/or luminosity class. Unfortunately, point sources in this colour had to be sourced from the low resolution WISE catalogue (which only detects the reddest cluster members), so clusters' measured extinctions will be redder than their true values. The $[H-K]$ colour is dependent of spectral type and luminosity class

and subsequently does not have a well defined zero point in the literature. However, point sources in this colour can be sourced from the 2MASS catalogue so about twice the number of members are used to measure a cluster extinction from $[H-K]$ than $[H-4.5]$. From a linear fit of a cluster sample's measured median $[H-K]$ colours and $A_H^{H45}$ values, the $[H-K]$ zero point was measured to be 0.06 mag.

# Chapter 6

# Age Determination

It is essential that the fundamental properties of a cluster sample (distances, extinctions, ages) are homogeneously derived to ensure that their uncertainties are systematic and any trends identified through large scale analyses undertaken with the sample are trustworthy. Methods to homogeneously derive clusters' distance and extinction values from photometry alone were presented in Chapter 4 and 5 respectively. This Chapter presents a method to homogeneously derive cluster ages.

## 6.1 Current Limitations

Age estimates for clusters which only have photometry available (and masses of members are unknown) can only be derived through fitting modelled cluster sequence isochrones to their CCM diagrams. In the literature, isochrone fitting is typically used to simultaneously identify a cluster's members and derive its distance, extinction, age and metallicity (e.g. Claria and Lapasset (1986), Jeffries et al. (2001), Naylor and Jeffries (2006), Glushkova et al. (2010), Piatti et al. (2010)). Unfortunately this approach enviably causes discrepancies between fundamental property values derived for a single cluster due to authors' different interpretations of their CCM diagrams (members, interlopers, MS/turn-off, giants etc.), particularly if these features are not well defined, as they typically are not for cluster candidates discovered as NIR overdensities.

Many examples of these discrepancies exist in the literature. One example is FSR1716 whose

distance, extinction, age and metallicity was derived by Froebrich et al. (2010) and Bonatto and Bica (2008b) who both fitted isochrones to the CCM diagrams of the cluster. Froebrich et al. (2010) found that FSR1716 was a Solar metallicity open cluster of 7.0 kpc, $A_H$ = 0.74 mag and 2 Gyr, whereas Bonatto and Bica (2008b) found that FSR1716 was either a Solar metallicity open cluster of 0.8 kpc, $A_H = 1.11$ mag and 7 Gyr or a globular cluster of 2.3 kpc, $A_H = 1.11$ mag and 12 Gyr. Another example is FSR0904 whose distance, extinction, age and metallicity was derived by Glushkova et al. (2010), Camargo et al. (2010) and Kharchenko et al. (2013) using isochrone fitting. Glushkova et al. (2010) found that FSR0904 was a Solar metallicity open cluster of 1.3 kpc, $A_H = 0.08$ mag and 630 Myr. Camargo et al. (2010) found that FSR0904 was a Solar metallicity open cluster of 2.2 kpc, $A_H = 0.35$ mag and 20 Myr. Kharchenko et al. (2013) found that FSR0904 was a Solar metallicity open cluster of 1.4 kpc, $A_H = 0.70$ mag and 63 Myr.

It has been argued that when multiple values of a cluster's fundamental properties have been derived for a cluster in the literature, they should be compared and an average taken (e.g. Netopil et al. (2015)), but this is impractical for large samples. Other approaches have attempted to address this issue by developing methods to homogeneously derive the properties of a sample using isochrone fitting (Monteiro et al. (2010), Kharchenko et al. (2012), Perren et al. (2015)), but as distance, extinction, age and metallicity values are initially unknown, individual cluster values remain questionable. The remainder of this Chapter addresses this issue by presenting an approach to homogeneously determine cluster sample ages using isochrone fitting, which has an emphasis on the accurate derivation of individual cluster property values.

## 6.2 Method

To ensure that an unbiased isochrone fit of each cluster in a sample is made, a *pipeline* is set-up. The pipeline fits isochrones to clusters' CCM diagrams to derive their distances, extinctions and ages.

The three steps of the pipeline are:

- Construction of clusters' CCM diagrams
- Cluster characterisation through isochrone fitting
- Derivation of cluster properties

### 6.2.1 Unbiased Isochrone Fits

At the time of development, a *manual* pipeline was the more prudent choice for:

(i) **Accuracy of fit**

Isochrones are fit to the prominent features (e.g. MS/turn-off, giants) of clusters' CCM diagrams. If these features are not well defined they are difficult to visually identify, and nearly impossible to identify using an automated process.

(ii) **Consistency of fit**

An automated pipeline would have a discreet approach to the fitting rather than 'the whole picture' approach which can only be achieved from a human perspective. Manually, fits can be subjective to individual interpretations of clusters' CCM diagrams. Thus manual fitting (performed by one human fitter), ensures a consistency in the fits.

The pipeline has an emphasis on fitting isochrones in an unbiased and homogeneous way. For this reason clusters' distance and extinction estimates are used as a starting point to fit isochrones to their CCM diagrams, and can be derived either from the methods set out in Chapter 4 and 5 or using an alternative method of the users choice. Any attempt to apply this pipeline to derive the properties of cluster samples which do not have distance and extinction estimates is not advised for the reasons discussed in Sect 6.1.

Solar metallicity Geneva isochrones (Lejeune and Schaerer, 2001) are fitted to cluster candidates which are suspected to have an intermediate or old age ($log(age/yr) > 8$). Solar metallicity PMS isochrones (Siess et al., 2000) are fitted to cluster candidates which are suspected to be young ($log(age/yr) < 8$) or contain members which are PMS. Both sets of isochrones were chosen due to their extensive mass and age ranges which are assumed to cover the majority of an open cluster sample. The Geneva isochrones have a stellar age range of ($3.0 < log(age/yr) < 10.2$) and masses of ($0.8\,M_{\odot} < M < 120\,M_{\odot}$); the PMS isochrones have a stellar age range of ($5.5 < log(age/yr) < 7.95$) and masses of ($0.1\,M_{\odot} < M < 7.0\,M_{\odot}$).

The reader should note the use of *Solar* metallicity isochrones. This pipeline is designed to derive the ages for samples of predominantly intermediate-old cluster candidates within $\sim 5$ kpc of the Solar Neighbourhood and whose metallicities are unknown (i.e. the FSR List catalogue). For large cluster samples of unknown metallicities it is prudent to assume a single

metallicity when fitting isochrones so that cluster properties are homogeneously derived. In order to decide which metallicity isochrones to use, all clusters in the WEBDA catalogue with a metallicity were selected and found to have a median of $Z = 0.02$ (i.e. Solar). Hence it is reasonable to assume a Solar metallicity for clusters in the Solar Neighbourhood. It should be noted that systematic uncertainties caused by using a (slightly) incorrect metallicity are statistically small. For example, if a Solar metallicity is incorrectly assumed for a cluster of $-0.4 < Z < 0.2$ there will be an intrinsic uncertainty comparable to $log(age/yr) \sim 0.1$. Thus, whilst in individual cluster cases a Solar metallicity may prove an inaccurate assumption, it is statistically justified.

### 6.2.2 STEP 1: Construction of CCM Diagrams

In Step 1 CCM diagrams are constructed for each cluster candidate. Membership probabilities are derived for all stars within the *cluster area* using the PDT (see Chapter 3 for details). The cluster area, $A_{cl}$, is defined as a circular area of radius $2 \times r_{cor}$ around the centre of the cluster. It was found that a cluster area with a radius of $1 \times r_{cor}$ typically did not display enough members for the MS/turn−off to be prominent on the CCM diagrams of most clusters. This is because the highest probability members are more easily identifiable with a cluster area of $2 \times r_{cor}$, i.e. the membership probability of stars that were identified as the most likely members for a cluster area of $1 \times r_{cor}$ increase, and additional stars are identified as having a high membership probability.

### 6.2.3 STEP 2: Cluster Characterisation

In Step 2 the fitter uses the flowchart shown in Fig. 6.1 to characterise the cluster candidate. The subsequent action to be taken is determined by the characterisation flag assigned to the candidate, either:

(I) **Non-cluster:** no feature(s) resembling an open cluster are visible in the candidate's CCM diagrams. This candidate is either not a real cluster or is real but its overdensity on the field is too low to reliably identify its most likely cluster members (e.g. candidate is typically positioned towards the GC).

**Action:** No attempt to fit an isochrone to the candidates CCM diagrams is made.

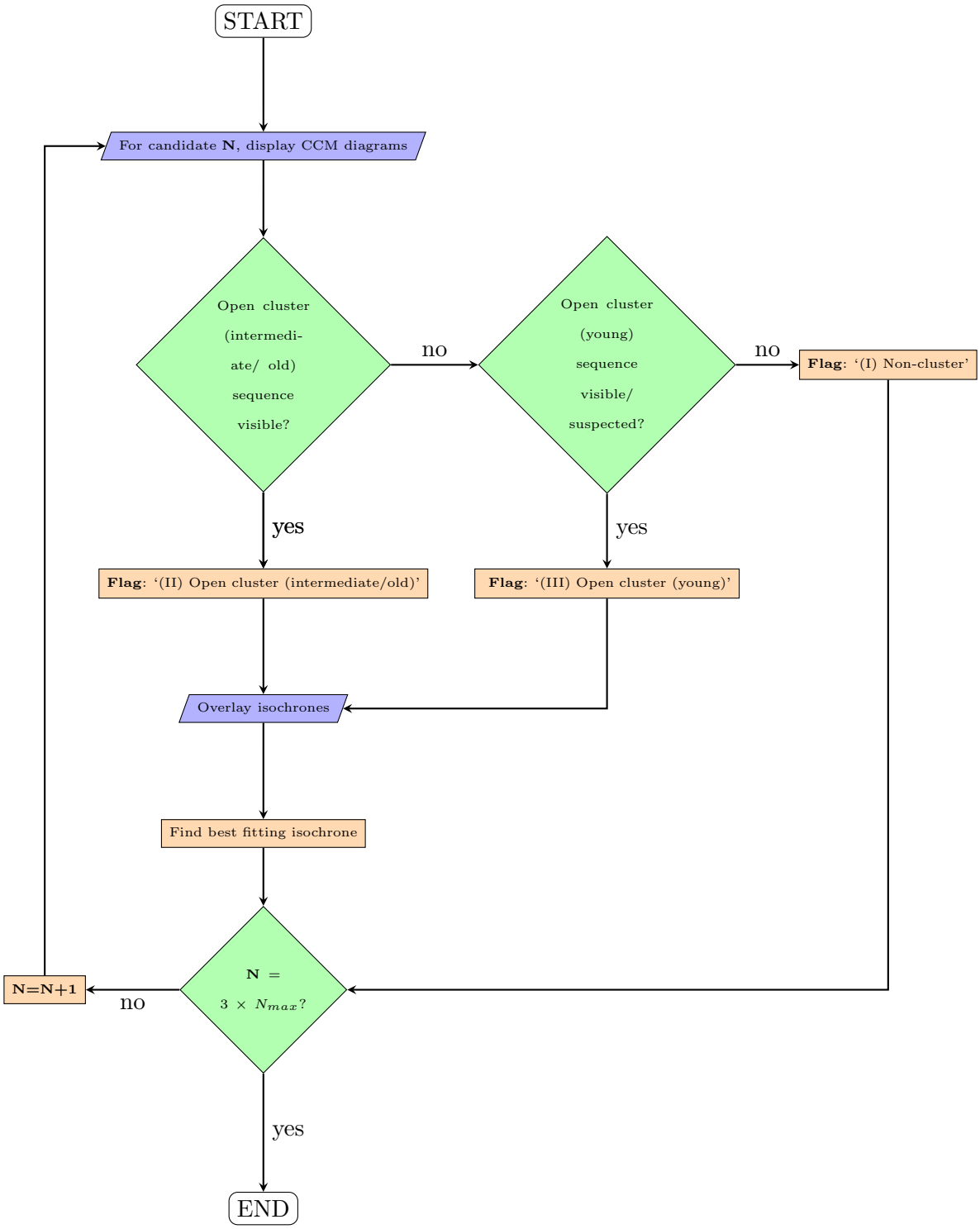


Figure 6.1: *Flowchart of STEP 2:* denotes the process of categorising the cluster candidates in a sample as (I) Non-cluster; (II) Open cluster (intermediate/old); or (III) Open cluster (young). Iterating over (and valid for) $1 \leq N \leq 3 \times N_{max}$ where $N_{max}$ is the total number of candidates in the sample.

(II) **Open cluster (intermediate/old):** A clear intermediate age or old open cluster sequence is visible ($log(age/yr) > 8$); feature(s) resembling a MS/turn−off (and ideally giants) are visible. No PMS track is visible or suspected.

**Action:** Four Geneva isochrones of $\log(age/yr) = 7.00$, 8.00, 9.00, 10.00 are overlaid on the CCM diagrams, configured using the candidates known distance and extinction estimates. The best fit of the four isochrones is chosen and overlaid with the two additional isochrones in steps of $\log(age/yr) = 0.05$. This process is repeated until a satisfactory fit has been made. For example, if a $\log(age/yr) = 9.00$ isochrone best fits the candidate's CCM diagrams, three isochrones of $\log(age/yr) = 8.95$, 9.00, 9.05 are overlaid (and so on). If isochrones of $\log(age/yr) = 9.00$ and 10.00 best fit the candidate's CCM diagrams, three isochrones of $\log(age/yr) = 9.45$, 9.50, 9.55 are overlaid (and so on).

(III) **Open cluster (young):** A clear young open cluster sequence and/or PMS stars are visible (or suspected below the magnitude limit of the photometry). Only the top of the cluster sequence may be visible on the CCM diagrams.

**Action:** Four PMS isochrones of $\log(age/yr) = 7.30$, 7.60, 7.80, 7.90 are overlaid on the CCM diagrams, configured using the candidates known distance and extinction estimates. The best fit of the four isochrones is chosen and overlaid with the two additional isochrones in steps of $\log(age/yr) = 7.00$ (10 Myr). If a candidate has a suspected age of $\log(age/yr) < 7.00$, isochrones are overlaid in steps of $\log(age/yr) = 6.00$ (1 Myr).

Each candidate in the sample is blindly characterised three times (i.e. the cluster ID and previous isochrone fits are unknown) in a randomised order to ensure that unbiased distance, extinction and age values are derived. For example, if a sample contains 1000 cluster candidates, 3000 candidate characterisations and isochrone fits are made.

### 6.2.4 STEP 3: Derivation of Cluster Properties

In this step the three characterisations made for each candidate in Step 2 (Sect. 6.2.3) are compared. A final characterisation is made for each candidate, and a single set of property values are derived using the flowchart shown in Fig. 6.2. A candidate is characterised as either:

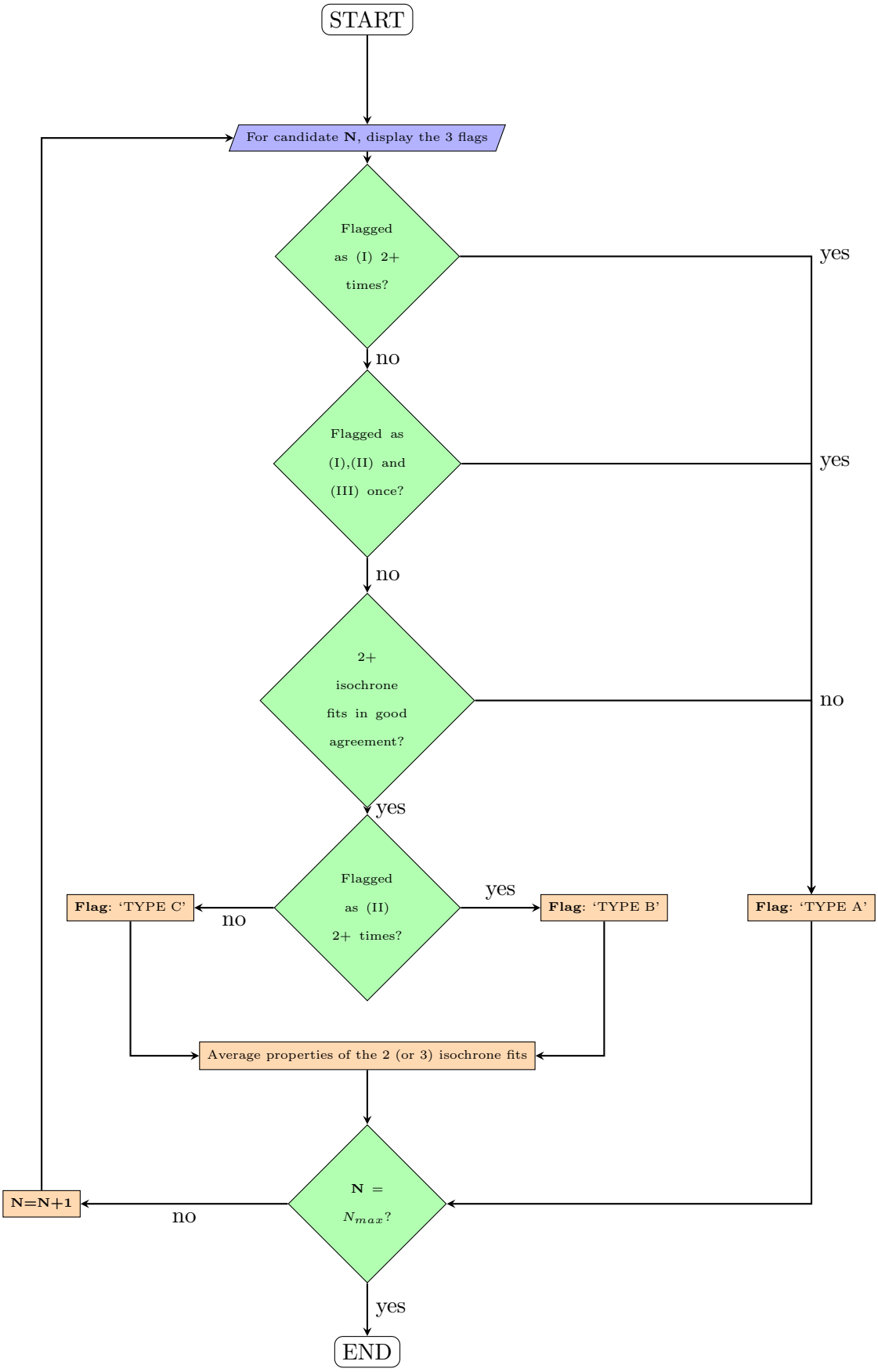


Figure 6.2: *Flowchart of STEP 3:* denotes the process in which cluster candidates receive their final classification as either TYPE A, TYPE B or TYPE C and their distance, extinction and age values are derived (see text for details). Iterating over (and valid for) $1 \leq N \leq N_{max}$ where $N_{max}$ is the total number of clusters in the sample.

**TYPE A - Non-cluster:** The candidate has been flagged in Step 2 as *'(I) Non-cluster'* two or three times. Alternatively, the candidate was flagged in Step 2 as each of the three categories (I, II, III) once, or at least two of the isochrone fits are in poor agreement.

**Action:** None. Cluster candidate is discarded.

**TYPE B - Open cluster (intermediate/old):** The candidate has been flagged in Step 2 as *'(II) Open cluster (intermediate/old)'* two or three times, and at least two of the isochrone fits are in good agreement.

**Action:** Properties are derived as the average of the two (or three) isochrone fits that are in good agreement.

**TYPE C - Open cluster (young):** The candidate has been flagged in Step 2 as *'(III) Open cluster (young)'* two or three times, and at least two of the isochrone fits are in good agreement.

**Action:** Properties are derived as the average of the two (or three) isochrone fits that are in good agreement.

### 6.2.5 An Example: FSR0071

The pipeline was applied to a sub-sample of the FSR List catalogue clusters (Sect. 8.3). In Step 1, CCM diagrams were generated for FSR0071 (Fig. 6.3). In Step 2, FSR0071 was flagged as '*(II) Open cluster (intermediate/old)*' because no PMS track was visible or suspected, and the cluster was fitted with Geneva isochrones three times. In Step 3, FSR0071 was characterised as '**TYPE B- Open cluster (intermediate/old)**' as all three isochrone fits were in good agreement (Fig. 6.4). The properties of the FSR0071 are derived as the average of the three isochrone fits, giving the cluster an age of $log(age/yr) = 7.60 \pm 0.17$, distance of $2.00 \pm 0.21$ kpc, and $H-$band extinction of $0.29 \pm 0.02$ mag (Table 6.1). Note, the uncertainties on these values are derived as the absolute statistical variation between the three fits and do not include the uncertainties caused by assuming the cluster has a Solar metallicity.

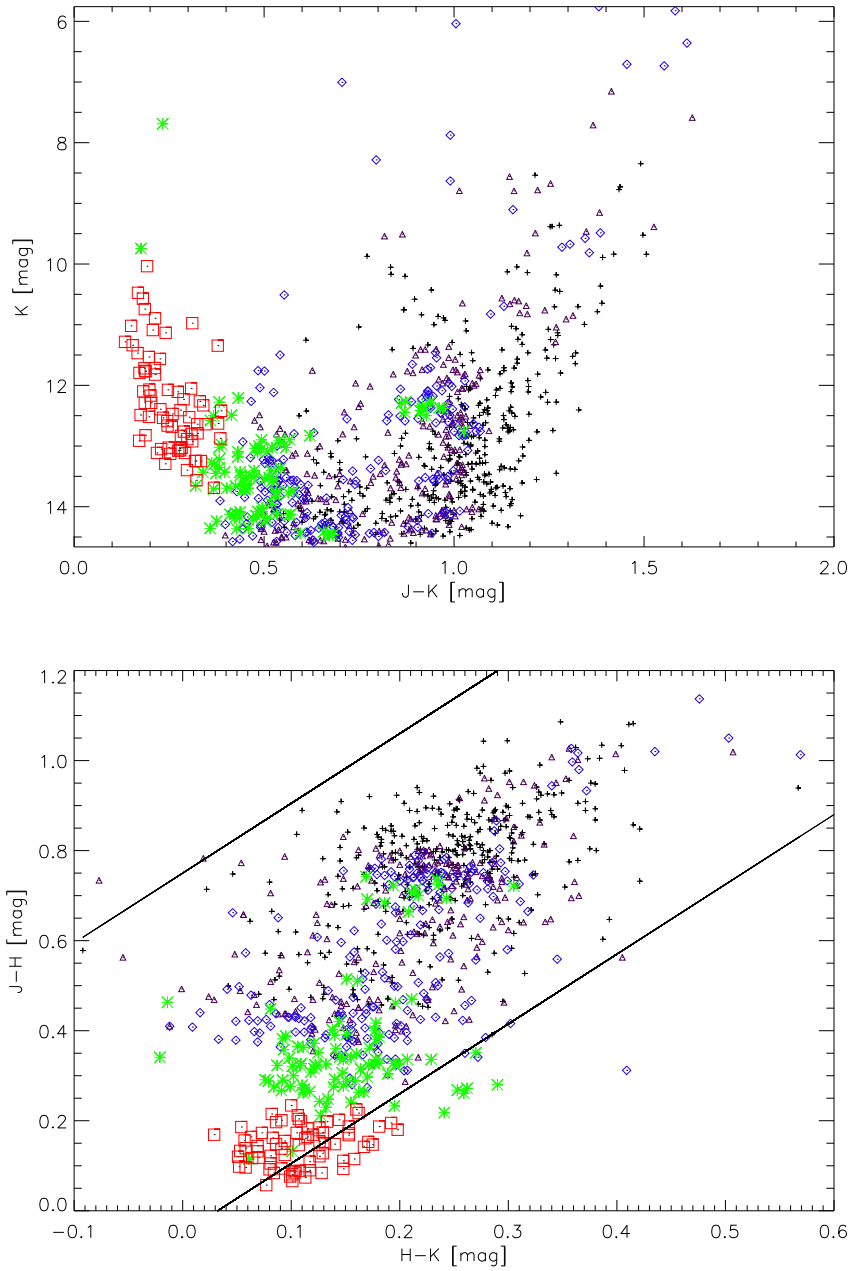


Figure 6.3: CCM diagrams of **FSR0071** for all stars within 2 × $r_{cor}$. Membership probabilities were determined using the PDT with a Nearest Neighbour number of $N = 15$ (see Chapter 3 for details). Symbols represent the determined cluster membership probabilities: $P^i_{cl} \geq 80\,\%$ red squares; $60\% < P^i_{cl} < 80\,\%$ green stars; $40\% < P^i_{cl} < 60\,\%$ blue diamonds; $20\% < P^i_{cl} < 40\,\%$ purple triangles; $P^i_{cl} < 20\,\%$ black plus signs.

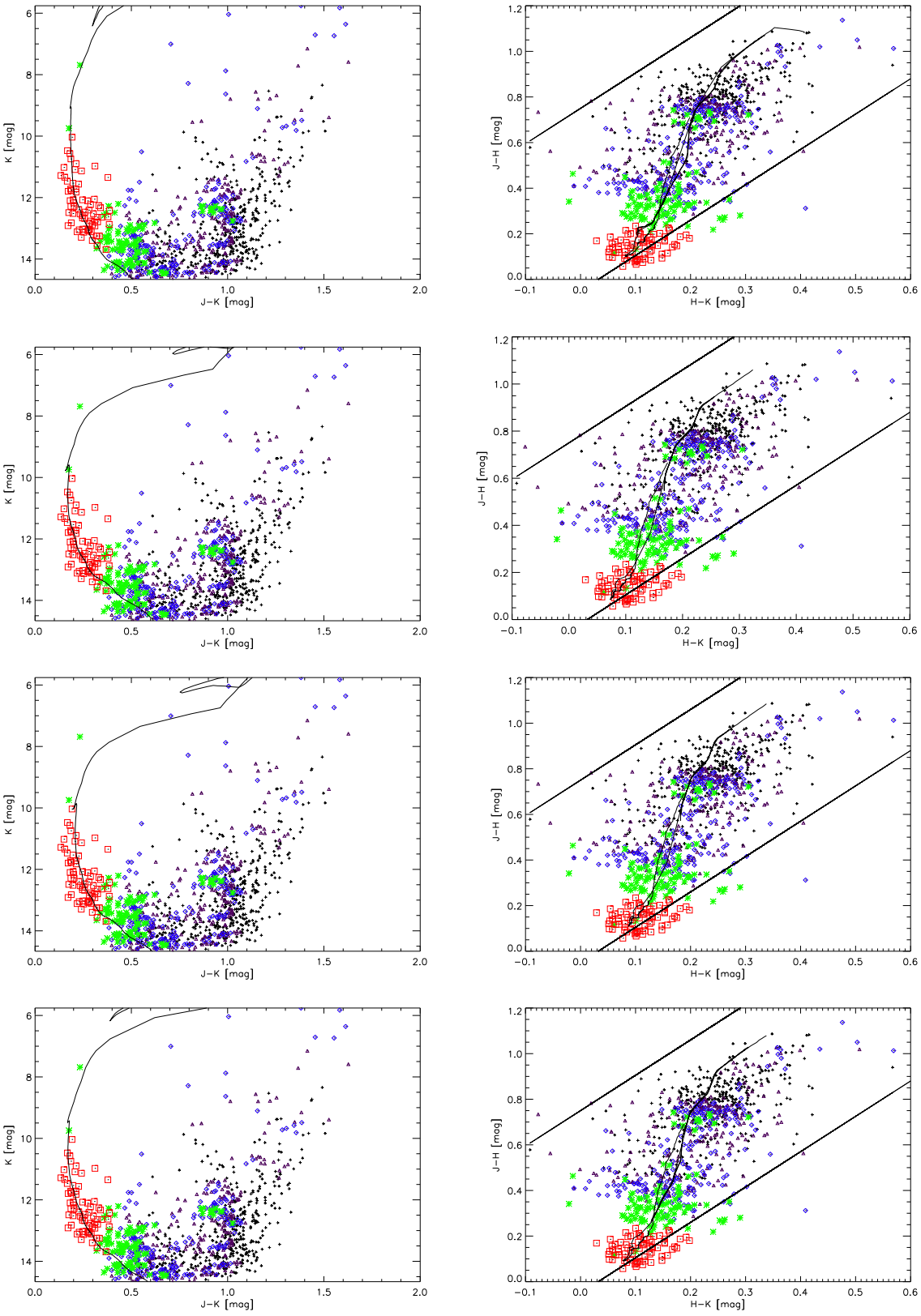


Figure 6.4: Isochrone fits for **FSR0071**. Membership probabilities were determined for all stars within $2 \times r_{cor}$ using the PDT with a Nearest Neighbour number of $N = 15$ (see Chapter 3 for details). Symbols represent the determined membership probabilities: $P^i_{cl} \geq 80\,\%$ red squares; $60\% < P^i_{cl} < 80\,\%$ green stars; $40\% < P^i_{cl} < 60\,\%$ blue diamonds; $20\% < P^i_{cl} < 40\,\%$ purple triangles; $P^i_{cl} < 20\,\%$ black plus signs. The left panels, show the isochrone fits in the $J - K/K$ Colour−Magnitude space, the right panels show the isochrone fits in the $H - K/J - H$ Colour−Colour space. Panels represent *(Top)* Fit 1; *(Upper Middle)* Fit 2; *(Lower Middle)* Fit 3; *(Bottom)* Average of Fits 1, 2 and 3 (see Table 6.1 for isochrone parameters).

Table 6.1: Shows the three sets of properties derived for **FSR0071** from its three best fitting isochrones and the average of these fits. The uncertainties on the averaged values are derived as the absolute statistical variation between the three fits and do not include the uncertainties caused by assuming the cluster has a Solar metallicity.

| **Fit No.** | **Age** [**log(age/yr)**] | **d** [**kpc**] | $A_H$ [**mag**] |
|---|---|---|---|
| Fit 1 | 7.30 | 2.40 | 0.32 |
| Fit 2 | 7.90 | 1.70 | 0.25 |
| Fit 3 | 7.60 | 1.90 | 0.29 |
| Averaged Fit | 7.60 $\pm$ 0.17 | 2.00 $\pm$ 0.21 | 0.29 $\pm$ 0.02 |

## 6.3 Potential Improvements

The pipeline assumes that clusters have a Solar metallicity, which will be incorrect for some clusters as there is a metallicity gradient in the Disk (Friel, 1995). A potential improvement therefore would be to incorporate metallicity measurements into the pipeline by inspecting cluster CCM diagrams which have been overlaid with isochrones of varying metallicities (e.g. Bonatto and Bica (2009)). However, assuming a Solar metallicity for clusters is statistically justified (Sect. 6.2.1), deriving cluster metallicity estimates would be too time-expensive to be practical for large cluster samples and their accuracy would be questionable (as cluster age is unknown).

## 6.4 Summary

This Chapter has presented a method to homogeneously derive the ages of cluster samples and refine their known distance and extinction estimates. The method consists of using a 3-step manual pipeline to fit modelled cluster sequence isochrones to the CCM diagrams of cluster candidates.

In *Step 1* CCM diagrams are constructed for the candidates. Members are statistically identified using the PDT (Chapter 3).

In *Step 2* candidates are blindly fitted with isochrones three times, in a randomised order. Candidates known distance and extinction estimates are used as a starting point to fit the isochrones. The 'blind' aspect ensures that the fits remain unbiased and that the fitter is

not influenced by previous fits of the candidate or known properties in the literature. Fitting isochrones three times is intended to counteract the subjective nature of how cluster CCM diagrams are interpreted, and to minimise human error in the derived properties of the candidate.

In *Step 3* the three isochrone fits are correlated for each candidate and inspected. If at least two of the fits are in good agreement, the age, distance and extinction values of the cluster are derived as the average of the fits.

# Chapter 7

# Scale Height Determination

To fully understand open cluster behaviour on a Galactic scale, it is important to begin to build up an observational picture of the temporal evolution of cluster scale height. This requires, in addition to the accurate derivation of cluster ages and distances, a method to accurately measure the scale height of samples.

Different authors have attempted to explore this issue. It has been argued that it is not possible to determine the scale height of old clusters ($> 1$ Gyr) due to their flattened vertical distribution perpendicular to the GP (e.g. Bonatto et al. (2006)), though it has been shown that old clusters have a scale height of 375 pc (Janes and Phelps (1994), Froebrich et al. (2010)). This is significantly larger than their young ($< 200$ Myr) and intermediate-aged (200 Myr to 1 Gyr) counterparts which have typical scale heights of 48 pc and 150 pc respectively (Bonatto et al. (2006), Moitinho (2010)). Unfortunately the methods employed to measure these scale heights are only applicable to sample sizes of a few 100 clusters (or more) and fail at smaller sample sizes. Consequently, a detailed analysis of the temporal evolution of cluster scale height has not been possible, as observationally, there are simply not enough known clusters to do this.

Additional difficulties lie in the nature of cluster samples. Ideally, for this kind of analysis, the properties of cluster samples would be homogeneously determined, so that uncertainties on the scale height measurements are systematic. A further issue that has to be considered is the role of cluster disruption and observational bias on the number and age spread of samples, which causes a decline in the number of clusters observed with cluster age. This has been a major stumbling block particularly for samples of (rare) old clusters, such that the scale

height evolution of clusters older than 1 Gyr is poorly understood. This Chapter explores the limitations mentioned above and presents a solution to determine cluster scale height for smaller sample sizes.

## 7.1 Current Limitations

As briefly discussed in the introduction of this Chapter, there are three main limitations for building up an observational picture of the evolution of scale height with cluster age: (i) the methods employed to measure scale height are only applicable to larger sample sizes and fail at smaller sample sizes; (ii) the nature of the cluster samples; (iii) the role of cluster disruption and observational bias on the number and age spread of cluster samples.

The second of these limitations relates to the heterogeneous nature of large cluster samples properties which are collated from the literature, i.e. different methods are used to determine clusters' fundamental properties. Any uncertainties in an analysis of the evolution of cluster scale height and age (which is dependent on cluster distance and age values) with such a sample would not be systematic and therefore any trends identified would be unreliable. Thus, a cluster sample with homogeneously determined distances and ages is required (methods for which have been presented in Chapters 4 and 5 respectively).

Limitations (i) and (iii) are intrinsically linked and are essentially the same problem: there are an insufficient number of known clusters with which to make scale height measurements for using small bin sizes, due to established methods' restraints on sample size.

In order to understand the nature of this problem, it is important to look at the theory behind it. To analyse the distribution of an open cluster sample perpendicular to the GP, it can be assumed that the sample's space density, $N(Z)$, follows an exponential or sech$^2$ function of the form:

$$N(Z) = N_0 \cdot \exp\left(-\frac{|Z - Z_0|}{h_0}\right), \tag{7.1}$$

or

$$N(Z) = N_0 \cdot sech^2\left(\frac{|Z - Z_0|}{2 \cdot h_0}\right), \tag{7.2}$$

where $h_0$ is the scale height of a cluster sample; $Z$ is the vertical distance of the clusters above/below the GP; $Z_0$ is the vertical zero point (plane of symmetry) of the sample; and $N_0$ is the central space density at $Z = Z_0$.

Eq. 7.1 assumes the stellar density to be exponentially vertically distributed, whilst Eq. 7.2 assumes a velocity dispersion which is not dependent on vertical height above/below the GP, and is thus expected for a self-gravitating disk. Both equations produce very similar distributions, but at $|Z - Z_0| = 0$ Eq. 7.2 is continuous and Eq. 7.1 is not. For finite distributions, which typically contain objects a few scale heights away from $Z_0$ (i.e. cluster samples), it is sufficient to fit a exponential *or* $\mathrm{sech}^2$ function to determine their scale height. Eq. 7.1 is the function of choice in the literature, most likely because cluster samples contain objects which are normally a few scale heights from the mid-plane, i.e. not at $|Z - Z_0| = 0$ (e.g. Piskunov et al. (2006), Janes and Phelps (1994), Bonatto et al. (2006), Pandey et al. (1988), Liu and Zhu (2011)).

To fit either function a minimum number of clusters is required, typically in the order of a few 100 for a good fit, with a minimum of $\sim 100$ required (e.g. Piskunov et al. (2006), Bonatto et al. (2006)). Unfortunately, the number of observed clusters diminishes with cluster age (e.g. Kharchenko et al. (2013), Schmeja et al. (2014)). This is most likely caused by observational biases. Firstly as discussed, older clusters have been shown to have larger scale heights than their younger counterparts (Buckner and Froebrich, 2014), which indicates that a significant proportion may be located at higher latitudes, and so escape detection from surveys that focus on the lower latitudes of the GP (e.g. Froebrich et al. (2007), Mercer et al. (2005)). Secondly, as the clusters evolve their apparent radius will increase (due to member loss through encounters and stellar evolution), such that at small distances (few hundred parsec) they become too extended on the sky to be detected. For example a cluster with an actual core radius of 3 pc, will have an apparent radius of 0.86° (51.57') at a distance of 200 pc, and 0.17° (10.31') at a distance at 1000 pc. Naturally, it is difficult to distinguish clusters' with large apparent radii as overdensities on the field in the absence of e.g. proper motion measurements.

This issue has been noted by several authors including Kharchenko et al. (2013), who found a lack of old open cluster candidates in the MWSC catalogue within $< 1$ kpc. In an attempt to find the 'missing' old clusters of the MWSC catalogue, Schmeja et al. (2014) used a star count algorithm on the 2MASS point source catalogue to look for the clusters at high latitudes ($|b| > 20°$), applying filters in Colour-Magnitude space to increase the contrast between field stars and the found overdensities (cluster candidates). In total they discovered

an additional 139 old open clusters ($8.3 < log(age/yr) < 9.7$ ) at distances from the GP of $0.3 < Z < 1$ kpc but about 60 old clusters up to 1 kpc from the Sun which remain 'missing' (Schmeja et al. (2014) − Fig. 7 therein). The authors speculate that this is due to these clusters' extended angular size.

Despite these limitations, it is still important to establish a relationship (if any) between cluster age and scale height. Thus, as the limitations on the data are yet to be resolved, a method to determine scale height which diminishes the restraints on sample size is required.

## 7.2 Parameter Determination

The aim of this Chapter is to establish a method to determine the scale height of (observed) cluster samples, which greatly reduces the restraints that established methods have on sample size.

To do this, modelled cluster distributions are randomly generated with a spectrum of different scale heights and vertical zero points values. The model $Z$-distributions are then compared to observed cluster samples $Z$-distributions using a two sample Kolmogorov- Smirnov test (2sKST) (Peacock, 1983), the aim of which is to determine the observed cluster sample's scale height and vertical zero points value. The observed samples parameters are taken as the values of the model distribution which shows the highest probability to be drawn from same parent distribution.

The remainder of this Chapter explains how the modelled cluster distributions are generated and details the process by which observed cluster samples scale heights vertical zero points are determined.

### 7.2.1 Modelling Cluster Distributions

#### 7.2.1.1 Setup

To generate modelled cluster distributions, a choice of using Eq. 7.1 or Eq. 7.2 must be made. The choice of function is essentially (used in this context) arbitrary and the distributions can be modelled using either equation. As cluster samples typically contain objects a few scale heights away from $Z_0$ (i.e. not at $|Z - Z_0| = h_0$), Eq. 7.1 is the function of choice.

The free parameters of the modelled cluster distributions are: the initial central space density, $N_0$; vertical zero point, $Z_0$; and scale height, $h_0$. For a fixed size distribution it can be assumed that its space density is equal to the number of clusters, i.e.

$$N(Z) = N_M \tag{7.3}$$

where $N_M$ is the number of clusters in the distribution.

Substituting Eq. 7.3 into Eq. 7.1 and integrating with respect to $Z$, gives the central space density of a distribution, $N_0$, as

$$N_0 = \frac{N_M}{2h_0} \cdot \left(1 - \exp\left(-\frac{|Z - Z_0|}{h_0}\right)\right)^{-1}, \tag{7.4}$$

#### 7.2.1.2 Parameter Ranges

The ranges of $Z_0$ and $h_0$ are set at $-160 < Z_0^{mod} < 100$ pc and $20 < h_0^{mod} < 1000$ pc both with 5 pc step sizes, as these cover the full range of potential values an observed cluster sample could take, i.e. a total of $53 \text{ x } 197 = 10441$ modelled cluster distributions will be generated, each with a unique combination of $Z_0^{mod}$ and $h_0^{mod}$ values.

Each modelled cluster distribution is generated randomly within a parameter space of ($[Z_{min}^{mod}, 0]$, $[Z_{max}^{mod}, N_0^{mod}]$). The maximum $Z-$value, $Z_{max}^{mod}$, of the modelled cluster distribution is set as the maximum vertical height the observed sample is complete for (i.e. has a flat surface density distribution), defined as:

$$Z_{max}^{mod} = d_{max}^{obs} \times \ sin(|b_{max}^{obs}|) \tag{7.5}$$

where $d_{max}^{obs}$ is the maximum distance the observed sample is complete in parsec; and $b_{max}^{obs}$ is the maximum latitude of the sample in degrees. For example, in Sect. 2.1 CS 1 was found to have $d_{max}^{obs}$ =1800 pc and $|b_{max}^{obs}| = 90°$, so for CS 1 $Z_{max}^{mod} = 1800 \times sin(90°) = 1800$ pc.

The minimum $Z-$value, $Z_{min}^{mod}$, is defined as

$$Z_{min}^{mod} = Z_0^{mod} - Z_{max}^{mod} \tag{7.6}$$

#### 7.2.1.3 Size

To determine an observed cluster sample's scale height and vertical zero point $(h_0^{obs}, Z_0^{obs})$, a 2sKST is employed to compare the observed sample to each of the modelled cluster distributions. The 2sKST operates by comparing the Cumulative Distribution Function (CDF) of the observed cluster sample and each modelled cluster distributions to determine the probability (known as the 'KS-statistic') that both are drawn from the same parent distribution. Thus it is imperative that the CDF of the modelled cluster distributions are smooth, i.e. contain a sufficient number of (modelled) clusters.

It is important to select a sufficiently large value for $N_M$ so as to avoid any unnecessary uncertainties caused by the random nature of the modelled cluster distributions, whilst limiting its value so that the computing time/power used to generate the distributions is not excessive. In principle the value of $N_M$ can be determined numerically or analytically from Eq 7.4. A numerical approach was chosen as it can ensure, through testing, that $N_M$ is of a sufficiently large size such that each modelled cluster distribution is representative of a (statistically) random sample.

To determine the value of $N_M$, modelled cluster distributions were generated between $300 < N_M^{mod} < 50,000$. The values of $Z_0^{mod}$ and $h_0^{mod}$ were kept constant and, for each value of $N_M^{mod}$, ten modelled cluster distribution realisations were made. The modelled cluster distributions were then compared with an observed distribution using the 2sKST and the probability they were drawn from the same parent distribution determined. Modelled cluster distributions were deemed to have a large enough value of $N_M^{mod}$ when 9 out of the 10 realisations produced identical results, i.e. distributions were large enough to remove any uncertainties resulting from their random nature. To discount any dependence of the results on the chosen $h_0^{mod}$ and/or $Z_0^{mod}$ values, the tests were repeated with varied constant $h_0^{mod}$ and $Z_0^{mod}$ values. The minimum value of $N_M^{mod}$ to produce identical KS-statistics for 9 out of each set of 10 realisations is $N_M^{mod} = 30000$. Hence each of the 10441 modelled cluster distributions have 30000 points.

### 7.2.2 Best Fit Parameters

The value of $h_0^{obs}$ and $Z_0^{obs}$ cannot simply be taken as the values of the model distribution which it has been identified as the most likely to be drawn from the same parent distribution (i.e. the highest KS-statistic). This is because there will be multiple modelled cluster distributions with which the observed sample has very high and similar KS-statistics (as these modelled cluster distributions will have near identical $h_0^{mod}$ and $Z_0^{mod}$ values).

For example, an observed cluster sample is found to have the highest KS-statistic with modelled cluster distribution A which has ($h_0^{mod} = 180\,\mathrm{pc}$, $Z_0^{mod} = 20\,\mathrm{pc}$), the second highest KS-statistic with B which has ($h_0^{mod} = 185\,\mathrm{pc}$, $Z_0^{mod} = 25\,\mathrm{pc}$), and third highest KS-statistic with C which has ($h_0^{mod} = 175\,\mathrm{pc}$, $Z_0^{mod} = 15\,\mathrm{pc}$). Each of the three statistics are very similar because A, B and C have near identical ($h_0^{mod}, Z_0^{mod}$) values. In fact, the observed sample may not have an exact match with *any* of the modelled cluster distributions, i.e. it has parameter values which are in-between the defined 5 pc step sizes e.g. $h_0^{obs} = 177\,\mathrm{pc}$, $Z_0^{obs} = 22\,\mathrm{pc}$.

To find the parameters of the observed sample all 10441 KS-statistics are plotted as a function of the modelled cluster distributions' $h_0^{mod}$ and $Z_0^{mod}$ values, and contouring is overlaid which represents the values of the KS-statistics (e.g. Fig. 7.1). A 2-D Gaussian distribution is fitted to find the central coordinates (highest value) of the contour, of the form

$$G(h_0^{mod}, Z_0^{mod}) = A_0 + A_1 \exp\left(-\frac{U}{2}\right) \tag{7.7}$$

Where, $G(h_0^{mod}, Z_0^{mod})$ is the 2-D Gaussian function, $U$ is the elliptical function:

$$U = \left(\frac{h_0^{mod'}}{A_2}\right)^2 + \left(\frac{Z_0^{mod'}}{A_3}\right)^2 \tag{7.8}$$

and $A_{0-4}$ are constants with,

$$h_0^{mod'} = (h_0^{mod} - h_0^c) \times cos(T) - (Z_0^{mod} - Z_0^c) \times sin(T) \tag{7.9}$$

$$Z_0^{mod'} = (h_0^{mod} - h_0^c) \times sin(T) + (Z_0^{mod} - Z_0^c) \times cos(T) \tag{7.10}$$

for a clockwise rotation $T$ of the ellipse around the $Z_0^{mod}$ axis, and a central peak of $(h_0^c, Z_0^c)$.

The central coordinates (peak) of the Gaussian fit are then taken as the best fit parameters for the observed distribution. Hence,

$$h_0^{obs} = h_0^c \tag{7.11}$$

$$Z_0^{obs} = Z_0^c \tag{7.12}$$

where $h_0^{obs}$ is the scale height and $Z_0^{obs}$ is the vertical zero point, of the observed cluster sample.

## 7.3 Parameter Uncertainties

It is important to ascertain how large the uncertainties $\Delta h_0^{obs}$ and $\Delta Z_0^{obs}$ are, and how they depend on (i) the value of the parameters and (ii) the size of the observed cluster sample.

### 7.3.1 Dependence on the Parameter Values

As the aim of this approach is to determine $h_0^{obs}$ and $Z_0^{obs}$, it is not possible to directly estimate the impact their values have on the uncertainties (as these values are initially unknown).

To overcome this, small cluster samples with simulated $Z$-distributions and a range of $h_0$ and $Z_0$ values were generated randomly using Eq. 7.1. For each simulated cluster sample, 50 different realisations were generated to avoid any unnecessary uncertainties caused by the random nature of their distributions. Since the value of $h_0^{obs}$ and $Z_0^{obs}$ is known for each of these simulated cluster samples, any uncertainties in these values as returned from the approach can be accurately evaluated.

To evaluate $\Delta h_0^{obs}$ and $\Delta Z_0^{obs}$ two tests were made:

1. **Evaluate $\Delta Z_0^{obs}$:** for this test $h_0^{obs}$ was kept constant at 200 pc and $Z_0^{obs}$ was varied over the range $-40 \leq Z_0^{obs} \leq +40$ pc.
2. **Evaluate $\Delta h_0^{obs}$:** for this test $Z_0^{obs}$ was kept constant at -30 pc and $h_0^{obs}$ was varied in the range $100 \leq h_0^{obs} \leq 350$ pc.

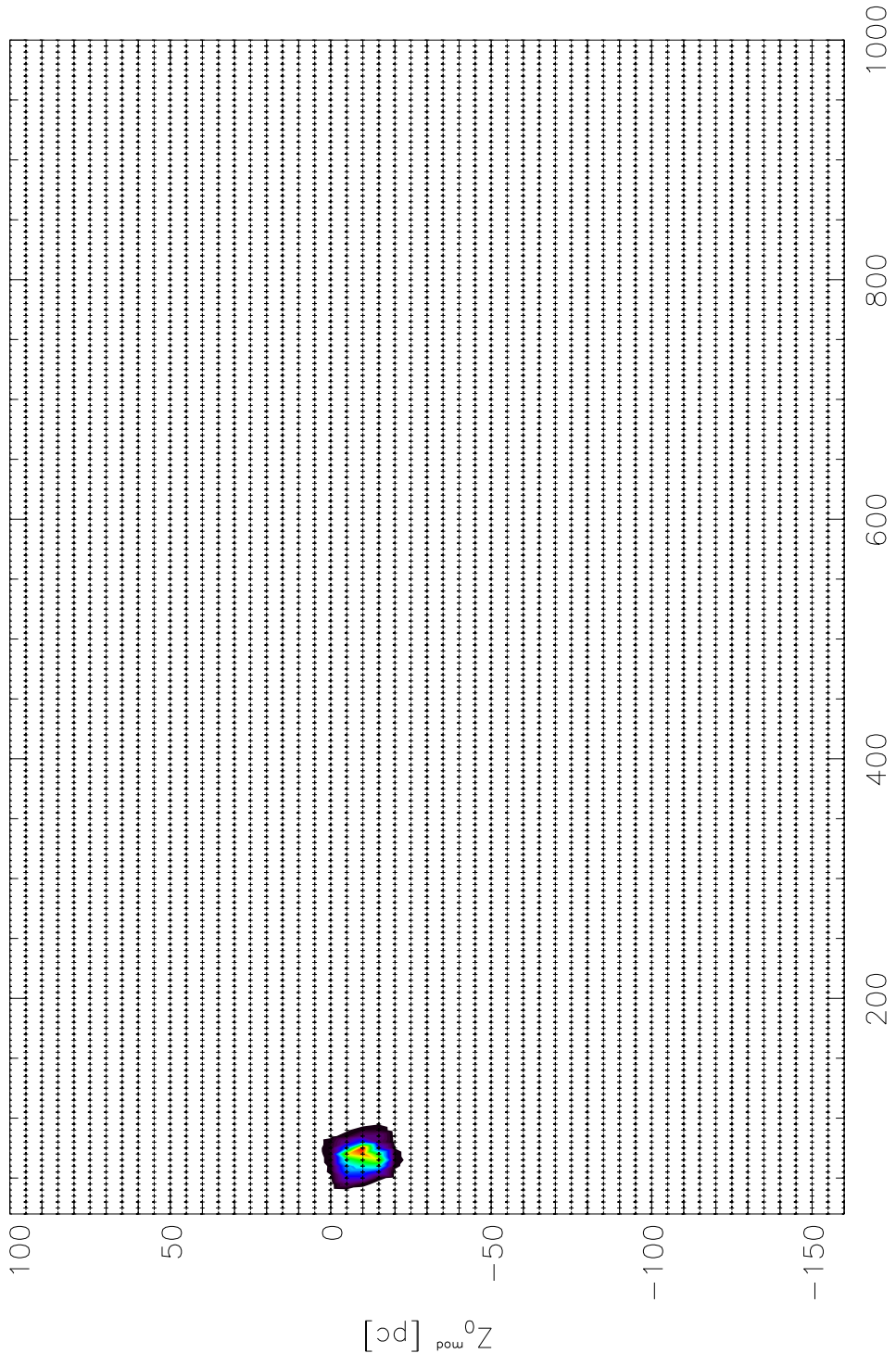


Figure 7.1: Plot of the KS-statistics obtained for an observed cluster sample (a sub-sample of CS 1, consisting of clusters positioned in the Fourth Galactic Quadrant with no age restriction). Crosses indicated each modelled cluster distribution's $h_0^{mod}$ and $Z_0^{mod}$ values. The colours and contouring indicate the highest KS-statistics, i.e. the modelled cluster distributions which are more likely to have been drawn from the same parent distribution as the observed sample: red represents the highest, black the lowest non-zero, and white null.

For both Test 1 and 2, it was found that $\Delta h_0^{obs}$ and $\Delta Z_0^{obs}$ had is no significant or systematic dependence on $h_0^{obs}$ or $Z_0^{obs}$.

### 7.3.2 Dependence on the Observed Cluster Sample Size

To determine the dependence (if any) of the observed cluster sample size on $\Delta h_0^{obs}$ and $\Delta Z_0^{obs}$, Test 1 and 2 were repeated for simulated cluster samples of sizes $N_D = 10$, 15, 30, 50, 75, 100, 200, 300 and 600.

A systematic dependence of $N_D$ on $\Delta h_0^{obs}$ and $\Delta Z_0^{obs}$ was found (Fig. 7.2). The tests failed for simulated cluster samples of size $N_D$ =10 as the distributions were too small, thus a minimum sample size of 15 clusters is established.

The uncertainty on $\Delta h_0^{obs}$ can be approximated by a power law of the form,

$$\frac{\Delta h_0^{obs}}{h_0^{obs}} = 1.12 \cdot (N_D)^{-0.41} \tag{7.13}$$

thus,

$$\frac{\Delta h_0^{obs}}{h_0^{obs}} \propto \frac{1}{\sqrt{N_D}} \tag{7.14}$$

The uncertainty on $\Delta Z_0^{obs}$ can be approximated by a power law for $N_D < 115$ and a constant for $N_D > 115$, where

$$\Delta Z_0^{obs} = \begin{cases} 419\,\mathrm{pc} \cdot (N_D)^{-1.07} & \text{if } N_D < 115 \\ 2.6\,\mathrm{pc} & \text{if } N_D > 115 \end{cases} \tag{7.15}$$

thus,

$$\Delta Z_0^{obs} \propto \frac{1}{N_D} \text{ if } N_D < 115 \tag{7.16}$$

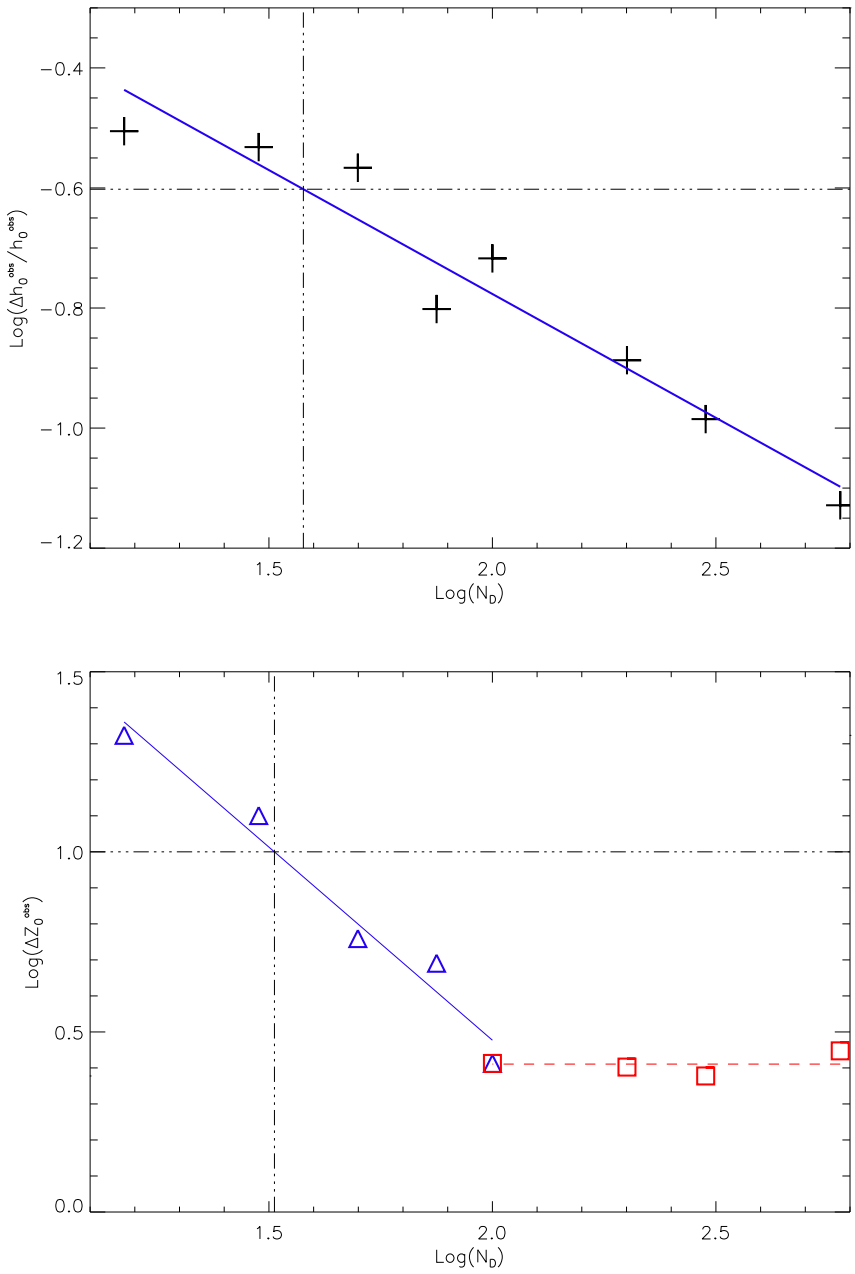


Figure 7.2: (*Top*) Logarithmic plot of scale height relative error against simulated cluster sample size. Black crosses represent the mean values for simulated cluster sample and the solid line represents the fitted power law. The dot-dash lines represent the 25 % uncertainty boundaries on the scale height, which is achieved for a sample size of 38 clusters or more. (*Bottom*) Logarithmic plot of vertical zero point absolute error against simulated cluster sample size. Blue triangles represent the mean values obtained for simulated cluster sample sizes of $N_D < 100$ and red squares for $N_D > 115$. The corresponding coloured lines represent the respective linear fits. The dot-dash lines identifies an error of 10 pc for $Z_0^{obs}$, which is achieved for a sample size of 32 clusters or more.

Note, the constants in Eq. 7.13 and Eq. 7.15 are calculated through comparing the simulated cluster samples against modelled cluster distributions which have parameter values in the range $20 < h_0^{mod} < 1000\,\mathrm{pc}$ and $-160 < Z_0^{mod} < 100\,\mathrm{pc}$ (5 pc step sizes, see Sect. 7.2.1.2). This is important as, if the modelled cluster distributions had different $h_0^{mod}$ and $Z_0^{mod}$ ranges and step sizes, the values of constants in Eq. 7.13 and Eq. 7.15 would change. Most significantly, the constant value of $\Delta Z_0^{obs}$ for $N_D > 115$ is a direct result of the step size, i.e. the simulated cluster samples are sufficiently large that the limiting factor becomes the step size rather than sample size. So for a step size of 5 pc, $\Delta Z_0^{obs} \approx 5/2\,\mathrm{pc}$. Thus if a smaller step size was used, $\Delta Z_0^{obs}$ (for $N_D > 115$) would decrease; if a larger step size was used, $\Delta Z_0^{obs}$ (for $N_D > 115$) would increase.

## 7.4 Potential Improvements

To derive $Z_0^{obs}$ and $h_0^{obs}$, an observed cluster sample is compared to 10441 modelled cluster distributions using 2sKST's to ascertain whether they are drawn from the same parent distribution (Sect. 7.2.1). The resulting KS-statistics are plotted as a function of the modelled cluster distributions $Z_0^{mod}$ and $h_0^{mod}$ values and a 2-D Gaussian function is fitted to the contour to find $Z_0^{obs}$ and $h_0^{obs}$ (Sect. 7.2.2). However, as evidenced by Figure 7.3, symmetry in not always observed in the $Z_0^{mod}$ and $h_0^{mod}$ axes of the non-zero contours. A potential improvement therefore would be to use multivariate central moment fitting to find $Z_0^{obs}$ and $h_0^{obs}$. However, it should be noted that fitting a 2-D Gaussian function has been shown to derive $Z_0^{obs}$ and $h_0^{obs}$ with a good accuracy (Fig. 7.2), and any decrease in the uncertainties of these values gained by finding the multivariate central moment is expected to be statistically small and less than the uncertainties on the cluster distances of observed samples.

## 7.5 Summary

This Chapter has presented a novel method to accurately measure the scale height of cluster samples, which significantly lessens established methods constraints on sample size from a few hundred to 15 clusters. The method was developed to enable the evolution of cluster age and scale height to be traced in detail for the first time (see Chapter 10).

The scale height and vertical zero point (plane of symmetry) of observed cluster samples are determined through a comparison with modelled cluster distributions using a two sample

KS-test. The resultant KS-statistics are fitted with a Gaussian function to find the best fit parameters for the observed cluster sample.

Until now, the scale height and vertical zero point of cluster samples have been determined in the literature by fitting an exponential or $\mathrm{sech}^2$ function to their $Z$-distributions. Unfortunately, a few hundred objects are required to accurately fit the functions, and fail for small sample sizes (e.g. Bonatto et al. (2006)). Using the method presented in this Chapter, the same parameters can be determined with a better than 25 % accuracy in $h_0^{obs}$ for a sample size of 38 or more.

The method is not limited to cluster samples and can be applied to samples of any object type e.g. Planetary and Proto-Planetary Nebulae, Jets, and photo-dissociation regions (Froebrich et al., 2015).

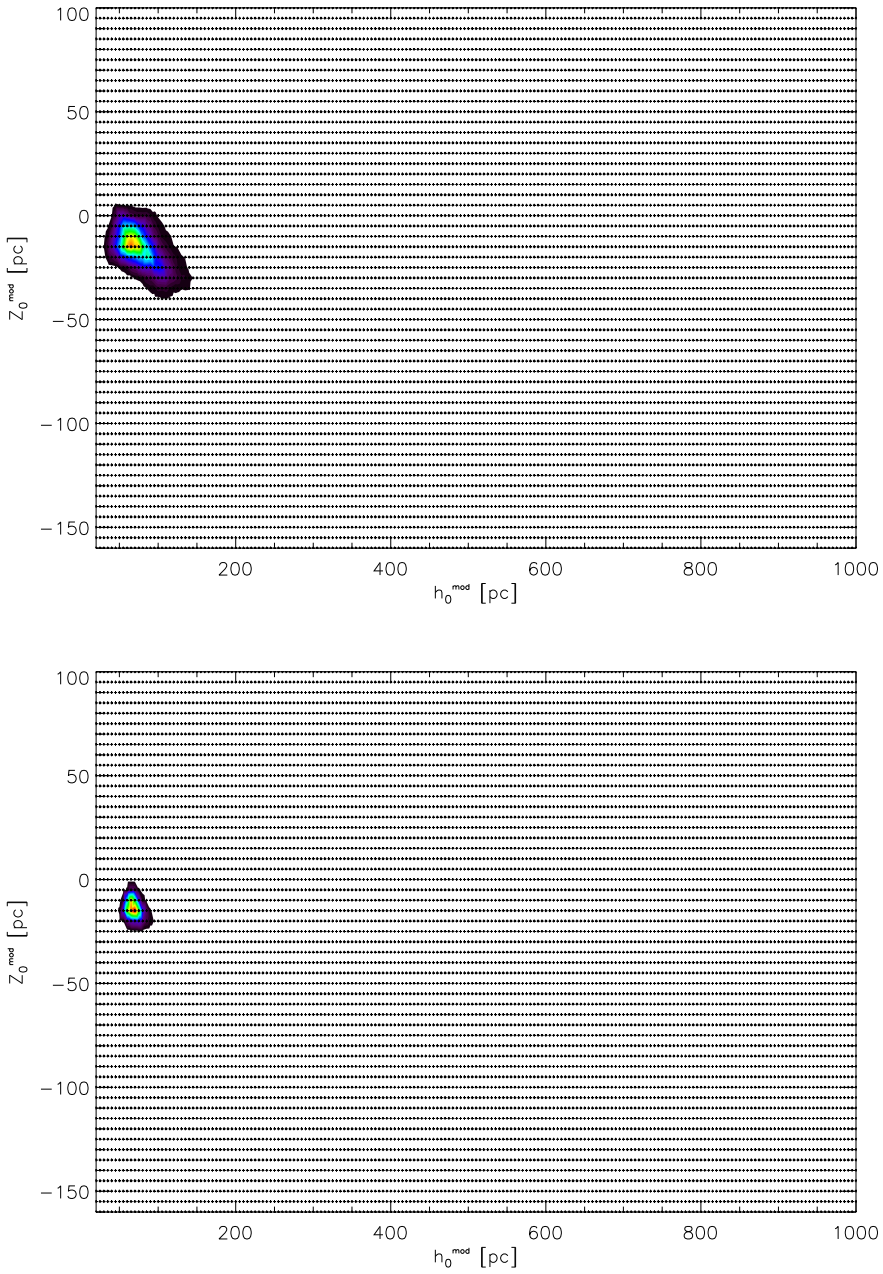


Figure 7.3: Plot of the KS-statistics obtained for an observed cluster sample (*Top*) a sub-sample of CS 1, consisting of clusters positioned in the Third Galactic Quadrant with ages $8.3 < log(age/yr) < 9.0$ and (*Bottom*) a sub-sample of CS 1, consisting of clusters in all four Galactic Quadrants with ages $8.3 < log(age/yr) < 9.0$. Crosses indicate each modelled cluster distribution's $h_0^{mod}$ and $Z_0^{mod}$ values. The colours and contour indicate the highest KS-statistics, i.e. the modelled cluster distributions which are more likely to have been drawn from the same parent distribution as the observed sample: red represents the highest, black the lowest non-zero, and white null. Note the non-symmetric shape of the non-zero contours.

# Part III

# Results

# Chapter 8

# Analysis of the FSR List Catalogue

Until now it has not been possible to collectively analyse the open clusters of the FSR List catalogue, as the task of determining their fundamental properties has been impeded by a severe lack of data, with only 2MASS photometry available for the majority of clusters. Although deeper, higher resolution photometry is available (from e.g. UKIDSS-GPS, GLIMPSE, VISTA-VVV), no survey has, to date, covered the extensive longitudinal and latitudinal range of the catalogue such that the benefit of this additional photometry has only been afforded to a select few clusters. Therefore any attempt to incorporate photometry from these surveys into an analysis of the FSR List catalogue would have had the undesirable effect of shifting the catalogue from one comprised of homogeneously to heterogeneously sourced data. Additionally, such an incorporation would compromise the reliability and validity of results obtained from any subsequently attempted large scale analyses undertaken with the FSR List catalogue. Thus ideally, the properties and distributions of the catalogue's open clusters would be analysed homogeneously utilising photometry from a single source (e.g. 2MASS).

As discussed in Chapters 1 and 2, some progress towards homogeneously analysing the FSR List catalogue has been made through selected sub-samples, in addition to the numerous studies of individual objects for which the deeper, high resolution photometry are available. Most relevant to this Chapter is the work by Froebrich et al. (2010) who determined the ages, distances and extinctions of the catalogue's oldest clusters ($\geq 1$ Gyr) by fitting modelled cluster sequence isochrones to their CCM diagrams which were constructed from 2MASS photometry. Older clusters have the advantage of a typically well defined, bright MS, turn-

off and giants which are prominent on their CCM diagrams, above the 2MASS magnitude limit. In contrast, younger clusters typically have a less defined/bright MS (the majority of which will be below the 2MASS magnitude limit), no turn-off/few (if any) giants and a comparatively larger proportion of PMS objects, i.e. fitting modelled cluster sequence isochrone tracks for older clusters is significantly easier (and more reliable) than for younger clusters. Hence, Froebrich et al. (2010) chose to analyse only the older clusters of the catalogue and the younger clusters have, collectively, remained unstudied in the literature.

In this Chapter, the methods presented in Chapters 4, 5 and 6 are applied to homogeneously derive the distance, extinction and age of the 1021 open clusters and 680 open cluster candidates of the FSR List catalogue using 2MASS photometry. A table of all derived cluster properties is provided in Appendix A. For many of these cluster/candidates this is the first time an attempt to derive their fundamental properties has been made. A global analysis of the Galactic distribution of the sample, as well as individual analyses of the more interesting clusters, is presented and the results are discussed.

## 8.1 Distance Distribution

The distances of 771 FSR List catalogue open cluster/candidates are determined using the automated distance method outlined in Chapter 4. Of these, 377 are clusters previously known in the literature and 394 are new cluster candidates (55 % and 39 % of the total number of objects of these types in the catalogue respectively). The marked discrepancy between the total number of known clusters and new candidates with distance estimates can be attributed to differences in their nature and the distance methodology conditions (see Sect 4.2.1.3). Compared to the known clusters, the new candidates typically have less pronounced features (e.g. poorly defined MS, few/no giants), slightly higher extinctions (Fig. 8.3), fewer members and fewer high quality photometry stars in their cluster/control areas; hence they had remained undetected. As such, many of the new candidates had less than 30 A-sample stars in their cluster and control areas, i.e. they failed to meet the conditions of the distance methodology and were excluded from further analysis.

Of course, it is also reasonable to expect that a proportion of the new candidates which were excluded are asterisms. Indeed, Froebrich et al. (2007) determined that only $\sim 50$ % of the total number of new candidates are real, and candidates with less members are more likely to be asterisms. Spatial analyses of selected sub-samples of the FSR List cluster candidates

by Bica et al. (2008) and Camargo et al. (2010) agree with this assessment. Furthermore, an examination of the ratio of cluster members to field stars shows that, on average, its value is twice as high for the known clusters than for the new candidates (Buckner and Froebrich, 2013), i.e. the more pronounced objects have a higher likelihood of being real.

However, this raises an important question: how many of the new candidates with distance estimates are actually real? From the above evidence at least three quarters of the sample are expected to be real, i.e. the contamination of the sample is less than 25 %. In addition, an inspection of the DAML02 catalogue reveals that, to date, 276 of the new candidates ($\sim 27$ % of the total contained in the FSR List catalogue) have been confirmed by the community and have distance, extinction and age values listed in the database. Furthermore, due to the condition that new candidates had to have a minimum of 30 A-sample stars in their cluster/control areas to be included in this analysis, it is reasonable to assume that the majority of asterisms have been excluded.

Figure 8.1 shows the Galactic distribution of the sample of clusters whose distance have been determined. As noted by Froebrich et al. (2007) there is distinct lack of clusters within $\pm 60^\circ$ of the GC in the FSR List catalogue, which is due to the high field star density associated with this region, i.e. there is a low contrast between clusters' and the field. Only clusters that appeared as significant density enhancements on the field were detected in 2MASS and hence are present in the catalogue.

The sample is distributed between about 1 kpc−12 kpc distance from the Sun, and has an average projected number density peak of 15 clusters per sq/kpc at 3 kpc. This density drops significantly either side of the peak, down to about half at 4 kpc. Towards larger distances clusters appear more compact, and so many would not have originally been included in the catalogue due to its apparent radii selection effect (Froebrich et al., 2010). Towards smaller distances clusters appear angularly extended, so were either (a) not included in the original catalogue due to the apparent radii selection effect, or (b) excluded from this analysis as their apparent radius was greater than $0.05^\circ$ (see Sect. 4.2.1.3). Furthermore, as the observed scale height of clusters increases with age (Moitinho (2010), Buckner and Froebrich (2014)), and the catalogue is latitude limited, it is reasonable to expect a lack of older open clusters in the Solar Neighbourhood, similar to that observed by Kharchenko et al. (2013) for the MWSC catalogue. Finally, it should be noted that at particularly small distances from the Sun (such as within 1 kpc), the density of field stars foreground to the clusters is extremely low, such that the accuracy of determined distances should be treated with caution.

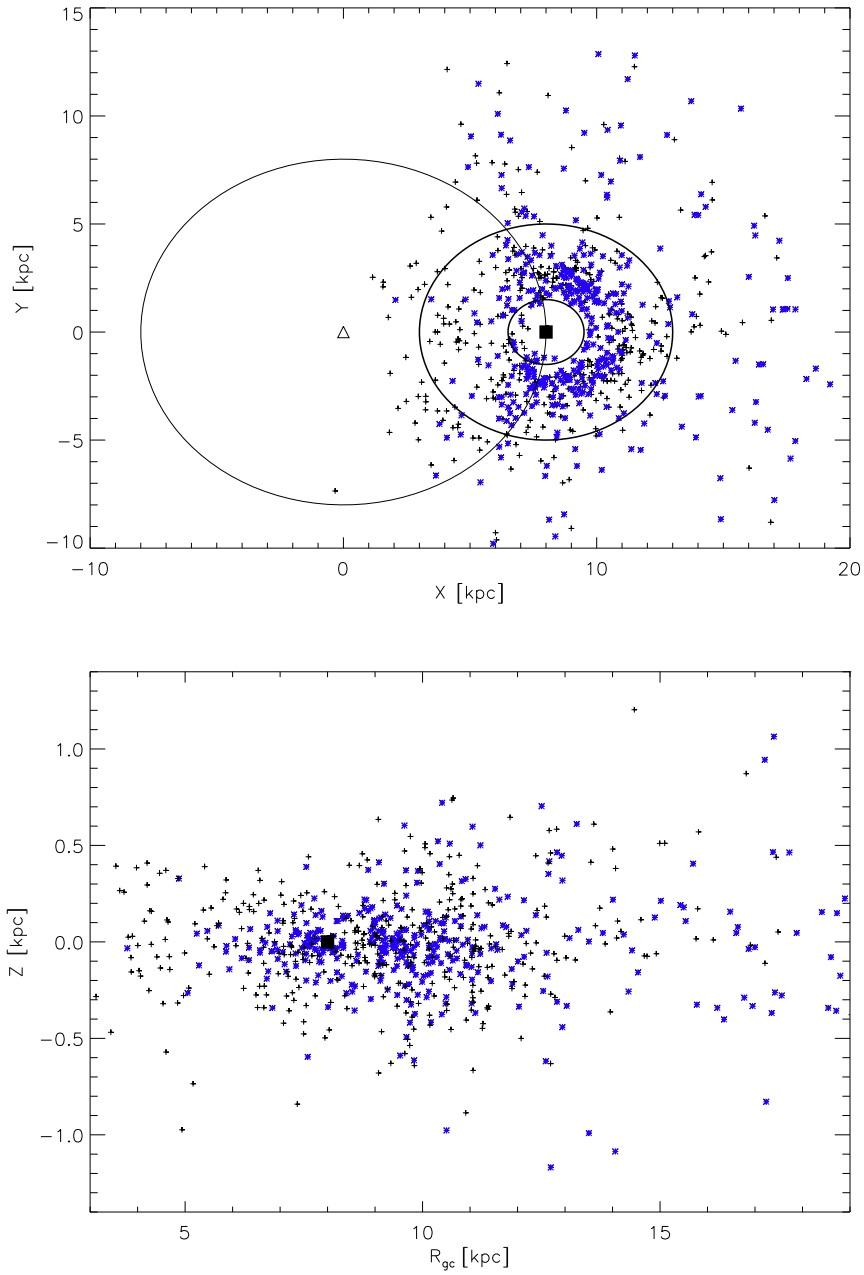


Figure 8.1: Plot of the distribution of the FSR List catalogue open clusters with derived distances (*Top*) in the Galactic Plane and (*Bottom*) as a function of their height, Z, above and below the Galactic Plane and Galactocentric distance, $R_{GC}$. Blue stars represent the known clusters and black crosses the new candidates. The Galactic Centre is represented by a black triangle and the Sun a filled black square. Concentric circles mark distances of 1.5 kpc and 5 kpc from the Sun which assumed to be at $R_{GC} = 8$ kpc as indicated by the largest circle.

The scale height of various sub-samples is determined. Clusters with a distance greater than 5 kpc are excluded from the measurement as they are typically further away from the Galactic mid-plane, and so would have been easier to detect due to extinction, i.e. their inclusion would have biased the scale height measurements. The new candidates and known clusters in the sample have a scale height of 315 ± 30 pc and 235 ± 20 pc, respectively. As discussed, the new candidates are typically less prominent than the known clusters, hence it would have been easier to detect them (and capture high quality photometry) away from the mid-plane where the field star density is lower and there is less stellar crowding. Similarly, known clusters typically appear as prominent overdensities (hence they have been previously detected), so it is easier to detect them in the mid-plane where the field star density is higher. Using the scale height age relation by Buckner and Froebrich (2014) (Fig. 6 and Eq. 7 therein), the new candidates are typically older than the known clusters with typical ages of ∼2.3 Gyr and ∼1.9 Gyr respectively.

## 8.2 Extinction Distribution

Extinction estimates are determined for 775 FSR List catalogue clusters (of which 771 have a distance estimate) using the automated extinction method outlined in Chapter 5. Two $H$-band extinction values were derived for each cluster in the sample from their measured median colours: (i) $A_H^{HK}$ from $[H-K]$ and (ii) $A_H^{H45}$ from $[H-4.5]$. Figure 8.2 shows that there is generally good linear one:one agreement between $A_H^{HK}$ and $A_H^{H45}$ for the majority of clusters in the sample, with scatter of 0.18 mag after fitting to the $3\sigma$ level (independent of distance). Figure 8.3 shows the extinction distributions of the sample. The majority of clusters have a $H$-band extinction in range 0 mag$\leq A_H^{HK,H45} \leq$ 2 mag, peaking between 0.1-0.2 mag.

In principle, $A_H^{H45}$ should be a more reliable measure of extinction than $A_H^{HK}$ as the $[H-4.5]$ colour measures the spectral energy distribution in the Rayleigh-Jeans part of the spectrum, and thus is almost independent of stellar spectral type and luminosity class (Majewski et al., 2011). This is unlike the intrinsic value of the $[H-K]$ colour which varies with stellar spectral type and luminosity class. However, in application $A_H^{HK}$ is the more reliable measure of extinction as clusters $H$- and $K$-band photometry were taken from the 2MASS survey and 4.5$\mu$m band photometry from the WISE survey, i.e. as only $\sim 50\,\%$ of 2MASS objects with a Qflag of "AAA" are detected by WISE, $A_H^{H45}$ is biased towards the brightest (redder)

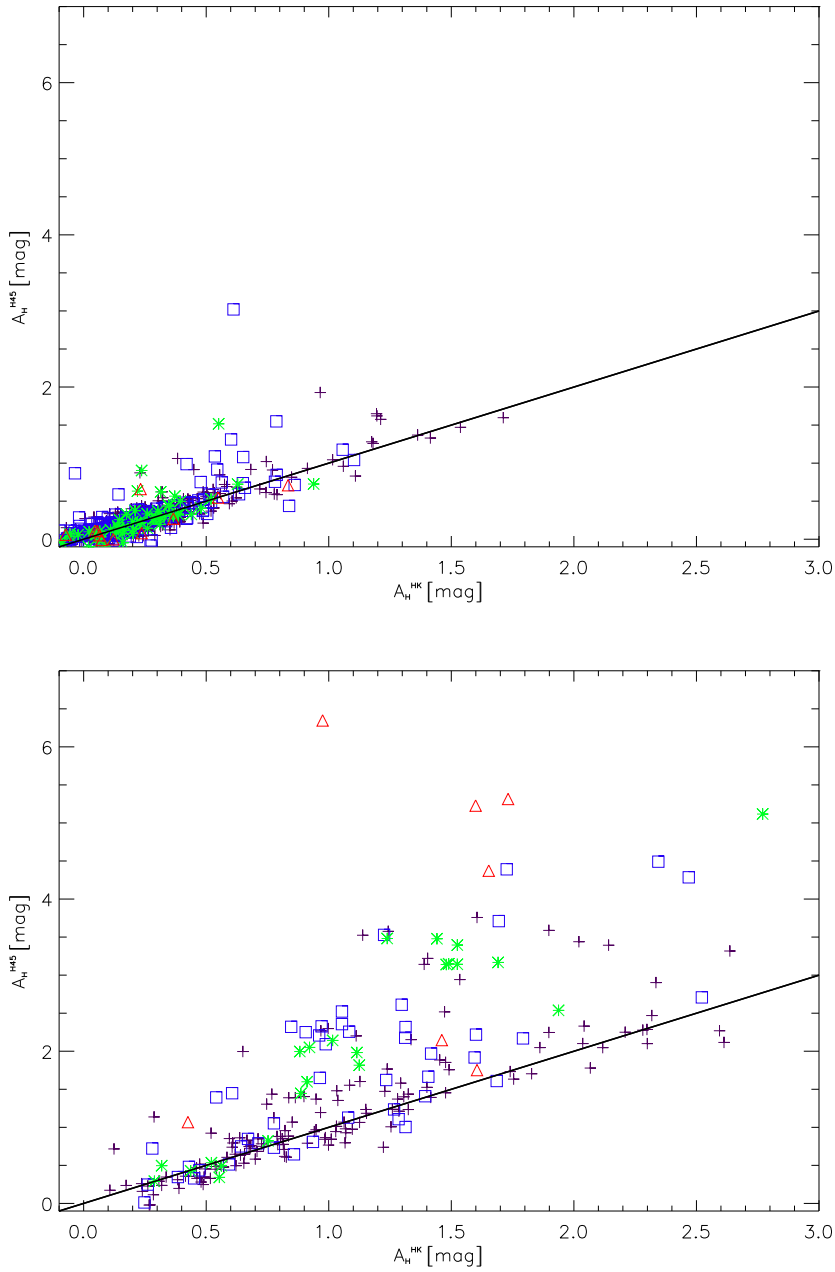


Figure 8.2: Plot of $A_H^{HK}$ against $A_H^{H45}$ of the sample, for clusters with distance estimates of (*Top*) less than 5 kpc and (*Bottom*) greater than 5 kpc or for which none were made. Symbols indicate the YSO fraction, $Y_{frac}$, of the clusters: red triangles for $Y_{frac} > 0.10$, green stars for $0.05 < Y_{frac} < 0.10$, blue squares for $0.01 < Y_{frac} < 0.05$ and purple crosses for $Y_{frac} < 0.01$. See text for details. The solid black one:one line has been fitted to the $3\sigma$ level.

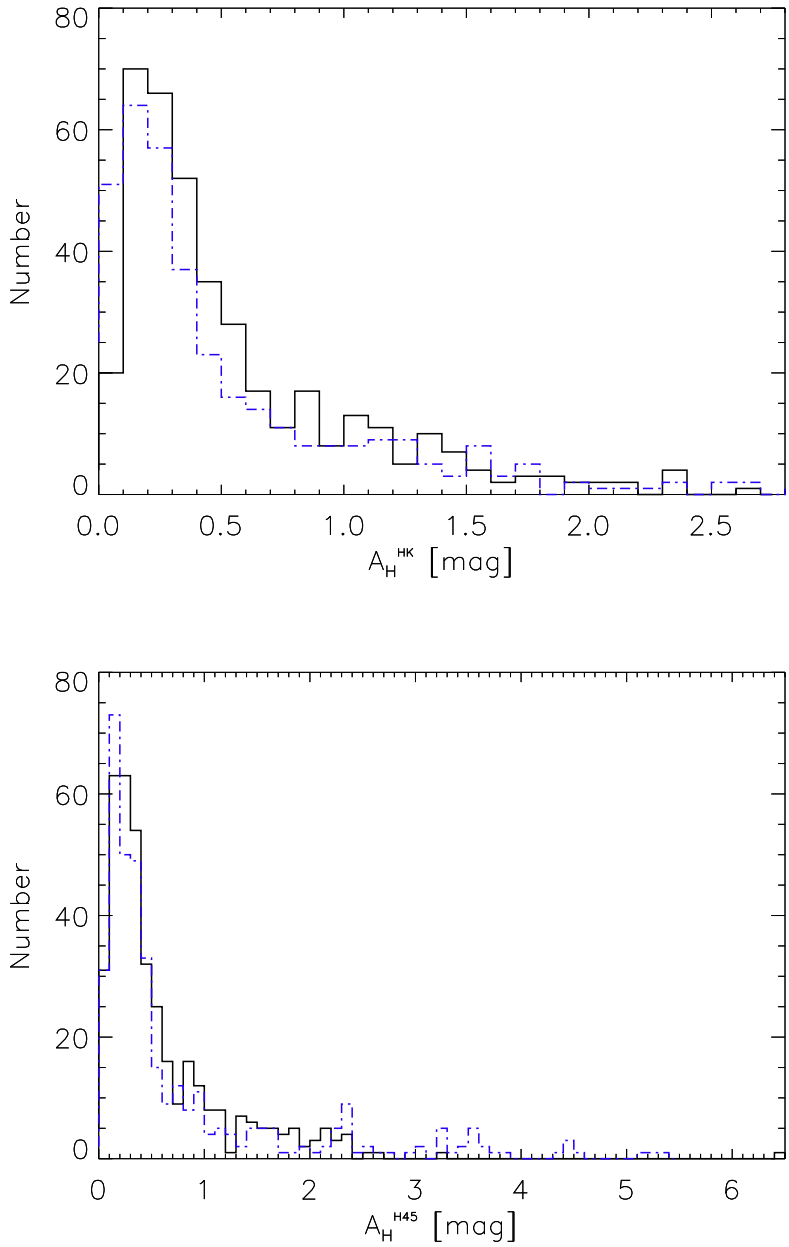


Figure 8.3: Histogram showing the distribution of the $H$-band extinctions of the clusters in the sample, measured from their median (*Top*) $[H-K]$ and (*Bottom*) $[H-4.5]$ colours. The distributions of the new candidates and known clusters in the sample are represented by solid black and dashed blue lines respectively.

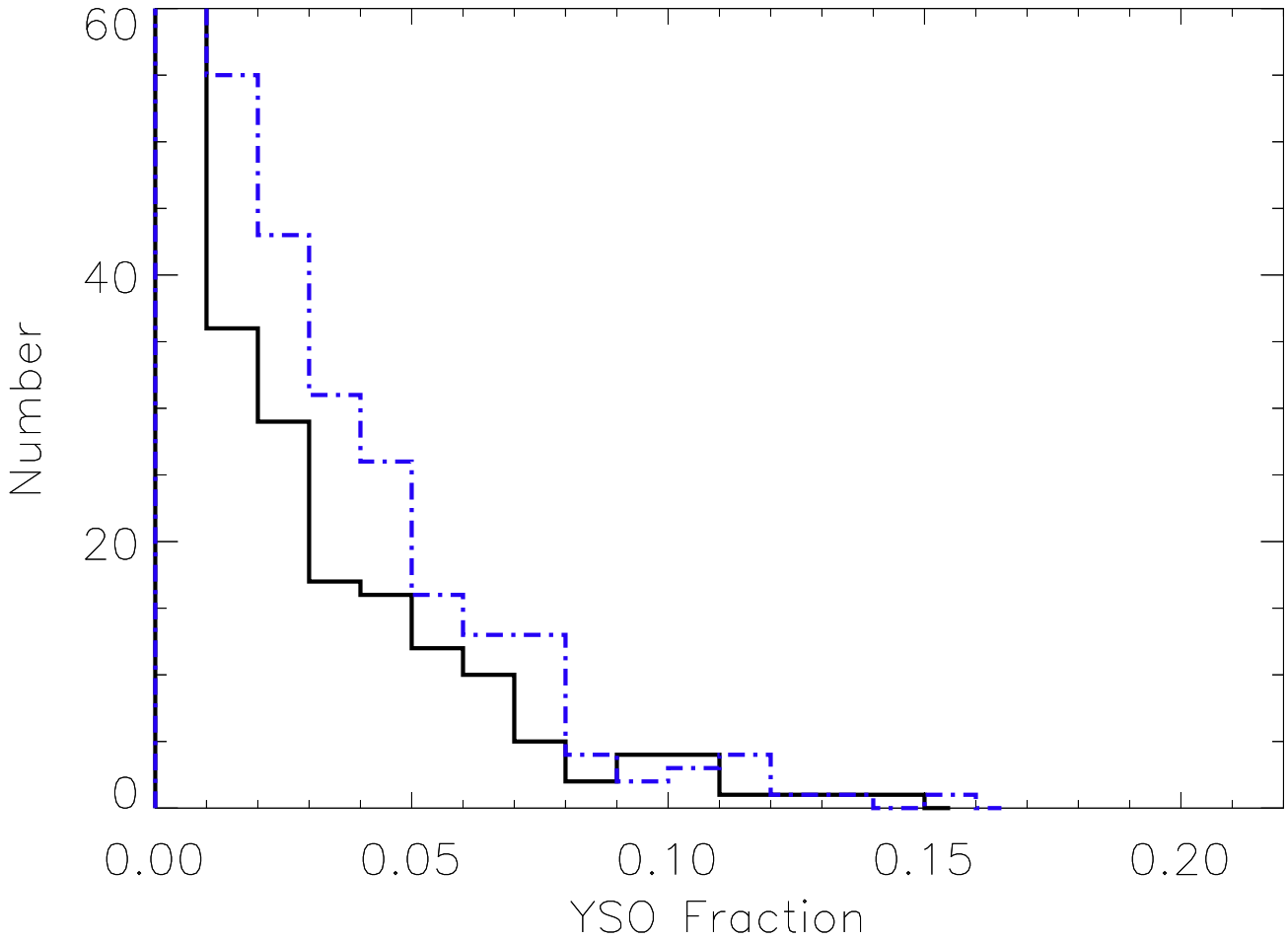


Figure 8.4: Histogram showing the YSO fraction distribution of the sample. The solid black line shows the distribution of the new candidates and the dashed blue line shows the distribution of the known clusters. Note, the first bin ($Y_{frac} = 0$) contains 258 new candidates and 165 known clusters.

objects. Naturally this bias is exaggerated at larger distances where foreground extinction will be typically higher, and so the correction for large foreground extinction (Sect. 4.2.4.1) cannot fully compensate for this effect. The effect of a large fraction of intrinsically red members (e.g. YSOs) must also be considered, as the bias on $A_H^{H45}$ will be particularity prominent for those clusters which are likely to be young and also associated with a GMC (where fainter or bluer members are potentially occluded). Hence, the cause of obvious outliers in Figure 8.2 is most likely due to only the brightest (reddest) members of the clusters being detected in WISE (i.e. 4.5$\mu$m), which has consequently increased the measured $A_H^{H45}$ value.

The fraction of YSOs, $Y_{frac}$, in each cluster in the sample is determined. Note, the $Y_{frac}$ values are a lower limit as L-band photometry was not available for the entire sample so L-band excess stars were not included in the calculations. The majority of clusters were found to have no YSO objects (Figure 8.4), suggesting that the sample is dominated by older clusters and has none younger than 4 Myr (Lada and Lada, 2003) which concurs with the ages derived in Sect. 8.1 from the scale height relation by Buckner and Froebrich (2014). Figure 8.2 demonstrates that, as expected, clusters with the highest fraction of YSO objects ($Y_{frac} > 0.1$) display a higher discrepancy between $A_H^{H45}$ and $A_H^{HK}$ than those with a lower fraction of YSO objects. After splitting the sample into potentially older ($Y_{frac} < 1\,\%$) and younger ($Y_{frac} > 1\,\%$) clusters, scale heights are determined of $300 \pm 20$ pc and $190 \pm 15$ pc respectively.

## 8.3 Age Distribution

The ages of 298 FSR List catalogue clusters are determined using the pipeline outlined in Chapter 6. Of these, 216 are known and 82 new candidates are confirmed as real. Based on the number of objects of these types in the sample, ages were successfully determined for 57 % and 21 % of the known and new candidates, respectively.

The lack of new candidates in the sample can, again, be attributed to their nature as discussed in Sect. 8.1, i.e. a poorly defined MS and lack of prominent features made fitting modelled cluster sequence isochrone tracks to their CCM diagrams, and thus age determinations, impossible. The CCM diagrams of the confirmed new candidates, like the known clusters, generally exhibited well defined MS and associated features. As expected, a proportion of the new candidates were confirmed as asterisms. Unfortunately the few overdensities of this variety exhibited cluster-type characteristics (believable radial star density profiles,

more than 30 stars in the cluster/control areas and sources with similar $H$- and $K$-band magnitudes) and thus had not previously been excluded from the analysis.

The sample ranges between 5 Myr and 10 Gyr with the majority of clusters in the 10 Myr to 5 Gyr range (Fig. 8.5). There is a deficit of clusters younger than 10 Myr in the sample which is expected as the majority of these objects will be embedded and thus more difficult to detect using 2MASS photometry. The mode of the sample's age distribution is $\sim 400$ Myr, which is slightly higher than the DAML02 and WEBDA catalogues which have a modal age value of $\sim 200$ Myr. It is important to investigate why the sample has a larger modal age value: does the pipeline derive ages that are systematically too old for the clusters? A comparison between the ages derived for the sample here and those given for them by the MWSC catalogue does not favour this position as the two sets of age values are in good linear agreement, albeit with a few clusters which are a factor of 10 or more out (most likely caused by an incorrect assumption that these clusters have a Solar metallicity, or incorrectly cross-identified). Removing these outliers, the two sets of age values have a Pearson correlation coefficient of $\rho = 0.73$ and a scatter of 0.19 for $log(age/yr)$.

Other considerations include the methods by which objects in the FSR List catalogue were discovered, and conditions under which the properties of the sample are derived, which perhaps do not favour younger clusters. Firstly, (as previously discussed) the FSR List catalogue was discovered using 2MASS star density maps, i.e. objects had to appear as strong over-densities to be distinguished from the field population. Therefore as younger clusters are typically closer to the Galactic mid-plane (and some will be associated with nebulosity), it is reasonable to assume that a proportion of those 'missing' from the sample are not present in the catalogue. Secondly, there were a set of quality control conditions that were required of all clusters for their extinctions and ages to be derived, which did not favour the (potentially) younger candidates of the FSR List catalogue. For example, one of the conditions required that objects had to have at least 30 A-sample stars in the cluster/control areas for their extinction to be derived, which would have potentially excluded many of the younger candidates due to associated nebulosity. Similarly, cluster ages were derived through successfully fitting modelled cluster sequence isochrones to their CCM diagrams, which is biased against younger clusters as they typically have less MS stars that are above the 2MASS magnitude limit i.e. accurate isochrone fits (and thus age determinations) can be extremely difficult.

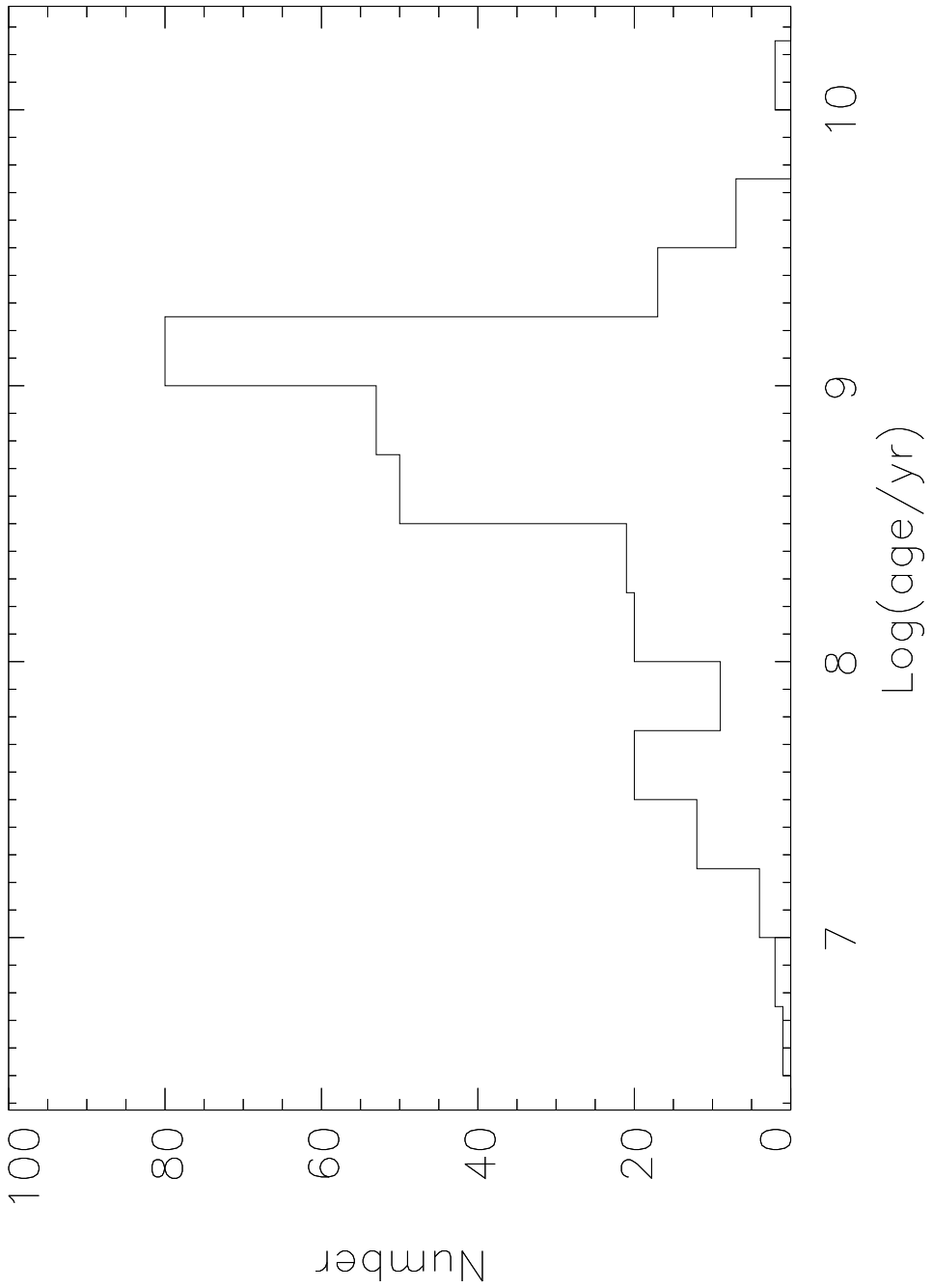


Figure 8.5: Histogram showing the age distribution of the sample.

### 8.3.1 Comparison of Distributions

The distance and extinction estimates of the sample were refined using the pipeline described in Chapter 6 (see Sect. 6.2). As such, it is important to compare the two sets of values to identify any significant differences that could indicate an error in either methodology which has been overlooked.

Herein, the distance estimates derived in Sect. 8.1 using the automated methodology shall be referred to as $D^{meth}$, and the refined distance estimates as $D^{iso}$. Figure 8.6 shows that there is a linear correlation between the $D^{meth}$ and $D^{iso}$, with a Pearson coefficient of $\rho = 0.89$ and a scatter of 63 %. The refined distance estimates are approximately a factor of 1.25 smaller than $D^{meth}$. Clusters at distances smaller than 3 kpc show the largest scatter as these are the clusters which have very few identified foreground stars, i.e. the more foreground stars the smaller the relative error on $D^{meth}$.

As discussed in Sect. 8.2, $A_H^{HK}$ is more reliable than $A_H^{H45}$, and so this is the $H$-band extinction that will be used for the comparison. Herein, the refined extinction estimates shall be referred to as $A_H^{iso}$. Figure 8.7 shows that there is a very strong linear correlation between $A_H^{HK}$ and $A_H^{iso}$, with a Pearson coefficient of $\rho = 0.95$ and a scatter of 9 %.

It is expected for there be a stronger linear agreement between the two sets of extinction values than the distance values. To determine $D^{meth}$ many steps were required to first estimate and calibrate the number density of stars foreground to each cluster ($\rho_{fg}^{cl}$), leading to an accumulation of errors where even very small inaccuracies in the value of $\rho_{fg}^{cl}$ can potentially lead to significant errors on $D^{meth}$. In contrast, only the median $[H-K]$ colour of the clusters members needed to be measured to derive $A_H^{HK}$, and small inaccuracies in this measurement do not significantly affect the accuracy of $A_H^{HK}$.

Two sample Kolmogorov- Smirnov tests (2sKST's) are used to assess if the following sub-samples are drawn from the same parent distribution:

- **S1** FSR List clusters with $Y_{frac} < 5\,\%$ (potentially old clusters)
- **S2** FSR List clusters with $Y_{frac} > 5\,\%$ (potentially young open clusters)
- **S3** All known open clusters in the FSR List catalogue
- **S4** All new open cluster candidates in the FSR List catalogue

Table 8.1: Table of 2sKST statistics (unit: %) of various sub-samples. Note that only statistics $< 1\,\%$ and $> 99\,\%$ are significant.

| | S1 | S2 | S3 | S4 | S5 | S6 | S7 | S8 | S9 | S10 |
|---|---|---|---|---|---|---|---|---|---|---|
| S1 | — | **0.25** | **0.06** | 2.53 | **0.43** | 32.75 | 52.85 | 13.66 | 6.37 | 10.98 |
| S2 | **0.25** | — | 39.51 | 4.07 | 9.89 | 9.61 | 3.28 | 15.72 | 2.17 | 2.95 |
| S3 | **0.06** | 39.51 | — | **0.51** | 15.40 | 9.02 | 1.99 | 28.99 | 2.52 | **0.37** |
| S4 | 2.53 | 4.07 | **0.51** | — | 44.59 | 3.31 | 7.47 | 11.77 | 7.77 | **0.05** |
| S5 | **0.43** | 9.89 | 15.40 | 44.59 | — | 4.21 | 3.79 | 15.10 | 6.20 | **0.06** |
| S6 | 32.75 | 9.61 | 9.02 | 3.31 | 4.21 | — | 44.91 | 98.62 | 12.80 | 56.28 |
| S7 | 52.85 | 3.28 | 1.99 | 7.47 | 3.79 | 44.91 | — | 14.69 | 6.04 | 95.75 |
| S8 | 13.66 | 15.72 | 28.99 | 11.77 | 15.10 | 98.62 | 14.69 | — | 25.24 | 31.14 |
| S9 | 6.37 | 2.17 | 2.52 | 7.77 | 6.20 | 12.80 | 6.04 | 25.24 | — | **0.61** |
| S10 | 10.98 | 2.95 | **0.37** | **0.05** | **0.06** | 56.28 | 95.75 | 31.14 | **0.61** | — |

- **S5** All open clusters in the FSR List catalogue
- **S6** FSR List clusters with an age estimate
- **S7** New cluster candidates in the FSR List catalogue with an age estimate
- **S8** Known open clusters in the FSR List catalogue with an age estimate
- **S9** FSR List clusters with $log(age/yr) \geq 9$ (old clusters)
- **S10** FSR List clusters with $log(age/yr) < 9$ (young open clusters)

Table 8.1 reveals that clusters with a low fraction of YSOs (S1) or that are young (S10) show the most dissimilarity to the other sub-samples. The (potentially) old and young samples (S9/S10 and S1/S2) possess significantly different distributions which suggests either a detection bias on the FSR List catalogue, a bias on the methodologies used to derive cluster properties, a physical effect, or some combination of all three.

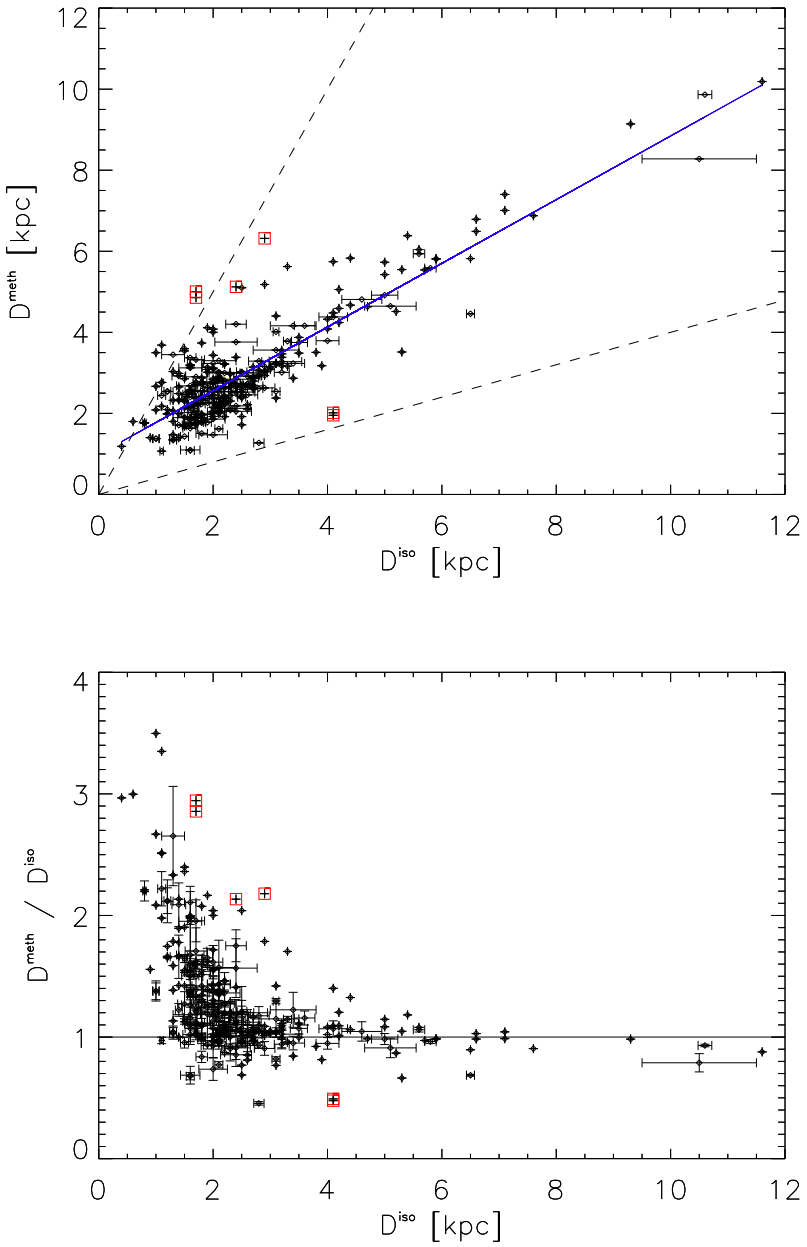


Figure 8.6: Plots comparing the refined distance estimates, $D^{iso}$, with those initially derived for the sample, $D^{meth}$. (*Top*) The black dashed lines mark a 40 % discrepancy between the two sets of values and the solid blue line represents the best linear fit to the data with $3\sigma$ clipping. (*Bottom*) The solid black line represents the one:one relationship (not fitted). In both plots, black diamonds and red squares represent clusters which have been included and excluded (respectively) from the linear fit in the *Top* plot.

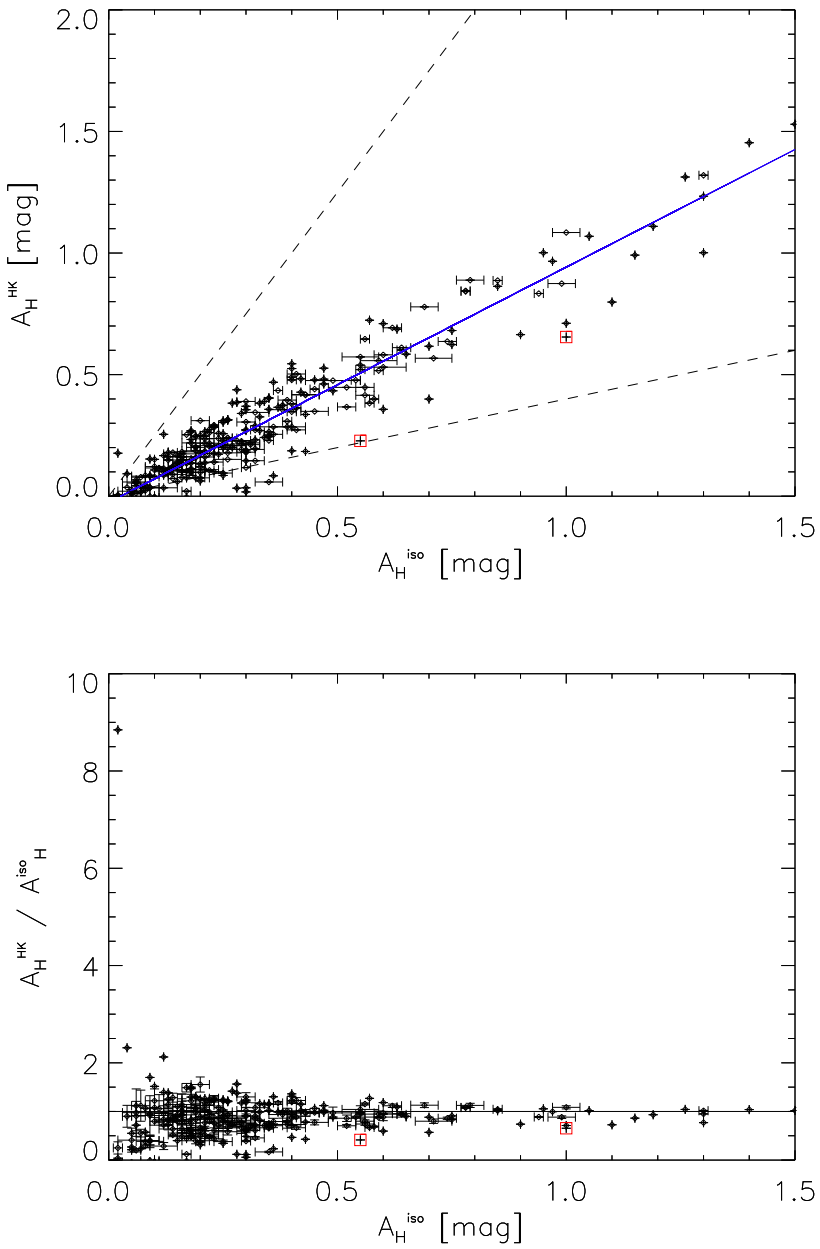


Figure 8.7: Plots comparing refined $H$-band extinction estimates for the sample, $A_H^{iso}$, with those initially derived from the clusters median $[H-K]$ colour, $A_H^{HK}$. (*Top*) The black dashed lines mark a 40 % discrepancy between the two sets of values and the solid red line represents the best linear fit to the data with $3\sigma$ clipping. (*Bottom*) The solid black line represents the one:one relationship (not fitted). In both plots, black diamonds and red squares represent clusters which have been included and excluded (respectively) from the linear fit in the *Top* plot.

## 8.4 Selected Individual Clusters

Following the above analysis, it became apparent that some objects in the FSR List catalogue warranted further investigation. These clusters have high resolution photometry available from either the UKIDSS-GPS or VISTA-VVV surveys and are: (i) suspected to contain a large number of PMS members, or (ii) at notable Galactocentric distances. In this Section their fundamental properties are redetermined using the pipeline described in Chapter 6 and the results are discussed. Cluster CCM diagrams were constructed using photometry from the UKIDSS-GPS/VISTA-VVV surveys for point sources at $K < 12$ mag, and 2MASS for point sources brighter than $K > 12$ mag as these bright members tend to be the earlier spectra types. A summary of the refitted properties is provided in Table 8.2.

### 8.4.1 Clusters with PMS Stars

Typically, the CCM diagrams of clusters which are suspected to have a large proportion of PMS stars had no markers to fit modelled cluster sequence isochrones to as only their brightest member stars were visible above the 2MASS $K$-band magnitude limit. Obviously, the properties derived/refined for these clusters in Sect. 8.3 are therefore questionable (and are certainly less reliable than for the rest of the sample), as with variable distance and extinction values there is little difference between the fit of a (e.g.) 10 Myr or 90 Myr modelled PMS isochrone to their brightest members. Hence, deeper magnitude photometry is required to derive accurate properties for these clusters and to confirm that these clusters' members are predominantly PMS.

In total 19 clusters were flagged as potentially having a large number of PMS members, of which UKIDSS-GPS survey photometry was available for 9. These are: FSR0195, FSR0207, FSR0301, FSR0636, FSR0718, FSR0794, FSR0870, FSR0904 and FSR1189.

**FSR0195:** A confirmed new cluster candidate, located in the first Galactic Quadrant. Its CCM diagrams (Fig. 8.8) show a young open cluster with a PMS track. The cluster has a redetermined Solar distance of $d = 3.00$ kpc, age of 37 Myr and a $H$-band extinction of $A_H = 1.10$ mag. The revised age and extinction values are consistent with those determined in Sect. 8.3. The revised distance is approximately 1.5 times greater, as the addition of dimmer stars below the 2MASS magnitude limit has helped to more accurately constrain its value.

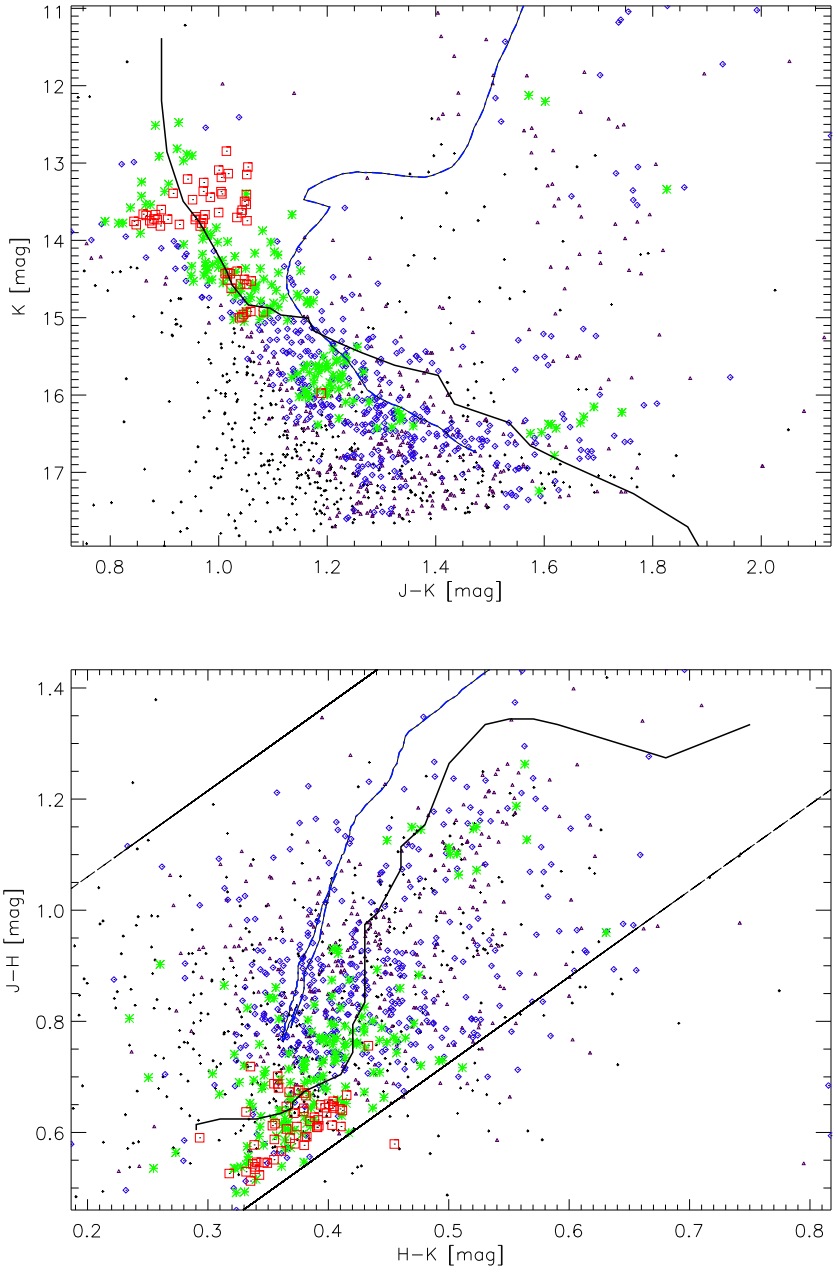


Figure 8.8: (*Top*) Colour-Magnitude and (*Bottom*) Colour-Colour diagrams of **FSR0195**. Photometric membership probabilities are determined for stars within $2 \times r_{cor}$, with $N = 15$ and are represented as follows: $P^i_{cl} \geq 80\%$ red squares; $60 \leq P^i_{cl} < 80\%$ green stars; $40 \leq P^i_{cl} < 60\%$ blue diamonds; $20 \leq P^i_{cl} < 40\%$ purple triangles; $P^i_{cl} < 20\%$ black plus signs. The best fitting modelled cluster sequence, as determined in Sect. 8.4, is plotted as a solid black isochrone. The dashed blue isochrone represents the best fitting modelled cluster sequence as determined by the MWSC catalogue. The parallel black lines in the Colour-Colour plot represent the reddening bands of the cluster.

FSR0195 features in the MWSC catalogue (Sect. 2.1) whose authors used their data processing pipeline and 2MASS photometry to derive the properties of the cluster (see Sect. 2.1 for a detailed description and discussion of this catalogue). The catalogue gives extinction and distance values which are slightly smaller than the revised values. Most notably, the age estimate is markedly older at 2.2 Gyr. An inspection of the CCM diagrams diagrams of FSR0195 clearly show that it is much younger than this value and therefore the values given by the MWSC catalogue are inaccurate, most likely caused by a combination of the systematic nature of their pipeline, and use of only the lower resolution 2MASS photometry (as the dimmer cluster stars cannot be detected).

**FSR0207:** A previously known cluster (IC 4996), located in the first Galactic Quadrant in the Cygnus constellation. Its CCM diagrams (Fig. 8.9) show a young open cluster with a PMS track. The redetermined properties of FSR0207 are $d = 1.20$ kpc, age of 20 Myr and $A_H = 0.25$ mag, which are in general agreement with the values derived in Sect. 8.3, albeit giving a slightly older age but smaller distance and extinction for the cluster.

A search of the literature reveals that the cluster has been extensively studied and it is generally agreed to have an age of $\sim 10$ Myr, Solar distance $\sim 1.9$ kpc and $H$-band extinction of $\sim 0.35$ mag, i.e. younger, further and more reddened than the revised values presented here suggest (see Table 8.2). However, it should be noted that authors predominantly used UBVRI photometry to derive these values and IRAS maps have shown there to be an IR dusty shell surrounding the cluster which is associated with the nearby Berkeley 87 (Lozinskaya and Repin, 1990). As such, the UKIDSS-GPS JHK photometry utilised here has a distinct advantage, revealing the dimmer stars in the cluster sequence which are crucial to accurately fit modelled cluster sequence isochrones to the CCM diagrams of FSR0207 (and derive the cluster's fundamental properties). The presence of PMS stars in FSR0207 has previously been confirmed through photometric and spectral analysis (see e.g. Delgado et al. (1999), Delgado et al. (1998), Zwintz et al. (2004), Zwintz and Weiss (2006), Bhavya et al. (2007)).

**FSR0301:** A previously known cluster (Berkeley 55), located in the second Galactic Quadrant in the Cygnus constellation. Its CCM diagrams (Fig. 8.10) show a young open cluster with a PMS track. The scattering of the brightest objects at the top of the MS could be real or could be caused by misidentification of members. The cluster's properties are redetermined as $d = 4.00$ kpc, age of 40 Myr and $A_H = 1.00$ mag. The revised age and extinction values are in agreement with those derived in Sect. 8.3, but the revised distance value is a factor of

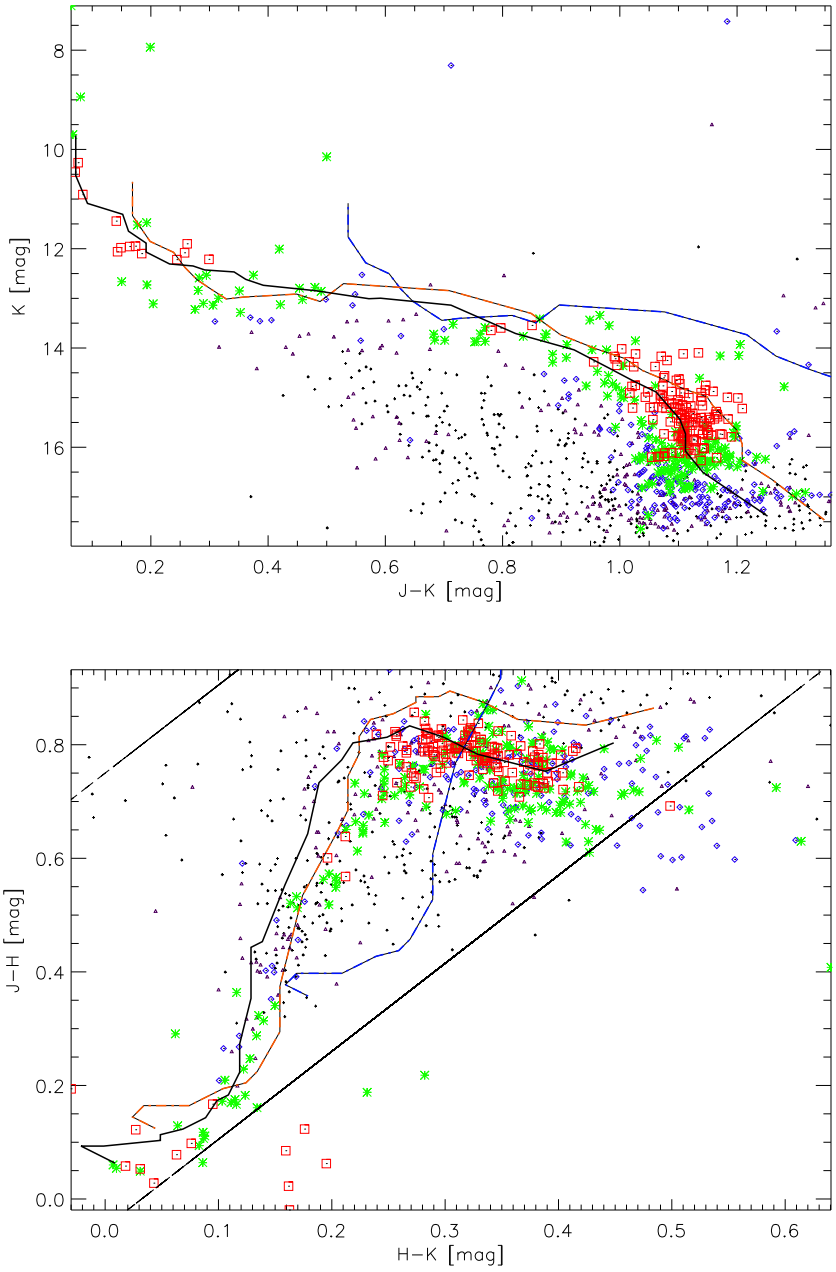


Figure 8.9: (*Top*) Colour-Magnitude and (*Bottom*) Colour-Colour diagrams of **FSR0207**. Photometric membership probabilities are determined for stars within $2 \times r_{cor}$, with $N = 15$ and are represented as follows: $P^i_{cl} \geq 80\%$ red squares; $60 \leq P^i_{cl} < 80\%$ green stars; $40 \leq P^i_{cl} < 60\%$ blue diamonds; $20 \leq P^i_{cl} < 40\%$ purple triangles; $P^i_{cl} < 20\%$ black plus signs. The best fitting modelled cluster sequence, as determined in Sect. 8.4, is plotted as a solid black isochrone. The dashed orange and blue isochrones represent the best fitting modelled cluster sequences as determined by Lynga (1995) and the MWSC catalogue respectively. The parallel black lines in the Colour-Colour plot represent the reddening bands of the cluster.

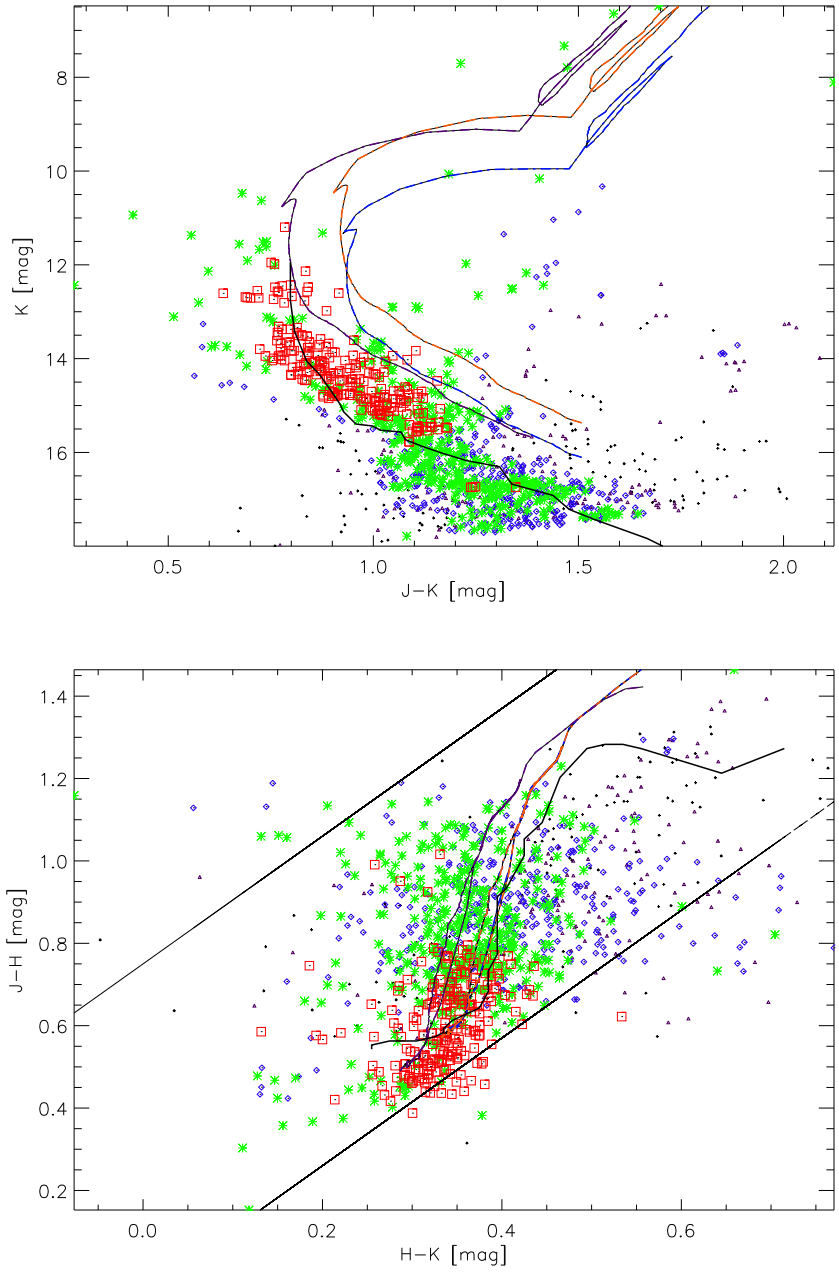


Figure 8.10: (*Top*) Colour-Magnitude and (*Bottom*) Colour-Colour diagrams of **FSR0301**. Photometric membership probabilities are determined for stars within $2 \times r_{cor}$, with $N = 15$ and are represented as follows: $P^i_{cl} \geq 80\%$ red squares; $60 \leq P^i_{cl} < 80\%$ green stars; $40 \leq P^i_{cl} < 60\%$ blue diamonds; $20 \leq P^i_{cl} < 40\%$ purple triangles; $P^i_{cl} < 20\%$ black plus signs. The best fitting modelled cluster sequence, as determined in Sect. 8.4, is plotted as a solid black isochrone. The dashed purple, orange and blue isochrones represent the best fitting modelled cluster sequences as determined by Tadross (2008), Maciejewski and Niedzielski (2007) and the MWSC catalogue respectively. The parallel black lines in the Colour-Colour plot represent the reddening bands of the cluster.

two larger. This was expected as although the cluster sequence is strongly defined, the majority of stars on it are below the 2MASS magnitude limit (i.e. not visible when the distance value was originally determined), and in the absence of its associated markers an accurate distance determination through isochrone fitting is difficult.

The revised values for FSR0301 are in complete agreement with Negueruela and Marco (2012) who conducted an in depth study of the cluster using UBVJHK photometry and $z$-band spectra. Other studies determined the cluster to have a significantly smaller Solar distance and to be much older at $\sim 300$ Myr (Tadross (2008), Maciejewski and Niedzielski (2007) and the MWSC catalogue), which is most likely a result of member misidentification. To demonstrate this, the reader is referred to Figure 8.10. Here it is shown that if objects within the ranges $6\,\mathrm{mag} \leq K \leq 10.5\,\mathrm{mag}$ and $1.2\,\mathrm{mag} \leq [J-H] \leq 2.2\,\mathrm{mag}$ are assumed part of the cluster, an age of about 300 Myr is derived. However, the CCM diagrams clearly show this 300 Myr isochrone is too old for the cluster, which is a notably poor fit to the cluster sequence below $K \approx 13\,\mathrm{mag}$. Furthermore, Negueruela and Marco (2012) showed that the brightest B-type stars on the MS are B3-6, which confirms the cluster's age to be greater than 40 Myr but less than 100 Myr.

**FSR0636:** A previously known cluster (King 6), located in the second Galactic Quadrant in the Local Spiral Arm. Its CCM diagrams (Fig. 8.11) show a young open cluster with a PMS track. The cluster's properties are redetermined as $d = 0.80\,\mathrm{kpc}$, age of 53 Myr and $A_H = 0.35\,\mathrm{mag}$, which are in agreement with the values derived in Sect. 8.3.

At the time of writing there are only three studies of FSR0636 in the literature. Of these, two (Ann et al. (2002), Maciejewski and Niedzielski (2007)) agree with the revised distance and extinction values but conclude the cluster to be much older at $\sim 250$ Myr. As demonstrated in Figure 8.11, although a 250 Myr isochrone can be fitted to the cluster it fails to fit the cluster sequence for objects with $K > 14\,\mathrm{mag}$ entirely, with the 50 Myr isochrone providing a better goodness of fit. Furthermore, the earliest stars on the MS are B-stars of type B5-7 (Straižys and Laugalys, 2007), i.e. the cluster has an age of less than 100 Myr.

The third study of FSR0636 by the MWSC catalogue should be treated with extreme caution, as the values indicate that they were derived by fitting a isochrone to field stars and not the cluster sequence.

**FSR0718:** A previously known cluster (Berkeley 15), located in the second Galactic Quadrant in the Auriga constellation. Its CCM diagrams (Fig. 8.12) show a young open cluster but without the PMS track it was assumed to have. The cluster's properties are redetermined as

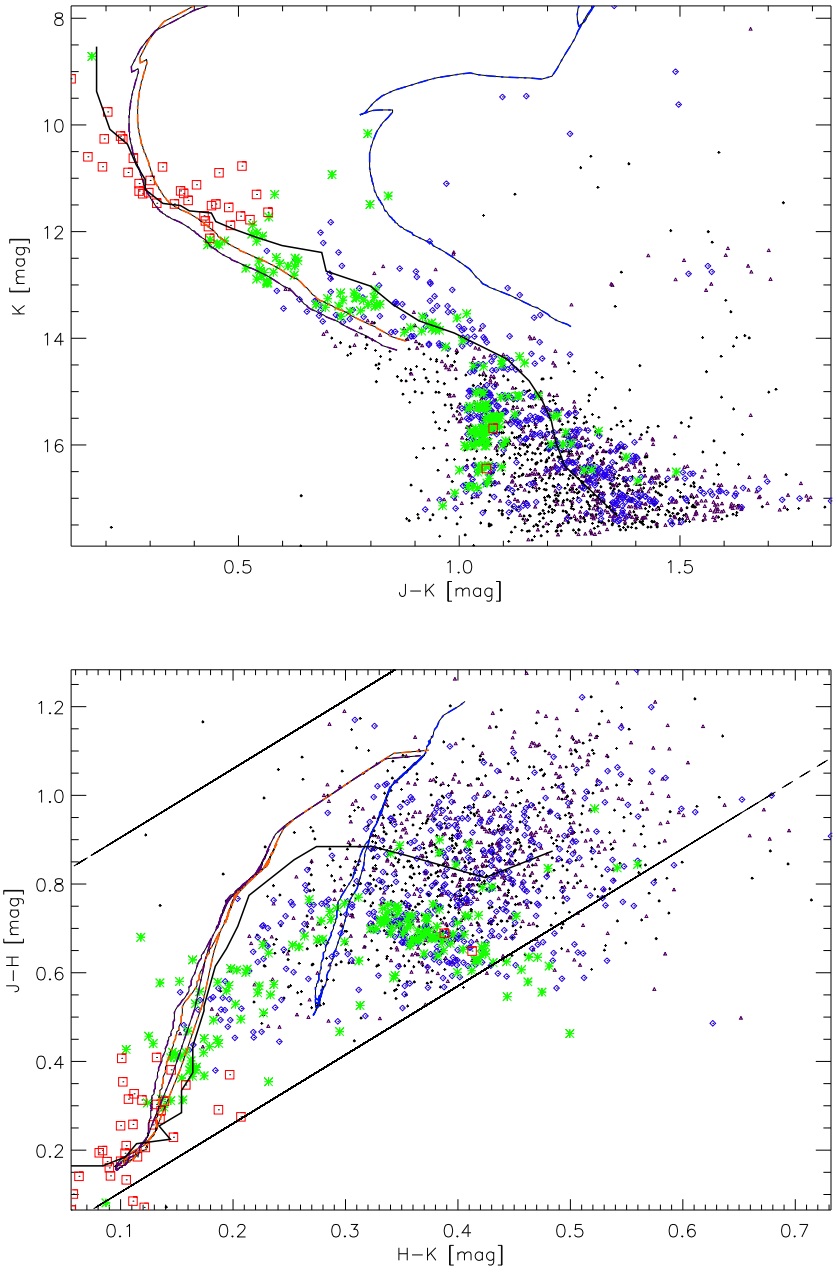


Figure 8.11: (*Top*) Colour-Magnitude and (*Bottom*) Colour-Colour diagrams of **FSR0636**. Photometric membership probabilities are determined for stars within $2 \times r_{cor}$, with $N = 15$ and are represented as follows: $P^i_{cl} \geq 80\%$ red squares; $60 \leq P^i_{cl} < 80\%$ green stars; $40 \leq P^i_{cl} < 60\%$ blue diamonds; $20 \leq P^i_{cl} < 40\%$ purple triangles; $P^i_{cl} < 20\%$ black plus signs. The best fitting modelled cluster sequence, as determined in Sect. 8.4, is plotted as a solid black isochrone. The dashed purple, orange and blue lines represent the best fitting isochrones as determined by Ann et al. (2002), Maciejewski and Niedzielski (2007) and the MWSC catalogue respectively. The parallel black lines in the Colour-Colour plot represent the reddening bands of the cluster.

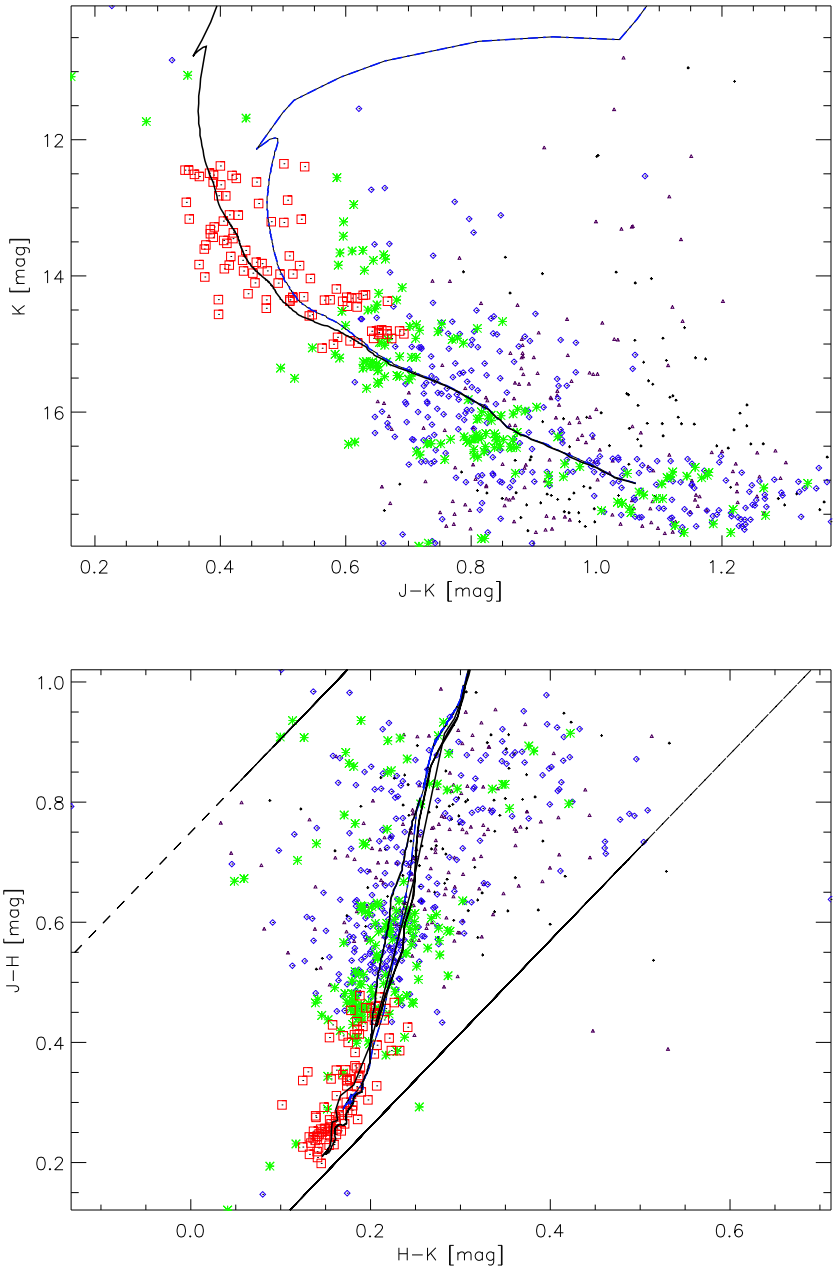


Figure 8.12: (*Top*) Colour-Magnitude and (*Bottom*) Colour-Colour diagrams of **FSR0718**. Photometric membership probabilities are determined for stars within $2 \times r_{cor}$, with $N = 15$ and are represented as follows: $P^i_{cl} \geq 80\%$ red squares; $60 \leq P^i_{cl} < 80\%$ green stars; $40 \leq P^i_{cl} < 60\%$ blue diamonds; $20 \leq P^i_{cl} < 40\%$ purple triangles; $P^i_{cl} < 20\%$ black plus signs. The best fitting isochrone, as determined in Sect. 8.4, is plotted as a solid black line and the dashed blue line represents a 300 Myr isochrone with the same distance and extinction. The parallel black lines in the Colour-Colour plot represent the reddening bands of the cluster.

$d = 3.00$ kpc, age of 50 Myr and $A_H = 0.48$ mag, which are in general agreement with the values derived in Sect. 8.3, albeit with a slightly smaller extinction.

The properties of FSR0718 are strongly disputed in the literature, but most authors derive an age in excess of $> 300$ Myr. This is much older than the revised value, which is most likely a result of member misidentification. To demonstrate, the reader is referred to the cluster's CCM diagrams in Figure 8.12, where it is shown that if low-probability membership objects at $K \leq 12$ mag and $0.9\,\text{mag} \leq [J-H] \leq 1.3$ mag are assumed giant members, the cluster would have an age in excess of $\sim$300 Myr. As observed by Tapia et al. (2010) further analysis in needed to discern the earliest member spectral types in FSR0718 for absolute clarification of the cluster's age.

**FSR0794:** A previously known and extensively studied cluster (NGC 1960/M36), located in the second Galactic Quadrant in the Auriga constellation. Its CCM diagrams (Fig. 8.13) show a young open cluster with well defined MS and PMS tracks. The cluster's properties are redetermined as $d = 1.20$ kpc, age of 23 Myr and $A_H = 0.17$ mag, which are in general agreement with those derived in Sect. 8.3. The revised values generally agree with the vast number given in the literature (except for those given by the MWSC catalogue), albeit with a slightly lower extinction value.

**FSR0870:** A previously known cluster (NGC 2129), located in the third Galactic Quadrant in the Gemini constellation. Its CCM diagrams (Fig. 8.14) clearly show a very young open cluster with a PMS track. The cluster's properties are redetermined as $d = 1.90$ kpc, age of 10 Myr and $A_H = 0.40$ mag. Even though the majority of the cluster sequence is below the 2MASS magnitude limit, the clump of bright, high probability members at the top of the MS ($K \approx 10$ mag) made a reasonably accurate derivation of the clusters properties possible in Sect. 8.3.

The nature of FSR0870 has been a subject for debate since its discovery. An early study by Cuffey (1938) placed the cluster at a distance of $\sim 0.6$ kpc from the Sun, but a study by Peña and Peniche (1994) cast doubt on the cluster's existence when the authors created a histogram of the distances of 37 stars in the direction of FSR0870 using $uvby-\beta$ photometry and concluded it was an asterism, despite a previous radial velocity study by Liu et al. (1991). Their conclusion prompted further studies which utilised proper motions and photometry confirm whether FSR0870 is real or an asterism (e.g. Baumgardt et al. (2000), Carraro et al. (2006)). It is now generally accepted that FSR0870 is a real Solar metallicity cluster, at a distance of $\sim 2$ kpc, age of $\sim 10$ Myr and extinction of $A_H \sim 0.4$ mag which is in agreement

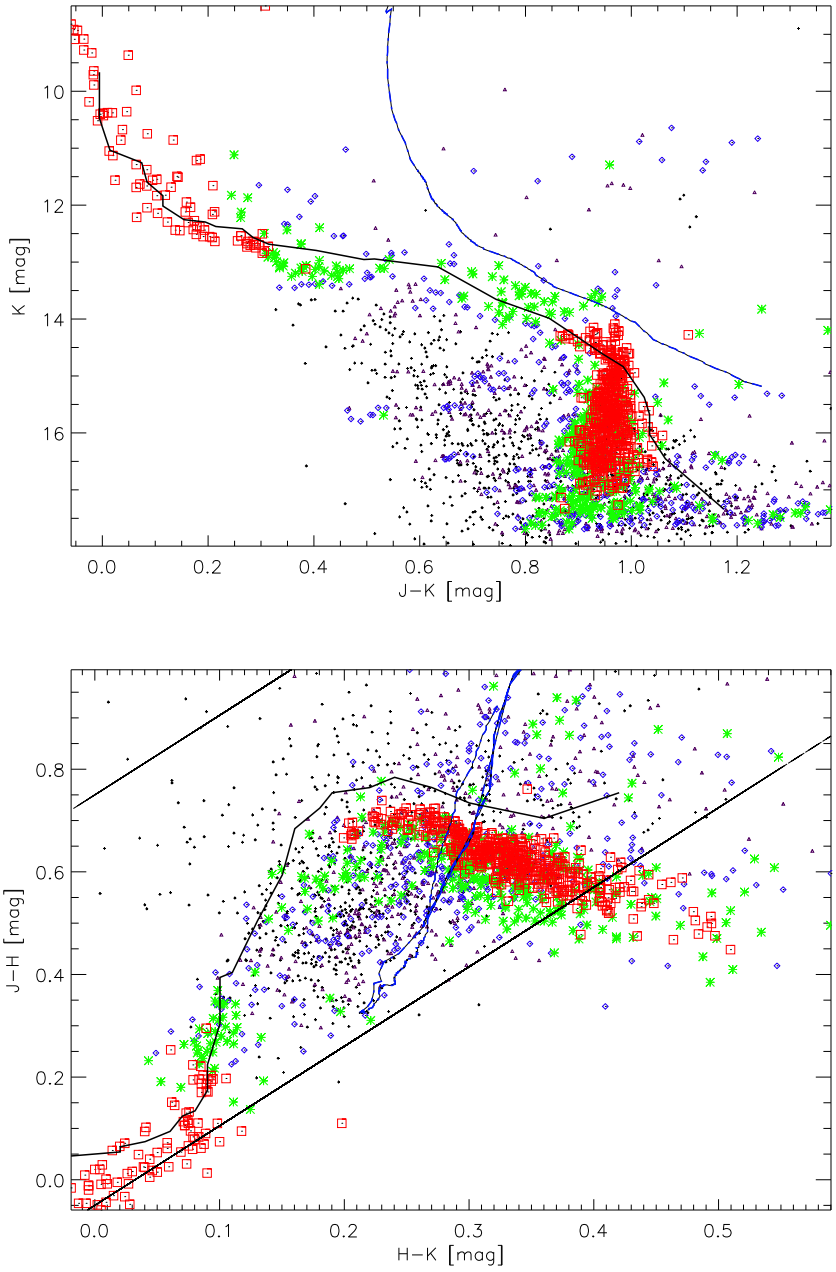


Figure 8.13: (*Top*) Colour-Magnitude and (*Bottom*) Colour-Colour diagrams of **FSR0794**. Photometric membership probabilities are determined for stars within $2 \times r_{cor}$, with $N = 15$ and are represented as follows: $P^i_{cl} \geq 80\%$ red squares; $60 \leq P^i_{cl} < 80\%$ green stars; $40 \leq P^i_{cl} < 60\%$ blue diamonds; $20 \leq P^i_{cl} < 40\%$ purple triangles; $P^i_{cl} < 20\%$ black plus signs. The best fitting modelled cluster sequence, as determined in Sect. 8.4, is plotted as a solid black isochrone. The dashed blue isochrone represents the best fitting modelled cluster sequence as determined by the MWSC catalogue. The parallel black lines in the Colour-Colour plot represent the reddening bands of the cluster.

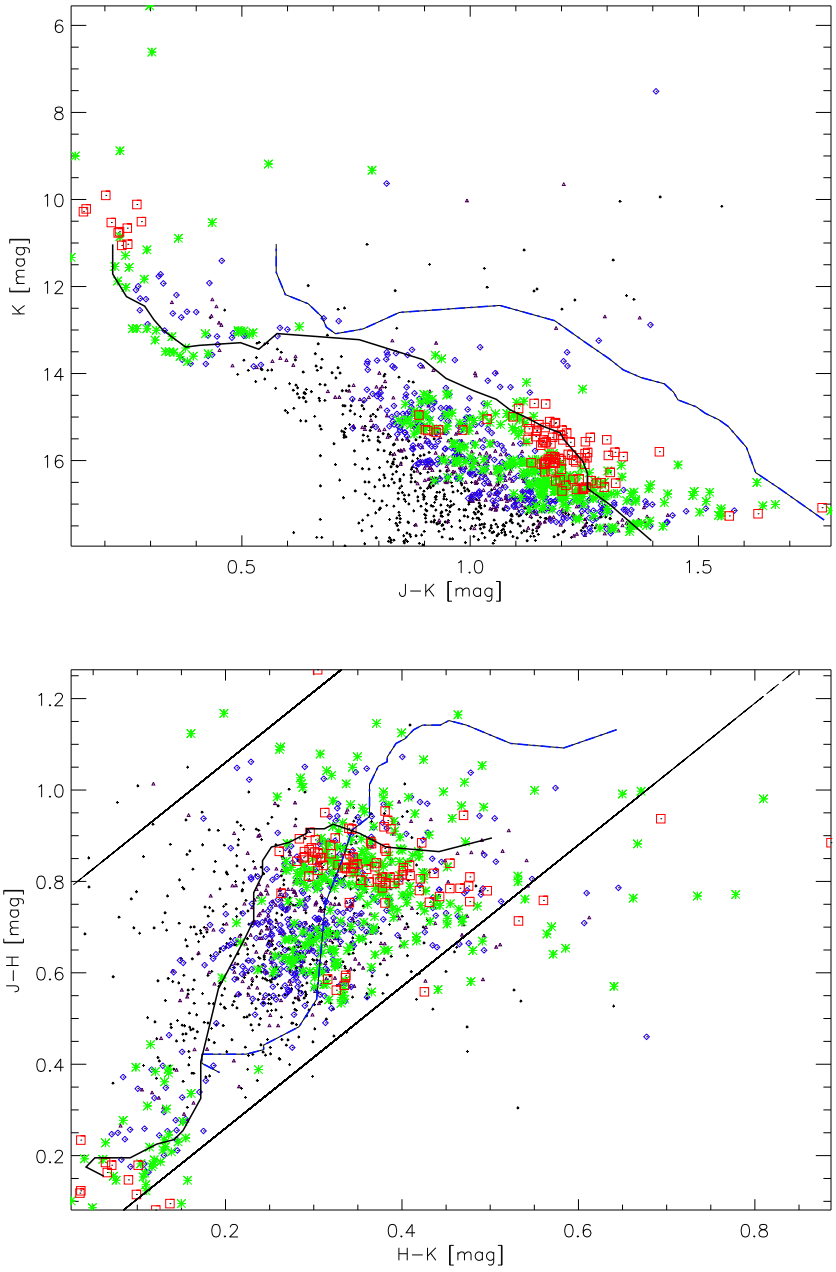


Figure 8.14: (*Top*) Colour-Magnitude and (*Bottom*) Colour-Colour diagrams of **FSR0870**. Photometric membership probabilities are determined for stars within $2 \times r_{cor}$, with $N = 15$ and are represented as follows: $P^i_{cl} \geq 80\%$ red squares; $60 \leq P^i_{cl} < 80\%$ green stars; $40 \leq P^i_{cl} < 60\%$ blue diamonds; $20 \leq P^i_{cl} < 40\%$ purple triangles; $P^i_{cl} < 20\%$ black plus signs. The best fitting modelled cluster sequence, as determined in Sect. 8.4, is plotted as a solid black isochrone. The dashed blue isochrone represents the best fitting modelled cluster sequence as determined by the MWSC catalogue. The parallel black lines in the Colour-Colour plot represent the reddening bands of the cluster.

with the revised values presented here. Note that the extinction value given by the MWSC catalogue differs significantly from the accepted value.

**FSR0904:** A new cluster candidate located in the third Galactic Quadrant. Its CCM diagrams (Fig. 8.15) show a very young open cluster without the PMS track it was suspected to have. The cluster's properties are redetermined as $d = 2.10\,\mathrm{kpc}$, age of 8 Myr and $A_H = 0.35\,\mathrm{mag}$, which are in general agreement with the values derived Sect. 8.3, albeit with slightly lower extinction and age estimates caused by the majority of the MS falling below the 2MASS magnitude limit.

There have been three previous studies of FSR0904, and whilst all have derived values for the clusters properties by fitting isochrones to 2MASS photometry, they have produced conflicting values. The revised values are in agreement with those derived by Camargo et al. (2010), but conflict with those of Glushkova et al. (2010) and the MWSC catalogue.

Glushkova et al. (2010) found the cluster to be a factor of $\sim 10$ older than the revised values suggest, with a significantly smaller extinction and distance. This discrepancy is caused by misidentification of cluster members by the authors (i.e. field stars as giants - see Figure 8.15), which was compounded by the majority of the MS not being visible to the authors when they determined the cluster's properties (as it is below the 2MASS magnitude limit). Members were identified as objects that lay along the isochrone fitted to the CCM diagrams and which formed the cluster's spatial density peak. Obviously, this approach is subjective on the authors interpretation of the CCM diagrams and subsequent choice of isochrone. Furthermore, assessing membership based on spatial positioning has been shown to be unreliable, especially for young clusters (such as FSR0904) which do not appear circular in projection, those projected onto a high density field star background, or with significant stellar crowding (for a full discussion see e.g. Froebrich et al. (2010), Buckner and Froebrich (2013)). Although Glushkova et al. (2010) identified the majority of members on the top of the MS with reasonable accuracy, the misidentification of field stars as the cluster's giants, in combination with 'missing' the majority of the cluster sequence (due to 2MASS magnitude limits), has resulted in the authors significantly overestimating FSR0904's age and underestimating its extinction and distance.

The values derived by the MWSC catalogue significantly vary from the revised values, giving the cluster a notably larger age and extinction estimate and as shown are not a good fit for the cluster.

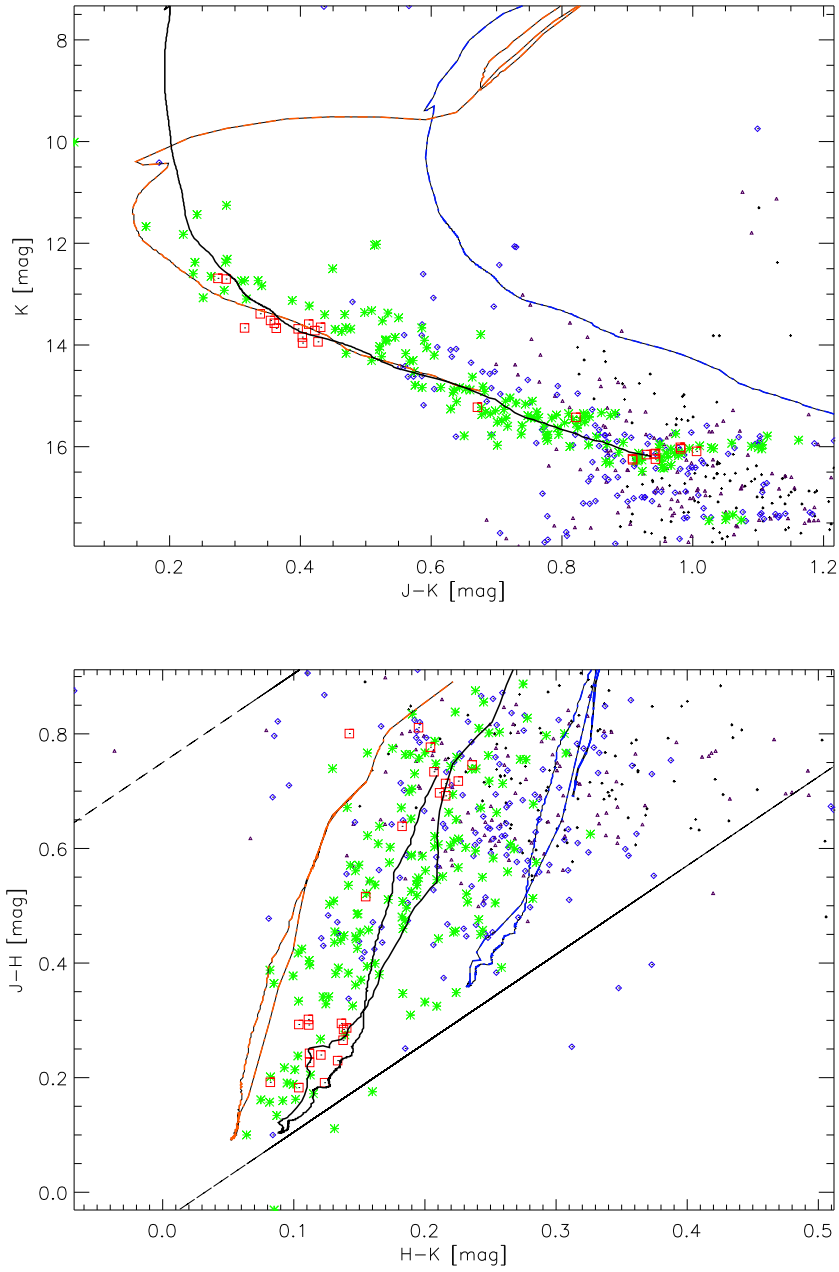


Figure 8.15: (*Top*) Colour-Magnitude and (*Bottom*) Colour-Colour diagrams of **FSR0904**. Photometric membership probabilities are determined for stars within $2 \times r_{cor}$, with $N = 15$ and are represented as follows: $P^i_{cl} \geq 80\%$ red squares; $60 \leq P^i_{cl} < 80\%$ green stars; $40 \leq P^i_{cl} < 60\%$ blue diamonds; $20 \leq P^i_{cl} < 40\%$ purple triangles; $P^i_{cl} < 20\%$ black plus signs. The best fitting modelled cluster sequence, as determined in Sect. 8.4, is plotted as a solid black isochrone. The dashed orange and blue isochrones represent the best fitting modelled cluster sequences as determined by Glushkova et al. (2010) (see text for details) and the MWSC catalogue respectively. The parallel black lines in the Colour-Colour plot represent the reddening bands of the cluster.

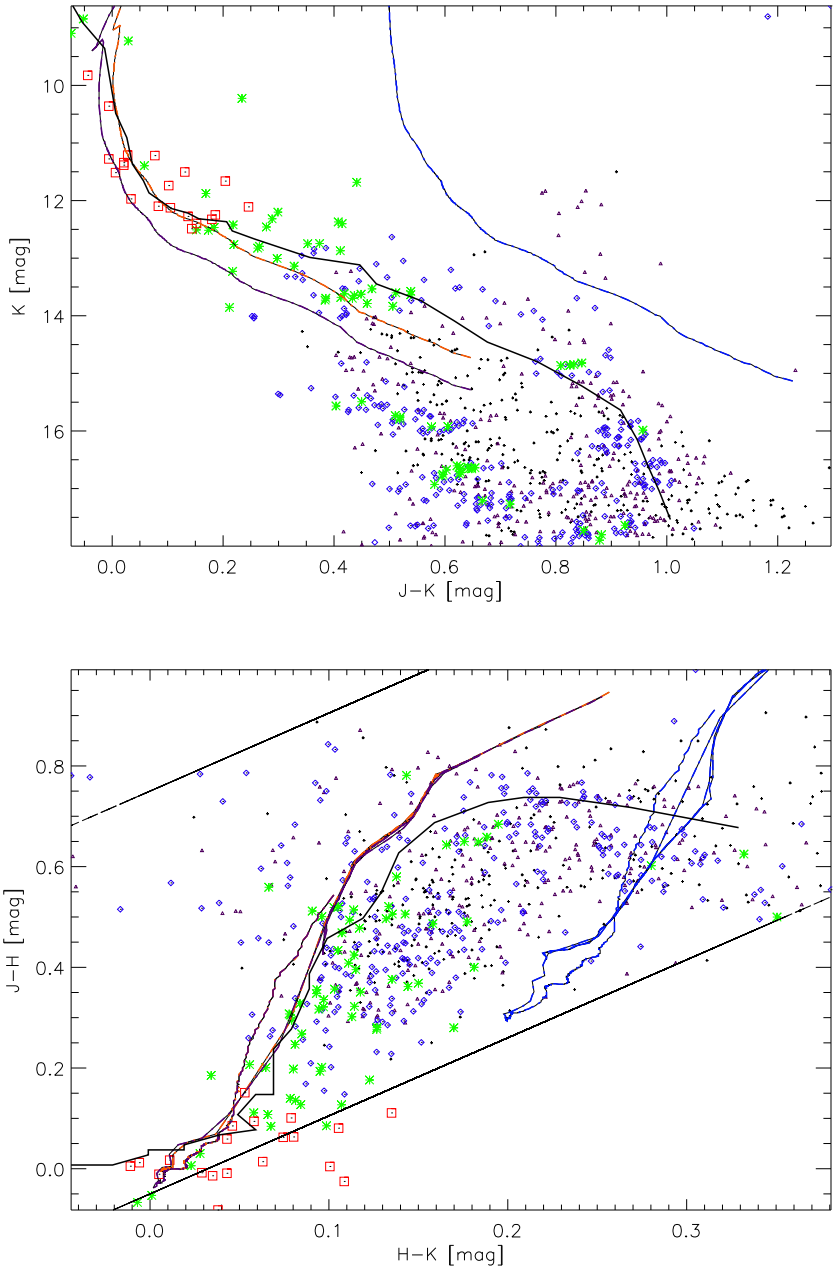


Figure 8.16: (*Top*) Colour-Magnitude and (*Bottom*) Colour-Colour diagrams of **FSR1189**. Photometric membership probabilities are determined for stars within $2 \times r_{cor}$, with $N = 15$ and are represented as follows: $P^i_{cl} \geq 80\%$ red squares; $60 \leq P^i_{cl} < 80\%$ green stars; $40 \leq P^i_{cl} < 60\%$ blue diamonds; $20 \leq P^i_{cl} < 40\%$ purple triangles; $P^i_{cl} < 20\%$ black plus signs. The best fitting modelled cluster sequence, as determined in Sect. 8.4, is plotted as a solid black isochrone. The dashed purple, orange and blue isochrones represent the best fitting modelled cluster sequences as determined by Segura et al. (2014), Lim et al. (2011) and the MWSC catalogue respectively. The parallel black lines in the Colour-Colour plot represent the reddening bands of the cluster.

**FSR1189:** A previously known cluster (NGC 2353), located in the third Galactic Quadrant near the Canis Major OB1 association. Its CCM diagrams (Fig. 8.16) show a moderately young open cluster with a PMS track. The cluster's properties are redetermined as $d = 1.20$ kpc, age of 90 Myr and $A_H = 0.11$ mag, which are in agreement with the values derived in Sect. 8.3.

The revised age and distance values are also in consensus with the literature. This age also agrees with the assessment of Fitzgerald et al. (1990) and Lim et al. (2011), that FSR1189 is unrelated to the much younger ($\sim 3$ Myr), but similarly distanced, Canis Major OB1 association. The revised extinction estimate is a factor of 2 larger than that given by various authors, but is accurate according to the isochrone fits shown in Figure 8.16. Literature studies have predominantly analysed FSR1189 using visual (UBV) photometry, whilst this work has conducted the analysis using NIR (JHK) photometry. Thus, a possible source of the discrepancy between the extinction values could be the presence of a dark cloud in the line of sight of the cluster (as proposed by Segura et al. (2014)). Again, the MWSC catalogue gives values for the cluster which are inconsistent with both the literature and the revised values given here, most likely caused by a combination of the systematic nature of the authors data processing pipeline and only utilising (the relatively) low resolution 2MASS photometry.

### 8.4.2 Clusters with Notable Galactocentric Distances

Five clusters were flagged as having notable Galactocentric distances with respect to the remainder of the sample. Of these, three are within 5 kpc of, and two approximately 13 kpc away from, the GC[1]. Inclusion of deeper magnitude photometry on the clusters CCM diagrams will make visible the dimmer members which are on the MS but below the 2MASS magnitude limit, thus enabling more accurate modelled cluster sequence isochrone fits to be made and ultimately the Galactocentric distances can be confirmed or revised.

Photometry from the UKIDSS-GPS/VISTA-VVV surveys was available for 4 of the clusters. These are: FSR0089, FSR0188, FSR0828 and FSR1716.

**FSR0089:** A new cluster candidate located in the first Galactic Quadrant, flagged as the nearest to the GC in the sample with a Galactocentric distance of $R_{GC} = 2.09$ kpc. Its CCM diagrams (Fig. 8.17) show an intermediate-old cluster with a well defined MS, turn-off and

[1]Assuming a Solar Galactocentric distance of $R_{GC}^{\odot} = 8.00$ kpc (Malkin, 2012)

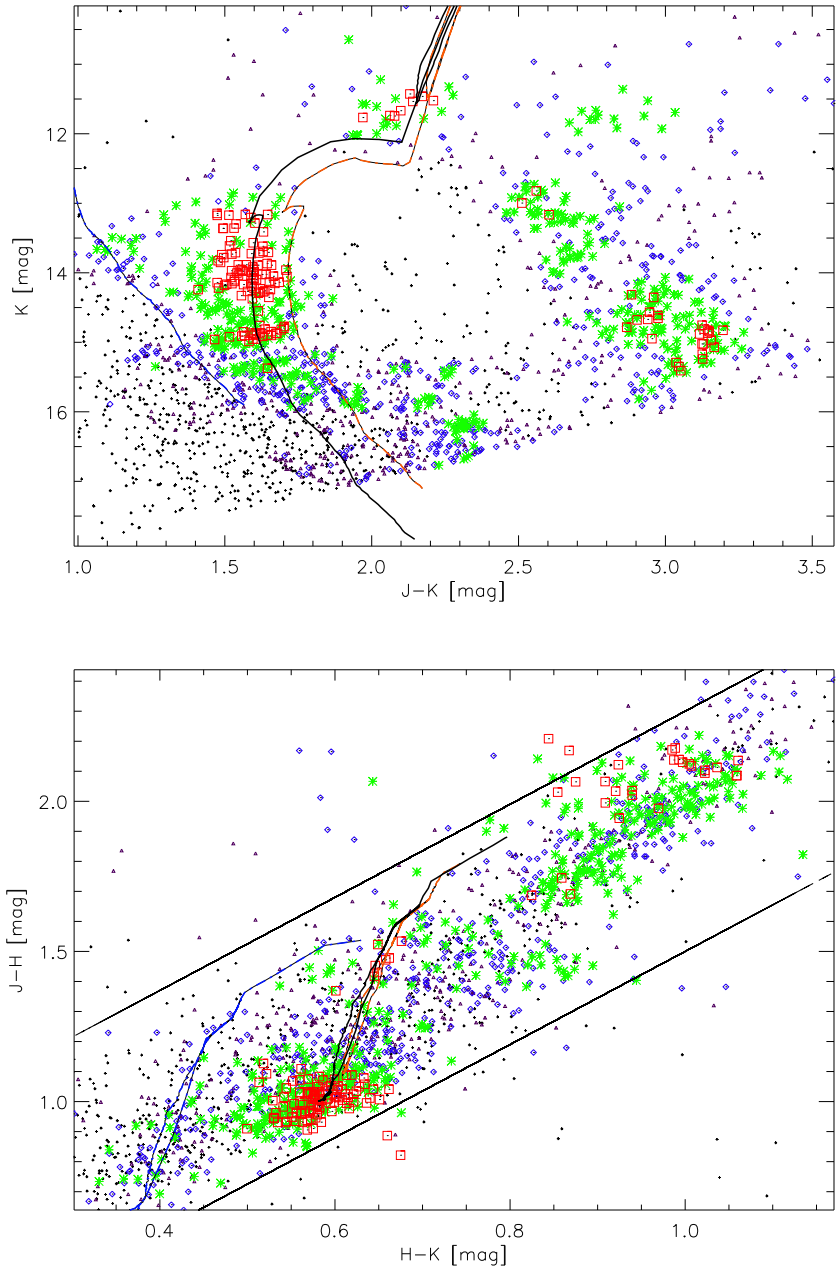


Figure 8.17: (*Top*) Colour-Magnitude and (*Bottom*) Colour-Colour diagrams of **FSR0089**. Photometric membership probabilities are determined for stars within $2 \times r_{cor}$, with $N = 15$ and are represented as follows: $P^i_{cl} \geq 80\%$ red squares; $60 \leq P^i_{cl} < 80\%$ green stars; $40 \leq P^i_{cl} < 60\%$ blue diamonds; $20 \leq P^i_{cl} < 40\%$ purple triangles; $P^i_{cl} < 20\%$ black plus signs. The best fitting modelled cluster sequence, as determined in Sect. 8.4, is plotted as a solid black isochrone. The dashed orange and blue isochrones represent the best fitting modelled cluster sequences as determined by Froebrich et al. (2008) and the MWSC catalogue respectively. The parallel black lines in the Colour-Colour plot represent the reddening bands of the cluster.

giants. The cluster's properties are redetermined as $d = 3.10$ kpc, age of 500 Myr and $A_H = 1.60$ mag.

The revised age and extinction values are in approximate agreement with those derived in Sect. 8.3, but the cluster's distance estimate has halved. As such, FSR0089 is no longer the nearest cluster to the GC in the sample, but still has a notable Galactocentric distance of $R_{GC} = 5.18$ kpc. The discrepancy in the distance estimate occurred because the majority of the cluster's MS is below the 2MASS magnitude limit and thus was not visible when the pipeline was originally applied to derive its fundamental properties.

The revised values are in generally good agreement with the literature, albeit with a slightly larger distance. The reader should note that the extinction value given by the MWSC catalogue is not in agreement with the revised values or the literature, and should therefore be treated with caution.

**FSR0188:** A new cluster candidate located in the first Galactic Quadrant, flagged as both one of the furthest clusters from the Sun and nearest to the GC at $R_{GC} = 4.52$ kpc. Its CCM diagrams (Fig. 8.18) show an old cluster with a well defined MS, turn-off and giants. The cluster's properties are redetermined as $d = 4.90$ kpc, age of 1 Gyr and $A_H = 0.61$ mag. The revised age and extinction values are in general agreement with those derived in Sect. 8.3, but the cluster's distance estimate has halved. As such, FSR0188 is no longer one of the nearest clusters to the GC in the sample. The majority of cluster's sequence was below the 2MASS magnitude limit, which impacted on accuracy of the distance estimate; it is a good example of the necessity for deeper magnitude photometry (from e.g. UKIDSS-GPS) when deriving cluster properties through isochrone fitting.

FSR0188 features in the MWSC catalogue which determines the cluster to be younger, nearer and redder than the revised values suggest. Figure 8.18 shows the CCM diagrams of the cluster with two sets of isochrones over-plotted: those depicting the revised values, and those given by the MWSC catalogue. Clearly, the revised values are a better fit for the cluster's sequence and the authors of MWSC catalogue have misidentified field stars as cluster members (in particular the giants) and vice versa, when fitting their isochrone to the photometry.

**FSR0828:** A new cluster candidate located in the second Galactic Quadrant, flagged as having the greatest Galactocentric distance in the sample at $R_{GC} = 13.00$ kpc. Its CCM diagrams (Fig. 8.19) show an old cluster with a well defined MS (below the 2MASS magnitude limit), turn-off and giants. The cluster's properties are redetermined as $d = 3.20$ kpc, age of 2 Gyr and $A_H = 0.22$ mag, which is slightly older and much closer than the values derived in

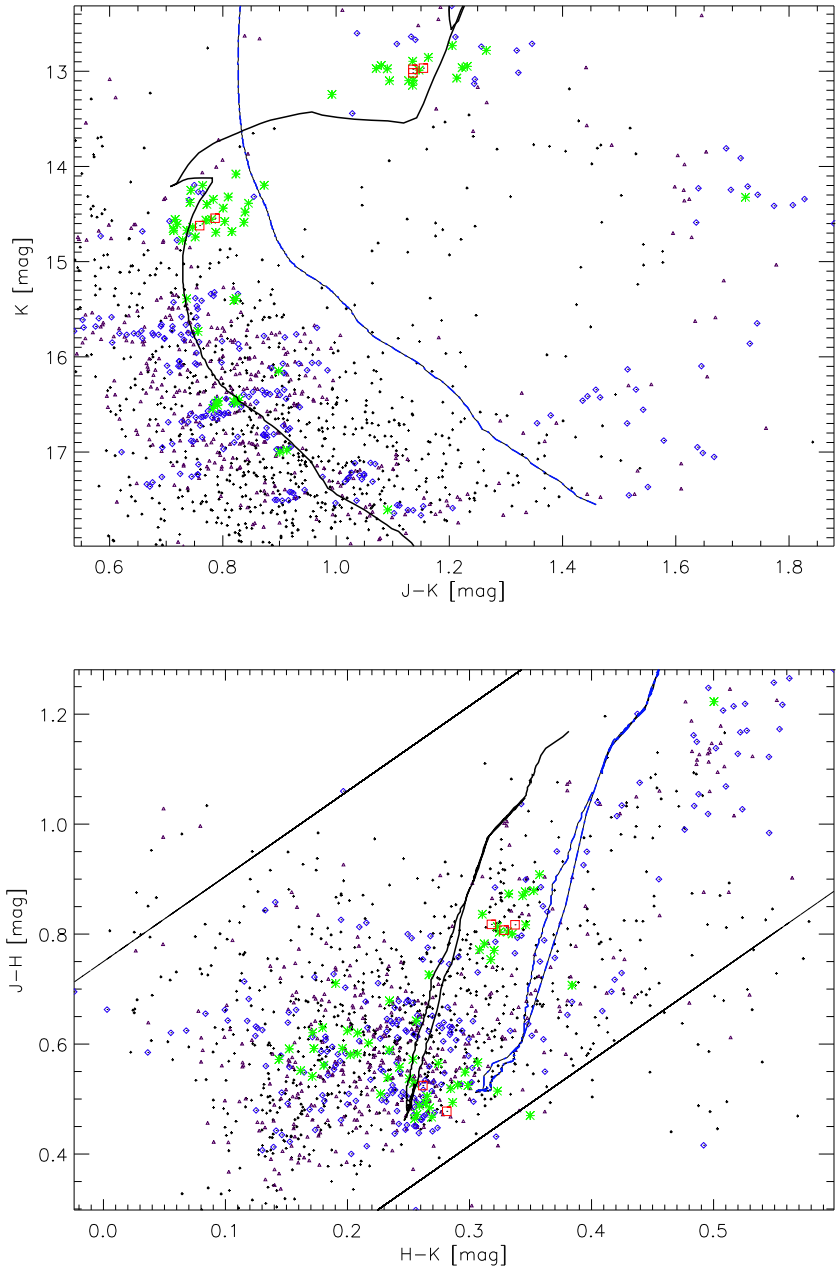


Figure 8.18: (*Top*) Colour-Magnitude and (*Bottom*) Colour-Colour diagrams of **FSR0188**. Photometric membership probabilities are determined for stars within $2 \times r_{cor}$, with $N = 15$ and are represented as follows: $P^i_{cl} \geq 80\%$ red squares; $60 \leq P^i_{cl} < 80\%$ green stars; $40 \leq P^i_{cl} < 60\%$ blue diamonds; $20 \leq P^i_{cl} < 40\%$ purple triangles; $P^i_{cl} < 20\%$ black plus signs. The best fitting modelled cluster sequence, as determined in Sect. 8.4, is plotted as a solid black isochrone. The dashed blue isochrone represents the best fitting modelled cluster sequence as determined by the MWSC catalogue. The parallel black lines in the Colour-Colour plot represent the reddening bands of the cluster.

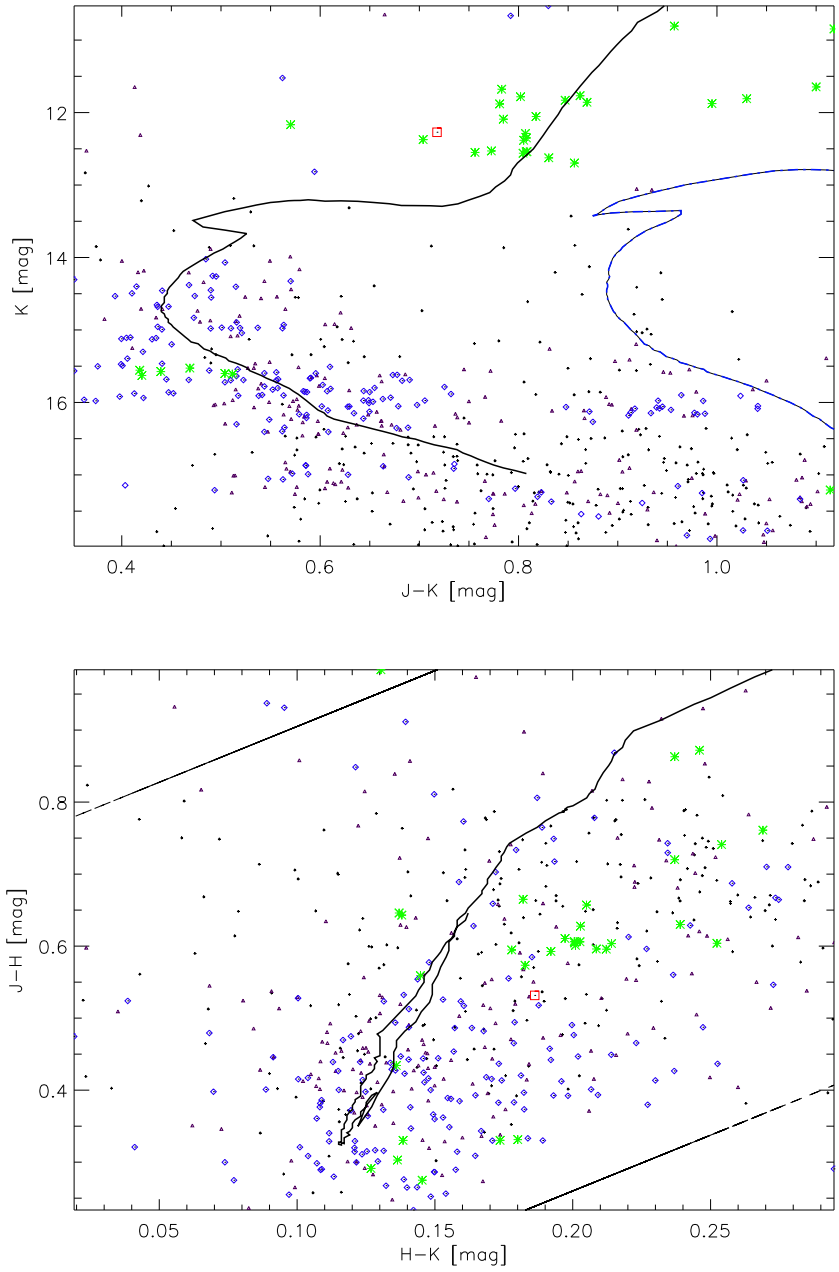


Figure 8.19: (*Top*) Colour-Magnitude and (*Bottom*) Colour-Colour diagrams of **FSR0828**. Photometric membership probabilities are determined for stars within $2 \times r_{cor}$, with $N = 15$ and are represented as follows: $P^i_{cl} \geq 80\%$ red squares; $60 \leq P^i_{cl} < 80\%$ green stars; $40 \leq P^i_{cl} < 60\%$ blue diamonds; $20 \leq P^i_{cl} < 40\%$ purple triangles; $P^i_{cl} < 20\%$ black plus signs. The best fitting isochrone, as determined in Sect. 8.4, is overplotted as a solid black line. The dashed blue isochrone represents the best fitting modelled cluster sequence as determined by the MWSC catalogue. The parallel black lines in the Colour-Colour plot represent the reddening bands of the cluster.

Sect. 8.3 suggested. As such, FSR0828 no longer has the largest Galactocentric distance in the sample.

The revised properties are in generally good agreement with the literature, but there is a conflict between the revised extinction value and that given by the MWSC catalogue.

**FSR1716:** A new cluster candidate located in the fourth Galactic Quadrant, flagged as one of the nearest to the GC at $R_{GC} = 3.33\,\mathrm{kpc}$. Its CCM diagrams (Fig. 8.20) show a very old open or possible globular cluster candidate. The cluster's properties are redetermined as $d = 7.30\,\mathrm{kpc}$, age of 10 Gyr and $A_H = 0.55\,\mathrm{mag}$, making it older, further away but less reddened than the values in Sect. 8.3 suggest. The revised values make FSR1716 the oldest cluster in the sample and nearest to the GC with $R_{GC} = 1.69\,\mathrm{kpc}$.

Deriving the age of old clusters such as FSR1716 is difficult. Unlike younger clusters, the CCM diagrams of the oldest clusters have only one detectable age defining feature: the position of the Red Giant Clump (RGC). Unfortunately in many instances this feature falls below, or is very close to, the magnitude limit of the photometry being employed to analyse the cluster, and its position had to be guesstimated by each author based on their individual interpretations of the CCM diagrams. Figure 8.20 clearly indicates the RGC of FSR1716 to be at $K \sim 15 - 15.5\,\mathrm{mag}$. The exact position of the RGC is derived as the weighted mean of the membership probabilities of stars in the cluster area, determined to be $K = 15.3\,\mathrm{mag}$ and is confirmed by Figure 8.21 which shows a histogram of the $K$-band magnitude of stars in the cluster area. The position of the RGC is fully/partially below to the magnitude limits of the photometry which have been previously used to derive the cluster's fundamental properties (2MASS, NTT). As such there has been no agreement in the literature of the age and distance of FSR1716, further complicated by a debate over its nature. Most studies have assumed that FSR1716 is an open cluster, deriving ages of $1.7 - 7.1\,\mathrm{Gyr}$ and distances of $0.8 - 7.0\,\mathrm{kpc}$. Meanwhile, Bonatto and Bica (2008b) concluded that it could be a low metallicity 12 Gyr globular cluster at a distance of 2.3 kpc.

The revised values presented here were determined by fitting an isochrone to the CCM diagrams of FSR1716, using the measured position of the RGC as a reference point. The revised age value of FSR1716 agrees with the assessment that it is a potential globular cluster candidate.

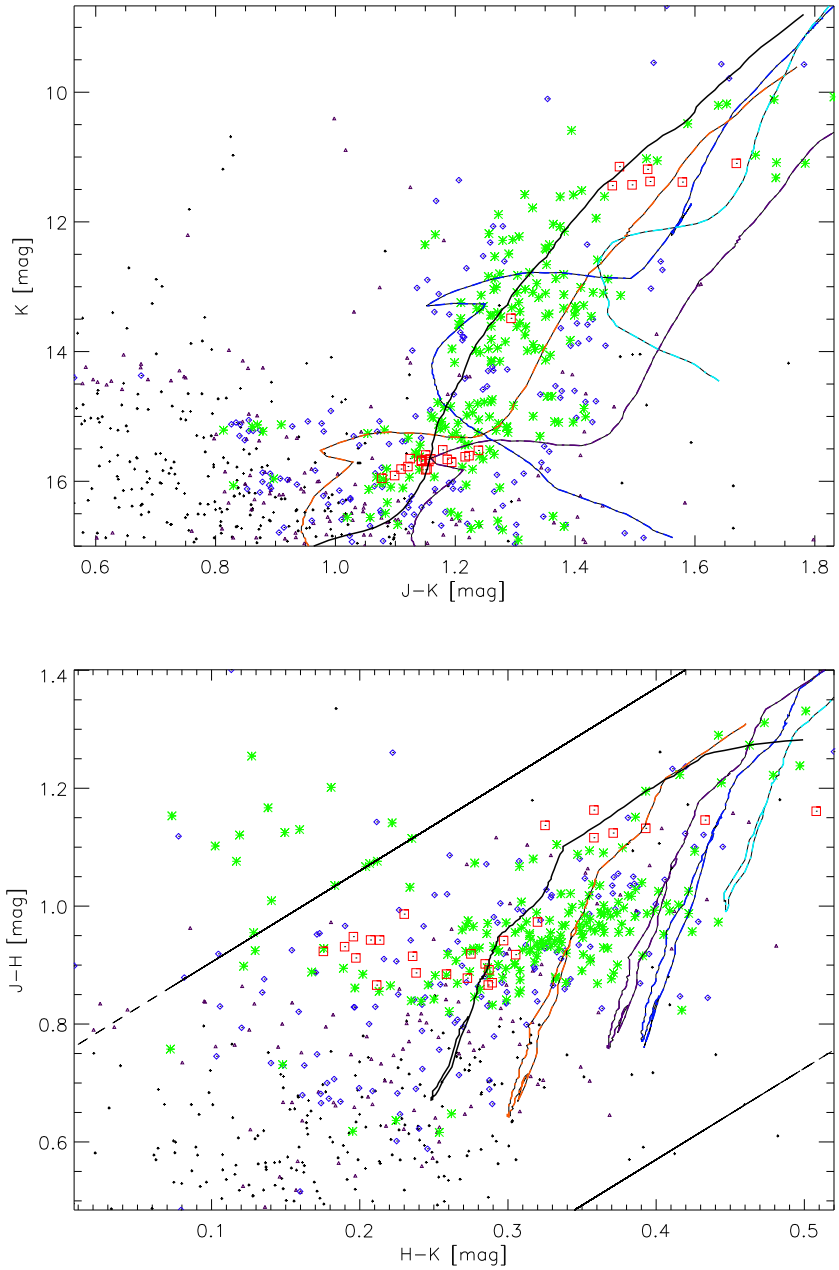


Figure 8.20: (*Top*) Colour-Magnitude and (*Bottom*) Colour-Colour diagrams of **FSR1716**. Photometric membership probabilities are determined for stars within $2 \times r_{cor}$, with $N = 15$ and are represented as follows: $P^i_{cl} \geq 80\%$ red squares; $60 \leq P^i_{cl} < 80\%$ green stars; $40 \leq P^i_{cl} < 60\%$ blue diamonds; $20 \leq P^i_{cl} < 40\%$ purple triangles; $P^i_{cl} < 20\%$ black plus signs. The best fitting modelled cluster sequence, as determined in Sect. 8.4, is plotted as a solid black isochrone. The dashed purple, orange, turquoise and blue lines represent the best fitting open cluster isochrones as determined by Froebrich et al. (2008), Froebrich et al. (2010), Bonatto and Bica (2008b) and the MWSC catalogue respectively. The parallel black lines in the Colour-Colour plot represent the reddening bands of the cluster.

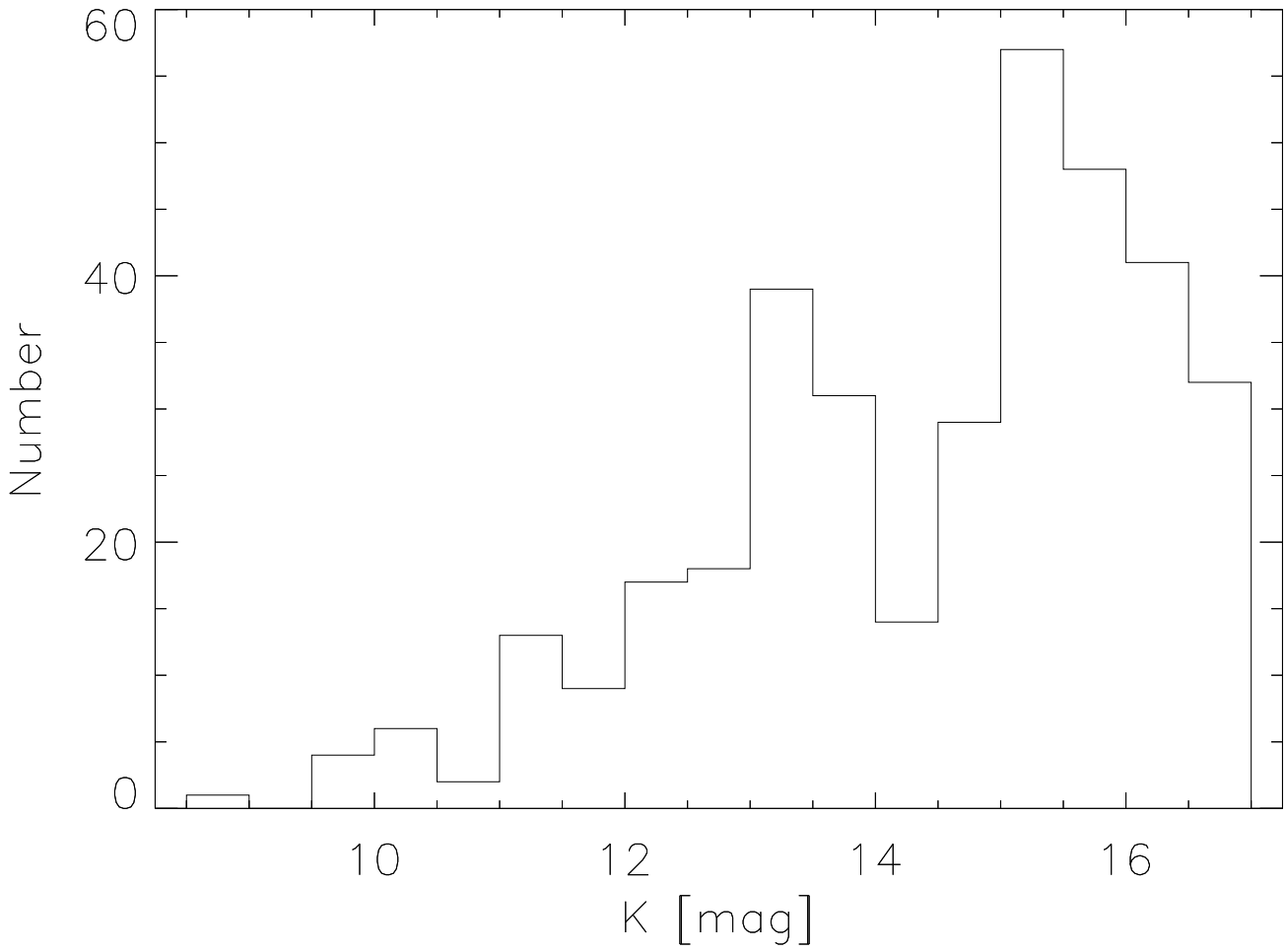


Figure 8.21: Histogram of the $K$-band magnitudes of **FSR1716** for stars within $2 \times r_{cor}$ and $P_{cl}^{i} \geq 40\%$ ($N = 15$). The peak at $K \sim 15 - 15.5$ mag indicates the position of the cluster's RGC.

## 8.5 Future Work

It is important to determine the properties of the remaining FSR List catalogue clusters and confirm the nature of the new cluster candidates. At present this is impeded by a lack of deep resolution photometry, with surveys such as UKIDSS-GPS and VISTA-VVV only covering a fraction of the longitudinal and latitudinal ranges of the FSR List catalogue. Therefore a starting point for any future work should be a focus on the sourcing and utilisation of deep resolution photometry for all objects in the catalogue. Deriving mass estimates should also be a priority as these will enrich the current understanding of open cluster distribution in the GP.

Additional future work should include the use of the methods presented by this Thesis to determine and analyse the properties of other photometric cluster catalogues as they become available. A comparative analysis of the distribution of the various cluster samples could then be undertaken, enabling the identification of biases and trends intrinsic to either the FSR List catalogue and/or other catalogues. Furthermore, as all cluster properties will have been homogeneously derived, the catalogues could be combined into a single sample with further cluster samples added as they are discovered. The existence of such a large cluster sample would enable a rigorous analysis of the distribution of open clusters in the GP to be undertaken.

Table 8.2: Details the refined properties of the clusters studied in Sect. 8.4. For each cluster the table lists its ID, class (PMS, OC or GlC), type (known open cluster or new cluster candidate), Galactic coordinates (l,b), age, distance in parsec, $H$-band extinction value, and the literature source of these values.

| **ID** | **Type** | **Class** | **l** [deg] | **b** [deg] | **Age** [log(age/yr)] | **d** [pc] | $A_H$ [mag] | **Source** |
|---|---|---|---|---|---|---|---|---|
| FSR0195, MWSC3298 | New | PMS | 72.07 | -00.99 | $7.57^{+6.48}_{-6.48}$ | $3000^{+120}_{-120}$ | 1.10 | [TWR] |
| | | | | | 7.60 | 1900 | 1.15 | [TW] |
| | | | | | 9.35 | 2331 | 0.91 | [1] |
| FSR0207, MWSC3297, IC 4996 | Known | PMS | 75.38 | 01.30 | 7.30 | $1200^{+70}_{-70}$ | 0.25 | [TWR] |
| | | | | | 7.00 | 1400 | 0.30 | [TW] |
| | | | | | 7.15 | 1764 | 0.73 | [1] |
| | | | | | $6.95^{+6.00}_{-6.00}$ | $1620^{+75}_{-75}$ | 0.34 | [2] |
| | | | | | $6.88^{+6.48}_{-6.48}$ | 2399 | $0.39^{+0.04}_{-0.04}$ | [3] |
| | | | | | 6.85 | $2291^{+995}_{-995}$ | 0.38 | [4] |
| | | | | | 7.00 | 1620 | 0.35 | [5] |
| FSR0301, MWSC3490, Berkeley 55 | Known | PMS | 93.04 | 01.80 | $7.60^{+6.78}_{-6.78}$ | $4000^{+30}_{-30}$ | $1.00^{+0.00}_{-0.00}$ | [TWR] |
| | | | | | 7.51 | 2000 | 1.00 | [TW] |
| | | | | | $8.57\ ^{+0.04}_{-0.04}$ | 1700 | 0.94 | [1] |
| | | | | | $7.70^{+7.00}_{-7.00}$ | 4000 | $1.00^{+0.09}_{-0.09}$ | [6] |
| | | | | | 8.48 | $1440^{+65}_{-65}$ | 0.81 | [7] |
| | | | | | 8.50 | $1210^{+310}_{-390}$ | $0.94^{+0.05}_{-0.06}$ | [8] |
| FSR0636, MWSC0277, King 6 | Known | PMS | 143.35 | -00.13 | $7.72^{+6.48}_{-6.48}$ | $800^{+0.00}_{-0.00}$ | $0.35^{+0.00}_{-0.00}$ | [TWR] |
| | | | | | 7.70 | 800 | 0.35 | [TW] |
| | | | | | 8.98 | 632 | 0.68 | [1] |
| | | | | | $8.40^{+7.70}_{-7.70}$ | $871^{+12}_{-12}$ | $0.27^{+0.05}_{-0.05}$ | [9] |
| | | | | | 8.40 | $800^{+290}_{-250}$ | $0.29^{+0.07}_{-0.06}$ | [8] |
| FSR0718, MWSC0453, Berkeley 15 | Known | OC | 162.27 | 01.62 | $7.70^{+0.37*}_{-0.37}$ | $3000^{+190}_{-190}$ | $0.48^{+0.01}_{-0.01}$ | [TWR] |
| | | | | | 7.30 | $2700^{+20}_{-20}$ | 0.55 | [TW] |
| | | | | | 9.40 | 1300 | 0.69 | [1] |
| | | | | | $8.50^{+0.10}_{-0.10}$ | $3000^{+300}_{-300}$ | $0.48^{+0.03}_{-0.03}$ | [10] |
| | | | | | 9.70 | $1259^{+135}_{-135}$ | 0.25 | [11] |
| | | | | | $9.35/9.95^{+0.05}_{-0.05}$ | $1406^{+10}_{-10}$ | $0.13^{+0.02}_{-0.02}$ | [12] |
| FSR0794, MWSC0594, NGC 1960 | Known | PMS | 174.55 | 01.08 | $7.36^{+6.48}_{-6.48}$ | $1200^{+30}_{-30}$ | $0.17^{+0.01}_{-0.01}$ | [TWR] |
| | | | | | 7.30 | 1200 | 0.20 | [TW] |
| | | | | | $7.57^{+0.08}_{-0.08}$ | 1200 | 0.67 | [1] |
| | | | | | 7.40 | 1330 | 0.12 | [13] |
| | | | | | $7.20^{+0.20}_{-0.2}$ | $1318^{+120}_{-120}$ | $0.14^{+0.01}_{-0.01}$ | [14] |
| | | | | | 7.48 | 1200 | 0.13 | [15] |
| | | | | | $7.42^{+6.51}_{-6.72}$ | $1164^{+11}_{-26}$ | 0.11 | [16] |

Continued on next page

**Table 8.2 – continued from previous page**

| ID | Type | Class | l [deg] | b [deg] | Age [log(age/yr)] | d [pc] | $A_H$ [mag] | Source |
|---|---|---|---|---|---|---|---|---|
| FSR0870, MWSC0704, NGC 2129 | Known | PMS | 186.61 | 00.15 | 7.00 | 1900 | 0.40 | [TWR] |
| | | | | | 7.30 | 1600 | 0.40 | [TW] |
| | | | | | 7.48 | 1651 | 0.77 | [1] |
| | | | | | 7.00 | $2200^{+200}_{-200}$ | $0.43^{+0.04}_{-0.04}$ | [17] |
| | | | | | $7.00^{+5.00}_{-5.00}$ | $2100^{+100}_{-100}$ | $0.42^{+0.03}_{-0.03}$ | [18] |
| FSR0904, MWSC0731, SAI61 | New | OC | 191.03 | -00.78 | $6.90^{+0.07}_{-0.07}$ | $2100^{+60}_{-60}$ | $0.35^{+0.02}_{-0.02}$ | [TWR] |
| | | | | | 7.30 | 2000 | 0.43 | [TW] |
| | | | | | 7.80 | 1427 | 0.70 | [1] |
| | | | | | $7.30^{+7.00}_{-7.00}$ | $2200^{+100}_{-100}$ | $0.35^{+0.02}_{-0.02}$ | [20] |
| | | | | | $8.80^{+0.05}_{-0.05}$ | $1265^{+10}_{-10}$ | $0.08^{+0.09}_{-0.09}$ | [21] |
| FSR1189, MWSC1152, NGC 2353 | Known | PMS | 224.67 | 00.40 | 7.95 | $1200^{+30}_{-30}$ | $0.11^{+0.01}_{-0.01}$ | [TWR] |
| | | | | | 8.00 | 1200 | 0.10 | [TW] |
| | | | | | 7.20 | 1180 | 0.65 | [1] |
| | | | | | $8.10^{+0.1}_{-0.1}$ | $1170^{+40}_{-40}$ | $0.05^{+0.01}_{-0.01}$ | [22] |
| | | | | | 7.88 | $1200^{+80}_{-80}$ | 0.06 | [23] |
| | | | | | 7.86 | $1513^{+646}_{-646}$ | $0.05^{+0.03**}_{-0.03}$ | [24] |
| FSR0089, MWSC2997 | New | OC | 29.49 | -00.98 | $8.70^{+0.03}_{-0.03}$ | $3100^{+90}_{-90}$ | $1.60^{+0.01}_{-0.01}$ | [TWR] |
| | | | | | $8.50^{+0.03}_{-0.03}$ | $6500^{+70}_{-70}$ | 1.50 | [TW] |
| | | | | | 8.30 | 1516 | 1.00 | [1] |
| | | | | | $9.00^{+8.00}_{-8.00}$ | $2200^{+100}_{-100}$ | $1.60\ ^{+0.05}_{-0.05}$ | [25] |
| | | | | | $9.00^{+8.48}_{-8.48}$ | $2200^{+300}_{-300}$ | $1.63\ ^{+0.08}_{-0.08}$ | [26] |
| FSR0188, MWSC3228 | New | OC | 70.65 | 01.74 | $9.00^{+0.02}_{-0.02}$ | $4900^{+180}_{-180}$ | $0.61^{+0.01}_{-0.01}$ | [TWR] |
| | | | | | $8.60^{+0.05}_{-0.05}$ | $10500^{+1000}_{-1000}$ | $0.62^{+0.02}_{-0.02}$ | [TW] |
| | | | | | $8.20\ ^{+0.10}_{-0.10}$ | 3354 | 0.89 | [1] |
| FSR0828, MWSC0687, Koposov 43 | New | OC | 179.92 | 01.75 | 9.30 | $3200^{+60}_{-60}$ | 0.22 | [TWR] |
| | | | | | 8.90 | 5000 | 0.28 | [TW] |
| | | | | | 9.30 | 2800 | 0.28 | [26] |
| | | | | | $9.12^{+0.02}_{-0.02}$ | 3000 | 0.75 | [1] |
| | | | | | $9.30^{+0.1}_{-0.1}$ | $2800^{+120}_{-120}$ | $0.21^{+0.05}_{-0.05}$ | [19] |
| FSR1716, MWSC2359 | New | OC/GlC? | 329.79 | -01.59 | 10.00 | $7300^{+90}_{-90}$ | 0.55 | [TWR] |
| | | | | | $9.10^{+0.07}_{-0.07}$ | 5400 | $0.79^{+0.03}_{-0.03}$ | [TW] |
| | | | | | 9.23 | 2396 | 1.00 | [1] |
| | | | | | $> 9.30$ | $7000^{+500}_{-500}$ | $0.93^{+0.08}_{-0.08}$ | [26] |
| | | | | | 9.30 | 7000 | 0.74 | [27] |
| | | OC | | | $9.85^{+9.0}_{-9.0}$ | $800^{+100}_{-100}$ | $1.11^{+0.04}_{-0.04}$ | [28] |
| | | GlC | | | $10.08^{+9.30}_{-9.30}$ | $2300^{+300}_{-300}$ | $1.11^{+0.07}_{-0.07}$ | [28] |

**Table notes:**

[TWR] This Work (revised)

*NB: the uncertainties on d, Age and $A_H$ are the statistical variations of the multiple isochrone fits used to derive the cluster's properties (see Chapter 6 for details).*

[TW] This Work (unrevised)

*NB: the uncertainties on d, Age and $A_H$ are the statistical variations of the multiple isochrone fits used to derive the cluster's properties (see Chapter 6 for details).*

[1] Kharchenko et al. (2013)

[2] Vansevicius et al. (1996)

[3] Delgado et al. (1998)

[4] Bhavya et al. (2007)

[5] Lynga (1995)

[6] Negueruela and Marco (2012)

[7] Tadross (2008)

[8] Maciejewski and Niedzielski (2007)

[9] Ann et al. (2002)

[10] Lata et al. (2004)

[11] Sujatha et al. (2004)

[12] Tapia et al. (2010)

[13] Sharma et al. (2006)

[14] Sanner et al. (2000)

[15] Barkhatova et al. (1985)

[16] Bell et al. (2013)

[17] Carraro et al. (2006)

[18] Tripathi et al. (2013)

[19] Koposov et al. (2008)

*NB: source paper misidentified cluster as FSR0848.*

[20] Camargo et al. (2010)

[21] Glushkova et al. (2010)

[22] Lim et al. (2011)

[23] Fitzgerald et al. (1990)

[24] Segura et al. (2014)

[25] Bonatto and Bica (2007a)

[26] Froebrich et al. (2008)

[27] Froebrich et al. (2010)

[28] Bonatto and Bica (2008b)

# Chapter 9

# Galactic Extinction Law

In the literature, interstellar absorption is typically assumed constant per unit distance in the GP, measured as the average of the Solar Neighbourhood, with a canonical value of $A_V = 0.7\,\mathrm{mag/kpc}$ (e.g. Froebrich et al. (2010)). However, it is reasonable to expect that this value varies with Galactic longitude, becoming significantly higher in lines of sight towards (e.g.) the GC, and lower in lines of sight towards (e.g.) the Anticentre.

It is essential to accurately constrain how the value of interstellar absorption varies with Galactic longitude for the generation of synthetic star fields with Galaxy models, i.e. if its value is set too high a model will underestimate the density of field stars, and if its value is set too low a model will overestimate the density of field stars. Cluster samples are ideal tools with which to do this as they contain a large number of objects of the same type, with known distances and extinctions. Indeed, Joshi (2005) (J05 hereafter) analysed a sub-sample of the DAML02 catalogue and found that the value of interstellar absorption varies sinusoidally with Galactic longitude. Unfortunately, there were some issues with the authors approach, namely the validity of their methodology, the small size and presence of a possible reddening/distance bias of their sample, as well as the heterogeneous nature of clusters' properties (see Chapter 1 for a discussion). Evidently, these issues need to be addressed to verify the findings of their analysis and then to build upon it. This Chapter provides that analysis, exploring how interstellar absorption varies with Galactic longitude using an consistent, unbiased approach with a large cluster sample whose properties have been homogeneously derived.

## 9.1 Cluster Sample

When using a cluster sample to determine how interstellar absorption varies with Galactic longitude, there are a number of factors which need to be considered. Most notably, clusters should be positioned in the GP to ensure that the line of sight is in the Galactic mid-plane. It is also important that both the cluster sample's distance and extinction estimates are derived homogeneously, as this ensures that any variation of the measured interstellar absorption values with Galactic longitude is real, and that the uncertainties are systematic. For this reason the sample of 771 FSR List catalogue clusters whose distance and extinction values were homogeneously and photometrically determined (Sect. 8.1 and 8.2) are used for the analysis.

It is important to ensure that the sample has no reddening or distance bias, as this will affect the accuracy of the analysis. Two $H$-band extinction estimates were measured for each cluster in the sample, from their measured median $[H-K]$ and $[H-4.5]$ colours ($A_H^{HK}$ and $A_H^{H45}$ respectively). In principle, $A_H^{H45}$ should be more reliable than $A_H^{HK}$ because the $[H-4.5]$ colour (unlike the $[H-K]$ colour) is almost independent of luminosity and spectral class. Unfortunately, due to photometry limitations $A_H^{H45}$ can only be measured from the brightest (reddest) $\sim 50\,\%$ of the cluster members, whereas $A_H^{HK}$ does not have this restriction. Consequently, there are a number of the clusters in the sample whose two $H$-band extinctions vary significantly. These discrepancies are most pronounced for clusters with a:

- **High YSO fraction**

  Disk ($K$-band) excess emission members will cause an underestimation of the clusters measured median $[H-K]$ colour and subsequently $A_H^{HK}$ (Eq. 5.4).

- **Distance $>5\,$kpc**

  At increasing distances interstellar material (dust, gas) accumulate in any given line of sight, such that two identical clusters placed in the same line of sight but at different distances will have different extinction values. Therefore at large distances only the brightest members of clusters are observable. As clusters' median $[H-4.5]$ colours are measured from their brightest (reddest) members, the accuracy of $A_H^{H45}$ decreases with increasing distance. This effect is most pronounced at cluster distances $>5\,$kpc (Fig. 8.2).

The reader should note that it is not possible to measure the value of interstellar absorption for Galactic longitudes of $l < 60^\circ$ and $l > 300^\circ$ with this sample because the sample contains far too few clusters in those regions for an accurate analysis to be undertaken (Fig. 8.1). The lack of clusters in these regions is caused by the (i) inherent deficit in the FSR List catalogue (Froebrich et al., 2007) and (ii) difficulty in deriving the distance and extinction values the catalogue's clusters in these regions. In both cases, the low resolution of 2MASS and the high projected number density of the field in these regions made it difficult to identify clusters and resolve individual cluster members.

For the above reasons, the following restrictions are applied to the cluster sample. A cluster must:

- **Be closer than 150 pc to the GP**
- **Have a YSO fraction of less than 10 %**
- **Have a distance of 5 kpc or less**
- **Have a Galactic longitude of** $30^\circ \leq l \leq 300^\circ$

Clusters that fail to comply with one or more of the above restrictions are excluded from the analysis. These selections leave 302 clusters in the sample.

## 9.2 Method

The value of interstellar absorption is measured in intervals of 10 degrees longitude, determined as the change in extinction per unit distance of the cluster sample.

The method measures the values of extinction per unit distance, $A_H[mag/kpc]$, as the gradient of a linear fit made on a plot of cluster distances against extinction (e.g. Fig. 9.1). It is ideal to have as many clusters as possible in each longitude bin, to ensure that the linear fits (and hence the values of interstellar absorption) are not influenced by random scatter caused by e.g. individual clusters which have an erroneous distance or extinction value. For this reason the method has a requirement that there are at least 10 clusters within each longitude bin.

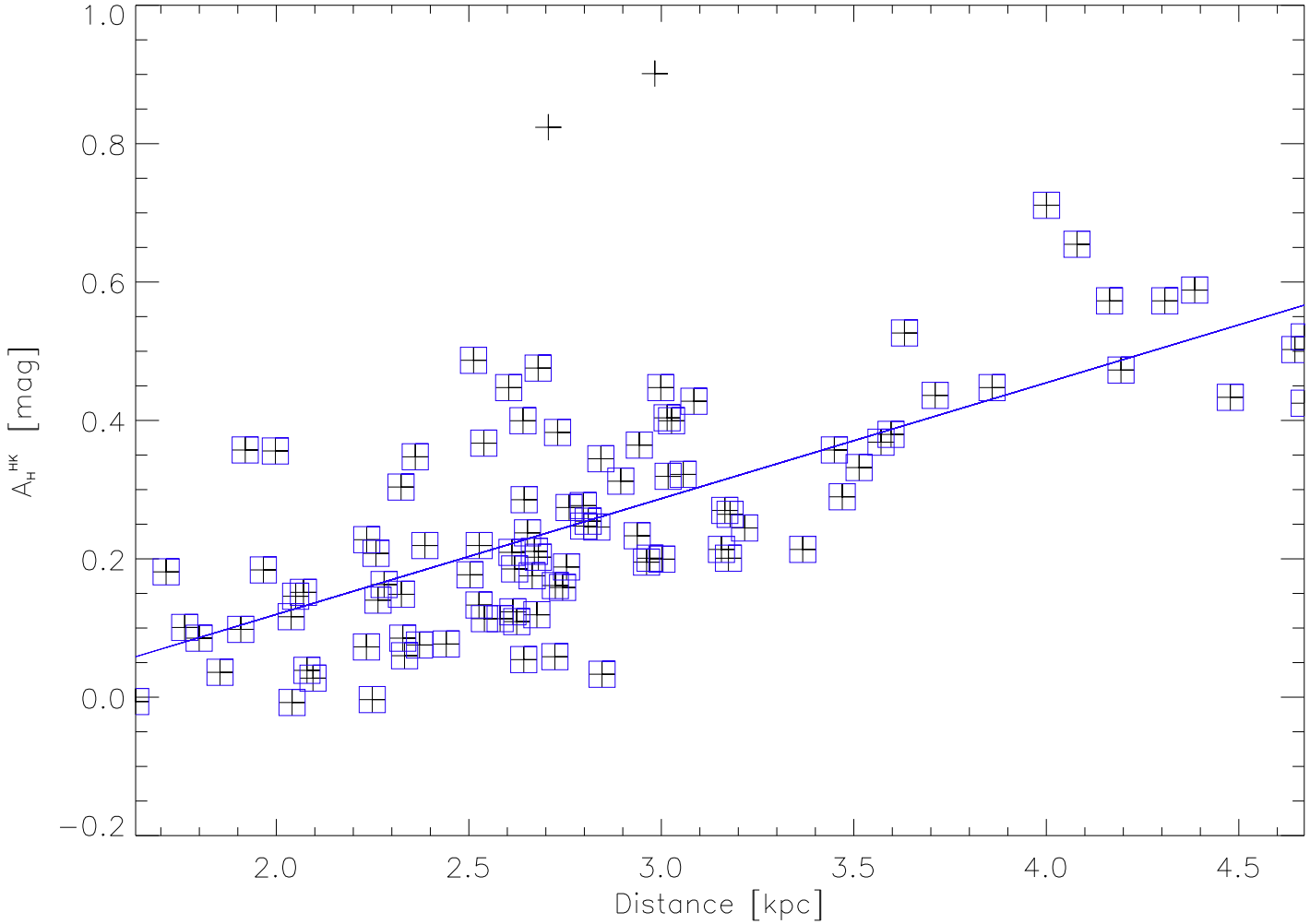


Figure 9.1: Plot shows cluster distances against their $H$-band extinctions, $A_H^{HK}$, for clusters in the region $l = 110° \pm 30°$ (see text for details). Black crosses represent clusters in this region, the solid blue line is the linear fit and blue boxed crosses are clusters included in the fit at the $3\sigma$ level.

To maximise the number of clusters used to determine the extinction per unit distance, clusters within $\pm 30^\circ$ from the target longitude are utilised, i.e. bins are not independent as they overlap. For example, to determine $A_H[mag/kpc]$ at $l = 110^\circ$, a plot of distance against extinction is made using clusters with a longitude in the range $80^\circ < l < 140^\circ$. The width of the bins (i.e. $60^\circ$) have no significant effect on the gradients of the linear fits, but do provide a compromise between the number of clusters (and thus the uncertainty on $A_H[mag/kpc]$) and the longitudinal resolution. To aid the reader in evaluating the trustworthiness of the determined interstellar absorption values, the number of clusters per bin/longitude range are provided in Appendix B, along with their respective plots and linear fits.

## 9.3 Extinction Law

A systematic dependence of Galactic longitude with the value of interstellar absorption is found, as described by

$$A_H(l)[mag/kpc] = 0.10 + 0.001 \times |l - 180^\circ|/^\circ \text{ For } 60^\circ < l < 300^\circ \tag{9.1}$$

where $A_H(l)[mag/kpc]$ is the $H$-band extinction per unit distance as a function of Galactic longitude, $l$.

Figure 9.2 shows that the shape of $A_H^{HK}(l)[mag/kpc]$ and $A_H^{H45}(l)[mag/kpc]$ (derived from $A_H^{HK}$ and $A_H^{H45}$ respectively) are very similar, and most points are indistinguishable within the uncertainties.

Evidently there is a systematic decrease in the value of interstellar absorption from the GC towards the Anticentre, i.e. $A_H(60^\circ, 300^\circ) = 0.22\,\text{mag/ kpc}$ and $A_H(180^\circ) = 0.10\,\text{mag/ kpc}$. There are marked variations between extinction law described by Eq. 9.1 and the canonical value of interstellar absorption of $A_V = 0.7$ mag/kpc or, converted to the $H$-band, $A_H = 0.12\,\text{mag/ kpc}$. The canonical value corresponds to the value measured towards the Anticentre and is approximately three times smaller than the measured value at $60^\circ$ from the GC. This result was expected as, due to the exponential distribution of dust across the Galactic Disk, it is reasonable for the value of interstellar absorption to vary with Galactic longitude and not to remain constant.

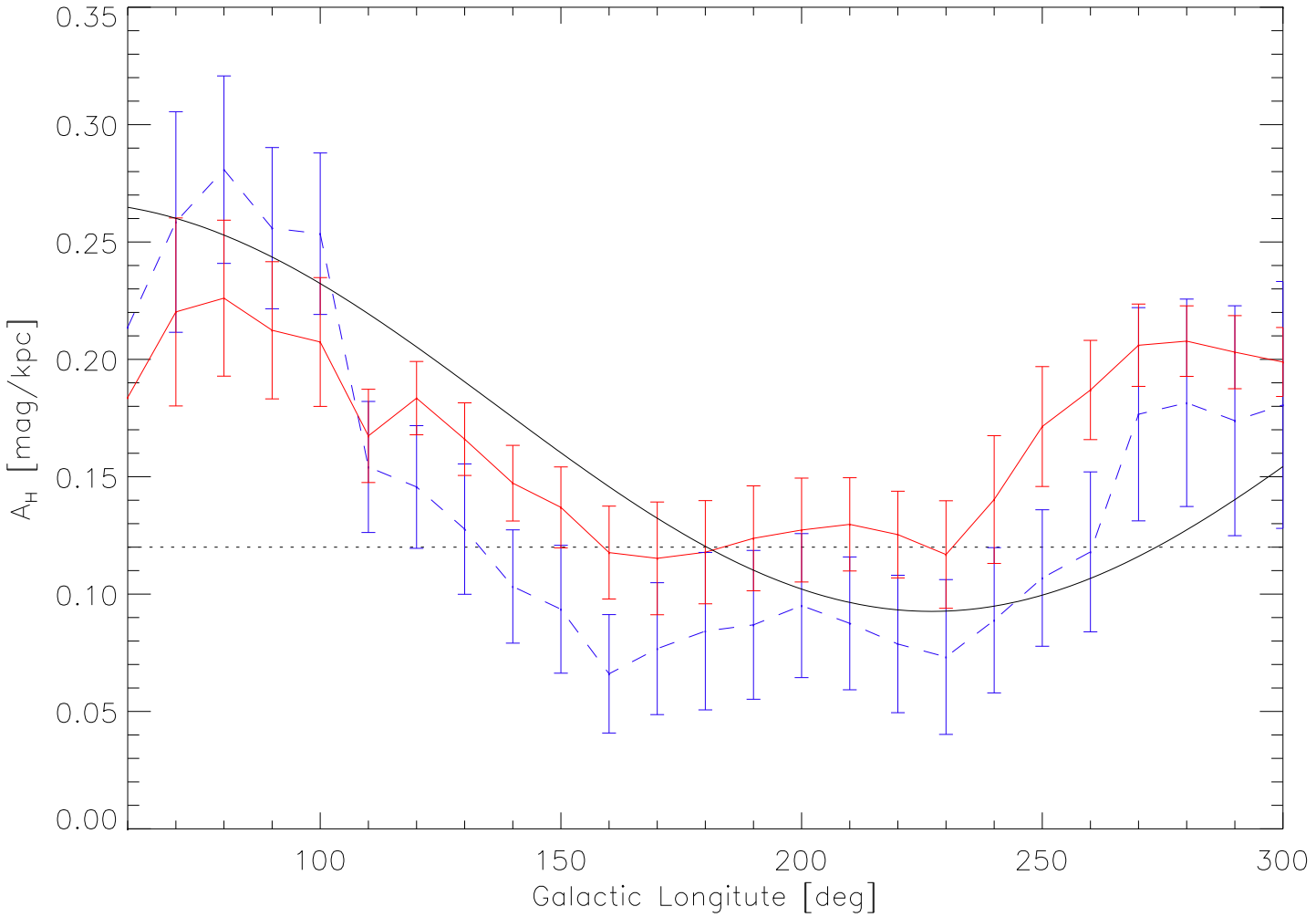


Figure 9.2: Plot shows the $H$-band extinction per unit distance, $A_H[mag/kpc]$, as a function of Galactic longitude. The solid red line represents $A_H^{HK}$ per kpc, and the dashed blue line $A_H^{H45}$ per kpc. The black dotted line represents the canonical value of $A_H[mag/kpc]$. The solid black line represents the function described by J05 (converted to $A_H$[mag/kpc] using Mathis (1990)).

The found variation of interstellar absorption with Galactic longitude is in agreement with the values measured by J05, but there is an offset of $\sim 50^\circ$ i.e. $A_H(180)[mag/kpc] \approx A_H^{J05}(230)[mag/kpc]$ etc. The reason for this offset can be clearly seen from Fig. 5 and 6 in the J05 paper:

- Between $140^\circ < l < 160^\circ$ their measured values of interstellar absorption are significantly higher than would be expected/described by their fit. These bins contained a notably small number of clusters (only 5 clusters were in the $150^\circ < l < 160^\circ$ bin), that were at small distances and were highly reddened compared to neighbouring bins (i.e. $A_H \gtrsim 0.20\,\mathrm{mag/\,kpc}$). These clusters are most likely in a line of sight for which interstellar absorption is higher than is typical for those regions (e.g. in the line of sight of a GMC etc.). Therefore it is reasonable to assume that these clusters have biased the authors values.

- Between $280^\circ < l < 310^\circ$ their measured values of interstellar absorption are significantly lower than would be expected/described by their fit. These were the only bins that included very distant clusters ($> 8\,\mathrm{kpc}$). Additionally these clusters had a notable low extinction ($A_H < 0.10\,\mathrm{mag/\,kpc}$), most likely because they are in a line of sight for which interstellar absorption is lower than is typical for those regions (e.g. at high latitudes). Therefore it is reasonable to assume that these clusters have biased the authors values.

- Attempts by the authors to fit a function to the above data points, whilst ensuring $A_H^{J05}(0)[mag/kpc] = A_H^{J05}(360)[mag/kpc]$, are the source of the observed offset.

## 9.4 Applications

Properly constrained extinction laws are essential for the generation of synthetic star fields with Galaxy models (e.g. BGM, TRILEGAL). If the canonical value is assumed in simulations, the value of interstellar absorption will be underestimated, and the projected number density of simulated field stars will be overestimated, in some lines of sight. In other lines of sight, the value of interstellar absorption will be overestimated and the projected number density of simulated stars will be underestimated. These effects will be most prominent towards the GC and Anticentre, thus particular caution is warranted if the canonical value is assumed for these regions. A good demonstration of this is seen in the distance method

presented in Chapter 4, for which a position dependent correction to the cluster distances as given by the Galactic model is required (Sect. 4.3.3.1). This correction is necessary as cluster distances are underestimated towards the Anticentre and overestimated towards the GC. In essence the positional correction is only necessary because the canonical value of interstellar absorption was assumed, i.e. the projected number density of stars was overestimated towards the Anticentre and underestimated towards the GC. This can be seen through a visual comparison of the positional correction function (Fig. 4.5) with the extinction law function (Fig. 9.2), which clearly shows that they are approximately the inverse of one another. Hence, if the extinction law is used instead of the canonical value, the positional distance correction is no longer required. It should be noted that if the positional distance correction was eliminated from the distance method, the calibration samples (Sect. 4.3) would no longer be required, as there would be no correction to the distance given by the Galactic model. Thus the distances to individual clusters (which are not part of a larger cluster sample) would now be determinable. Finally, the relationship between the extinction law and positional distance correction shows that a cluster's $H45_{med}$ can (statistically) be used as distance indicator, provided that the cluster is in the GP and is not projected onto GMCs. Unfortunately, a cluster's $HK_{med}$ cannot be relied upon in the same manner as its value is dependent on stellar luminosities and spectral types.

## 9.5 Future Work

To investigate the variation of interstellar absorption with Galactic longitude, a cluster sample with homogeneously determined distances and extinctions values was used. Cluster members were statistically identified using the PDT which assigns membership probabilities based on stellar colours (Chapter 3). Whilst the PDT has been shown to identify members with good accuracy (Bonatto and Bica (2007b), Buckner and Froebrich (2013)), it is, of course, not infallible. In particular, difficulties are encountered when attempting to identify members in clusters which are projected onto a high star density field (e.g. towards the GC), in the line of sight of a GMC, have a large proportion of intrinsically red members, and/or have blue straggler members. As the sample's two sets of $H$-band extinction values were determined from the median colours of the cluster's highest probability members, any inaccuracies in the measured colours of the cluster would result in inaccuracies in the cluster's determined extinction values, and by extension, the extinction law. Hence, confirmation of cluster membership (from e.g. spectroscopy, astrometry, X-ray emissions) will reduce uncertainties in the here presented extinction law. Similarly, refinement of cluster distance values (from e.g. the

forthcoming Gaia-ESO Public Spectroscopic Survey data releases, Gilmore et al. (2012)), will further refine and reduce the uncertainties on the extinction law.

It is important to note, however, that any cluster distance and extinction refinements are not expected to change the approximate shape or function of the extinction law, just to lower the uncertainty (as demonstrated by the agreement and systematic offset of its function as determined by the two sets of extinction values - see Fig. 9.2). Future cluster discoveries, and the subsequent expansion of cluster samples with homogeneously derived parameters, will also lower the uncertainty and refine the extinction law. For example, in this work the change in interstellar absorption was explored at 10° longitude intervals using clusters positioned within ±30° from the target longitude. With additional clusters the change in interstellar absorption could explored at e.g. 5° longitude intervals using clusters positioned within ±10° from the target longitude. In particular, an increase in the number of discovered clusters towards the GC will enable the extinction law to be defined for the inner 120° of the GP. Refinements to the interstellar absorption law would further benefit the accuracy of simulations performed with Galactic models, including the cluster distances derived using the distance method in Chapter 4.

# Chapter 10

# Scale Height Evolution

In Chapter 7 a novel method to measure the scale height of cluster samples was presented that significantly lessened established methods' restraints on sample size. In this Chapter the method is applied to three cluster samples, to trace the temporal evolution of cluster scale height in detail for the first time, and to begin to build up an observational understanding of open cluster behaviour on a Galactic scale.

## 10.1 Cluster Samples

The cluster samples CS 1, CS 2 and CS 3 are used for the scale height analyses. Both CS 1 and CS 2 have a large number of clusters with ages in excess of 1 Gyr and so are good tracers of the evolution of scale height, $h_0$, for old clusters. CS 3, however, only has the ability to trace the evolution of $h_0$ below 1 Gyr as it contains few clusters in excess of 1 Gyr. Note, CS 1, CS 2 and CS 3 are not independent of each other, i.e. most clusters are included in at least one of the other two samples. A full discussion of the properties and compositions of each sample is provided in Chapter 2.

The CS 4 sample will not be included in the analyses presented in this Chapter as it contains only 96 clusters. Unfortunately, even with a lessened restraint on sample size, a sample of 96 clusters is simply too small to trace the temporal evolution cluster scale height. Furthermore, unlike CS 1−3, CS 4 is comprised of predominantly older clusters (Fig. 2.4) which is not conducive with an analysis performed uniformly across a wide age range. An additional

consideration is that CS 4 is latitude restricted at $|b| \leq 20°$, whereas CS 1−3 which have no such restrictions (i.e. $|b| \leq 90°$). Potentially a latitude restricted cluster sample can have biased age and vertical distance distributions, which is a particular concern for CS 4 as older clusters have a larger scale height than their younger counterparts (Moitinho, 2010), so will typically be positioned at higher latitudes. Hence, CS 4 potentially consists of older clusters which are not necessary 'typical' or collectively representative of the behaviour of their age group i.e. any trends identified by a scale height analysis undertaken with CS 4 would unlikely be a true representation founded in underlying physics.

## 10.2 Age Bins

Each cluster sample is sorted by age and divided into bins. It is desirable for the bins to be the same size so that the relative scale height uncertainties are constant, and thus any trend with cluster age is more easily identifiable. A bin size of 40 clusters is chosen to achieve a relative scale height uncertainty of $\sim 25\%$ (Fig. 7.2).

Bins are created in two formats:

- **Type A**

  A cluster sample is sorted by age and divided into bins of 40 clusters. The measured scale height values correspond to the median cluster ages of each bin, i.e.

  - The first bin contains clusters 1-40 and the determined scale height corresponds to the age of the $20^{th}$ cluster.
  - The second bin contains cluster 41-80 and the determined scale height corresponds to the age of the $60^{th}$ cluster.
  - The third bin contains clusters 81-120 and the determined scale height corresponds to the age of the $100^{th}$ cluster.

  and so on. For example, a sample of 400 clusters would have 10 bins (each consisting of 40 clusters) with 10 scale height measurements.

- **Type B**

  A cluster sample is sorted by age and divided into continuous bins of 40 clusters. The measured scale height values correspond to the age of each bin which are determined as a running median, i.e.

- The first bin contains clusters 1-40 and the determined scale height corresponds to the age of the $20^{th}$ cluster.
- The second bin contains cluster 2-41 and the determined scale height corresponds to the age of the $21^{st}$ cluster.
- The third bin contains clusters 3-42 and the determined scale height corresponds to the age of the $22^{nd}$ cluster.

and so on. For example, a sample of 400 clusters would have 360 bins (each consisting of 40 clusters) with 360 scale height measurements.

In principle, any trends identified between cluster scale height and age would be independent of the choice of the bin borders. The purpose of Type B binning is to verify any trends (identified from Type A binning) are real, and not dependent on the particular combination of objects per bin. In particular this is useful in cases where a cluster sample is not divisible by 40, i.e. at least one bin contains less than 40 clusters.

## 10.3 Scale Height Analysis

### 10.3.1 Stellar Component of the Galactic Disk

The scale height of the stellar component of the Galactic Disk (GD) changes as a function of age, as shown through scale height measurements of stars with spectral classes O−M (e.g. Pirzkal et al. (2005), Elias et al. (2006)). It is therefore expected that the scale height of clusters is also a function of age, however due to restrictions of sample size, it has not been possible until now to make a comparison between the cluster and stellar scale heights functions.

To determine the scale height function of the stellar component of the GD, scale heights measurements for the different spectral classes are required. For consistency, a compilation of scale height measurements for different spectral types has not been taken from literature as the values would not have been systematically derived. Instead, the scale height function has been calculated from the colour dependent velocity dispersion's for the MS from Dehnen and Binney (1998) which have been converted into spectral types using Popper (1980). Ages for each spectral class are taken as half of their typical expected lifetimes.

Assuming that the kinetic energy is proportional to the potential energy of a spectral class sample gives:

$$0.5mv^2 \propto mh_0 \tag{10.1}$$

thus,

$$h_0 = \kappa v^2 \tag{10.2}$$

where $h_0$ is the scale height in parsec; $v$ is the stellar velocity dispersion; and $\kappa$ is the constant of proportionality. This relation holds for a tracer population in the GD with a constant velocity dispersion (i.e. the $sech^2$ model is assumed - see Eq. 7.2).

From the literature, the stellar scale height function is approximately an exponential, from about 90 pc for O-F classes to about 400 pc for K-M classes. Using these values as a guideline, it is reasonable to assign a value of $\kappa = 3$ as this would give approximately the same scale height values for the spectral classes. Note, the exact value of $\kappa$ is unimportant as it is a scaling factor and the shape of the scale height function (Eq. 10.2) which will be used for comparison, not the scale height measurements for individual spectral types.

A function of the scale height evolution of the stellar component of the GD is generated using Eq. 10.2 and spectral type ages.

### 10.3.2 Age Relation

Figure 10.1 and 10.2 show the scale height values derived for CS 1, CS 2 and CS 3 over a range of age bins. There is a clear trend of increasing scale height with cluster age, with a marked change of gradient at $log(age/yr) = 9$ (1 Gyr). Using linear regression, the evolution of cluster scale height can be characterised by two linear functions of the form:

$$h_0 \propto \begin{cases} 11.0\,\text{pc} \cdot log(age/yr) & \text{if age} \leq 1\,\text{Gyr} \\ 880\,\text{pc} \cdot log(age/yr) & \text{if age} \geq 1\,\text{Gyr} \end{cases} \tag{10.3}$$

where $h_0$ is scale height in parsec.

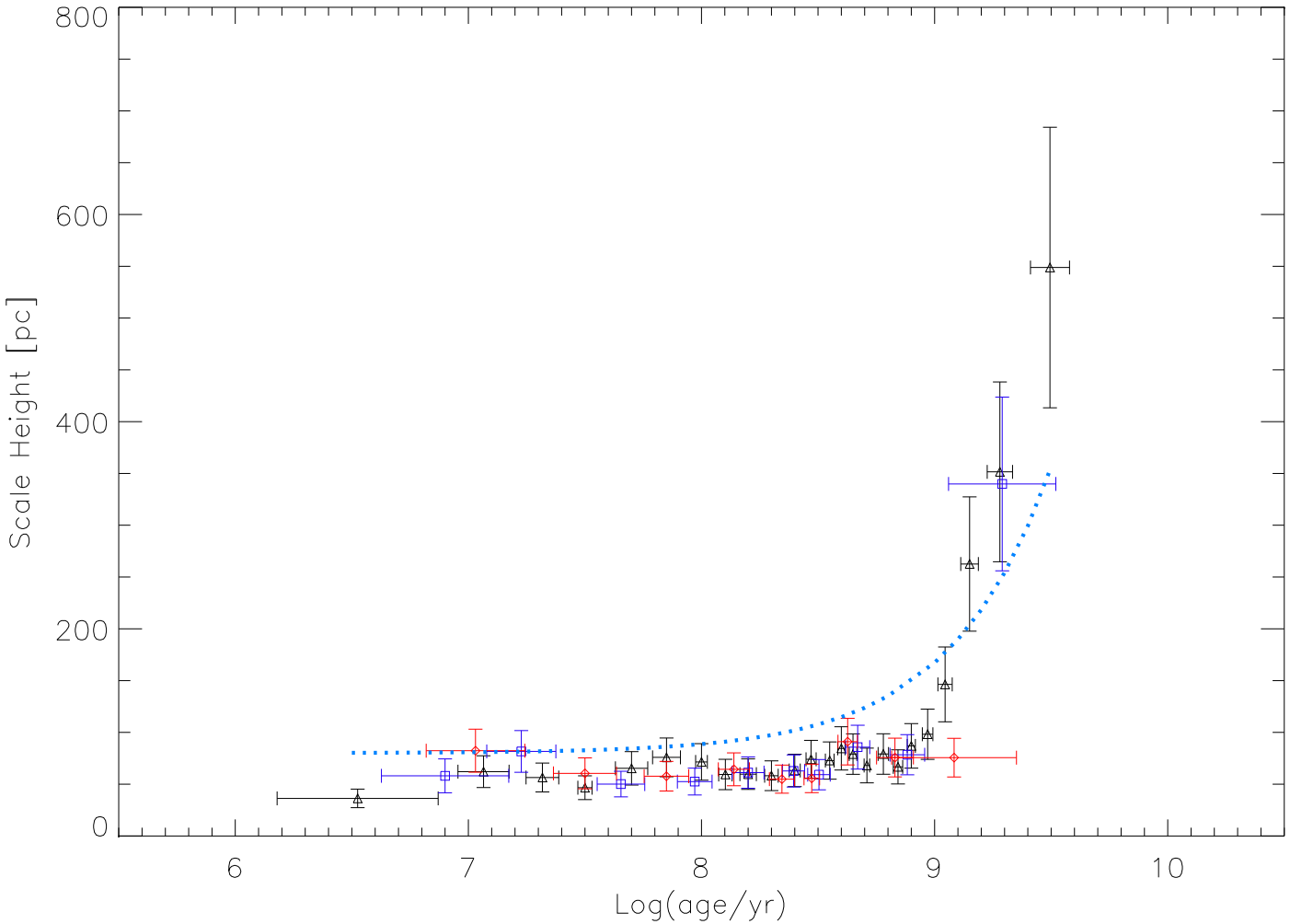


Figure 10.1: Evolution of the cluster scale height $h_0$ with age for the 3 investigated samples with Type A age bins. Black triangles represent CS 1, blue squares represent CS 2 and red diamonds represent CS 3. The horizontal error bars indicate the typical rms of log(age/yr) from the median age in each bin. The blue dotted line is the qualitative scale height-age relation for the stellar component of the Galactic Disk (see Sect. 10.3.1).

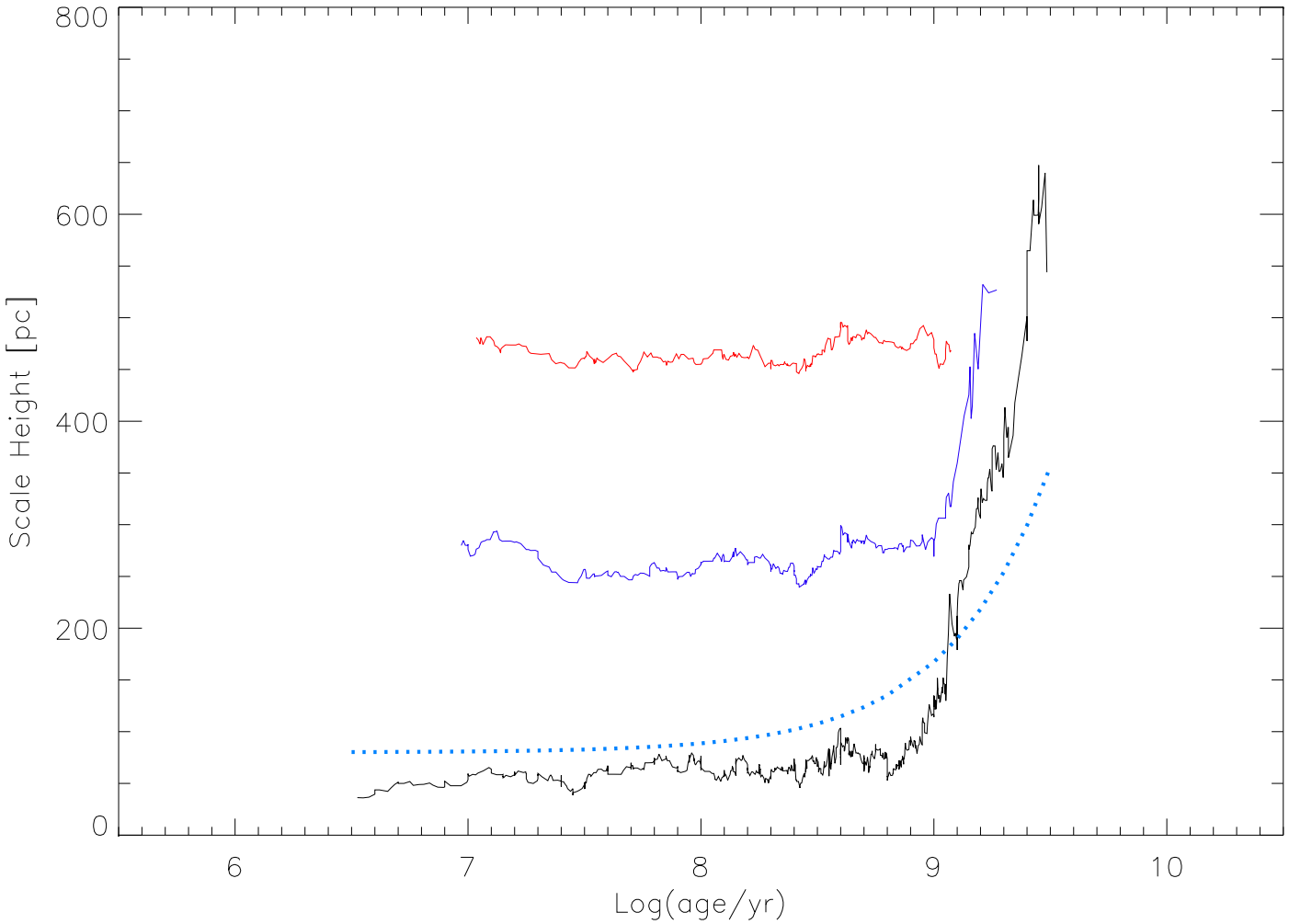


Figure 10.2: Evolution of the cluster scale height $h_0$ with age for the 3 investigated samples with Type B age bins. The solid black line represents CS 1, the solid blue line represents CS 2 with a shift of +200 pc in scale height and the solid red line represents CS 3 with a shift of +400 pc in scale height. The blue dotted line is the qualitative scale height-age relation for the stellar component of the Galactic Disk (see Sect. 10.3.1).

A table of the Type A bin parameters (age, $h_0$, $Z_0$ values and their associated errors) for each sample is provided in Appendix C. The weighted Pearson correlation coefficients of the data points for a cluster age of $< 300$ Myr, 300 Myr$-$1 Gyr and $>1$ Gyr are $\rho = 0.05$, 0.52 and 0.99 respectively, suggesting that there is no evolution in cluster scale height for the first few 100 Myr.

The inability of CS 3 to trace $h_0$ above 1 Gyr is clearly illustrated in Fig. 10.1 and 10.2. The median age of the 40 oldest clusters in CS 3 is $\sim 1$ Gyr, although a few of the clusters are up to a factor of 13 in age larger than this. The presence of these very old clusters in the bin is too few to increase its measured scale height, but enough to inflate the median age of the bin (i.e. right shift the point on the age axis). Resultantly, in both figures the oldest age bin (furthest right plotted point) of CS 3 has a smaller scale height that predicted by Eq. 10.3. One solution is to lower the median age of the bin by excluding the very old clusters. However, removal of clusters from the bin would negate the attempt to keep the bin sizes uniform and would increase the uncertainty on its measured scale height value (which is dependent on sample size $-$ Sect. 7.3.2).

#### 10.3.2.1 Discussion

There is no significant increase in cluster scale height between a few million years and 300 Myr, remaining constant at about 40 pc. This value is comparable to that of: (i) OB stars (30$-$50 pc; Elias et al. (2006), Reed (2006)) which is expected as massive stars rarely form in isolation, instead forming in a clustered environment (e.g. Habing and Israel (1979)) and their short life span means that they do not have sufficient time to significantly increase in scale height; and (ii) the mid-plane at 1/3 scale height of the dust scale height (125 pc; Drimmel et al. (2003), Marshall et al. (2006)). Therefore the formation of clusters and massive stars is only possible in the densest part of the ISM and no significant fraction of observed clusters form (with or without OB stars) away from the mid-plane in lower density environments.

Between the ages of 300 Myr and 1 Gyr there is a gradual increase in cluster scale height of about 10 pc per *dex* in cluster age, with a scale height of 75 pc corresponding to a cluster age of 1 Gyr. Young objects in the Disk have comparable scale heights e.g. young White Dwarfs (55$-$120 pc; Wegg and Phinney (2012)), bipolar Planetary Nebulae (130 pc; Corradi and Schwarz (1995)). The dominant cluster disruption process in this age range is member loss which can occur through an interaction with e.g. GMCs, stellar evolution, tidal relaxation

or a combination of all three processes. Most importantly, if a cluster survives a disruption event, it will gain vertical velocity (and thus scale height). These disruptive processes are well understood from numerical models and full discussions can be found in e.g. Lamers et al. (2005), Lamers and Gieles (2006), Gieles et al. (2008), Gieles (2009).

At 1 Gyr there is a marked increase in cluster scale height of about 880 pc per *dex* in cluster age, with a scale height of 550 pc corresponding to a cluster age of 3 Gyr. Previous attempts to measure the scale height of clusters older than 1 Gyr have had little success. Until now, restraints on sample sizes have severely restricted analyses of the scale height for clusters older than 1 Gyr as the number of observed clusters in this age range is significantly smaller than their younger counterparts. Subsequently only a single literature value of 375 pc for clusters $>1$ Gyr had been measured (Janes and Phelps (1994), Froebrich et al. (2010)). From Eq. 10.3 a value of 375 pc corresponds to a cluster age of about 2.2 Gyr, i.e. in the middle of the old cluster age bin (Fig. 10.1). Hence the literature value is an average scale height for clusters older than 1 Gyr. This finding effectively demonstrates why a new method to determine scale height which greatly reduced restraints on sample size, and a detailed analysis of cluster scale height evolution, was needed.

The change of the cluster scale height function at 1 Gyr is considerably different to the behaviour of the stellar component of the GD, which does not show a marked increase in scale height at 1 Gyr, but instead a gradual increase from a few million years to 3 Gyr (see Fig. 10.1). Its plausible that the older clusters were formed at larger distances from the Galactic mid-plane than their younger counterparts i.e. the change in cluster scale height function at 1 Gyr is a historical marker of the formation behaviour of Galactic star clusters (see e.g. de la Fuente Marcos et al. (2013)). However, it is reasonable to expect the temporal scale height evolution of clusters and the observed stellar components of the Disk to be near-identical if the scale height of clusters was governed solely by their stellar components. Therefore, as it has been shown that younger clusters ($<1$ Gyr) have scale heights comparable to the stellar component of the Disk, the marked change in scale height at 1 Gyr indicates that a change in the underlying physical processes governing the evolutionary behaviour of clusters occurs. A consensus in the literature has not yet been reached on the role that initial cluster mass plays in disruption (see e.g. Bastian (2011)), but the change in the scale height function at 1 Gyr closely corresponds to the mass-dependent destruction time-scale for clusters with an initial mass of $10^4\,M_\odot$ within 1 kpc of the Sun (Boutloukos and Lamers, 2003). As CS 1, 2 and 3 consist of clusters that are within 1.8 kpc, 1.0 kpc and 1.0 kpc of the Sun respectively (Chapter 2), it is reasonable to expect that the older clusters in these

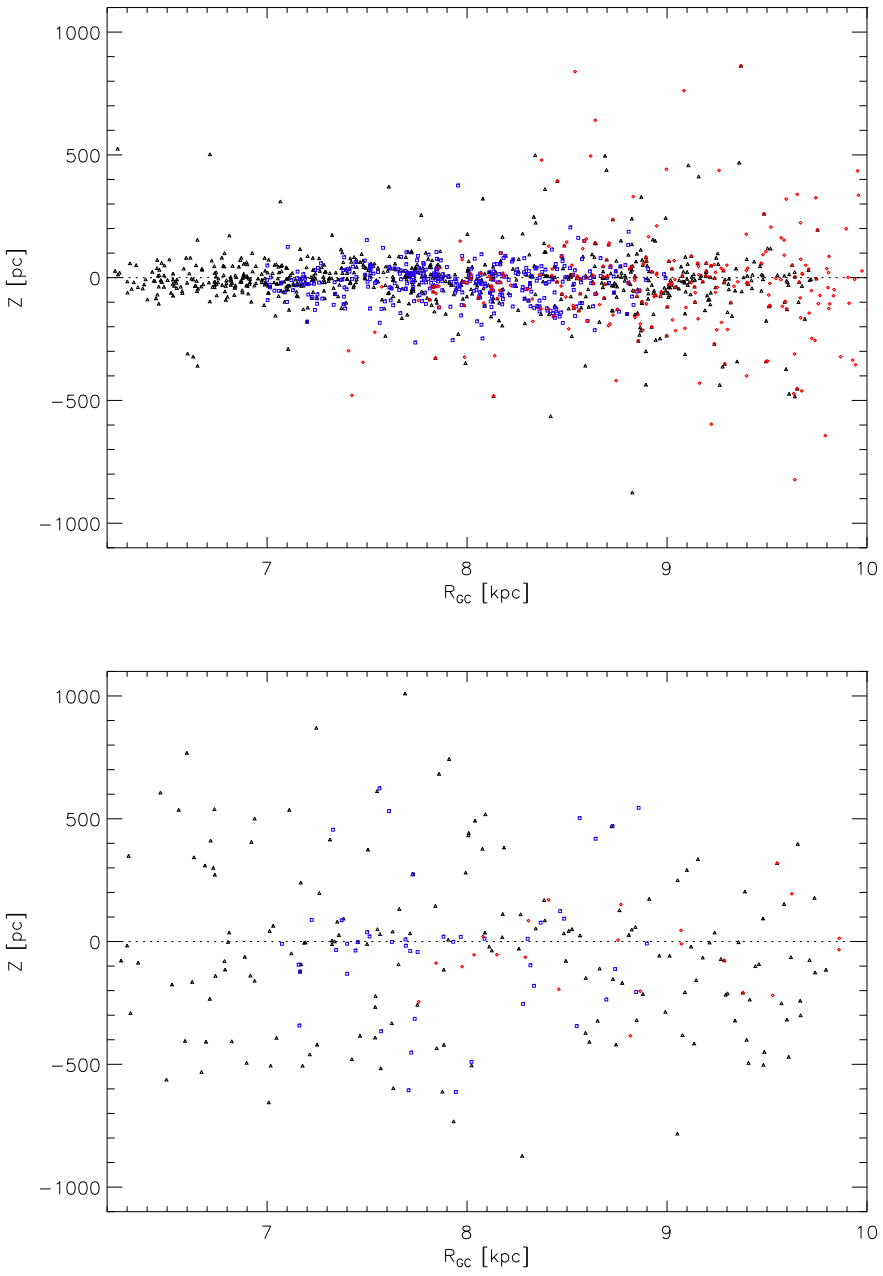


Figure 10.3: Plot of Galactocentric distance, $R_{GC}$, against vertical distance from the Plane, $Z$, of clusters with an age (*Top*) less than 1 Gyr and (*Bottom*) greater than 1 Gyr. The different symbols and colours represent the different cluster samples: black triangles (CS 1), blue squares (CS 2) and red diamonds (CS 3).

samples ($>1$ Gyr) are predominantly those which were initially massive ($> 10^4\,M_{\odot}$). Furthermore, whilst the heating of the stellar component of the Disk occurs gradually via N-body interactions, the tidal field and GMCs, the discontinuity in the clusters scale height function around 1 Gyr implies additional sources of heating. Assuming a mass-dependent disruption time scale, by 1 Gyr only initially massive clusters are expected to have survived and had at least one violent interaction (e.g. Lamers et al. (2005)). These interactions would have caused the clusters to undergo mass loss through tidal shocks, scattering them into higher orbits away from the GP mid-plane, simultaneously decreasing the likelihood of further violent interactions (and disruption) and prolonging their chances of survival. Indeed, Fig. 10.3 shows there is a notable lack of clusters $>1$ Gyr close to the Galactic mid-plane comparative to their younger counterparts.

To date there have been no simulations of the temporal evolution of cluster scale height, most likely caused by the complex nature and number of variables that need to be considered i.e. the affects of gravitational interactions, Galactic structure and chemical composition, individual cluster parameters, cluster initial formation conditions and internal cluster processes. However, there have been simulations of the effects of heating (from interactions) on clusters' vertical height above the GP. In order to ascertain if the inclined orbit and vertical height above the plane 4 Gyr old open cluster M67 ($\mathrm{Z} = 450$ pc) was a result of interactions or an inherent property, Gustafsson et al.(in prep) traced the evolution of clusters in a spiral galaxy over a 5 Gyr period. The simulations showed that interactions of the clusters with spiral arms and GMCs could cause the increase in vertical velocity needed through member ejection, rather than the formation of clusters at higher latitudes. Their work also showed that heating from stellar evolution and interactions with globular clusters, High Velocity Clouds (HVC) and dark matter halos either had little affect on clusters vertical height above the plane or were rare occurrences. As cluster samples with large scale heights are typically associated with having greater vertical heights above/below the plane, the authors findings provide the first numerical agreement with the here presented observational evidence.

### 10.3.3 Dependence on Galactic Position

To investigate if cluster scale height changes with Galactocentric radius, $R_{GC}$, the age dependence identified in Sect. 10.3.2 has to be eliminated. To do this, CS 1, 2 and 3 are divided into four age bins: (1) $age < 80$ Myr; (2) $80\,\mathrm{Myr} \leq age < 200$ Myr; (3) $200\,\mathrm{Myr} \leq age < 1$ Gyr; (4) $age \geq 1$ Gyr. Each age bin is then separated into three Galactocentric distance ranges and $h_0$ is determined for each sub-sample. To aid the reader in evaluating the trustworthiness

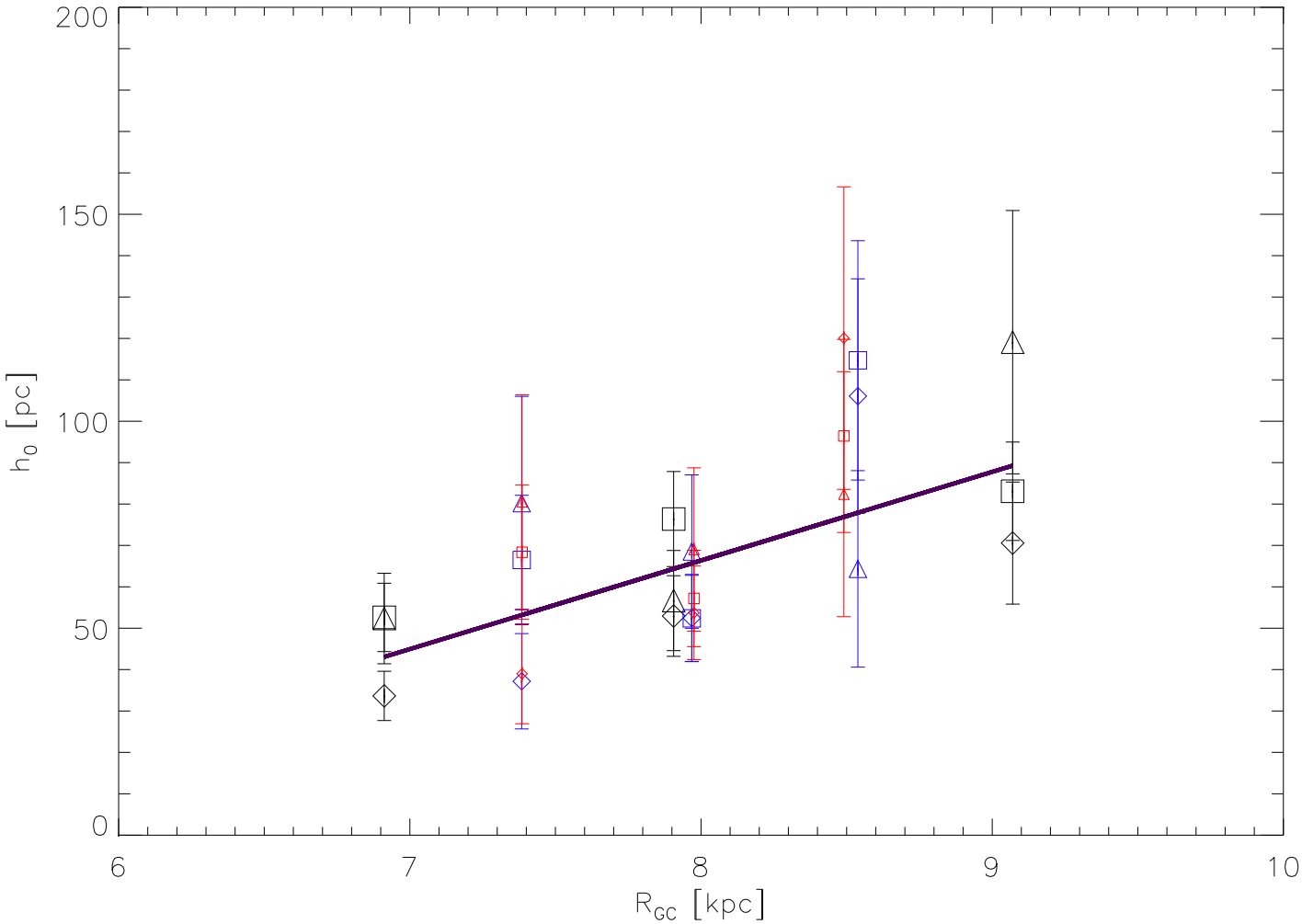


Figure 10.4: Shows cluster scale height, $h_0$, as a function of Galactocentric distance, $R_{GC}$. The symbols indicate different age ranges. Diamonds indicate clusters younger than 80 Myr, triangles indicate clusters with ages between 80 Myr and 200 Myr and squares indicate clusters with ages between 200 Myr and 1 Gyr. The different cluster samples are distinguished by different colours and symbol sizes: large black (CS 1), medium blue (CS 2), small red (CS 3).

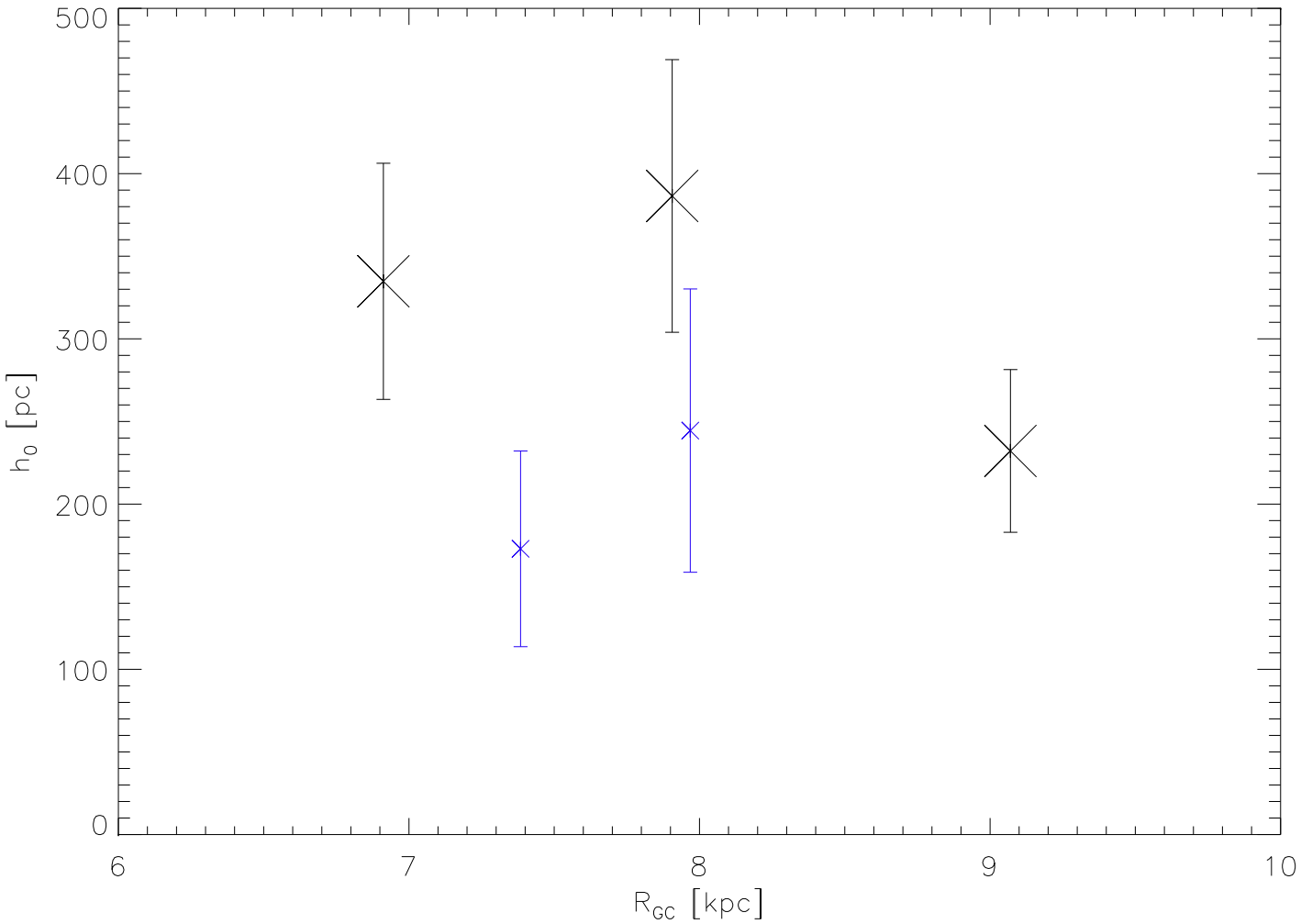


Figure 10.5: Shows cluster scale height, $h_0$, as a function of Galactocentric distance, $R_{GC}$, for clusters $> 1$ Gyr. The different cluster samples are distinguished by different colours and symbol sizes: large black (CS 1), small blue (CS 2).

of the determined scale height measurements, a table with the number of clusters per bin (and their respective measurements) is provided in Appendix C.

A weak trend between scale height and Galactocentric distance is identified for the younger clusters ($< 1$ Gyr), with:

$$h_0 \propto 0.02 \cdot R_{GC}[pc] \quad \text{if age} < 1\,\text{Gyr} \tag{10.4}$$

where $h_0$ is cluster scale height; and $R_{GC}$ is Galactocentric distance in parsecs. The weighted Pearson correlation coefficient for the younger clusters is $\rho = 0.80$.

#### 10.3.3.1 Discussion

The trend between scale height and Galactocentric distance (characterised by Eq. 10.4) is consistent with the results of Sect. 10.3.2 as, typically, sufficient time has not passed to guarantee that the younger clusters have had at least one violent interaction which has either disrupted or scattered them out of the mid-plane. Models have shown there to be a higher density of visible mass (stars, gas) in the Disk towards the GC for $R_{GC} < 5$ kpc (Klypin et al. (2002), Rodriguez-Fernandez and Combes (2008)). Thus, at smaller $R_{GC}$ values it is reasonable to expect a higher frequency of disruptive processes acting on clusters. A secondary effect is more high mass clusters forming at smaller $R_{GC}$ values (close to the mid-plane), than at larger $R_{GC}$ values. Potentially, therefore, the observed difference in scale height is due to the higher mass clusters dominating the samples towards low $R_{GC}$, and lower mass clusters dominating the samples at larger $R_{GC}$. Furthermore it has been shown that there is moderate flaring of the molecular (star forming) material in the Disk (e.g. Sanders et al. (1984), Wouterloot et al. (1990)) which, as clusters are formed in the mid-plane of the Disk, provides a partial explanation of the trend between scale height and Galactocentric distance.

An alternative explanation is that the trend is caused by the assumption of incorrect metallicity values for clusters when their fundamental properties (distances, extinctions and ages) were derived. For CS 1, 2 and 3 these properties were (mostly) derived through fitting modelled cluster sequence isochrones to clusters' CCM diagrams. If an incorrect metallicity (e.g. Solar) is assumed for a cluster, incorrect metallicity isochrones are fitted and hence incorrect fundamental property values are derived. In the presence of a Galactic metallicity gradient,

it is reasonable to expect that a proportion of the cluster samples fundamental properties would be erroneous due to incorrect metallicity values. In principle, clusters' Solar distances (and thus vertical distances) would be underestimated towards the GC and overestimated towards the Anticentre, which would produce the observed correlation between cluster scale height and $R_{GC}$. However, two of the three cluster samples' parameters (CS 2 and CS 3) were compiled from literature, i.e. a constant metallicity was not assumed. Whilst CS 1 does (mostly) assume that clusters have a Solar metallicity, all three samples show the same scale height/Galactocentric distance correlation. Hence it is unlikely that the identified trend is caused by incorrect assumptions of cluster metallicities. Furthermore, any errors on the clusters determined vertical distances incurred from assuming an erroneous metallicity will be smaller than the errors on the determined scale heights, and therefore would not have significantly contributed to the observed trend.

No trend was found between scale height and Galactocentric distance for the old clusters ($\geq$ 1 Gyr). The weighted Pearson correlation coefficient for the old clusters is $\rho = -0.29$ (Fig. 10.5). This is consistent with the results of Sect. 10.3.2, i.e. clusters which survive $>$ 1 Gyr are scattered away from the mid-plane after one or more violent interactions. With increasing vertical distance from the mid-plane, the probability of violent interactions decreases, and once out of the mid-plane, i.e. where GMCs are concentrated (Stark and Lee, 2005), the expected likelihood of an interaction becomes independent of Galactic position.

The lack of a relationship between scale height and Galactocentric distance for the old clusters supports the argument that the identified trend for the younger clusters is not caused by the use of erroneous metallicities. However, it should be noted that the paucity of old clusters meant that scale height values could not be measured for the old clusters in CS 3 and those in the largest Galactocentric distance bin for CS 2. Thus interpretations of the relationship (lack there of) between old clusters and Galactocentric distance should be treated with a degree of scepticism, until an analysis with additional old open clusters can be made.

To fully understand the trends identified here further investigation is required, including determination of mass estimates for the cluster samples and numerical simulations of cluster populations in the Galaxy; both of which are outside the scope of this work.

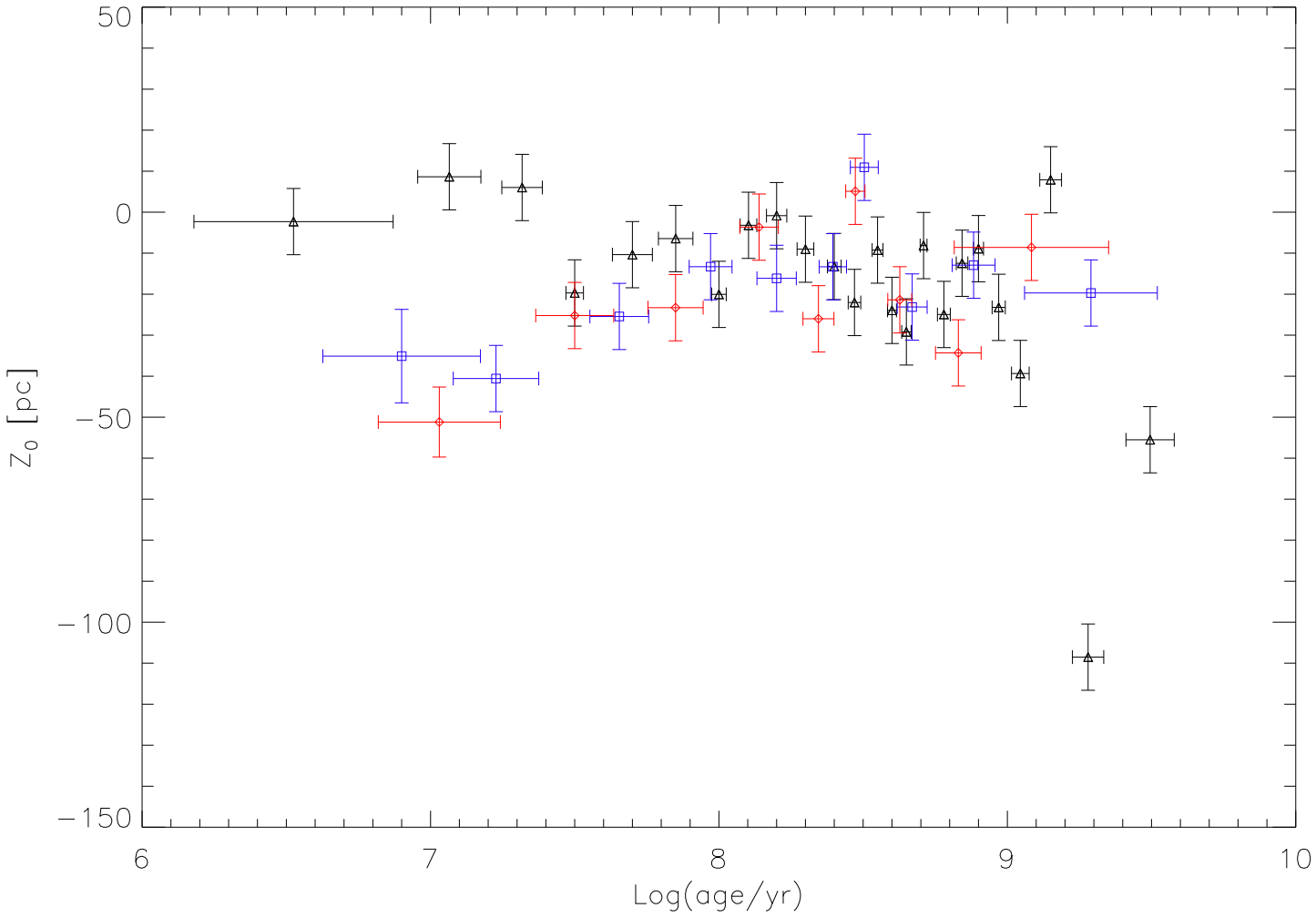


Figure 10.6: Shows cluster vertical zero points, $Z_0$, with cluster age. The different symbols and colours represent the different cluster samples: black triangles (CS 1), blue squares (CS 2) and red diamonds (CS 3). The horizontal error bars represent the *rms* of log(age/yr) from the median age.

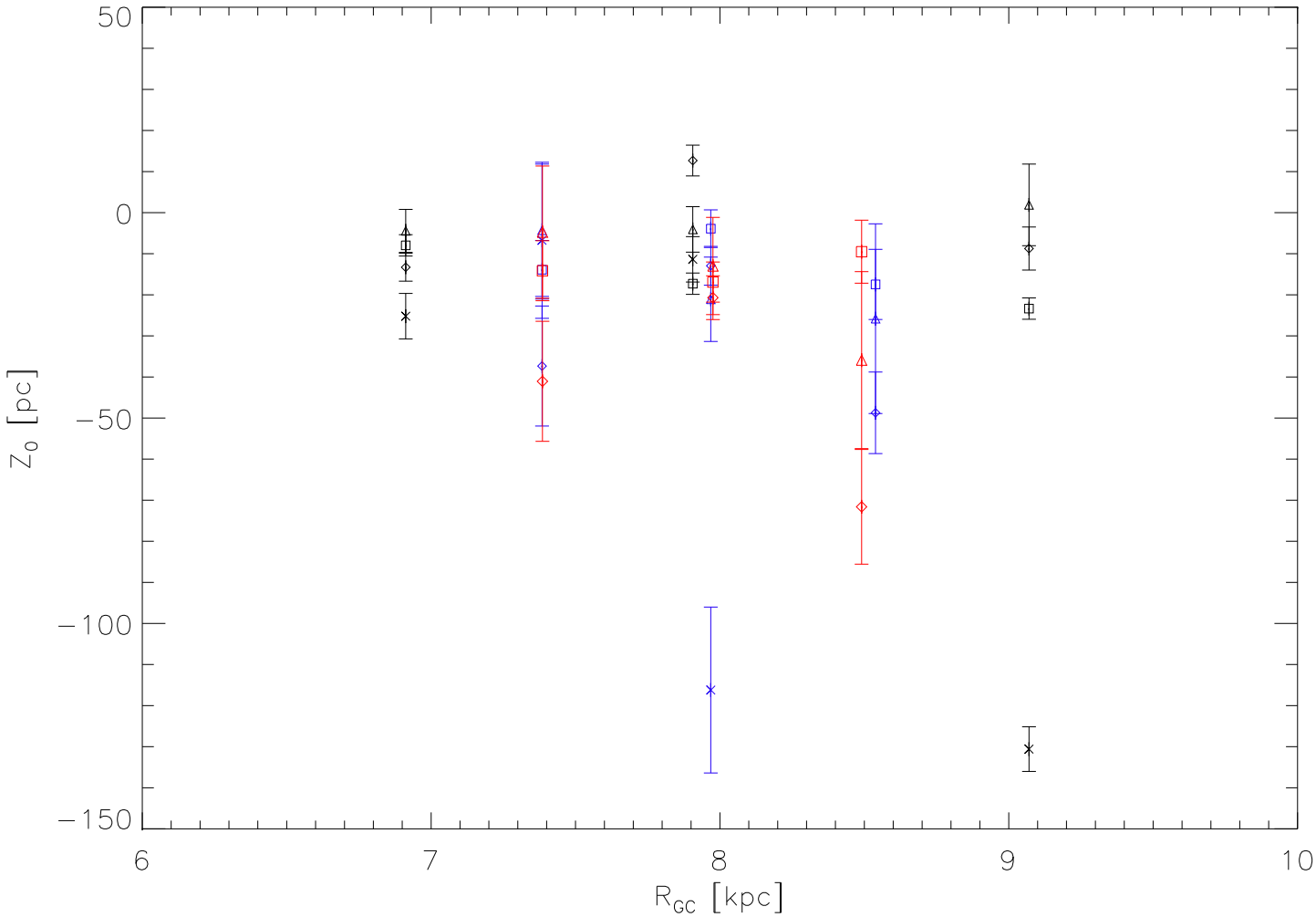


Figure 10.7: Shows cluster vertical zero points, $Z_0$, as a function of Galactocentric distance, $R_{GC}$. The symbols indicate different age ranges. Diamonds indicate clusters younger than 80 Myr, triangles indicate clusters with ages between 80 Myr and 200 Myr, squares indicate clusters with ages between 200 Myr and 1 Gyr and crosses indicate clusters with ages $> 1$ Gyr. The different cluster samples are distinguished by different colours: black (CS 1), blue (CS 2), red (CS 3).

## 10.4 Vertical Zero Point Analysis

No correlation was found between samples' vertical zero point, $Z_0$, and cluster age or Galactocentric distance (Fig. 10.6 and 10.7). This is an expected result as the spatial distribution of clusters is symmetric around the mid-plane (Eq. 7.1 and 7.2), and therefore clusters should be perturbed/disrupted equally above and below the plane such that the plane of symmetry (i.e. $Z_0$) will remain constant. Note, the outliers in Fig. 10.6 and 10.7 are an observational effect: samples with large scale heights typically contain clusters at large vertical distances above/below the Plane, so that clusters in these samples below the GP have significantly larger vertical distances compared to clusters above the plane with respect to the Sun (as $Z_\odot$ is positive), thus as the distribution of clusters around $Z_0$ is symmetric, the value is observed to decline with increasing scale height.

### 10.4.1 Solar Vertical Displacement

The Solar vertical displacement is determined as the weighted mean of the measured $Z_0$ values of the Type A bins for each sample, such that

$$Z_\odot = -\frac{\sum_{i=1}^{N_{ss}} w_i Z_0}{\sum_{i=1}^{N_{ss}} w_i} \tag{10.5}$$

where

$$w_i = \frac{1}{\sqrt{\Delta Z_0}} \tag{10.6}$$

and

$$\Delta Z_\odot^2 = \frac{1}{\left(\sum_{i=1}^{N_{ss}} w_i\right)} \tag{10.7}$$

where $Z_\odot$ is the Solar vertical displacement; $\Delta Z_\odot$ is the error on $Z_\odot$; $N_{ss}$ is the number of Type A bins for each sample (i.e. 24 for CS 1, 10 for CS 2, 9 for CS 3); $w_i$ are the weights; and $\Delta Z_0$ is the uncertainty on $Z_0$.

Note the multiplication correction of $-1$ applied to Eq. 10.5. In principle, clusters will typically form in, and thus samples distributions will be symmetric around, the mid-plane of the

GD (where the molecular material lies). Hence, if the Sun is positioned above the mid-plane the calculated weighted mean of the samples $Z_0$ values will be negative, or positive if the Sun is positioned below the mid-plane.

From Eq. 10.5 and 10.7 a Solar vertical displacement above the GP of $Z_\odot = 18.5 \pm 1.2$ pc is derived, which is in agreement with values determined from other tracers e.g. OB stars ($19.6 \pm 2.1$ pc; Reed (2006)), optical star counts ($20.5 \pm 3.5$ pc; Humphreys and Larsen (1995)), reddening material ($22.8 \pm 3.3$ pc; Joshi (2005)).

## 10.5 Future Work

A detailed understanding of the here presented results can only be achieved through further research. Observationally, it would be advantageous to include additional clusters with high precision parameters (distances, metallicities, ages). Unfortunately at present there are a limited number of clusters available in the literature (the majority of which have been used in this analysis). Large scale surveys (such as VISTA-VVV, Gaia-ESO, and UKIDSS-GPS) are expected to identify a significant number of previously undiscovered clusters within the next few years, providing both high precision parameter measurements for these new clusters and a refinement of those currently known in the literature.

To date there are no numerical simulations of the temporal evolution of cluster scale height on a Galactic scale. This is most likely due to the extensively complex nature of simulating the physics governing cluster evolution. For example, the affects of gravitational interactions (of clusters with e.g. GMCs, HVCs, spiral arms, the Galactic Bar, globular clusters, black holes), Galactic structure and chemical composition (Disk warping and potential, metallicity and matter density gradients), cluster sample parameters (Galactic orbits and positions; distance, ages, metallicities and extinction distributions; tidal and half mass radii; stellar velocities etc.), cluster formation (stellar density and composition, stellar and cluster infant mortality, initial mass function etc.) and internal processes (stellar evolution, viral and tidal relaxation), on cluster scale height need to be considered. It is reasonable to anticipate large scale numerical simulations of the evolution of cluster scale height will become available in coming years, with the continuous improvements in both computational power and the scientific communities understanding of the physics governing cluster evolution. The observational evidence presented provides constraints for future numerical models of cluster evolution and disruption in the context of the entire Galactic Disk.

# Part IV

# Conclusions

This Thesis has successfully conducted a homogeneous analysis of Galactic open clusters, achieved through the development and implementation of new methods to derive the distances, extinctions, ages and scale heights of cluster samples. Below, the conclusions of this research are presented.

## Methodology

A novel automated calibration and optimisation method to derive open cluster distances from NIR photometry alone has been presented. Using the Photometric Decontamination Technique (PDT) from Bonatto and Bica (2007b) and Froebrich et al. (2010), and a Galactic Model, distances are derived on the principle that they are related to the projected number density of stars foreground to the cluster. The method can estimate distances with a better than 40 % accuracy for clusters within 5 kpc of the Sun, and significantly better for those more distant, when calibrated with a cluster sample which has an intrinsic scatter of 30 %. A comparison of a cluster sample's derived distance estimates with their literature values showed a good correlation, albeit with a large scatter which can be attributed to the difficulty in accurately deriving distances for clusters within 3 kpc of the Sun.

An automated method to derive open cluster extinction values from NIR photometry alone has been presented. Using the PDT, two $H$-band extinction estimates are derived for clusters from their members' median $[H-K]$ and $[H-4.5]$ colours. The method requires the value of the zero points of both colours to be known, but the $[H-K]$ zero point is not well defined in the literature, as it is difficult to measure because the colour intrinsically depends on stellar spectral type and luminosity class. A sample consisting of clusters with a low fraction of $K$-band excess objects was used to measure the value of the $[H-K]$ zero point to be 0.06 mag. The validity of this value was confirmed through a cross-comparison of the two sets of derived $H$-band extinction estimates for a cluster sample, which were shown to generally be in good linear agreement.

A pipeline to derive cluster ages through fitting modelled cluster sequences to their CCM diagrams has been presented. This pipeline has a secondary application of refining the distance and extinction values given by the automated methods discussed above. It was designed to be robust and to minimise the variation between multiple distance, reddening and age values, often derived for a single cluster by multiple authors using traditional isochrone fitting, which is subjective to each fitter's personal interpretation of the cluster's CCM diagrams. A cross-

comparison of a cluster sample's derived ages with those given by the literature showed them to be in good agreement, although a few cluster's age values disagreed by up to a factor of 10. The discrepancies were most likely caused by (i) the pipeline incorrectly assuming they were of Solar metallicity, and (ii) uncertainties in the methodology employed to derive the literature values. Distance values derived using the pipeline are approximately 1.25 times smaller than those derived using the automated calibration and optimisation method (well within the 40 % uncertainty). The refined pipeline extinction values are in general 1:1 agreement with the automated extinction estimates.

A novel method to derive the scale height and vertical zero point for cluster distributions has been presented. Using modelled distributions and Kolmogorov-Smirnov tests, measurements can be made for sample sizes of 15 or more, with an uncertainty of 25 % on the scale height value for a sample size of 38. This is a significant improvement on previously established methodologies used in the literature, which require a minimum of a few hundred objects per sample to make a reasonably accurate measurement. As such, the novel method enabled a detailed analysis of the scale height evolution of Galactic open clusters to be undertaken for the first time. Furthermore, the method is not limited to cluster samples and can be applied to samples of any type of object, as demonstrated by Froebrich et al. (2015) for Planetary and Proto-Planetary Nebulae, Jets, and photo-dissociation regions.

## Results

### The FSR List Catalogue

An in-depth homogeneous analysis of the entire FSR List catalogue was undertaken for the first time, utilising photometry from the 2MASS and WISE surveys. Distances, extinctions and YSO fractions were derived for 55 % and 39 % of the total known and new open cluster candidates in the catalogue, respectively. The distribution of the sample is biased towards its spatial density peak in the Galactic Plane at a Solar distance of about 3 kpc, most likely caused by apparent radii selection effects on the catalogue and the analysis. Known clusters within 5 kpc were found to have a scale height of $235 \pm 20$ pc and new cluster candidates $315 \pm 30$ pc, indicating typical ages of $\sim 1.9$ Gyr and $\sim 2.3$ Gyr respectively.

Most clusters in the sample have an extinction in the range $0\,\mathrm{mag} \leq A_H \leq 2\,\mathrm{mag}$, and the

distribution is biased towards its peak of 0.1−0.2 mag. Clusters were typically found to have a YSO fraction of $Y_{frac} < 10\,\%$. Those with a $Y_{frac} > 1\,\%$ were measured to have a scale height of $190 \pm 15$ pc, whilst those with $Y_{frac} < 1\,\%$ were measured to have a scale height of $300 \pm 20$ pc. All clusters were found to have a $Y_{frac} < 20\,\%$, which suggests that the sample potentially contains no clusters with an age of $< 4$ Myr.

Ages were derived for 32 % of the known and 8 % of the new open cluster candidates. Confirmed new cluster candidates are predominantly young, hence the comparative lack of new cluster candidates in the sample is a reflection of the difficulty in deriving their ages through modelled cluster sequence isochrone fitting, due to e.g. less well defined/prominent features (Main Sequence/turn-off, giants etc.), a large proportion of members falling below photometry magnitude limits.

The age distribution of the sample ranges between 5 Myr and 10 Gyr with the majority of clusters in the 10 Myr−5 Gyr range. There is a deficit of clusters younger than 10 Myr in the sample, most likely because these objects are typically embedded and thus more difficult to detect in 2MASS. The modal value of distribution is $\sim 400$ Myr, which is higher than expected when compared to other cluster catalogues such as DAML02 and WEBDA. A cross-comparison between the ages derived for the sample and those given for them by the MWSC catalogue were found to be in good agreement, suggesting that the methods employed to discover the FSR List catalogue, and derive cluster properties, perhaps favour older clusters. This is supported by the finding that the old and young clusters of the sample possess significantly different distributions.

Thirteen clusters were studied using additional deep, high resolution photometry UKIDSS-GPS and VISTA-VVV surveys, because they were suspected to either contain PMS sequences or had notable Galactocentric distances. Of these, seven were confirmed to contain PMS stars, one of which is a confirmed new cluster candidate. Notably, the analysis identified FSR1716 as both the oldest open cluster in the catalogue and nearest to the Galactic Centre at $< 2$ kpc. Due to its age of 10 Gyr, this cluster is a potential globular cluster candidate. In many cases these were the first analyses of the clusters using deep, high resolution photometry, and as such their derived properties differed substantially from literature estimates. For the majority of these clusters there was a marked discrepancy between the properties derived in this Thesis (and the literature) with those listed in the MWSC catalogue. This is most likely caused by (i) the pipeline presented by this Thesis (and the literature) incorrectly assuming a Solar metallicity for these clusters and/or (ii) due to the nature of these clusters the pipeline employed by the authors of the MWSC catalogue to homogeneously derive cluster ages has

produced systematic (but sometimes erroneous) values, particularly in the absence of deep, high resolution photometry.

The accuracy of the results presented here could be further improved through the inclusion of deep, high resolution photometry (from e.g. UKIDSS-GPS and VISTA-VVV surveys), for all objects in the catalogue, but unfortunately this photometry is only available for a minority at present. Mass estimates would enrich the understanding of the here observed cluster distributions in the Galactic Plane.

### Extinction Law

Interstellar absorption in the Solar Neighbourhood is typically assumed constant, derived as an average over all lines of sight, with a canonical value of $A_H[mag/kpc] = 0.12$ mag. This Thesis has investigated the variation of interstellar absorption with Galactic longitude using a sub-sample of the FSR List catalogue. A systematic dependence was found and is characterised by the function: $A_H(l)[mag/kpc] = 0.10 + 0.001 \times |l - 180°|/°$ for $60° \leq l \leq 300°$, i.e. the value of interstellar absorption varies up to a factor of two, depending on the observer's line of sight. The canonical value corresponds to the value measured towards the Anticentre and is approximately three times smaller than the value measured at 60° from the Galactic Centre.

Therefore the extinction law presented here (and not the canonical value), should be adopted for all simulations performed with Galactic models. A relevant example of the importance of adopting the law is in the discussed automated distance method presented by this Thesis: the methodology requires simulations with a Galactic model to derive cluster distance estimates, and then a correction to those estimates based on clusters' longitudinal positions. However, the positional correction is only necessary because the canonical value is adopted instead of the extinction law; consequently the density of observable stars foreground to clusters (and thus their distance) is overestimated by the model towards the Galactic Centre, and underestimated towards the Anticentre. Furthermore as the $[H - 4.5]$ colour is independent of spectral type and luminosity, the extinction law also demonstrates that this colour can statistically be used as an indicator of cluster distance, provided that the cluster is not in the line of sight of a GMC and is in the Galactic Plane.

### Scale Height Evolution

The temporal scale height evolution of Galactic open clusters has been traced in detail for the first time using three cluster catalogues. A strong correlation between cluster scale height and age was found. From their formation until an age of approximately 300 Myr, there is no significant increase in cluster scale height which remains constant at about 40 pc. This is comparable to the scale height of OB stars, providing a good example of the link between massive and clustered star formation. Between 300 Myr and 1 Gyr cluster scale height gradually increases at a rate of about 10 pc per *dex* in cluster age. At 1 Gyr clusters are found to have reached a typical scale height of 75 pc with a significant increase in the rate at which they gain scale height of about 880 pc per *dex* in cluster age, which is also markedly different to the stellar component in the Galactic Disk. It is plausible that the older clusters were formed at larger distances from the Galactic mid-plane than their younger counterparts i.e. the change in cluster scale height function at 1 Gyr is a historical marker of the formation behaviour of Galactic star clusters (see e.g. de la Fuente Marcos et al. (2013)). However, if cluster scale height was governed solely by the ages of their stellar components, one would expect for them to have a very similar scale height evolution to that of the observed stellar components of the Galactic Disk. The reason older clusters gain scale height at a faster rate than their younger counterparts is most likely due to the older sample being dominated by initially massive clusters, which have survived one or more violent interactions and have been scattered into Galactic orbits away from the Galactic mid-plane.

A weak positive correlation between cluster scale height and Galactocentric distance was found for clusters with an age $< 1$ Gyr. In principle, if an erroneous metallicity was assumed for clusters when deriving their distances (through fitting modelled isochrone sequence isochrones to their CCM diagrams), their vertical distance from the Plane would be underestimated towards the Galactic Centre and overestimated towards the Anticentre. However, this is unlikely to be the source of the correlation as it was found for all cluster samples (for which various methods had been employed to derive metallicity values), and if an erroneous metallicity was assumed, the uncertainties on the cluster scale height measurements would be larger than those on cluster vertical distance values. Thus the most likely cause of the correlation is the matter density gradient and moderate flaring of the Galactic Disk, i.e. similarly aged clusters positioned towards the Galactic Centre would be expected to typically have higher masses and to have formed close to the mid-plane, but lower masses are typically formed further away from the (flared) mid-plane towards the Anticentre. This explanation

is further supported by the finding that there is no correlation between scale height and Galactocentric distance for clusters $> 1\,\mathrm{Gyr}$, but further investigation is warranted.

No correlation between cluster age, Galactocentric distance and the samples' vertical zero points was found. Clusters' planes of symmetry remain constant regardless of age, scale height or Galactic position as their distribution is symmetric around the mid-plane and therefore cluster disruption is homogeneous around the mid-plane.

The Solar vertical displacement above the Galactic Plane was measured from the distribution of clusters around the mid-plane and found to be $Z_{\odot} = 18.5 \pm 1.2\,\mathrm{pc}$. This is in agreement with various established literature values derived from other tracers (e.g. OB stars, optical star counts, reddening material).

At present there are no numerical simulations of the scale height evolution of Galactic open clusters, which are needed for a detailed understanding of the here presented observational evidence. Future analyses will benefit from increased accuracy of already known cluster properties from new data releases (e.g. distances from Gaia-ESO), mass estimates and the expansion of current cluster samples, in addition to any future cluster samples that are discovered.

# Acknowledgements

This Thesis would not have been possible without my supervisor Dirk Froebrich whose input, guidance, support and attention to detail have been 'stellar'; and the funding awarded to me by the Science & Technologies Facilities Council and the University of Kent to conduct my research.

I would like to thank my family for their continuous support. Will, I will never be able to sufficiently express in words my eternal gratitude for your love, patience and support throughout this process - thank you. A big thanks must go to my fabulous fellow Ph.D.'s in room 104 for both academically stimulating conversations and friendship.

Finally I would like to thank the reader for taking the time to read my Thesis in its entirety, as (to paraphrase a philosophical thought experiment): *if a thesis is written and nobody reads it, what contribution does it really make?* I hope you found my work as interesting and as stimulating to read as I did to research (which was immensely!).

# Bibliography

I. Akkaya, W. J. Schuster, R. Michel, C. Chavarría-K, A. Moitinho, R. Vázquez, and Y. Karatas. CCD UBVRI Photometry of the Galactic Open Clusters: Be 89, Ru 135, and Be 10. *Revista Mexicana de Astronomia y Astrofisica*, 46:385–430, October 2010.

B. S. Alessi, A. Moitinho, and W. S. Dias. Searching for unknown open clusters in the Tycho-2 catalog. *Astronomy and Astrophysics*, 410:565–575, November 2003. doi: 10.1051/0004-6361:20031280.

L. Allen, S. T. Megeath, R. Gutermuth, P. C. Myers, S. Wolk, F. C. Adams, J. Muzerolle, E. Young, and J. L. Pipher. The Structure and Evolution of Young Stellar Clusters. *Protostars and Planets V*, pages 361–376, 2007.

G. Alter, B. Balazs, J. Ruprecht, and J. Vanysek. *Catalogue of star clusters and associations*. 1970.

H. B. Ann, S. H. Lee, H. Sung, M. G. Lee, S.-L. Kim, M.-Y. Chun, Y.-B. Jeon, B.-G. Park, and I.-S. Yuk. BOAO Photometric Survey of Galactic Open Clusters. II. Physical Parameters of 12 Open Clusters. *Astronomical Journal*, 123:905–914, February 2002. doi: 10.1086/338309.

H. G. Arce and A. A. Goodman. Measuring Galactic Extinction: A Test. *Astrophysical Journal, Letters*, 512:L135–L138, February 1999. doi: 10.1086/311885.

R. H. Barbá, A. Roman-Lopes, J. L. Nilo Castellón, V. Firpo, D. Minniti, P. Lucas, J. P. Emerson, M. Hempel, M. Soto, and R. K. Saito. Hundreds of new cluster candidates in the VISTA Variables in the Vía Láctea survey DR1. *Astronomy and Astrophysics*, 581:A120, September 2015. doi: 10.1051/0004-6361/201424048.

K. A. Barkhatova, P. E. Zakharova, L. P. Shashkina, and L. K. Orekhova. The open cluster NGC 1960. *Astronomicheskii Zhurnal*, 62:854–859, October 1985.

N. Bastian. Cluster Disruption: From Infant Mortality to Long Term Survival. In *Stellar Clusters & Associations: A RIA Workshop on Gaia*, pages 85–97, 2011.

H. Baumgardt and P. Kroupa. The Influence of Gas Expulsion on the Evolution of Star Clusters. In E. Vesperini, M. Giersz, and A. Sills, editors, *IAU Symposium*, volume 246 of *IAU Symposium*, pages 36–40, May 2008. doi: 10.1017/S1743921308015238.

H. Baumgardt, C. Dettbarn, and R. Wielen. Absolute proper motions of open clusters. I. Observational data. *Astronomy and Astrophysics, Supplement*, 146:251–258, October 2000. doi: 10.1051/aas:2000362.

C. P. M. Bell, T. Naylor, N. J. Mayne, R. D. Jeffries, and S. P. Littlefair. Pre-main-sequence isochrones - II. Revising star and planet formation time-scales. *Monthly Notices of the RAS*, 434:806–831, September 2013. doi: 10.1093/mnras/stt1075.

R. A. Benjamin, E. Churchwell, B. L. Babler, T. M. Bania, D. P. Clemens, M. Cohen, J. M. Dickey, R. Indebetouw, J. M. Jackson, H. A. Kobulnicky, A. Lazarian, A. P. Marston, J. S. Mathis, M. R. Meade, S. Seager, S. R. Stolovy, C. Watson, B. A. Whitney, M. J. Wolff, and M. G. Wolfire. GLIMPSE. I. An SIRTF Legacy Project to Map the Inner Galaxy. *Publications of the ASP*, 115:953–964, August 2003. doi: 10.1086/376696.

B. Bhavya, B. Mathew, and A. Subramaniam. Pre-main sequence stars, emission stars and recent star formation in the Cygnus region. *Bulletin of the Astronomical Society of India*, 35:383–411, 2007.

E. Bica, C. Bonatto, and D. Camargo. Probing FSR star cluster candidates in bulge/disc directions with 2MASS colour-magnitude diagrams. *Monthly Notices of the RAS*, 385: 349–360, March 2008. doi: 10.1111/j.1365-2966.2007.12812.x.

C. Bonatto and E. Bica. Old open clusters in the inner Galaxy: FSR1744, FSR89 and FSR31. *Astronomy and Astrophysics*, 473:445–455, October 2007a. doi: 10.1051/0004-6361:20077675.

C. Bonatto and E. Bica. Open clusters in dense fields: the importance of field-star decontamination for NGC 5715, Lyngå 4, Lyngå 9, Trumpler 23, Trumpler 26 and Czernik 37. *Monthly Notices of the RAS*, 377:1301–1323, May 2007b. doi: 10.1111/j.1365-2966.2007.11691.x.

C. Bonatto and E. Bica. Exploring FSR open cluster candidates within $|\Delta\ell| = 20\,\mathrm{deg}$ of the Galactic anticentre. *Astronomy and Astrophysics*, 485:81–93, July 2008a. doi: 10.1051/0004-6361:200809764.

C. Bonatto and E. Bica. The old Galactic open clusters FSR 1716 and Czernik 23. *Astronomy and Astrophysics*, 491:767–780, December 2008b. doi: 10.1051/0004-6361:200810332.

C. Bonatto and E. Bica. Investigating the age and structure of the infrared old open clusters LK1, LK10, FSR1521 and FSR1555. *Monthly Notices of the RAS*, 392:483–496, January 2009. doi: 10.1111/j.1365-2966.2008.14093.x.

C. Bonatto, L. O. Kerber, E. Bica, and B. X. Santiago. Probing disk properties with open clusters. *Astronomy and Astrophysics*, 446:121–135, January 2006. doi: 10.1051/0004-6361:20053573.

C. Bonatto, S. Ortolani, B. Barbuy, and E. Bica. Open cluster survival within the solar circle: Teutsch145 and Teutsch146. *Monthly Notices of the RAS*, 402:1685–1692, March 2010. doi: 10.1111/j.1365-2966.2009.15980.x.

J. Borissova, P. Pessev, V. D. Ivanov, I. Saviane, R. Kurtev, and G. R. Ivanov. Discovery of new Milky Way star cluster candidates in the 2MASS Point Source Catalog. II. Physical properties of the star cluster CC 01. *Astronomy and Astrophysics*, 411:83–90, November 2003. doi: 10.1051/0004-6361:20034009.

J. Borissova, C. Bonatto, R. Kurtev, J. R. A. Clarke, F. Peñaloza, S. E. Sale, D. Minniti, J. Alonso-García, E. Artigau, R. Barbá, E. Bica, G. L. Baume, M. Catelan, A. N. Chenè, B. Dias, S. L. Folkes, D. Froebrich, D. Geisler, R. de Grijs, M. M. Hanson, M. Hempel, V. D. Ivanov, M. S. N. Kumar, P. Lucas, F. Mauro, C. Moni Bidin, M. Rejkuba, R. K. Saito, M. Tamura, and I. Toledo. New Galactic star clusters discovered in the VVV survey. *Astronomy and Astrophysics*, 532:A131, August 2011. doi: 10.1051/0004-6361/201116662.

J. Borissova, A.-N. Chené, S. Ramírez Alegría, S. Sharma, J. R. A. Clarke, R. Kurtev, I. Negueruela, A. Marco, P. Amigo, D. Minniti, E. Bica, C. Bonatto, M. Catelan, C. Fierro, D. Geisler, M. Gromadzki, M. Hempel, M. M. Hanson, V. D. Ivanov, P. Lucas, D. Majaess, C. Moni Bidin, B. Popescu, and R. K. Saito. New galactic star clusters discovered in the VVV survey. Candidates projected on the inner disk and bulge. *Astronomy and Astrophysics*, 569:A24, September 2014. doi: 10.1051/0004-6361/201322483.

S. G. Boutloukos and H. J. G. L. M. Lamers. Star cluster formation and disruption timescales - I. An empirical determination of the disruption time of star clusters in four galaxies. *Monthly Notices of the RAS*, 338:717–732, January 2003. doi: 10.1046/j.1365-8711.2003.06083.x.

A. S. M. Buckner and D. Froebrich. Properties of star clusters - I. Automatic distance and extinction estimates. *Monthly Notices of the RAS*, 436:1465–1478, December 2013. doi: 10.1093/mnras/stt1665.

A. S. M. Buckner and D. Froebrich. Properties of star clusters - II. Scaleheight evolution of clusters. *Monthly Notices of the RAS*, 444:290–302, October 2014. doi: 10.1093/mnras/stu1440.

D. Camargo, C. Bonatto, and E. Bica. Astrophysical parameters of 14 open clusters projected close to the Galactic plane. *Astronomy and Astrophysics*, 508:211–220, December 2009. doi: 10.1051/0004-6361/200912786.

D. Camargo, C. Bonatto, and E. Bica. Towards a census of the Galactic anticentre star clusters: colour-magnitude diagram and structural analyses of a sample of 50 objects. *Astronomy and Astrophysics*, 521:A42, October 2010. doi: 10.1051/0004-6361/201014756.

D. Camargo, C. Bonatto, and E. Bica. Towards a census of the Galactic anticentre star clusters - II. Exploring lower overdensities. *Monthly Notices of the RAS*, 423:1940–1954, June 2012. doi: 10.1111/j.1365-2966.2012.21018.x.

D. Camargo, E. Bica, and C. Bonatto. Towards a census of the Galactic anticentre star clusters - III. Tracing the spiral structure in the outer disc. *Monthly Notices of the RAS*, 432:3349–3360, July 2013. doi: 10.1093/mnras/stt703.

D. Camargo, E. Bica, and C. Bonatto. New Galactic embedded clusters and candidates from a WISE Survey. *New Astronomy*, 34:84–97, January 2015. doi: 10.1016/j.newast.2014.05.007.

J. M. Carpenter. 2MASS Observations of the Perseus, Orion A, Orion B, and Monoceros R2 Molecular Clouds. *Astronomical Journal*, 120:3139–3161, December 2000. doi: 10.1086/316845.

G. Carraro. The Milky Way thin disk structure as revealed by stars and young open clusters. In S. Feltzing, G. Zhao, N. A. Walton, and P. Whitelock, editors, *IAU Symposium*, volume 298 of *IAU Symposium*, pages 7–16, January 2014. doi: 10.1017/S1743921313006157.

G. Carraro and E. Costa. Photometry of the five marginally studied open clusters Collinder 74, Berkeley 27, Haffner 8, NGC 2509, and VdB-Hagen 4. *Astronomy and Astrophysics*, 464:573–580, March 2007. doi: 10.1051/0004-6361:20066350.

G. Carraro, B. Chaboyer, and J. Perencevich. The young open cluster NGC 2129. *Monthly Notices of the RAS*, 365:867–873, January 2006. doi: 10.1111/j.1365-2966.2005.09762.x.

G. Carraro, A. Moitinho, M. Zoccali, R. A. Vázquez, and G. Baume. Photometry of a Galactic Field at l=232deg, b=-6deg: The Old Open Cluster Auner 1, the Norma-Cygnus Spiral Arm, and the Signature of the Warped Galactic Thick Disk. *Astronomical Journal*, 133:1058–1066, March 2007. doi: 10.1086/510331.

A.-N. Chené, J. Borissova, C. Bonatto, D. J. Majaess, G. Baume, J. R. A. Clarke, R. Kurtev, O. Schnurr, J.-C. Bouret, M. Catelan, J. P. Emerson, C. Feinstein, D. Geisler, R. de Grijs, A. Hervé, V. D. Ivanov, M. S. N. Kumar, P. Lucas, L. Mahy, F. Martins, F. Mauro, D. Minniti, and C. Moni Bidin. Massive open star clusters using the VVV survey. II. Discovery of six clusters with Wolf-Rayet stars. *Astronomy and Astrophysics*, 549:A98, January 2013. doi: 10.1051/0004-6361/201220107.

J. J. Claria and E. Lapasset. Fundamental parameters of the open cluster NGC 2567. *Astronomical Journal*, 91:326–337, February 1986. doi: 10.1086/114013.

J. L. Clem, A. U. Landolt, D. W. Hoard, and S. Wachter. Deep, Wide-field CCD Photometry for the Open Cluster NGC 3532. *Astronomical Journal*, 141:115, April 2011. doi: 10.1088/0004-6256/141/4/115.

R. L. M. Corradi and H. E. Schwarz. Morphological populations of planetary nebulae: which progenitors? I. Comparative properties of bipolar nebulae. *Astronomy and Astrophysics*, 293:871–888, January 1995.

J. Cuffey. Red indices in galactic clusters. II.Messier 35, NGC 2158, IC 2157, NGC 2129, 1817, 2266, 2281. *Annals of Harvard College Observatory*, 106:39–74, 1938.

B. Davies, D. F. Figer, R.-P. Kudritzki, J. MacKenty, F. Najarro, and A. Herrero. A Massive Cluster of Red Supergiants at the Base of the Scutum-Crux Arm. *Astrophysical Journal*, 671:781–801, December 2007. doi: 10.1086/522224.

R. de la Fuente Marcos, C. de la Fuente Marcos, C. Moni Bidin, G. Carraro, and E. Costa. NGC 1252: a high altitude, metal poor open cluster remnant. *Monthly Notices of the RAS*, 434:194–208, September 2013. doi: 10.1093/mnras/stt996.

W. Dehnen and J. J. Binney. Local stellar kinematics from HIPPARCOS data. *Monthly Notices of the RAS*, 298:387–394, August 1998. doi: 10.1046/j.1365-8711.1998.01600.x.

A. J. Delgado, E. J. Alfaro, A. Moitinho, and J. Franco. Pre-Main-Sequence Stars in the Young Galactic Cluster IC 4996: A CCD Photometric Study. *Astronomical Journal*, 116: 1801–1809, October 1998. doi: 10.1086/300547.

A. J. Delgado, L. F. Miranda, and E. J. Alfaro. Spectroscopy of Pre-Main-Sequence Candidates of Spectral Type AF in the Young Galactic Cluster IC 4996. *Astronomical Journal*, 118:1759–1765, October 1999. doi: 10.1086/301058.

W. S. Dias and J. R. D. Lépine. Direct Determination of the Spiral Pattern Rotation Speed of the Galaxy. *Astrophysical Journal*, 629:825–831, August 2005. doi: 10.1086/431456.

W. S. Dias, B. S. Alessi, A. Moitinho, and J. R. D. Lépine. New catalogue of optically visible open clusters and candidates. *Astronomy and Astrophysics*, 389:871–873, July 2002. doi: 10.1051/0004-6361:20020668.

W. S. Dias, H. Monteiro, T. C. Caetano, and A. F. Oliveira. Fitting isochrones to open cluster photometric data. II. Nonparametric open cluster membership likelihood estimation and its application in optical and 2MASS near-IR data. *Astronomy and Astrophysics*, 539: A125, March 2012. doi: 10.1051/0004-6361/201118206.

K. Dobashi, H. Uehara, R. Kandori, T. Sakurai, M. Kaiden, T. Umemoto, and F. Sato. Atlas and Catalog of Dark Clouds Based on Digitized Sky Survey I. *Publications of Astronomical Soc of Japan*, 57:1, February 2005.

R. Drimmel, A. Cabrera-Lavers, and M. López-Corredoira. A three-dimensional Galactic extinction model. *Astronomy and Astrophysics*, 409:205–215, October 2003. doi: 10.1051/0004-6361:20031070.

C. M. Dutra and E. Bica. New infrared star clusters and candidates in the Galaxy detected with 2MASS. *Astronomy and Astrophysics*, 376:434–440, September 2001. doi: 10.1051/0004-6361:20010978.

C. M. Dutra, E. Bica, J. Soares, and B. Barbuy. New infrared star clusters in the southern Milky Way with 2MASS. *Astronomy and Astrophysics*, 400:533–539, March 2003. doi: 10.1051/0004-6361:20030005.

F. Elias, E. J. Alfaro, and J. Cabrera-Caño. OB Stars in the Solar Neighborhood. II. Kinematics. *Astronomical Journal*, 132:1052–1060, September 2006. doi: 10.1086/505941.

N. Epchtein, B. de Batz, L. Capoani, L. Chevallier, E. Copet, P. Fouqué, P. Lacombe, T. Le Bertre, S. Pau, D. Rouan, S. Ruphy, G. Simon, D. Tiphène, W. B. Burton, E. Bertin, E. Deul, H. Habing, J. Borsenberger, M. Dennefeld, F. Guglielmo, C. Loup, G. Mamon, Y. Ng, A. Omont, L. Provost, J.-C. Renault, F. Tanguy, S. Kimeswenger, C. Kienel, F. Garzon, P. Persi, M. Ferrari-Toniolo, A. Robin, G. Paturel, I. Vauglin, T. Forveille,

X. Delfosse, J. Hron, M. Schultheis, I. Appenzeller, S. Wagner, L. Balazs, A. Holl, J. Lépine, P. Boscolo, E. Picazzio, P.-A. Duc, and M.-O. Mennessier. The deep near-infrared southern sky survey (DENIS). *The Messenger*, 87:27–34, March 1997.

M. Fang, R. van Boekel, R. R. King, T. Henning, J. Bouwman, Y. Doi, Y. K. Okamoto, V. Roccatagliata, and A. Sicilia-Aguilar. Star formation and disk properties in Pismis 24. *Astronomy and Astrophysics*, 539:A119, March 2012. doi: 10.1051/0004-6361/201015914.

M. P. Fitzgerald, G. L. Harris, and B. C. Reed. The moderately young open cluster NGC 2353. *Publications of the ASP*, 102:865–880, August 1990. doi: 10.1086/132711.

J. B. Foster, J. J. Stead, R. A. Benjamin, M. G. Hoare, and J. M. Jackson. Distances to Dark Clouds: Comparing Extinction Distances to Maser Parallax Distances. *Astrophysical Journal*, 751:157, June 2012. doi: 10.1088/0004-637X/751/2/157.

E. D. Friel. The Old Open Clusters Of The Milky Way. *Annual Review of Astronomy and Astrophysics*, 33:381–414, 1995. doi: 10.1146/annurev.aa.33.090195.002121.

D. Froebrich, A. Scholz, and C. L. Raftery. A systematic survey for infrared star clusters with $|b| < 20^\circ$ using 2MASS. *Monthly Notices of the RAS*, 374:399–408, January 2007. doi: 10.1111/j.1365-2966.2006.11148.x.

D. Froebrich, H. Meusinger, and A. Scholz. NTT follow-up observations of star cluster candidates from the FSR catalogue. *Monthly Notices of the RAS*, 390:1598–1618, November 2008. doi: 10.1111/j.1365-2966.2008.13849.x.

D. Froebrich, S. Schmeja, D. Samuel, and P. W. Lucas. Old star clusters in the FSR catalogue. *Monthly Notices of the RAS*, 409:1281–1288, December 2010. doi: 10.1111/j.1365-2966.2010.17390.x.

D. Froebrich, S. V. Makin, C. J. Davis, T. M. Gledhill, Y. Kim, B.-C. Koo, J. Rowles, J. Eislöffel, J. Nicholas, J. J. Lee, J. Williamson, and A. S. M. Buckner. Extended $H_2$ emission line sources from UWISH2. *Monthly Notices of the RAS*, 454:2586–2605, December 2015. doi: 10.1093/mnras/stv1729.

M. P. Geyer and A. Burkert. The effect of gas loss on the formation of bound stellar clusters. *Monthly Notices of the RAS*, 323:988–994, May 2001. doi: 10.1046/j.1365-8711.2001.04257.x.

M. Gieles, S. F. Portegies Zwart, H. Baumgardt, E. Athanassoula, H. J. G. L. M. Lamers, M. Sipior, and J. Leenaarts. Star cluster disruption by giant molecular clouds. *Monthly Notices of the RAS*, 371:793–804, September 2006. doi: 10.1111/j.1365-2966.2006.10711.x.

M. Gieles, H. J. G. L. M. Lamers, and H. Baumgardt. Star Cluster Life-times: Dependence on Mass, Radius and Environment. In E. Vesperini, M. Giersz, and A. Sills, editors, *IAU Symposium*, volume 246 of *IAU Symposium*, pages 171–175, May 2008. doi: 10.1017/S1743921308015536.

Mark Gieles. Star cluster disruption. In *Star clusters: basic galactic building blocks throughout time and space*, volume 5 of *Proceedings of the International Astronomical Union*, pages 69–80, 8 2009. doi: 10.1017/S1743921309990895.

G. Gilmore, S. Randich, M. Asplund, J. Binney, P. Bonifacio, J. Drew, S. Feltzing, A. Ferguson, R. Jeffries, G. Micela, and et al. The Gaia-ESO Public Spectroscopic Survey. *The Messenger*, 147:25–31, March 2012.

L. Girardi, M. Barbieri, M. A. T. Groenewegen, P. Marigo, A. Bressan, H. J. Rocha-Pinto, B. X. Santiago, J. I. B. Camargo, and L. N. da Costa. *TRILEGAL, a TRIdimensional modeL of thE GALaxy: Status and Future*, page 165. 2012. doi: 10.1007/978-3-642-18418-5_17.

E. V. Glushkova, S. E. Koposov, I. Y. Zolotukhin, Y. V. Beletsky, A. D. Vlasov, and S. I. Leonova. Automated search for star clusters in large multiband surveys: II. Discovery and investigation of open clusters in the galactic plane. *Astronomy Letters*, 36:75–85, February 2010. doi: 10.1134/S1063773710020015.

T. P. Greene and E. T. Young. Near-infrared observations of young stellar objects in the Rho Ophiuchi dark cloud. *Astrophysical Journal*, 395:516–528, August 1992. doi: 10.1086/171672.

J. Gregorio-Hetem, A. Hetem, T. Santos-Silva, and B. Fernandes. Statistical fractal analysis of 25 young star clusters. *Monthly Notices of the RAS*, 448:2504–2513, April 2015. doi: 10.1093/mnras/stv111.

O. Güneş, Y. Karataş, and C. Bonatto. Astrophysical and structural parameters of the open clusters NGC 6866, NGC 7062, and NGC 2360. *New Astronomy*, 17:720–731, November 2012. doi: 10.1016/j.newast.2012.05.003.

H. J. Habing and F. P. Israel. Compact H II regions and OB star formation. *Annual Review of Astronomy and Astrophysics*, 17:345–385, 1979. doi: 10.1146/annurev.aa.17.090179.002021.

R. B. Hanson. A study of the motion, membership, and distance of the Hyades cluster. *Astronomical Journal*, 80:379–401, May 1975. doi: 10.1086/111753.

J. G. Hills. The effect of mass loss on the dynamical evolution of a stellar system - Analytic approximations. *Astrophysical Journal*, 235:986–991, February 1980. doi: 10.1086/157703.

E. Høg, C. Fabricius, V. V. Makarov, S. Urban, T. Corbin, G. Wycoff, U. Bastian, P. Schwekendiek, and A. Wicenec. The Tycho-2 catalogue of the 2.5 million brightest stars. *Astronomy and Astrophysics*, 355:L27–L30, March 2000.

R. M. Humphreys and J. A. Larsen. The Sun's Distance Above the Galactic Plane. *Astronomical Journal*, 110:2183, November 1995. doi: 10.1086/117677.

R. Indebetouw, J. S. Mathis, B. L. Babler, M. R. Meade, C. Watson, B. A. Whitney, M. J. Wolff, and M. G. Wolfire. The Wavelength Dependence of Interstellar Extinction from 1.25 to 8.0 $\mu$m Using GLIMPSE Data. *Astrophysical Journal*, 619:931–938, February 2005. doi: 10.1086/426679.

G. Ioannidis and D. Froebrich. YSO jets in the Galactic plane from UWISH2 - II. Outflow luminosity and length distributions in Serpens and Aquila. *Monthly Notices of the RAS*, 425:1380–1393, September 2012. doi: 10.1111/j.1365-2966.2012.21556.x.

K. Janes and D. Adler. Open clusters and galactic structure. *Astrophysical Journal, Supplement*, 49:425–445, July 1982. doi: 10.1086/190805.

K. A. Janes and R. L. Phelps. The galactic system of old star clusters: The development of the galactic disk. *Astronomical Journal*, 108:1773–1785, November 1994. doi: 10.1086/117192.

R. D. Jeffries, M. R. Thurston, and N. C. Hambly. Photometry and membership for low mass stars in the young open cluster NGC 2516. *Astronomy and Astrophysics*, 375:863–889, September 2001. doi: 10.1051/0004-6361:20010918.

Y. C. Joshi. Interstellar extinction towards open clusters and Galactic structure. *Monthly Notices of the RAS*, 362:1259–1266, October 2005. doi: 10.1111/j.1365-2966.2005.09391.x.

T. C. Junqueira, C. Chiappini, J. R. D. Lépine, I. Minchev, and B. X. Santiago. A new method for estimating the pattern speed of spiral structure in the Milky Way. *Monthly Notices of the RAS*, 449:2336–2344, May 2015. doi: 10.1093/mnras/stv464.

A. A. Kaas. K-Band Variability as a Method to Select Young Stellar Object Candidates. *Astronomical Journal*, 118:558–571, July 1999. doi: 10.1086/300941.

M. J. Kenyon, R. D. Jeffries, T. Naylor, J. M. Oliveira, and P. F. L. Maxted. Membership, binarity and accretion among very low-mass stars and brown dwarfs of the $\sigma$ Orionis cluster. *Monthly Notices of the RAS*, 356:89–106, January 2005. doi: 10.1111/j.1365-2966.2004.08455.x.

N. V. Kharchenko. All-sky compiled catalogue of 2.5 million stars. *Kinematika i Fizika Nebesnykh Tel*, 17:409–423, October 2001.

N. V. Kharchenko, A. E. Piskunov, S. Röser, E. Schilbach, and R.-D. Scholz. 109 new Galactic open clusters. *Astronomy and Astrophysics*, 440:403–408, September 2005. doi: 10.1051/0004-6361:20052740.

N. V. Kharchenko, A. E. Piskunov, E. Schilbach, S. Röser, and R.-D. Scholz. Global survey of star clusters in the Milky Way. I. The pipeline and fundamental parameters in the second quadrant. *Astronomy and Astrophysics*, 543:A156, July 2012. doi: 10.1051/0004-6361/201118708.

N. V. Kharchenko, A. E. Piskunov, E. Schilbach, S. Röser, and R.-D. Scholz. Global survey of star clusters in the Milky Way. II. The catalogue of basic parameters. *Astronomy and Astrophysics*, 558:A53, October 2013. doi: 10.1051/0004-6361/201322302.

A. Klypin, H. Zhao, and R. S. Somerville. ΛCDM-based Models for the Milky Way and M31. I. Dynamical Models. *Astrophysical Journal*, 573:597–613, July 2002. doi: 10.1086/340656.

J. Koornneef. Near-infrared photometry. II - Intrinsic colours and the absolute calibration from one to five micron. *Astronomy and Astrophysics*, 128:84–93, November 1983.

S. E. Koposov, E. V. Glushkova, and I. Y. Zolotukhin. Automated search for Galactic star clusters in large multiband surveys. I. Discovery of 15 new open clusters in the Galactic anti-center region. *Astronomy and Astrophysics*, 486:771–777, August 2008. doi: 10.1051/0004-6361:20078630.

A. Krone-Martins and A. Moitinho. UPMASK: unsupervised photometric membership assignment in stellar clusters. *Astronomy and Astrophysics*, 561:A57, January 2014. doi: 10.1051/0004-6361/201321143.

C. J. Lada. The physics and modes of star cluster formation: observations. *Royal Society of London Philosophical Transactions Series A*, 368:713–731, January 2010. doi: 10.1098/rsta.2009.0264.

C. J. Lada and E. A. Lada. Embedded Clusters in Molecular Clouds. *Annual Review of Astronomy and Astrophysics*, 41:57–115, 2003. doi: 10.1146/annurev.astro.41.011802.094844.

H. J. G. L. M. Lamers and M. Gieles. Clusters in the solar neighbourhood: how are they destroyed? *Astronomy and Astrophysics*, 455:L17–L20, August 2006. doi: 10.1051/0004-6361:20065567.

H. J. G. L. M. Lamers, M. Gieles, N. Bastian, H. Baumgardt, N. V. Kharchenko, and S. Portegies Zwart. An analytical description of the disruption of star clusters in tidal fields with an application to Galactic open clusters. *Astronomy and Astrophysics*, 441:117–129, October 2005. doi: 10.1051/0004-6361:20042241.

S. Lata, V. Mohan, and R. Sagar. CCD photometry of the galactic star clusters Be 15, Be 71 and King 1. *Bulletin of the Astronomical Society of India*, 32:371–383, December 2004.

T. Lejeune and D. Schaerer. Database of Geneva stellar evolution tracks and isochrones for $(UBV)_J(RI)_C$ JHKLL'M, HST-WFPC2, Geneva and Washington photometric systems. *Astronomy and Astrophysics*, 366:538–546, February 2001. doi: 10.1051/0004-6361:20000214.

B. Lim, H. S. Sung, R. Karimov, and M. Ibrahimov. Sejong Open Cluster Survey. I. NGC 2353. *Journal of Korean Astronomical Society*, 44:39–48, April 2011. doi: 10.5303/JKAS.2011.44.2.39.

J. Liu and Z. Zhu. Galactic Structure and Kinematics Defined by Open Clusters. In S. Qain, K. Leung, L. Zhu, and S. Kwok, editors, *Astronomical Society of the Pacific Conference Series*, volume 451 of *Astronomical Society of the Pacific Conference Series*, page 339, December 2011.

T. Liu, K. A. Janes, and T. M. Bania. More radial-velocity measurements in young open clusters. *Astronomical Journal*, 102:1103–1107, September 1991. doi: 10.1086/115936.

T. A. Lozinskaya and S. V. Repin. An infrared shell in the CYG X - CYG OB 1 region. *Astronomicheskii Zhurnal*, 67:1152–1164, December 1990.

P. W. Lucas, M. G. Hoare, A. Longmore, A. C. Schröder, C. J. Davis, A. Adamson, R. M. Bandyopadhyay, R. de Grijs, M. Smith, A. Gosling, S. Mitchison, A. Gáspár, M. Coe,

M. Tamura, Q. Parker, M. Irwin, N. Hambly, J. Bryant, R. S. Collins, N. Cross, D. W. Evans, E. Gonzalez-Solares, S. Hodgkin, J. Lewis, M. Read, M. Riello, E. T. W. Sutorius, A. Lawrence, J. E. Drew, S. Dye, and M. A. Thompson. The UKIDSS Galactic Plane Survey. *Monthly Notices of the RAS*, 391:136–163, November 2008. doi: 10.1111/j.1365-2966.2008.13924.x.

G. Lynga. Galactic dust and extinction. In W. B. Burton, editor, *The Large-Scale Characteristics of the Galaxy*, volume 84 of *IAU Symposium*, pages 87–92, 1979.

G. Lynga. VizieR Online Data Catalog: Open Cluster Data 5th Edition (Lynga 1987). *VizieR Online Data Catalog*, 7092:0, February 1995.

G. Maciejewski and A. Niedzielski. CCD BV survey of 42 open clusters. *Astronomy and Astrophysics*, 467:1065–1074, June 2007. doi: 10.1051/0004-6361:20066588.

F. F. S. Maia, W. J. B. Corradi, and J. F. C. Santos, Jr. Characterization and photometric membership of the open cluster NGC1981. *Monthly Notices of the RAS*, 407:1875–1886, September 2010. doi: 10.1111/j.1365-2966.2010.17034.x.

D. Majaess. Discovering protostars and their host clusters via WISE. *Astrophysics and Space Science*, 344:175–186, March 2013. doi: 10.1007/s10509-012-1308-y.

S. R. Majewski, G. Zasowski, and D. L. Nidever. Lifting the Dusty Veil with Near- and Mid-infrared Photometry. I. Description and Applications of the Rayleigh-Jeans Color Excess Method. *Astrophysical Journal*, 739:25, September 2011. doi: 10.1088/0004-637X/739/1/25.

Z. Malkin. The current best estimate of the Galactocentric distance of the Sun based on comparison of different statistical techniques. *ArXiv e-prints*, February 2012.

E. E. Mamajek, W. A. Lawson, and E. D. Feigelson. The $\eta$ Chamaeleontis Cluster: A Remarkable New Nearby Young Open Cluster. *Astrophysical Journal, Letters*, 516:L77–L80, May 1999. doi: 10.1086/312005.

L. A. Marschall, W. F. van Altena, and L.-T. G. Chiu. Membership of the Rosette Nebula cluster, NGC 2244. *Astronomical Journal*, 87:1497–1506, November 1982. doi: 10.1086/113240.

D. J. Marshall, A. C. Robin, C. Reylé, M. Schultheis, and S. Picaud. Modelling the Galactic interstellar extinction distribution in three dimensions. *Astronomy and Astrophysics*, 453: 635–651, July 2006. doi: 10.1051/0004-6361:20053842.

E. L. Martín, W. Brandner, J. Bouvier, K. L. Luhman, J. Stauffer, G. Basri, M. R. Zapatero Osorio, and D. Barrado y Navascués. Membership and Multiplicity among Very Low Mass Stars and Brown Dwarfs in the Pleiades Cluster. *Astrophysical Journal*, 543:299–312, November 2000. doi: 10.1086/317089.

J. S. Mathis. Interstellar dust and extinction. *Annual Review of Astronomy and Astrophysics*, 28:37–70, 1990. doi: 10.1146/annurev.aa.28.090190.000345.

S. Meibom, J. Andersen, and B. Nordström. Critical tests of stellar evolution in open clusters. III. Stellar population and dynamical evolution of IC 4651. *Astronomy and Astrophysics*, 386:187–203, April 2002. doi: 10.1051/0004-6361:20020183.

E. P. Mercer, D. P. Clemens, M. R. Meade, B. L. Babler, R. Indebetouw, B. A. Whitney, C. Watson, M. G. Wolfire, M. J. Wolff, T. M. Bania, R. A. Benjamin, M. Cohen, J. M. Dickey, J. M. Jackson, H. A. Kobulnicky, J. S. Mathis, J. R. Stauffer, S. R. Stolovy, B. Uzpen, and E. B. Churchwell. New Star Clusters Discovered in the GLIMPSE Survey. *Astrophysical Journal*, 635:560–569, December 2005. doi: 10.1086/497260.

J.-C. Mermilliod. The database for galactic open clusters (BDA). In D. Egret and M. A. Albrecht, editors, *Information and On-Line Data in Astronomy*, volume 203 of *Astrophysics and Space Science Library*, pages 127–138, 1995.

D. K. Milne and L. H. Aller. An average model for the galactic absorption. *Astronomical Journal*, 85:17–21, January 1980. doi: 10.1086/112628.

D. Minniti, P. W. Lucas, J. P. Emerson, R. K. Saito, M. Hempel, P. Pietrukowicz, A. V. Ahumada, M. V. Alonso, J. Alonso-Garcia, J. I. Arias, R. M. Bandyopadhyay, R. H. Barbá, B. Barbuy, L. R. Bedin, E. Bica, J. Borissova, L. Bronfman, G. Carraro, M. Catelan, J. J. Clariá, N. Cross, R. de Grijs, I. Dékány, J. E. Drew, C. Fariña, C. Feinstein, E. F. Lajús, R. C. Gamen, D. Geisler, W. Gieren, B. Goldman, O. A. Gonzalez, G. Gunthardt, S. Gurovich, N. C. Hambly, M. J. Irwin, V. D. Ivanov, A. Jordán, E. Kerins, K. Kinemuchi, R. Kurtev, M. López-Corredoira, T. Maccarone, N. Masetti, D. Merlo, M. Messineo, I. F. Mirabel, L. Monaco, L. Morelli, N. Padilla, T. Palma, M. C. Parisi, G. Pignata, M. Rejkuba, A. Roman-Lopes, S. E. Sale, M. R. Schreiber, A. C. Schröder, M. Smith, L. S. , Jr., M. Soto, M. Tamura, C. Tappert, M. A. Thompson, I. Toledo, M. Zoccali, and G. Pietrzynski. VISTA Variables in the Via Lactea (VVV): The public ESO near-IR variability survey of the Milky Way. *New Astronomy*, 15:433–443, July 2010. doi: 10.1016/j.newast.2009.12.002.

A. Moitinho. Star Formation and Spatial Structure in the Galactic Disk: Open Cluster Data. In E. K. Grebel and W. Brandner, editors, *Modes of Star Formation and the Origin*

*of Field Populations*, volume 285 of *Astronomical Society of the Pacific Conference Series*, page 256, 2002.

A. Moitinho. Observational properties of the open cluster system of the Milky Way and what they tell us about our Galaxy. In R. de Grijs and J. R. D. Lépine, editors, *IAU Symposium*, volume 266 of *IAU Symposium*, pages 106–116, January 2010. doi: 10.1017/S1743921309990949.

Y. Momany, S. Ortolani, C. Bonatto, E. Bica, and B. Barbuy. Multi-Conjugate Adaptive Optics VLT imaging of the distant old open cluster FSR1415. *Monthly Notices of the RAS*, 391:1650–1658, December 2008. doi: 10.1111/j.1365-2966.2008.14019.x.

H. Monteiro, W. S. Dias, and T. C. Caetano. Fitting isochrones to open cluster photometric data. A new global optimization tool. *Astronomy and Astrophysics*, 516:A2, June 2010. doi: 10.1051/0004-6361/200913677.

D. Montes, J. López-Santiago, M. C. Gálvez, M. J. Fernández-Figueroa, E. De Castro, and M. Cornide. Late-type members of young stellar kinematic groups - I. Single stars. *Monthly Notices of the RAS*, 328:45–63, November 2001. doi: 10.1046/j.1365-8711.2001.04781.x.

E. F. E. Morales, F. Wyrowski, F. Schuller, and K. M. Menten. Stellar clusters in the inner Galaxy and their correlation with cold dust emission. *Astronomy and Astrophysics*, 560: A76, December 2013. doi: 10.1051/0004-6361/201321626.

T. Naylor and R. D. Jeffries. A maximum-likelihood method for fitting colour-magnitude diagrams. *Monthly Notices of the RAS*, 373:1251–1263, December 2006. doi: 10.1111/j.1365-2966.2006.11099.x.

I. Negueruela and A. Marco. The Young Open Cluster Berkeley 55. *Astronomical Journal*, 143:46, February 2012. doi: 10.1088/0004-6256/143/2/46.

M. Netopil, E. Paunzen, and G. Carraro. A comparative study on the reliability of open cluster parameters. *Astronomy and Astrophysics*, 582:A19, October 2015. doi: 10.1051/0004-6361/201526372.

A. K. Pandey, B. C. Bhatt, and H. S. Mahra. Open clusters and galactic structure. *Astronomy and Astrophysics*, 189:66–69, January 1988.

D. B. Pavani, L. O. Kerber, E. Bica, and W. J. Maciel. Diagnostic tool to analyse colour-magnitude diagrams of poorly populated stellar concentrations. *Monthly Notices of the RAS*, 412:1611–1626, April 2011. doi: 10.1111/j.1365-2966.2010.17999.x.

J. H. Peña and R. Peniche. uvby-$\beta$ photometry of open clusters. IV. NGC 1444, NGC 1662, NGC 2129, NGC 2169, and NGC 7209. *Revista Mexicana de Astronomia y Astrofisica*, 28: 139–152, October 1994.

J. A. Peacock. Two-dimensional goodness-of-fit testing in astronomy. *Monthly Notices of the RAS*, 202:615–627, February 1983.

F. I. Pelupessy and S. Portegies Zwart. The evolution of embedded star clusters. *Monthly Notices of the RAS*, 420:1503–1517, February 2012. doi: 10.1111/j.1365-2966.2011.20137.x.

G. I. Perren, R. A. Vázquez, and A. E. Piatti. ASteCA: Automated Stellar Cluster Analysis. *Astronomy and Astrophysics*, 576:A6, April 2015. doi: 10.1051/0004-6361/201424946.

M. A. C. Perryman, L. Lindegren, J. Kovalevsky, E. Hoeg, U. Bastian, P. L. Bernacca, M. Crézé, F. Donati, M. Grenon, M. Grewing, F. van Leeuwen, H. van der Marel, F. Mignard, C. A. Murray, R. S. Le Poole, H. Schrijver, C. Turon, F. Arenou, M. Froeschlé, and C. S. Petersen. The HIPPARCOS Catalogue. *Astronomy and Astrophysics*, 323:L49–L52, July 1997.

A. E. Piatti, J. J. Clariá, and A. V. Ahumada. First CCD UBVI photometric analysis of four moderately young open clusters in the third galactic quadrant. *Monthly Notices of the RAS*, 408:1147–1167, October 2010. doi: 10.1111/j.1365-2966.2010.17196.x.

N. Pirzkal, K. C. Sahu, A. Burgasser, L. A. Moustakas, C. Xu, S. Malhotra, J. E. Rhoads, A. M. Koekemoer, E. P. Nelan, R. A. Windhorst, N. Panagia, C. Gronwall, A. Pasquali, and J. R. Walsh. Stars in the Hubble Ultra Deep Field. *Astrophysical Journal*, 622:319–332, March 2005. doi: 10.1086/427896.

A. E. Piskunov, N. V. Kharchenko, S. Röser, E. Schilbach, and R.-D. Scholz. Revisiting the population of Galactic open clusters. *Astronomy and Astrophysics*, 445:545–565, January 2006. doi: 10.1051/0004-6361:20053764.

I. Platais, V. Kozhurina-Platais, and F. van Leeuwen. A Search for Star Clusters from the HIPPARCOS Data. *Astronomical Journal*, 116:2423–2430, November 1998. doi: 10.1086/300606.

D. M. Popper. Stellar masses. *Annual Review of Astronomy and Astrophysics*, 18:115–164, 1980. doi: 10.1146/annurev.aa.18.090180.000555.

A. Porras, M. Christopher, L. Allen, J. Di Francesco, S. T. Megeath, and P. C. Myers. A Catalog of Young Stellar Groups and Clusters within 1 Kiloparsec of the Sun. *Astronomical Journal*, 126:1916–1924, October 2003. doi: 10.1086/377623.

C. F. Prosser. Membership of low-mass stars in the open cluster Alpha Persei. *Astronomical Journal*, 103:488–513, February 1992. doi: 10.1086/116077.

B. C. Reed. The Sun's Displacement from the Galactic Plane from Spectroscopic Parallaxes of 2500 OB Stars. *Journal of the Royal Astronomical Society of Canada*, 100:146, August 2006.

C. Reylé and A. C. Robin. Search for star clusters close to the Galactic plane with DENIS. *Astronomy and Astrophysics*, 384:403–407, March 2002. doi: 10.1051/0004-6361:20020018.

A. C. Robin, C. Reylé, S. Derrière, and S. Picaud. A synthetic view on structure and evolution of the Milky Way. *Astronomy and Astrophysics*, 409:523–540, October 2003. doi: 10.1051/0004-6361:20031117.

N. J. Rodriguez-Fernandez and F. Combes. Gas flow models in the Milky Way embedded bars. *Astronomy and Astrophysics*, 489:115–133, October 2008. doi: 10.1051/0004-6361:200809644.

S. Roeser, M. Demleitner, and E. Schilbach. The PPMXL Catalog of Positions and Proper Motions on the ICRS. Combining USNO-B1.0 and the Two Micron All Sky Survey (2MASS). *Astronomical Journal*, 139:2440–2447, June 2010. doi: 10.1088/0004-6256/139/6/2440.

J. Rowles and D. Froebrich. The structure of molecular clouds - I. All-sky near-infrared extinction maps. *Monthly Notices of the RAS*, 395:1640–1648, May 2009. doi: 10.1111/j.1365-2966.2009.14655.x.

N. Sánchez and E. J. Alfaro. The Spatial Distribution of Stars in Open Clusters. *Astrophysical Journal*, 696:2086–2093, May 2009. doi: 10.1088/0004-637X/696/2/2086.

D. B. Sanders, P. M. Solomon, and N. Z. Scoville. Giant molecular clouds in the Galaxy. I - The axisymmetric distribution of H2. *Astrophysical Journal*, 276:182–203, January 1984. doi: 10.1086/161602.

J. Sanner, M. Altmann, J. Brunzendorf, and M. Geffert. Photometric and kinematic studies of open star clusters. II. NGC 1960 (M 36) and NGC 2194. *Astronomy and Astrophysics*, 357:471–483, May 2000.

D. J. Schlegel, D. P. Finkbeiner, and M. Davis. Maps of Dust Infrared Emission for Use in Estimation of Reddening and Cosmic Microwave Background Radiation Foregrounds. *Astrophysical Journal*, 500:525–553, June 1998. doi: 10.1086/305772.

S. Schmeja, N. V. Kharchenko, A. E. Piskunov, S. Röser, E. Schilbach, D. Froebrich, and R.-D. Scholz. Global survey of star clusters in the Milky Way. III. 139 new open clusters at high Galactic latitudes. *Astronomy and Astrophysics*, 568:A51, August 2014. doi: 10.1051/0004-6361/201322720.

R.-D. Scholz, N. V. Kharchenko, A. E. Piskunov, S. Röser, and E. Schilbach. Global survey of star clusters in the Milky Way. IV. 63 new open clusters detected by proper motions. *Astronomy and Astrophysics*, 581:A39, September 2015. doi: 10.1051/0004-6361/201526312.

J. Segura, A. Juárez, and J. H. Peña. uvby-$\beta$ Photoelectric photometry and membership determination of the Open Cluster NGC 2353. *Revista Mexicana de Astronomia y Astrofisica*, 50:15–22, April 2014.

S. Sharma, A. K. Pandey, K. Ogura, H. Mito, K. Tarusawa, and R. Sagar. Wide-Field CCD Photometry around Nine Open Clusters. *Astronomical Journal*, 132:1669–1691, October 2006. doi: 10.1086/507094.

L. Siess, E. Dufour, and M. Forestini. An internet server for pre-main sequence tracks of low- and intermediate-mass stars. *Astronomy and Astrophysics*, 358:593–599, June 2000.

M. F. Skrutskie, R. M. Cutri, R. Stiening, M. D. Weinberg, S. Schneider, J. M. Carpenter, C. Beichman, R. Capps, T. Chester, J. Elias, J. Huchra, J. Liebert, C. Lonsdale, D. G. Monet, S. Price, P. Seitzer, T. Jarrett, J. D. Kirkpatrick, J. E. Gizis, E. Howard, T. Evans, J. Fowler, L. Fullmer, R. Hurt, R. Light, E. L. Kopan, K. A. Marsh, H. L. McCallon, R. Tam, S. Van Dyk, and S. Wheelock. The Two Micron All Sky Survey (2MASS). *Astronomical Journal*, 131:1163–1183, February 2006. doi: 10.1086/498708.

O. Solin, E. Ukkonen, and L. Haikala. Mining the UKIDSS Galactic Plane Survey: star formation and embedded clusters. *Astronomy and Astrophysics*, 542:A3, June 2012. doi: 10.1051/0004-6361/201118531.

A. A. Stark and Y. Lee. The Scale Height of Giant Molecular Clouds Is Less than That of Smaller Clouds. *Astrophysical Journal, Letters*, 619:L159–L162, February 2005. doi: 10.1086/427936.

V. Straižys and V. Laugalys. Young Stars in the Camelopardalis Dust and Molecular Clouds. I. The Cam OB1 Association. *Baltic Astronomy*, 16:167–182, 2007.

S. Sujatha, G. S. D. Babu, and S. Ananthamurthy. UBVRI CCD photometric studies of open clusters Berkeley 15, Czernik 18 and NGC 2401. *Bulletin of the Astronomical Society of India*, 32:295–309, December 2004.

A. L. Tadross. A Catalogue of previously unstudied Berkeley clusters. *Monthly Notices of the RAS*, 389:285–291, September 2008. doi: 10.1111/j.1365-2966.2008.13554.x.

M. T. Tapia, W. J. Schuster, R. Michel, C. Chavarría-K., W. S. Dias, R. Vázquez, and A. Moitinho. UBV(RI)$_C$ photometry of the open clusters Be 15, Be 80 and NGC 2192. *Monthly Notices of the RAS*, 401:621–632, January 2010. doi: 10.1111/j.1365-2966.2009.15685.x.

A. Tripathi, U. S. Pandey, and B. Kumar. Photometric study of Galactic open cluster NGC 2129, NGC 1502 and King 12. *Bulletin of the Astronomical Society of India*, 41:209, September 2013.

V. Vansevicius, A. Bridzius, A. Pucinskas, and T. S. Sasaki. BVRI CCD Photometry of the Open Cluster IC 4996. *Baltic Astronomy*, 5:539–548, 1996.

R. A. Vázquez, J. May, G. Carraro, L. Bronfman, A. Moitinho, and G. Baume. Spiral Structure in the Outer Galactic Disk. I. The Third Galactic Quadrant. *Astrophysical Journal*, 672:930–939, January 2008. doi: 10.1086/524003.

J.-L. Vergely, D. Egret, R. Freire Ferrero, B. Valette, and J. Koeppen. The Extinction in the Solar Neighbourhood from the HIPPARCOS Data. In R. M. Bonnet, E. Høg, P. L. Bernacca, L. Emiliani, A. Blaauw, C. Turon, J. Kovalevsky, L. Lindegren, H. Hassan, M. Bouffard, B. Strim, D. Heger, M. A. C. Perryman, and L. Woltjer, editors, *Hipparcos - Venice '97*, volume 402 of *ESA Special Publication*, pages 603–606, August 1997.

N. Vogt and A. F. J. Moffat. Galactic structure based on young southern open star clusters. *Astronomy and Astrophysics*, 39:477–479, March 1975.

C. Wegg and E. S. Phinney. White dwarf kinematics versus mass. *Monthly Notices of the RAS*, 426:427–439, October 2012. doi: 10.1111/j.1365-2966.2012.21394.x.

J. G. A. Wouterloot, J. Brand, W. B. Burton, and K. K. Kwee. IRAS sources beyond the solar circle. II - Distribution in the Galactic warp. *Astronomy and Astrophysics*, 230:21–36, April 1990.

E. L. Wright, P. R. M. Eisenhardt, A. K. Mainzer, M. E. Ressler, R. M. Cutri, T. Jarrett, J. D. Kirkpatrick, and D. Padgett. The Wide-field Infrared Survey Explorer (WISE): Mission

Description and Initial On-orbit Performance. *Astronomical Journal*, 140:1868, December 2010. doi: 10.1088/0004-6256/140/6/1868.

K. Zwintz and W. W. Weiss. Pulsating pre-main sequence stars in IC 4996 and NGC 6530. *Astronomy and Astrophysics*, 457:237–248, October 2006. doi: 10.1051/0004-6361:20065449.

K. Zwintz, M. Marconi, T. Kallinger, and W. W. Weiss. Pulsating pre-Main sequence stars in young open clusters. In J. Zverko, J. Ziznovsky, S. J. Adelman, and W. W. Weiss, editors, *The A-Star Puzzle*, volume 224 of *IAU Symposium*, pages 353–358, December 2004. doi: 10.1017/S1743921304004752.

# Appendix A

Appendix A contains a summary table of the FSR List catalogue cluster properties derived in this Thesis. A discussion of these properties is provided in Chapter 8.

**Note:**

- The revised properties of the 13 clusters that were analysed in Sect. 8.4 using UKIDSS-GPS or VISTA-VVV photometry are not listed in this Table. These revised properties can instead be found in Table 8.2 .
- The data contained in this table has been published in Buckner and Froebrich (2013) and Buckner and Froebrich (2014).

Table A.1: This table lists clusters' ID number, type (known open cluster or new cluster candidate), Galactic position (l,b), distance in kiloparsec determined using the novel photometric method outlined in Chapter 4 ($D^{meth}$), the pipeline outlined in Chapter 6 ($D^{iso}$) and uncertainty ($\Delta D^{iso}$); H-band extinction value derived from their measured median $[H-K]$ colour using the photometric method outlined in Chapter 5 ($A_H^{HK}$), the pipeline ($A_H^{iso}$) and uncertainty ($\Delta A_H^{iso}$); age derived from the pipeline outlined in Chapter 6 (Age) and uncertainty ($\Delta$ Age).

| **FSR ID** | **Type** | **l** [**deg**] | **b** [**deg**] | $D^{meth}$ [**kpc**] | $D^{iso}$ [**kpc**] | $\Delta D^{iso}$ [**kpc**] | $A_H^{HK}$ [**mag**] | $A_H^{iso}$ [**mag**] | $\Delta A_H^{iso}$ [**mag**] | **Age** [log($age/yr$)] | **$\Delta$Age** [log($age/yr$)] |
|---|---|---|---|---|---|---|---|---|---|---|---|
| 0001 | New | 0.03 | 3.47 | 4.4 | - | - | 1.06 | - | - | - | - |
| 0002 | New | 0.05 | 3.44 | 4.3 | - | - | 1.05 | - | - | - | - |
| 0009 | New | 1.86 | -9.52 | 3.4 | - | - | 0.32 | - | - | - | - |
| 0018 | New | 5.34 | 5.41 | 4.1 | - | - | 0.53 | - | - | - | - |
| 0019 | New | 5.52 | 6.08 | 3.8 | - | - | 0.44 | - | - | - | - |
| 0022 | New | 6.18 | 0.84 | 6.3 | - | - | 0.99 | - | - | - | - |
| 0023 | New | 6.58 | 0.78 | - | - | - | 1.28 | - | - | - | - |
| 0025 | New | 7.54 | 5.65 | 3.6 | - | - | 0.52 | - | - | - | - |
| 0027 | New | 7.78 | 8.45 | 2.6 | - | - | 0.34 | - | - | - | - |
| 0031 | New | 8.91 | -0.27 | 4.1 | - | - | 2.35 | - | - | - | - |
| 0032 | Known | 9.28 | -2.53 | 2.8 | 1.70 | 0.00 | 0.21 | 0.22 | 0.00 | 9.10 | 0.00 |
| 0035 | New | 9.69 | 0.76 | - | - | - | 2.09 | - | - | - | - |

Continued on next page

**Table A.1 – continued from previous page**

| **FSR ID** | **Type** | **l** [deg] | **b** [deg] | $D^{meth}$ [kpc] | $D^{iso}$ [kpc] | $\Delta D^{iso}$ [kpc] | $A_H^{HK}$ [mag] | $A_H^{iso}$ [mag] | $\Delta A_H^{iso}$ [mag] | **Age** [log(*age*/*yr*)] | **ΔAge** [log(*age*/*yr*)] |
|---|---|---|---|---|---|---|---|---|---|---|---|
| 0039 | New | 10.25 | 0.32 | 4.3 | - | - | 2.12 | - | - | - | - |
| 0042 | New | 11.79 | 16.13 | 0.7 | - | - | 0.25 | - | - | - | - |
| 0045 | Known | 12.87 | -1.32 | 2.2 | 2.60 | 0.00 | 0.20 | 0.32 | 0.00 | 8.50 | 0.00 |
| 0047 | Known | 14.04 | -0.82 | 6.1 | - | - | 2.65 | - | - | - | - |
| 0050 | New | 16.39 | 11.41 | 1.0 | - | - | 0.44 | - | - | - | - |
| 0051 | New | 16.71 | 2.24 | 4.0 | - | - | 1.12 | - | - | - | - |
| 0052 | New | 16.79 | -2.92 | 5.6 | - | - | 0.75 | - | - | - | - |
| 0053 | Known | 16.97 | 0.83 | 3.0 | - | - | 0.89 | - | - | - | - |
| 0054 | New | 17.16 | -2.28 | 3.6 | - | - | 0.32 | - | - | - | - |
| 0055 | New | 17.99 | -0.28 | 6.8 | - | - | 2.35 | - | - | - | - |
| 0057 | Known | 18.46 | -0.40 | 4.8 | - | - | 1.51 | - | - | - | - |
| 0059 | New | 19.74 | -0.56 | 6.8 | - | - | 2.67 | - | - | - | - |
| 0060 | New | 20.29 | -0.56 | 7.3 | - | - | 2.33 | - | - | - | - |
| 0062 | New | 20.86 | 4.30 | 2.0 | - | - | 0.54 | - | - | - | - |
| 0063 | New | 21.26 | 4.14 | 5.4 | - | - | 0.97 | - | - | - | - |
| 0068 | Known | 22.85 | -0.63 | - | - | - | 2.26 | - | - | - | - |
| 0070 | New | 23.44 | -15.27 | 3.6 | - | - | 0.57 | - | - | - | - |
| 0071 | Known | 23.89 | -2.91 | 1.9 | 2.00 | 0.21 | 0.21 | 0.29 | 0.02 | 7.60 | 0.17 |
| 0072 | New | 24.70 | 0.31 | 5.3 | - | - | 1.88 | - | - | - | - |
| 0074 | Known | 25.36 | -4.31 | 3.5 | 5.30 | 0.00 | 0.18 | 0.02 | 0.00 | 9.50 | 0.00 |
| 0076 | New | 25.56 | 5.08 | 1.9 | - | - | 0.47 | - | - | - | - |
| 0077 | New | 25.71 | 5.05 | 1.8 | - | - | 0.44 | - | - | - | - |

Continued on next page

**Table A.1 – continued from previous page**

| **FSR ID** | **Type** | **l** [deg] | **b** [deg] | $D^{meth}$ [kpc] | $D^{iso}$ [kpc] | $\Delta D^{iso}$ [kpc] | $A_H^{HK}$ [mag] | $A_H^{iso}$ [mag] | $\Delta A_H^{iso}$ [mag] | **Age** [log(*age*/*yr*)] | **ΔAge** [log(*age*/*yr*)] |
|---|---|---|---|---|---|---|---|---|---|---|---|
| 0080 | New | 26.64 | 12.19 | 1.1 | - | - | 0.26 | - | - | - | - |
| 0082 | Known | 27.31 | -2.77 | 1.1 | 1.60 | 0.07 | 0.09 | 0.14 | 0.03 | 8.60 | 0.09 |
| 0087 | New | 29.09 | -0.44 | - | - | - | 2.37 | - | - | - | - |
| 0089 | New | 29.49 | -0.98 | 4.5 | 6.50 | 0.07 | 1.53 | 1.50 | 0.00 | 8.50 | 0.03 |
| 0090 | New | 29.62 | -1.39 | 6.2 | - | - | 1.34 | - | - | - | - |
| 0094 | New | 31.82 | -0.12 | 6.0 | - | - | 1.79 | - | - | - | - |
| 0098 | New | 33.03 | 1.15 | 5.1 | - | - | 1.09 | - | - | - | - |
| 0100 | New | 34.33 | -2.79 | 3.4 | - | - | 0.32 | - | - | - | - |
| 0101 | New | 35.15 | 1.75 | 3.2 | 1.60 | 0.00 | 1.07 | 1.05 | 0.00 | 9.20 | 0.00 |
| 0107 | New | 36.31 | -3.21 | 5.0 | - | - | 0.53 | - | - | - | - |
| 0109 | Known | 37.17 | 2.62 | 1.7 | 1.50 | 0.03 | 0.52 | 0.59 | 0.01 | 9.00 | 0.00 |
| 0111 | Known | 38.66 | -1.64 | 2.0 | 1.80 | 0.00 | 0.19 | 0.30 | 0.00 | 8.80 | 0.00 |
| 0112 | New | 38.68 | -18.70 | 1.2 | - | - | 0.17 | - | - | - | - |
| 0113 | Known | 39.10 | -1.68 | 1.6 | 2.10 | 0.07 | 0.29 | 0.39 | 0.04 | 8.60 | 0.18 |
| 0115 | Known | 40.35 | -0.70 | 2.4 | 2.20 | 0.00 | 0.80 | 1.10 | 0.00 | 7.10 | 0.00 |
| 0122 | Known | 45.70 | -0.12 | 2.1 | 2.30 | 0.30 | 0.64 | 0.74 | 0.02 | 8.60 | 0.12 |
| 0124 | New | 46.48 | 2.65 | 3.7 | 1.10 | 0.00 | 0.48 | 0.45 | 0.00 | 9.30 | 0.00 |
| 0126 | New | 48.55 | -0.18 | 6.2 | - | - | 1.53 | - | - | - | - |
| 0127 | Known | 48.89 | -0.94 | 2.6 | 2.90 | 0.18 | 0.60 | 0.64 | 0.01 | 8.20 | 0.02 |
| 0129 | New | 49.39 | -1.32 | 7.0 | - | - | 1.37 | - | - | - | - |
| 0133 | New | 51.12 | -1.17 | 4.2 | 2.40 | 0.18 | 0.87 | 0.99 | 0.03 | 8.70 | 0.09 |
| 0138 | Known | 53.22 | 3.34 | 2.5 | 3.10 | 0.07 | 0.36 | 0.41 | 0.01 | 9.10 | 0.09 |

Continued on next page

**Table A.1 – continued from previous page**

| **FSR ID** | **Type** | **l** [deg] | **b** [deg] | $D^{meth}$ [kpc] | $D^{iso}$ [kpc] | $\Delta D^{iso}$ [kpc] | $A_H^{HK}$ [mag] | $A_H^{iso}$ [mag] | $\Delta A_H^{iso}$ [mag] | **Age** [log($age/yr$)] | **ΔAge** [log($age/yr$)] |
|---|---|---|---|---|---|---|---|---|---|---|---|
| 0142 | New | 55.79 | -0.19 | 7.0 | - | - | 1.34 | - | - | - | - |
| 0143 | New | 56.32 | -4.38 | 3.6 | - | - | 0.28 | - | - | - | - |
| 0144 | Known | 56.34 | -4.69 | 1.9 | 1.70 | 0.20 | 0.02 | 0.05 | 0.03 | 7.80 | 0.10 |
| 0148 | New | 57.03 | 0.02 | 2.8 | - | - | 0.61 | - | - | - | - |
| 0153 | Known | 59.40 | -0.15 | 4.1 | - | - | 0.60 | - | - | - | - |
| 0154 | New | 60.00 | -1.08 | 3.2 | 3.90 | 0.00 | 0.54 | 0.55 | 0.00 | 8.60 | 0.13 |
| 0157 | New | 62.02 | -0.70 | 2.2 | 1.10 | 0.00 | 0.58 | 0.65 | 0.00 | 6.80 | 0.00 |
| 0160 | New | 62.71 | 1.34 | 7.8 | - | - | 0.87 | - | - | - | - |
| 0161 | New | 63.10 | -17.39 | 1.3 | - | - | 0.12 | - | - | - | - |
| 0162 | New | 63.21 | -2.75 | 3.2 | - | - | 0.48 | - | - | - | - |
| 0163 | New | 63.23 | -2.42 | 4.2 | - | - | 0.51 | - | - | - | - |
| 0165 | New | 64.10 | -1.30 | 2.9 | - | - | 0.54 | - | - | - | - |
| 0166 | New | 64.87 | -4.94 | 2.2 | - | - | 0.35 | - | - | - | - |
| 0167 | New | 65.16 | -2.41 | 2.4 | 1.60 | 0.15 | 0.42 | 0.43 | 0.03 | 8.70 | 0.12 |
| 0168 | Known | 65.53 | -3.97 | 1.4 | 1.00 | 0.05 | 0.09 | 0.09 | 0.00 | 8.60 | 0.03 |
| 0169 | Known | 65.69 | 1.18 | 2.5 | 2.40 | 0.00 | 0.08 | 0.36 | 0.00 | 7.60 | 0.00 |
| 0170 | New | 65.93 | -2.69 | 6.7 | - | - | 1.14 | - | - | - | - |
| 0171 | Known | 66.10 | -0.94 | 3.7 | - | - | 0.70 | - | - | - | - |
| 0172 | New | 66.43 | -0.36 | 4.8 | - | - | 0.87 | - | - | - | - |
| 0177 | Known | 67.64 | 0.85 | 3.1 | 2.80 | 0.00 | 0.15 | 0.30 | 0.00 | 9.20 | 0.00 |
| 0180 | Known | 68.01 | 2.87 | 8.2 | - | - | 0.48 | - | - | - | - |
| 0181 | Known | 68.53 | 0.45 | 4.3 | - | - | 0.63 | - | - | - | - |

Continued on next page

**Table A.1 – continued from previous page**

| **FSR ID** | **Type** | **l** [deg] | **b** [deg] | $D^{meth}$ [kpc] | $D^{iso}$ [kpc] | $\Delta D^{iso}$ [kpc] | $A_H^{HK}$ [mag] | $A_H^{iso}$ [mag] | $\Delta A_H^{iso}$ [mag] | **Age** [log($age/yr$)] | **ΔAge** [log($age/yr$)] |
|---|---|---|---|---|---|---|---|---|---|---|---|
| 0182 | New | 69.18 | 3.36 | 2.7 | - | - | 0.07 | - | - | - | - |
| 0183 | New | 69.52 | -9.54 | 2.8 | - | - | 0.28 | - | - | - | - |
| 0186 | Known | 69.97 | 10.91 | 2.0 | 4.10 | 0.00 | 0.25 | 0.12 | 0.00 | 9.50 | 0.00 |
| 0187 | Known | 70.31 | 1.76 | 4.5 | 5.20 | 0.00 | 0.34 | 0.29 | 0.00 | 8.70 | 0.00 |
| 0188 | New | 70.65 | 1.74 | 8.3 | 10.50 | 1.00 | 0.69 | 0.62 | 0.02 | 8.60 | 0.05 |
| 0189 | New | 70.66 | -0.15 | 4.0 | - | - | 0.84 | - | - | - | - |
| 0190 | New | 70.73 | 0.96 | 10.2 | 11.60 | 0.00 | 1.31 | 1.26 | 0.00 | 8.80 | 0.00 |
| 0191 | New | 70.99 | 2.58 | 3.8 | 2.40 | 0.37 | 0.56 | 0.59 | 0.04 | 8.50 | 0.18 |
| 0192 | New | 71.10 | 0.85 | 8.6 | - | - | 0.88 | - | - | - | - |
| 0193 | New | 71.31 | 8.12 | 3.1 | - | - | 0.16 | - | - | - | - |
| 0194 | Known | 71.87 | 2.42 | 9.5 | - | - | 0.92 | - | - | - | - |
| 0195 | New | 72.07 | -0.99 | 4.1 | 1.90 | 0.00 | 0.99 | 1.15 | 0.00 | 7.60 | 0.00 |
| 0196 | Known | 72.12 | -0.51 | 2.9 | - | - | 0.44 | - | - | - | - |
| 0197 | New | 72.16 | 0.30 | 3.7 | 1.80 | 0.00 | 0.62 | 0.70 | 0.00 | 8.90 | 0.00 |
| 0198 | New | 72.18 | 2.62 | 12.8 | - | - | 1.02 | - | - | - | - |
| 0199 | Known | 72.40 | 0.94 | 2.9 | - | - | 0.28 | - | - | - | - |
| 0200 | Known | 73.25 | 0.95 | 3.8 | - | - | 0.34 | - | - | - | - |
| 0201 | Known | 73.27 | 1.17 | 5.3 | - | - | 0.36 | - | - | - | - |
| 0202 | Known | 73.99 | 8.49 | 1.5 | 1.80 | 0.10 | 0.02 | 0.07 | 0.00 | 9.20 | 0.05 |
| 0204 | New | 74.78 | 0.61 | 8.1 | - | - | 1.14 | - | - | - | - |
| 0205 | Known | 75.24 | -0.67 | 6.9 | 7.60 | 0.00 | 1.45 | 1.40 | 0.00 | 8.50 | 0.00 |
| 0206 | Known | 75.35 | -0.49 | 3.8 | - | - | 0.84 | - | - | - | - |

Continued on next page

**Table A.1 – continued from previous page**

| **FSR ID** | **Type** | **l** [deg] | **b** [deg] | $D^{meth}$ [kpc] | $D^{iso}$ [kpc] | $\Delta D^{iso}$ [kpc] | $A_H^{HK}$ [mag] | $A_H^{iso}$ [mag] | $\Delta A_H^{iso}$ [mag] | **Age** [log(*age*/*yr*)] | **ΔAge** [log(*age*/*yr*)] |
|---|---|---|---|---|---|---|---|---|---|---|---|
| 0207 | Known | 75.38 | 1.30 | 2.0 | 1.40 | 0.00 | 0.03 | 0.30 | 0.00 | 7.00 | 0.00 |
| 0208 | Known | 75.70 | 0.99 | 3.2 | 3.40 | 0.20 | 0.42 | 0.56 | 0.02 | 8.20 | 0.12 |
| 0210 | New | 76.21 | -0.55 | 6.6 | - | - | 1.33 | - | - | - | - |
| 0211 | Known | 76.39 | -0.60 | 7.5 | - | - | 2.39 | - | - | - | - |
| 0212 | Known | 76.94 | 2.02 | 11.8 | - | - | 1.65 | - | - | - | - |
| 0213 | New | 77.63 | 0.38 | 5.7 | - | - | 1.13 | - | - | - | - |
| 0214 | New | 77.71 | 4.18 | 5.8 | 6.50 | 0.00 | 0.29 | 0.23 | 0.01 | 8.90 | 0.05 |
| 0216 | Known | 78.01 | -3.36 | 1.7 | 1.40 | 0.06 | 0.10 | 0.16 | 0.02 | 8.90 | 0.08 |
| 0218 | Known | 78.10 | 2.79 | 2.7 | 1.00 | 0.00 | 0.37 | 0.38 | 0.00 | 7.40 | 0.00 |
| 0219 | New | 78.14 | 3.52 | 7.9 | - | - | 0.67 | - | - | - | - |
| 0220 | Known | 78.15 | -0.54 | 3.6 | - | - | 1.11 | - | - | - | - |
| 0224 | New | 78.47 | 1.36 | 5.5 | - | - | 0.70 | - | - | - | - |
| 0225 | New | 78.58 | -2.80 | 4.0 | - | - | 0.65 | - | - | - | - |
| 0226 | Known | 79.00 | 3.67 | 9.3 | - | - | 0.90 | - | - | - | - |
| 0230 | Known | 79.31 | 1.31 | 10.3 | - | - | 2.07 | - | - | - | - |
| 0231 | Known | 79.57 | 6.83 | 1.3 | 1.30 | 0.06 | -0.00 | 0.05 | 0.02 | 8.80 | 0.03 |
| 0233 | Known | 79.87 | -0.93 | 3.4 | 1.60 | 0.10 | 1.23 | 1.30 | 0.00 | 9.00 | 0.05 |
| 0234 | Known | 80.13 | 0.75 | 5.6 | - | - | 1.15 | - | - | - | - |
| 0238 | New | 80.48 | 0.62 | 3.0 | - | - | 0.90 | - | - | - | - |
| 0239 | New | 80.52 | 2.94 | 11.2 | - | - | 1.47 | - | - | - | - |
| 0240 | Known | 80.94 | -0.17 | 9.0 | - | - | 2.69 | - | - | - | - |
| 0241 | New | 81.23 | 8.03 | 1.8 | - | - | 0.07 | - | - | - | - |

Continued on next page

**Table A.1 – continued from previous page**

| **FSR ID** | **Type** | **l** [deg] | **b** [deg] | $D^{meth}$ [kpc] | $D^{iso}$ [kpc] | $\Delta D^{iso}$ [kpc] | $A_H^{HK}$ [mag] | $A_H^{iso}$ [mag] | $\Delta A_H^{iso}$ [mag] | **Age** [log(*age*/*yr*)] | **ΔAge** [log(*age*/*yr*)] |
|---|---|---|---|---|---|---|---|---|---|---|---|
| 0243 | Known | 81.46 | 1.11 | 5.4 | - | - | 1.21 | - | - | - | - |
| 0244 | Known | 81.48 | 0.46 | 5.8 | - | - | 1.30 | - | - | - | - |
| 0245 | New | 81.50 | 0.62 | 6.5 | - | - | 1.47 | - | - | - | - |
| 0248 | New | 81.72 | -0.60 | 7.6 | - | - | 1.91 | - | - | - | - |
| 0250 | New | 82.16 | -16.99 | 1.6 | - | - | 0.10 | - | - | - | - |
| 0251 | New | 82.33 | 0.76 | 5.6 | - | - | 1.18 | - | - | - | - |
| 0254 | New | 82.81 | 5.79 | 3.9 | - | - | 0.37 | - | - | - | - |
| 0255 | New | 82.93 | 2.20 | 12.5 | - | - | 1.81 | - | - | - | - |
| 0256 | Known | 83.08 | -4.13 | 3.7 | - | - | 0.55 | - | - | - | - |
| 0257 | New | 83.13 | 4.84 | 2.8 | 2.30 | 0.00 | 0.26 | 0.24 | 0.00 | 9.50 | 0.00 |
| 0258 | New | 83.58 | 0.68 | 2.5 | - | - | 0.49 | - | - | - | - |
| 0261 | New | 83.99 | -1.09 | 2.7 | - | - | 0.82 | - | - | - | - |
| 0262 | Known | 84.89 | 3.80 | 7.7 | - | - | 0.73 | - | - | - | - |
| 0263 | Known | 84.97 | -0.22 | 5.4 | - | - | 1.28 | - | - | - | - |
| 0265 | New | 85.50 | -4.44 | 2.5 | - | - | 0.37 | - | - | - | - |
| 0266 | New | 85.62 | -16.15 | 1.6 | - | - | 0.12 | - | - | - | - |
| 0267 | Known | 85.68 | -1.52 | 2.0 | 2.10 | 0.00 | 0.36 | 0.38 | 0.03 | 8.80 | 0.10 |
| 0268 | Known | 85.90 | -4.14 | 3.6 | 3.10 | 0.40 | 0.43 | 0.37 | 0.01 | 9.10 | 0.15 |
| 0271 | New | 86.17 | -5.28 | 3.0 | - | - | 0.33 | - | - | - | - |
| 0275 | New | 87.20 | 0.97 | 5.1 | 2.40 | 0.00 | 0.52 | 0.40 | 0.00 | 9.30 | 0.00 |
| 0276 | New | 87.32 | 5.75 | 7.4 | 7.10 | 0.00 | 0.62 | 0.75 | 0.00 | 8.60 | 0.00 |
| 0278 | New | 87.86 | 6.84 | 3.8 | - | - | 0.29 | - | - | - | - |

Continued on next page

**Table A.1 – continued from previous page**

| **FSR ID** | **Type** | **l** [deg] | **b** [deg] | $D^{meth}$ [kpc] | $D^{iso}$ [kpc] | $\Delta D^{iso}$ [kpc] | $A_H^{HK}$ [mag] | $A_H^{iso}$ [mag] | $\Delta A_H^{iso}$ [mag] | **Age** [log($age/yr$)] | **ΔAge** [log($age/yr$)] |
|---|---|---|---|---|---|---|---|---|---|---|---|
| 0280 | Known | 88.24 | 0.26 | 4.5 | 4.10 | 0.00 | 0.43 | 0.49 | 0.00 | 9.00 | 0.00 |
| 0282 | New | 88.75 | 1.05 | 2.6 | 2.70 | 0.00 | 0.45 | 0.56 | 0.02 | 8.80 | 0.09 |
| 0284 | New | 89.07 | 2.60 | 2.7 | - | - | 0.18 | - | - | - | - |
| 0285 | Known | 89.62 | -0.39 | 2.4 | 2.50 | 0.00 | 0.22 | 0.31 | 0.02 | 8.50 | 0.06 |
| 0286 | Known | 89.98 | -2.73 | 1.8 | 1.80 | 0.06 | 0.09 | 0.18 | 0.01 | 8.90 | 0.06 |
| 0290 | New | 90.42 | 3.19 | 10.9 | - | - | 1.12 | - | - | - | - |
| 0293 | New | 91.03 | -2.75 | 2.3 | 1.40 | 0.00 | 0.06 | 0.15 | 0.00 | 8.30 | 0.00 |
| 0294 | New | 91.27 | 2.34 | 2.7 | 1.60 | 0.24 | 0.48 | 0.49 | 0.06 | 7.60 | 0.32 |
| 0295 | New | 92.32 | -0.16 | 2.9 | - | - | 0.36 | - | - | - | - |
| 0300 | Known | 92.94 | 2.81 | 3.5 | - | - | 0.68 | - | - | - | - |
| 0301 | Known | 93.04 | 1.80 | 4.0 | 2.00 | 0.00 | 0.71 | 1.00 | 0.00 | 7.50 | 0.00 |
| 0304 | New | 93.56 | 0.67 | 3.6 | - | - | 0.53 | - | - | - | - |
| 0308 | Known | 94.40 | -5.51 | 10.3 | - | - | 1.74 | - | - | - | - |
| 0309 | Known | 94.42 | 0.19 | 1.7 | 1.60 | 0.09 | 0.18 | 0.30 | 0.02 | 8.20 | 0.06 |
| 0313 | Known | 95.28 | 2.07 | 7.6 | - | - | 0.76 | - | - | - | - |
| 0316 | New | 96.07 | -0.33 | 2.8 | - | - | 0.25 | - | - | - | - |
| 0318 | New | 96.15 | -4.72 | 2.8 | - | - | 0.20 | - | - | - | - |
| 0320 | New | 96.38 | 1.24 | 2.3 | 1.40 | 0.15 | 0.15 | 0.16 | 0.03 | 7.40 | 0.20 |
| 0322 | New | 96.47 | -2.10 | 2.1 | - | - | 0.15 | - | - | - | - |
| 0324 | New | 96.54 | 1.26 | 2.5 | - | - | 0.18 | - | - | - | - |
| 0326 | New | 96.75 | 1.08 | 8.6 | - | - | 0.86 | - | - | - | - |
| 0327 | Known | 97.34 | 0.45 | 3.1 | 1.90 | 0.00 | 0.43 | 0.42 | 0.00 | 7.90 | 0.00 |

Continued on next page

**Table A.1 – continued from previous page**

| **FSR ID** | **Type** | **l** [deg] | **b** [deg] | $D^{meth}$ [kpc] | $D^{iso}$ [kpc] | $\Delta D^{iso}$ [kpc] | $A_H^{HK}$ [mag] | $A_H^{iso}$ [mag] | $\Delta A_H^{iso}$ [mag] | **Age** [log(*age*/*yr*)] | **ΔAge** [log(*age*/*yr*)] |
|---|---|---|---|---|---|---|---|---|---|---|---|
| 0334 | New | 98.71 | 1.54 | 3.0 | - | - | 0.20 | - | - | - | - |
| 0336 | New | 99.09 | 0.96 | 2.5 | 2.30 | 0.12 | 0.37 | 0.52 | 0.02 | 7.30 | 0.38 |
| 0337 | Known | 99.14 | 7.49 | 13.0 | - | - | 0.89 | - | - | - | - |
| 0340 | Known | 99.31 | 3.74 | 9.3 | - | - | 0.70 | - | - | - | - |
| 0341 | New | 99.65 | -1.83 | 2.5 | - | - | 0.13 | - | - | - | - |
| 0342 | New | 99.76 | -2.21 | 2.5 | 2.50 | 0.23 | 0.22 | 0.18 | 0.02 | 8.90 | 0.03 |
| 0343 | Known | 99.96 | -2.69 | 2.1 | 2.30 | 0.10 | 0.04 | 0.07 | 0.01 | 8.80 | 0.06 |
| 0348 | Known | 101.37 | -1.86 | 2.0 | 2.10 | 0.00 | -0.01 | 0.01 | 0.01 | 9.00 | 0.03 |
| 0349 | Known | 101.41 | -0.60 | 3.2 | 3.20 | 0.00 | 0.20 | 0.19 | 0.02 | 8.80 | 0.03 |
| 0351 | New | 102.51 | 5.14 | 7.2 | - | - | 0.57 | - | - | - | - |
| 0352 | Known | 102.69 | 0.80 | 2.7 | 1.80 | 0.15 | 0.06 | 0.35 | 0.03 | 7.60 | 0.19 |
| 0353 | Known | 102.81 | -0.69 | 5.3 | - | - | 0.59 | - | - | - | - |
| 0357 | New | 103.10 | -3.41 | 2.9 | - | - | 0.12 | - | - | - | - |
| 0358 | New | 103.35 | 2.21 | 9.9 | 10.60 | 0.12 | 1.08 | 1.00 | 0.03 | 8.70 | 0.02 |
| 0359 | Known | 103.72 | -2.09 | 3.0 | - | - | 0.20 | - | - | - | - |
| 0363 | Known | 104.05 | 0.92 | 2.9 | 2.90 | 0.00 | 0.23 | 0.18 | 0.00 | 9.10 | 0.00 |
| 0365 | New | 104.18 | -2.21 | 3.1 | - | - | 0.32 | - | - | - | - |
| 0367 | Known | 104.56 | 1.30 | 9.7 | - | - | 1.05 | - | - | - | - |
| 0372 | Known | 105.31 | 4.07 | 13.3 | - | - | 1.58 | - | - | - | - |
| 0373 | Known | 105.35 | 9.50 | 2.2 | 2.20 | 0.00 | 0.15 | 0.13 | 0.01 | 9.50 | 0.00 |
| 0374 | Known | 105.41 | 9.90 | 12.1 | - | - | 1.71 | - | - | - | - |
| 0375 | Known | 105.47 | 1.20 | 2.6 | 2.60 | 0.00 | 0.40 | 0.70 | 0.00 | 7.60 | 0.00 |

Continued on next page

**Table A.1 – continued from previous page**

| **FSR ID** | **Type** | **l** [deg] | **b** [deg] | $D^{meth}$ [kpc] | $D^{iso}$ [kpc] | $\Delta D^{iso}$ [kpc] | $A_H^{HK}$ [mag] | $A_H^{iso}$ [mag] | $\Delta A_H^{iso}$ [mag] | **Age** [log(*age*/*yr*)] | **ΔAge** [log(*age*/*yr*)] |
|---|---|---|---|---|---|---|---|---|---|---|---|
| 0377 | New | 105.78 | 0.06 | 3.6 | - | - | 0.37 | - | - | - | - |
| 0378 | New | 105.86 | 3.91 | 12.8 | - | - | 1.45 | - | - | - | - |
| 0381 | New | 106.64 | -0.39 | 2.3 | 2.20 | 0.00 | 0.16 | 0.16 | 0.03 | 8.80 | 0.06 |
| 0382 | Known | 106.64 | 0.36 | 2.8 | 2.40 | 0.25 | 0.34 | 0.32 | 0.03 | 8.60 | 0.10 |
| 0383 | Known | 106.68 | 5.29 | 7.6 | - | - | 0.72 | - | - | - | - |
| 0384 | New | 106.75 | -2.95 | 2.1 | 1.20 | 0.00 | 0.03 | 0.05 | 0.00 | 7.60 | 0.00 |
| 0385 | New | 106.96 | 0.12 | 3.0 | 1.90 | 0.00 | 0.40 | 0.35 | 0.00 | 9.00 | 0.00 |
| 0387 | Known | 107.18 | -0.91 | 10.0 | - | - | 1.02 | - | - | - | - |
| 0388 | New | 107.32 | 5.13 | 4.9 | 5.00 | 0.23 | 0.89 | 0.85 | 0.01 | 8.90 | 0.03 |
| 0391 | Known | 107.62 | -2.27 | 3.7 | - | - | 0.44 | - | - | - | - |
| 0392 | Known | 107.79 | -1.02 | 2.6 | 2.10 | 0.20 | 0.19 | 0.21 | 0.01 | 8.70 | 0.03 |
| 0395 | Known | 108.49 | -2.79 | 3.0 | 2.50 | 0.21 | 0.20 | 0.26 | 0.01 | 7.70 | 0.13 |
| 0396 | Known | 108.51 | -0.38 | 3.0 | 2.50 | 0.09 | 0.40 | 0.58 | 0.01 | 7.80 | 0.03 |
| 0398 | New | 108.89 | 5.05 | 5.1 | - | - | 0.46 | - | - | - | - |
| 0399 | Known | 109.10 | -0.34 | 4.4 | - | - | 0.59 | - | - | - | - |
| 0400 | Known | 109.13 | 1.12 | 4.1 | 2.00 | 0.00 | 0.65 | 1.00 | 0.00 | 7.30 | 0.00 |
| 0401 | New | 109.40 | -0.23 | 3.5 | - | - | 0.33 | - | - | - | - |
| 0405 | New | 109.77 | 7.38 | 2.3 | - | - | 0.29 | - | - | - | - |
| 0406 | New | 109.86 | 2.76 | 8.5 | - | - | 1.16 | - | - | - | - |
| 0408 | Known | 110.19 | 2.72 | 7.4 | - | - | 0.83 | - | - | - | - |
| 0409 | Known | 110.25 | 0.01 | 8.5 | - | - | 1.29 | - | - | - | - |
| 0411 | Known | 110.58 | 0.14 | 2.9 | 2.10 | 0.00 | 0.31 | 0.26 | 0.00 | 9.00 | 0.00 |

Continued on next page

**Table A.1 – continued from previous page**

| **FSR ID** | **Type** | **l** [deg] | **b** [deg] | $D^{meth}$ [kpc] | $D^{iso}$ [kpc] | $\Delta D^{iso}$ [kpc] | $A_H^{HK}$ [mag] | $A_H^{iso}$ [mag] | $\Delta A_H^{iso}$ [mag] | **Age** [log($age/yr$)] | **ΔAge** [log($age/yr$)] |
|---|---|---|---|---|---|---|---|---|---|---|---|
| 0412 | Known | 110.70 | 0.48 | 6.8 | 6.60 | 0.00 | 0.84 | 0.78 | 0.01 | 8.90 | 0.00 |
| 0414 | New | 110.86 | 2.75 | 5.6 | - | - | 0.73 | - | - | - | - |
| 0415 | Known | 110.92 | 0.07 | 2.0 | 1.80 | 0.10 | 0.18 | 0.43 | 0.00 | 7.40 | 0.05 |
| 0416 | New | 110.93 | 2.76 | 3.5 | - | - | 0.41 | - | - | - | - |
| 0417 | New | 110.97 | -0.75 | 3.2 | - | - | 0.26 | - | - | - | - |
| 0418 | New | 111.20 | 2.75 | 4.3 | - | - | 0.56 | - | - | - | - |
| 0420 | Known | 111.27 | -0.67 | 6.7 | - | - | 1.19 | - | - | - | - |
| 0421 | Known | 111.34 | -0.22 | 2.8 | - | - | 0.19 | - | - | - | - |
| 0422 | New | 111.47 | 0.14 | 3.0 | - | - | 0.32 | - | - | - | - |
| 0423 | New | 111.48 | 5.19 | 3.2 | 3.10 | 0.12 | 0.42 | 0.43 | 0.03 | 9.20 | 0.03 |
| 0425 | New | 111.57 | 0.56 | 8.5 | - | - | 1.38 | - | - | - | - |
| 0427 | New | 111.92 | -4.17 | 3.2 | - | - | 0.27 | - | - | - | - |
| 0429 | New | 112.53 | 8.66 | 3.1 | - | - | 0.43 | - | - | - | - |
| 0430 | New | 112.71 | 3.22 | 2.3 | 1.50 | 0.00 | 0.30 | 0.25 | 0.00 | 8.70 | 0.00 |
| 0431 | Known | 112.71 | 0.91 | 3.9 | - | - | 0.45 | - | - | - | - |
| 0433 | Known | 112.86 | 0.17 | 2.3 | 1.80 | 0.00 | 0.09 | 0.25 | 0.00 | 8.10 | 0.00 |
| 0434 | Known | 112.86 | -2.86 | 2.2 | 2.10 | 0.00 | 0.23 | 0.25 | 0.00 | 8.40 | 0.03 |
| 0440 | New | 113.68 | -11.73 | 2.2 | - | - | 0.17 | - | - | - | - |
| 0444 | New | 114.51 | 2.63 | 2.4 | 2.20 | 0.00 | 0.35 | 0.40 | 0.01 | 8.80 | 0.07 |
| 0445 | Known | 114.61 | 0.24 | 8.9 | - | - | 1.02 | - | - | - | - |
| 0447 | New | 115.19 | -18.21 | 2.1 | - | - | 0.11 | - | - | - | - |
| 0448 | New | 115.20 | -0.99 | 4.3 | - | - | 0.57 | - | - | - | - |

Continued on next page

**Table A.1 – continued from previous page**

| **FSR ID** | **Type** | **l** [deg] | **b** [deg] | $D^{meth}$ [kpc] | $D^{iso}$ [kpc] | $\Delta D^{iso}$ [kpc] | $A_H^{HK}$ [mag] | $A_H^{iso}$ [mag] | $\Delta A_H^{iso}$ [mag] | **Age** [log($age/yr$)] | **ΔAge** [log($age/yr$)] |
|---|---|---|---|---|---|---|---|---|---|---|---|
| 0454 | Known | 115.80 | 1.01 | 2.7 | - | - | 0.16 | - | - | - | - |
| 0455 | Known | 115.94 | 10.15 | 4.0 | - | - | 0.31 | - | - | - | - |
| 0457 | Known | 116.13 | -0.14 | 1.9 | 1.60 | 0.12 | 0.04 | 0.09 | 0.02 | 8.40 | 0.09 |
| 0458 | Known | 116.44 | -0.78 | 2.2 | 1.80 | 0.06 | 0.07 | 0.14 | 0.01 | 8.00 | 0.08 |
| 0461 | Known | 116.60 | -1.01 | 2.7 | 2.60 | 0.12 | 0.16 | 0.16 | 0.04 | 8.40 | 0.23 |
| 0465 | New | 116.87 | 4.03 | 4.3 | - | - | 0.53 | - | - | - | - |
| 0467 | Known | 117.15 | 6.49 | 3.2 | 3.10 | 0.00 | 0.40 | 0.39 | 0.02 | 9.40 | 0.10 |
| 0468 | Known | 117.22 | 5.86 | 1.8 | 0.80 | 0.00 | 0.23 | 0.32 | 0.00 | 9.00 | 0.00 |
| 0471 | Known | 117.64 | 2.25 | 10.3 | - | - | 0.94 | - | - | - | - |
| 0475 | Known | 117.99 | -1.30 | 2.7 | 2.70 | 0.17 | 0.20 | 0.23 | 0.02 | 9.10 | 0.00 |
| 0476 | Known | 118.23 | 5.02 | 12.1 | - | - | 1.35 | - | - | - | - |
| 0479 | New | 118.55 | -7.81 | 2.1 | - | - | 0.07 | - | - | - | - |
| 0480 | New | 118.59 | -1.09 | 6.0 | 5.60 | 0.00 | 0.65 | 0.56 | 0.01 | 8.80 | 0.03 |
| 0488 | New | 119.65 | 3.19 | 10.2 | - | - | 1.66 | - | - | - | - |
| 0490 | Known | 119.78 | 1.70 | 3.6 | 1.50 | 0.00 | 0.38 | 0.40 | 0.01 | 9.10 | 0.00 |
| 0491 | Known | 119.80 | -1.38 | 2.0 | 2.00 | 0.10 | 0.12 | 0.11 | 0.03 | 8.80 | 0.07 |
| 0493 | Known | 119.93 | -0.09 | 2.6 | 2.20 | 0.15 | 0.05 | 0.06 | 0.02 | 8.30 | 0.09 |
| 0494 | New | 120.07 | 1.03 | 3.2 | 2.90 | 0.00 | 0.21 | 0.25 | 0.02 | 9.40 | 0.07 |
| 0495 | New | 120.13 | -4.83 | 2.5 | - | - | 0.14 | - | - | - | - |
| 0496 | New | 120.26 | 1.29 | 3.4 | 1.30 | 0.20 | 0.36 | 0.35 | 0.00 | 9.10 | 0.05 |
| 0501 | Known | 120.75 | -0.94 | 2.7 | - | - | 0.21 | - | - | - | - |
| 0502 | Known | 120.88 | 0.51 | 2.2 | 2.10 | 0.00 | -0.00 | 0.17 | 0.00 | 8.00 | 0.00 |

Continued on next page

**Table A.1 – continued from previous page**

| **FSR ID** | **Type** | **l** [deg] | **b** [deg] | $D^{meth}$ [kpc] | $D^{iso}$ [kpc] | $\Delta D^{iso}$ [kpc] | $A_H^{HK}$ [mag] | $A_H^{iso}$ [mag] | $\Delta A_H^{iso}$ [mag] | **Age** [log($age/yr$)] | **ΔAge** [log($age/yr$)] |
|---|---|---|---|---|---|---|---|---|---|---|---|
| 0510 | Known | 121.97 | -2.66 | 2.7 | - | - | 0.12 | - | - | - | - |
| 0512 | Known | 122.09 | 1.33 | 2.6 | 2.20 | 0.12 | 0.11 | 0.21 | 0.03 | 8.80 | 0.06 |
| 0514 | Known | 122.62 | 4.33 | 4.2 | - | - | 0.42 | - | - | - | - |
| 0515 | New | 122.83 | -8.10 | 2.6 | - | - | 0.11 | - | - | - | - |
| 0519 | New | 123.05 | 1.78 | 3.2 | 3.30 | 0.00 | 0.27 | 0.30 | 0.00 | 8.30 | 0.00 |
| 0523 | New | 123.59 | 5.60 | 2.2 | 2.10 | 0.00 | 0.22 | 0.22 | 0.03 | 9.20 | 0.14 |
| 0525 | Known | 124.01 | 1.07 | 2.3 | 2.00 | 0.06 | 0.14 | 0.23 | 0.02 | 7.90 | 0.10 |
| 0528 | Known | 124.69 | -0.60 | 2.7 | 2.40 | 0.12 | 0.38 | 0.57 | 0.01 | 7.50 | 0.15 |
| 0529 | Known | 124.95 | -1.21 | 2.4 | 1.10 | 0.07 | 0.08 | 0.16 | 0.01 | 8.50 | 0.06 |
| 0533 | Known | 125.90 | -2.60 | 2.6 | - | - | 0.21 | - | - | - | - |
| 0536 | New | 126.13 | 0.37 | 3.0 | 2.20 | 0.27 | 0.45 | 0.52 | 0.04 | 8.50 | 0.13 |
| 0537 | New | 126.32 | -2.34 | 2.6 | - | - | 0.11 | - | - | - | - |
| 0540 | Known | 126.64 | -4.38 | 1.6 | 1.60 | 0.13 | -0.01 | 0.02 | 0.01 | 8.20 | 0.03 |
| 0541 | Known | 126.67 | -0.78 | 12.9 | - | - | 2.52 | - | - | - | - |
| 0542 | New | 126.83 | 0.38 | 4.7 | 4.40 | 0.00 | 0.52 | 0.55 | 0.01 | 9.10 | 0.09 |
| 0543 | Known | 127.20 | 0.76 | 2.7 | 2.40 | 0.00 | 0.24 | 0.24 | 0.03 | 8.90 | 0.12 |
| 0546 | New | 127.60 | 3.40 | 4.2 | - | - | 0.44 | - | - | - | - |
| 0547 | New | 127.62 | -1.80 | 2.6 | - | - | 0.12 | - | - | - | - |
| 0548 | Known | 127.75 | 2.09 | 3.5 | 3.20 | 0.03 | 0.29 | 0.32 | 0.00 | 9.00 | 0.00 |
| 0549 | New | 127.83 | 3.51 | 3.6 | - | - | 0.36 | - | - | - | - |
| 0550 | Known | 128.03 | -1.80 | 1.8 | 1.70 | 0.00 | -0.02 | 0.01 | 0.01 | 8.10 | 0.19 |
| 0552 | Known | 128.22 | -1.11 | 2.4 | 2.00 | 0.00 | 0.08 | 0.17 | 0.00 | 7.80 | 0.00 |

Continued on next page

**Table A.1 – continued from previous page**

| **FSR ID** | **Type** | **l** [deg] | **b** [deg] | $D^{meth}$ [kpc] | $D^{iso}$ [kpc] | $\Delta D^{iso}$ [kpc] | $A_H^{HK}$ [mag] | $A_H^{iso}$ [mag] | $\Delta A_H^{iso}$ [mag] | **Age** [log(*age*/*yr*)] | **ΔAge** [log(*age*/*yr*)] |
|---|---|---|---|---|---|---|---|---|---|---|---|
| 0553 | New | 128.24 | 2.15 | 3.4 | - | - | 0.21 | - | - | - | - |
| 0554 | Known | 128.56 | 1.74 | 2.8 | 2.00 | 0.00 | 0.03 | 0.28 | 0.00 | 8.00 | 0.00 |
| 0555 | New | 128.81 | 8.65 | 3.0 | - | - | 0.30 | - | - | - | - |
| 0556 | Known | 129.08 | -0.35 | 1.8 | 1.60 | 0.00 | 0.10 | 0.23 | 0.02 | 8.30 | 0.09 |
| 0557 | Known | 129.38 | -1.53 | 2.5 | 2.00 | 0.15 | 0.11 | 0.18 | 0.01 | 8.40 | 0.08 |
| 0559 | Known | 129.51 | -0.96 | 2.1 | 2.40 | 0.27 | 0.15 | 0.32 | 0.02 | 7.20 | 0.15 |
| 0563 | Known | 130.05 | -0.16 | 4.6 | 5.10 | 0.45 | 0.50 | 0.41 | 0.02 | 8.90 | 0.06 |
| 0567 | Known | 130.13 | 0.38 | 3.2 | 2.20 | 0.00 | 0.24 | 0.35 | 0.00 | 7.70 | 0.00 |
| 0570 | New | 130.56 | -0.56 | 4.2 | - | - | 0.47 | - | - | - | - |
| 0574 | Known | 132.42 | -6.14 | 2.5 | 1.20 | 0.06 | 0.10 | 0.13 | 0.00 | 8.50 | 0.00 |
| 0576 | New | 133.28 | 8.82 | 7.7 | - | - | 1.74 | - | - | - | - |
| 0578 | New | 133.44 | 0.06 | 9.5 | - | - | 1.54 | - | - | - | - |
| 0582 | Known | 133.85 | 1.16 | 8.8 | - | - | 1.28 | - | - | - | - |
| 0585 | Known | 134.21 | 1.07 | 4.2 | 3.60 | 0.18 | 0.57 | 0.55 | 0.04 | 8.80 | 0.19 |
| 0588 | Known | 134.74 | 0.94 | 4.7 | - | - | 0.42 | - | - | - | - |
| 0592 | Known | 135.34 | -0.37 | 2.8 | 1.10 | 0.00 | 0.27 | 0.22 | 0.00 | 6.70 | 0.00 |
| 0594 | Known | 135.44 | -0.49 | 2.8 | 2.20 | 0.17 | 0.25 | 0.36 | 0.02 | 9.00 | 0.03 |
| 0597 | Known | 135.78 | -1.55 | 2.8 | - | - | 0.28 | - | - | - | - |
| 0598 | Known | 135.85 | 0.27 | 1.9 | 2.20 | 0.00 | 0.36 | 0.60 | 0.00 | 7.30 | 0.00 |
| 0599 | Known | 136.05 | -1.15 | 2.3 | 1.90 | 0.12 | 0.21 | 0.24 | 0.06 | 8.70 | 0.26 |
| 0600 | Known | 136.18 | -0.97 | 2.8 | - | - | 0.25 | - | - | - | - |
| 0602 | Known | 136.24 | 2.83 | 4.4 | - | - | 0.24 | - | - | - | - |

Continued on next page

**Table A.1 – continued from previous page**

| **FSR ID** | **Type** | **l** [deg] | **b** [deg] | $D^{meth}$ [kpc] | $D^{iso}$ [kpc] | $\Delta D^{iso}$ [kpc] | $A_H^{HK}$ [mag] | $A_H^{iso}$ [mag] | $\Delta A_H^{iso}$ [mag] | **Age** [log(*age*/*yr*)] | **ΔAge** [log(*age*/*yr*)] |
|---|---|---|---|---|---|---|---|---|---|---|---|
| 0603 | Known | 136.31 | -2.63 | 1.9 | 1.50 | 0.12 | 0.10 | 0.18 | 0.03 | 8.10 | 0.24 |
| 0608 | New | 137.03 | 1.10 | 9.0 | - | - | 1.20 | - | - | - | - |
| 0610 | Known | 137.20 | 0.91 | 8.0 | - | - | 0.65 | - | - | - | - |
| 0613 | Known | 137.41 | 1.28 | 8.6 | - | - | 0.96 | - | - | - | - |
| 0615 | Known | 137.82 | -1.75 | 2.6 | 1.90 | 0.00 | 0.29 | 0.40 | 0.00 | 7.70 | 0.00 |
| 0616 | New | 137.94 | -15.73 | 2.1 | - | - | 0.05 | - | - | - | - |
| 0617 | New | 137.95 | -8.09 | 2.7 | - | - | 0.13 | - | - | - | - |
| 0618 | Known | 138.04 | 1.51 | 8.1 | - | - | 0.83 | - | - | - | - |
| 0619 | Known | 138.10 | -4.75 | 2.5 | 1.40 | 0.00 | 0.11 | 0.10 | 0.00 | 9.20 | 0.00 |
| 0623 | New | 138.62 | 8.90 | 2.4 | 1.80 | 0.00 | 0.32 | 0.26 | 0.00 | 9.10 | 0.00 |
| 0624 | Known | 139.42 | 0.18 | 5.9 | 5.60 | 0.10 | 0.71 | 0.60 | 0.00 | 9.10 | 0.03 |
| 0636 | Known | 143.34 | -0.13 | 1.8 | 0.80 | 0.00 | 0.25 | 0.35 | 0.00 | 7.70 | 0.00 |
| 0637 | Known | 143.68 | 7.65 | 3.7 | - | - | 0.29 | - | - | - | - |
| 0639 | Known | 143.78 | -4.27 | 2.4 | 2.10 | 0.07 | 0.26 | 0.35 | 0.01 | 8.80 | 0.00 |
| 0641 | Known | 143.94 | 3.60 | 2.5 | 1.60 | 0.05 | 0.23 | 0.35 | 0.01 | 8.40 | 0.05 |
| 0643 | New | 144.78 | 13.65 | 3.0 | - | - | 0.30 | - | - | - | - |
| 0644 | Known | 145.11 | -3.99 | 2.5 | 2.00 | 0.09 | 0.24 | 0.21 | 0.02 | 8.30 | 0.03 |
| 0645 | Known | 145.92 | -2.99 | 3.2 | 1.60 | 0.00 | 0.38 | 0.33 | 0.00 | 7.60 | 0.00 |
| 0646 | Known | 146.06 | -2.82 | 2.9 | - | - | 0.30 | - | - | - | - |
| 0648 | Known | 146.67 | -8.92 | 1.9 | 2.50 | 0.00 | 0.03 | 0.08 | 0.00 | 8.90 | 0.00 |
| 0650 | Known | 146.97 | -3.71 | 2.5 | - | - | 0.31 | - | - | - | - |
| 0651 | Known | 147.08 | -0.50 | 3.9 | 3.50 | 0.00 | 0.68 | 0.75 | 0.00 | 9.20 | 0.00 |

Continued on next page

**Table A.1 – continued from previous page**

| **FSR ID** | **Type** | **l** [deg] | **b** [deg] | $D^{meth}$ [kpc] | $D^{iso}$ [kpc] | $\Delta D^{iso}$ [kpc] | $A_H^{HK}$ [mag] | $A_H^{iso}$ [mag] | $\Delta A_H^{iso}$ [mag] | **Age** [log($age/yr$)] | **ΔAge** [log($age/yr$)] |
|---|---|---|---|---|---|---|---|---|---|---|---|
| 0652 | Known | 147.52 | 5.66 | 3.3 | 3.20 | 0.35 | 0.31 | 0.25 | 0.00 | 9.10 | 0.06 |
| 0655 | New | 148.12 | 0.29 | 10.2 | - | - | 1.99 | - | - | - | - |
| 0657 | Known | 149.08 | -1.99 | 9.6 | - | - | 1.39 | - | - | - | - |
| 0658 | Known | 149.81 | -1.01 | 3.6 | 3.20 | 0.00 | 0.57 | 0.71 | 0.04 | 8.10 | 0.05 |
| 0659 | Known | 149.85 | 0.19 | 2.7 | 1.40 | 0.00 | 0.23 | 0.28 | 0.03 | 8.60 | 0.10 |
| 0662 | New | 150.39 | 3.89 | 7.5 | - | - | 1.08 | - | - | - | - |
| 0665 | New | 150.68 | -0.59 | 7.2 | - | - | 0.81 | - | - | - | - |
| 0666 | New | 150.79 | -0.58 | 7.2 | - | - | 0.94 | - | - | - | - |
| 0668 | Known | 151.61 | -0.23 | 9.4 | - | - | 1.49 | - | - | - | - |
| 0671 | New | 152.41 | 1.48 | 5.0 | - | - | 0.39 | - | - | - | - |
| 0676 | Known | 154.50 | -3.42 | 3.3 | - | - | 0.25 | - | - | - | - |
| 0677 | Known | 154.84 | 2.49 | 3.0 | 2.10 | 0.20 | 0.31 | 0.39 | 0.01 | 9.10 | 0.03 |
| 0679 | Known | 155.01 | -15.32 | 1.8 | 0.60 | 0.00 | 0.18 | 0.20 | 0.00 | 8.60 | 0.00 |
| 0681 | Known | 155.36 | 2.62 | 10.1 | - | - | 1.29 | - | - | - | - |
| 0684 | New | 156.45 | 5.76 | 3.3 | - | - | 0.28 | - | - | - | - |
| 0687 | New | 156.93 | 0.97 | 6.4 | - | - | 0.61 | - | - | - | - |
| 0690 | New | 157.91 | 5.13 | 2.8 | - | - | 0.07 | - | - | - | - |
| 0694 | Known | 158.59 | -1.57 | 2.7 | 2.60 | 0.13 | 0.23 | 0.29 | 0.03 | 8.80 | 0.07 |
| 0699 | New | 159.36 | 2.58 | 9.7 | - | - | 1.03 | - | - | - | - |
| 0702 | New | 160.13 | 0.96 | 6.8 | - | - | 0.62 | - | - | - | - |
| 0704 | Known | 160.50 | -17.81 | 1.9 | - | - | 1.02 | - | - | - | - |
| 0705 | New | 160.71 | 4.86 | 4.8 | 4.60 | 0.35 | 0.31 | 0.20 | 0.02 | 8.90 | 0.10 |

Continued on next page

**Table A.1 – continued from previous page**

| **FSR ID** | **Type** | **l** [deg] | **b** [deg] | $D^{meth}$ [kpc] | $D^{iso}$ [kpc] | $\Delta D^{iso}$ [kpc] | $A_H^{HK}$ [mag] | $A_H^{iso}$ [mag] | $\Delta A_H^{iso}$ [mag] | **Age** [log(*age*/*yr*)] | **ΔAge** [log(*age*/*yr*)] |
|---|---|---|---|---|---|---|---|---|---|---|---|
| 0706 | New | 161.17 | -7.75 | 2.6 | - | - | 0.31 | - | - | - | - |
| 0707 | New | 161.20 | 5.42 | 4.9 | - | - | 0.27 | - | - | - | - |
| 0710 | Known | 161.65 | -2.01 | 4.0 | 3.10 | 0.05 | 0.44 | 0.45 | 0.01 | 9.00 | 0.00 |
| 0713 | Known | 162.02 | -2.39 | 3.1 | 2.70 | 0.00 | 0.27 | 0.30 | 0.00 | 9.10 | 0.00 |
| 0716 | New | 162.26 | 3.62 | 2.6 | - | - | 0.03 | - | - | - | - |
| 0718 | Known | 162.27 | 1.62 | 2.9 | 2.70 | 0.00 | 0.23 | 0.55 | 0.00 | 7.30 | 0.00 |
| 0720 | Known | 162.31 | -2.33 | 8.4 | - | - | 1.07 | - | - | - | - |
| 0726 | Known | 162.81 | 0.66 | 5.4 | 5.00 | 0.00 | 0.37 | 0.30 | 0.00 | 8.80 | 0.00 |
| 0727 | New | 162.91 | 4.31 | 2.9 | 1.70 | 0.19 | 0.16 | 0.21 | 0.02 | 8.80 | 0.09 |
| 0728 | New | 162.92 | -6.88 | 2.3 | 1.30 | 0.00 | 0.25 | 0.20 | 0.00 | 9.00 | 0.00 |
| 0731 | Known | 163.58 | 5.05 | 5.1 | 4.20 | 0.00 | 0.36 | 0.30 | 0.00 | 9.30 | 0.00 |
| 0732 | New | 163.87 | 0.49 | 6.3 | - | - | 0.34 | - | - | - | - |
| 0735 | New | 164.21 | -1.84 | 3.0 | - | - | 0.12 | - | - | - | - |
| 0736 | New | 164.84 | 5.69 | 4.5 | - | - | 0.25 | - | - | - | - |
| 0739 | Known | 165.35 | -9.01 | 9.9 | - | - | 2.40 | - | - | - | - |
| 0740 | New | 165.50 | -7.66 | 3.3 | - | - | 0.54 | - | - | - | - |
| 0743 | Known | 166.87 | 3.62 | 5.0 | - | - | 0.41 | - | - | - | - |
| 0747 | Known | 167.59 | -4.10 | 1.8 | - | - | 0.19 | - | - | - | - |
| 0749 | New | 167.77 | 4.44 | 2.9 | - | - | 0.10 | - | - | - | - |
| 0753 | New | 168.39 | -3.08 | 3.4 | - | - | 0.21 | - | - | - | - |
| 0755 | Known | 168.44 | 1.22 | 3.3 | 2.80 | 0.18 | 0.13 | 0.20 | 0.01 | 8.50 | 0.03 |
| 0763 | New | 170.15 | 3.49 | 3.1 | - | - | 0.15 | - | - | - | - |

Continued on next page

**Table A.1 – continued from previous page**

| **FSR ID** | **Type** | **l** [deg] | **b** [deg] | $D^{meth}$ [kpc] | $D^{iso}$ [kpc] | $\Delta D^{iso}$ [kpc] | $A_H^{HK}$ [mag] | $A_H^{iso}$ [mag] | $\Delta A_H^{iso}$ [mag] | **Age** [log($age/yr$)] | **ΔAge** [log($age/yr$)] |
|---|---|---|---|---|---|---|---|---|---|---|---|
| 0769 | Known | 171.90 | 0.45 | 5.8 | 4.40 | 0.00 | 0.48 | 0.42 | 0.00 | 9.10 | 0.00 |
| 0774 | Known | 172.64 | 0.33 | 2.5 | 1.50 | 0.03 | 0.11 | 0.22 | 0.01 | 8.70 | 0.03 |
| 0777 | New | 173.05 | -0.12 | 4.2 | - | - | 0.33 | - | - | - | - |
| 0778 | New | 173.08 | -3.47 | 6.0 | - | - | 0.66 | - | - | - | - |
| 0781 | Known | 173.37 | -0.17 | 9.0 | - | - | 0.90 | - | - | - | - |
| 0785 | Known | 173.57 | -1.59 | 9.4 | - | - | 0.96 | - | - | - | - |
| 0786 | Known | 173.60 | -1.66 | 9.6 | - | - | 0.82 | - | - | - | - |
| 0787 | Known | 173.65 | 2.83 | 9.4 | - | - | 1.78 | - | - | - | - |
| 0790 | New | 173.75 | -5.87 | 3.4 | 3.20 | 0.00 | 0.26 | 0.18 | 0.00 | 9.20 | 0.00 |
| 0791 | Known | 173.93 | 0.27 | 9.9 | - | - | 1.01 | - | - | - | - |
| 0792 | Known | 174.10 | -8.85 | 2.4 | 1.90 | 0.10 | 0.14 | 0.18 | 0.02 | 8.60 | 0.06 |
| 0793 | New | 174.44 | -1.86 | 4.3 | 4.00 | 0.00 | 0.39 | 0.34 | 0.00 | 8.80 | 0.00 |
| 0794 | Known | 174.54 | 1.08 | 2.0 | 1.20 | 0.00 | 0.06 | 0.20 | 0.00 | 7.30 | 0.00 |
| 0796 | New | 174.75 | -5.60 | 3.4 | - | - | 0.20 | - | - | - | - |
| 0800 | Known | 175.67 | -3.67 | 4.8 | - | - | 0.42 | - | - | - | - |
| 0802 | New | 176.17 | 6.02 | 2.6 | 2.00 | 0.00 | 0.17 | 0.24 | 0.00 | 8.70 | 0.00 |
| 0807 | New | 176.53 | -0.11 | 8.9 | - | - | 1.17 | - | - | - | - |
| 0808 | New | 176.56 | -16.66 | 1.7 | - | - | 0.19 | - | - | - | - |
| 0812 | New | 176.78 | 0.12 | 7.8 | - | - | 0.80 | - | - | - | - |
| 0814 | New | 177.06 | -0.41 | 3.1 | 1.60 | 0.20 | 0.35 | 0.45 | 0.03 | 8.00 | 0.15 |
| 0816 | New | 177.10 | 0.19 | 6.1 | - | - | 0.57 | - | - | - | - |
| 0817 | New | 177.63 | -0.10 | 5.8 | - | - | 0.55 | - | - | - | - |

Continued on next page

**Table A.1 – continued from previous page**

| **FSR ID** | **Type** | **l** [deg] | **b** [deg] | $D^{meth}$ [kpc] | $D^{iso}$ [kpc] | $\Delta D^{iso}$ [kpc] | $A_H^{HK}$ [mag] | $A_H^{iso}$ [mag] | $\Delta A_H^{iso}$ [mag] | **Age** [log($age/yr$)] | **ΔAge** [log($age/yr$)] |
|---|---|---|---|---|---|---|---|---|---|---|---|
| 0821 | New | 178.75 | -0.18 | 3.4 | - | - | 0.25 | - | - | - | - |
| 0822 | Known | 179.11 | -10.46 | 1.8 | 0.80 | 0.03 | 0.10 | 0.18 | 0.02 | 8.60 | 0.12 |
| 0825 | New | 179.32 | 1.26 | 3.0 | 2.90 | 0.00 | 0.14 | 0.21 | 0.00 | 8.80 | 0.00 |
| 0826 | New | 179.68 | -0.51 | 6.9 | - | - | 0.77 | - | - | - | - |
| 0828 | New | 179.92 | 1.75 | 5.7 | 5.00 | 0.00 | 0.44 | 0.28 | 0.00 | 8.90 | 0.00 |
| 0829 | Known | 179.96 | -0.29 | 2.8 | 2.10 | 0.00 | 0.27 | 0.21 | 0.00 | 9.20 | 0.00 |
| 0839 | New | 180.87 | 4.12 | 7.1 | - | - | 1.46 | - | - | - | - |
| 0842 | New | 181.51 | -3.89 | 4.2 | - | - | 0.32 | - | - | - | - |
| 0845 | Known | 182.40 | 0.26 | 14.0 | - | - | 1.95 | - | - | - | - |
| 0846 | New | 182.56 | -0.74 | 4.8 | - | - | 0.61 | - | - | - | - |
| 0847 | Known | 182.74 | 0.48 | 4.1 | 4.00 | 0.00 | 0.48 | 0.54 | 0.01 | 9.00 | 0.03 |
| 0852 | New | 184.13 | -0.41 | 3.5 | - | - | 0.29 | - | - | - | - |
| 0854 | Known | 184.77 | -13.51 | 1.7 | 1.70 | 0.00 | 0.06 | 0.06 | 0.03 | 9.30 | 0.12 |
| 0866 | New | 186.33 | 13.84 | 2.1 | 1.30 | 0.00 | 0.01 | 0.05 | 0.00 | 9.10 | 0.00 |
| 0867 | Known | 186.37 | 1.26 | 2.5 | 1.60 | 0.07 | 0.11 | 0.13 | 0.03 | 8.40 | 0.16 |
| 0870 | Known | 186.61 | 0.15 | 2.6 | 1.60 | 0.00 | 0.19 | 0.40 | 0.00 | 7.30 | 0.00 |
| 0872 | Known | 186.64 | 1.80 | 4.4 | 3.10 | 0.00 | 0.25 | 0.19 | 0.00 | 9.40 | 0.00 |
| 0873 | Known | 186.73 | 2.49 | 3.2 | - | - | 0.08 | - | - | - | - |
| 0881 | New | 188.06 | -2.22 | 4.6 | 4.20 | 0.00 | 0.40 | 0.35 | 0.00 | 8.90 | 0.00 |
| 0882 | New | 188.06 | -9.84 | 2.6 | - | - | 0.25 | - | - | - | - |
| 0883 | New | 188.11 | 0.15 | 2.7 | 2.50 | 0.00 | 0.18 | 0.26 | 0.03 | 8.60 | 0.10 |
| 0889 | Known | 189.02 | 0.79 | 10.8 | - | - | 1.75 | - | - | - | - |

Continued on next page

**Table A.1 – continued from previous page**

| **FSR ID** | **Type** | **l** [deg] | **b** [deg] | $D^{meth}$ [kpc] | $D^{iso}$ [kpc] | $\Delta D^{iso}$ [kpc] | $A_H^{HK}$ [mag] | $A_H^{iso}$ [mag] | $\Delta A_H^{iso}$ [mag] | **Age** [log($age/yr$)] | **ΔAge** [log($age/yr$)] |
|---|---|---|---|---|---|---|---|---|---|---|---|
| 0896 | Known | 189.88 | 0.51 | 8.7 | - | - | 1.78 | - | - | - | - |
| 0898 | Known | 190.08 | 0.81 | 7.6 | - | - | 0.95 | - | - | - | - |
| 0899 | Known | 190.14 | 1.05 | 8.5 | - | - | 1.11 | - | - | - | - |
| 0900 | New | 190.78 | -0.77 | 4.3 | - | - | 0.42 | - | - | - | - |
| 0902 | New | 190.98 | 2.29 | 4.6 | - | - | 0.29 | - | - | - | - |
| 0903 | New | 191.01 | -0.61 | 3.1 | - | - | 0.33 | - | - | - | - |
| 0904 | New | 191.03 | -0.78 | 3.1 | 2.00 | 0.00 | 0.34 | 0.43 | 0.00 | 7.30 | 0.00 |
| 0905 | New | 191.07 | 6.29 | 2.5 | - | - | 0.08 | - | - | - | - |
| 0908 | Known | 191.93 | 0.84 | 10.5 | - | - | 1.11 | - | - | - | - |
| 0910 | Known | 192.18 | -3.82 | 11.5 | - | - | 1.58 | - | - | - | - |
| 0911 | New | 192.30 | 3.36 | 3.4 | - | - | 0.12 | - | - | - | - |
| 0914 | New | 192.42 | -16.67 | 3.0 | - | - | 0.17 | - | - | - | - |
| 0921 | New | 192.87 | -2.27 | 3.2 | - | - | 0.49 | - | - | - | - |
| 0923 | New | 193.23 | -1.02 | 5.3 | - | - | 0.64 | - | - | - | - |
| 0924 | New | 193.33 | -1.12 | 4.9 | - | - | 0.50 | - | - | - | - |
| 0925 | New | 193.34 | -2.59 | 3.8 | - | - | 0.27 | - | - | - | - |
| 0932 | New | 194.61 | -3.49 | 4.0 | - | - | 0.40 | - | - | - | - |
| 0934 | New | 195.13 | -11.97 | 3.1 | - | - | 0.40 | - | - | - | - |
| 0939 | New | 195.54 | -2.19 | 3.5 | - | - | 0.24 | - | - | - | - |
| 0941 | New | 195.57 | 0.78 | 4.0 | - | - | 0.29 | - | - | - | - |
| 0942 | New | 195.58 | -3.59 | 2.9 | 2.80 | 0.05 | 0.29 | 0.36 | 0.03 | 8.90 | 0.10 |
| 0952 | New | 196.66 | -3.00 | 4.3 | - | - | 0.30 | - | - | - | - |

Continued on next page

**Table A.1 – continued from previous page**

| **FSR ID** | **Type** | **l** [deg] | **b** [deg] | $D^{meth}$ [kpc] | $D^{iso}$ [kpc] | $\Delta D^{iso}$ [kpc] | $A_H^{HK}$ [mag] | $A_H^{iso}$ [mag] | $\Delta A_H^{iso}$ [mag] | **Age** [log(*age*/*yr*)] | **ΔAge** [log(*age*/*yr*)] |
|---|---|---|---|---|---|---|---|---|---|---|---|
| 0953 | New | 196.68 | -0.58 | 3.3 | - | - | 0.26 | - | - | - | - |
| 0959 | Known | 197.21 | 8.92 | 2.0 | 4.10 | 0.00 | -0.02 | 0.03 | 0.00 | 8.80 | 0.00 |
| 0961 | Known | 197.24 | -2.34 | 3.0 | 2.90 | 0.00 | 0.13 | 0.17 | 0.01 | 8.80 | 0.03 |
| 0962 | New | 197.28 | 0.42 | 3.9 | - | - | 0.13 | - | - | - | - |
| 0971 | Known | 198.04 | -5.80 | 3.1 | 3.00 | 0.00 | 0.25 | 0.19 | 0.00 | 9.40 | 0.00 |
| 0972 | Known | 198.11 | 19.65 | 1.7 | 1.50 | 0.00 | -0.01 | 0.02 | 0.00 | 9.40 | 0.00 |
| 0973 | Known | 199.03 | -10.38 | 2.3 | 1.70 | 0.00 | 0.17 | 0.15 | 0.00 | 8.50 | 0.00 |
| 0974 | New | 199.63 | 1.60 | 3.2 | - | - | 0.20 | - | - | - | - |
| 0979 | New | 200.79 | 0.63 | 4.0 | - | - | 0.33 | - | - | - | - |
| 0981 | Known | 201.35 | 0.30 | 8.9 | - | - | 1.65 | - | - | - | - |
| 0982 | Known | 201.79 | 2.11 | 2.6 | 2.50 | 0.00 | 0.18 | 0.22 | 0.01 | 9.00 | 0.05 |
| 0985 | New | 202.12 | -5.52 | 3.2 | - | - | 0.17 | - | - | - | - |
| 0987 | New | 202.42 | -5.12 | 3.2 | 2.00 | 0.17 | 0.21 | 0.31 | 0.02 | 8.10 | 0.18 |
| 0990 | Known | 202.96 | 2.17 | 2.8 | - | - | 0.47 | - | - | - | - |
| 0995 | Known | 203.38 | 11.82 | 1.8 | 1.80 | 0.07 | -0.02 | 0.03 | 0.01 | 9.00 | 0.07 |
| 1000 | New | 203.83 | -6.26 | 3.2 | - | - | 0.13 | - | - | - | - |
| 1002 | Known | 204.37 | -1.69 | 2.9 | 2.60 | 0.24 | 0.13 | 0.16 | 0.02 | 9.00 | 0.12 |
| 1008 | Known | 205.93 | -0.37 | 6.8 | - | - | 0.54 | - | - | - | - |
| 1011 | Known | 206.17 | -2.27 | 8.2 | - | - | 1.02 | - | - | - | - |
| 1012 | Known | 206.25 | 5.14 | 5.2 | - | - | 0.32 | - | - | - | - |
| 1014 | Known | 206.35 | -2.19 | 6.7 | - | - | 0.69 | - | - | - | - |
| 1019 | Known | 206.54 | -16.35 | 17.0 | - | - | 3.38 | - | - | - | - |

Continued on next page

**Table A.1 – continued from previous page**

| **FSR ID** | **Type** | **l** [deg] | **b** [deg] | $D^{meth}$ [kpc] | $D^{iso}$ [kpc] | $\Delta D^{iso}$ [kpc] | $A_H^{HK}$ [mag] | $A_H^{iso}$ [mag] | $\Delta A_H^{iso}$ [mag] | **Age** [log(*age*/*yr*)] | **ΔAge** [log(*age*/*yr*)] |
|---|---|---|---|---|---|---|---|---|---|---|---|
| 1026 | Known | 207.01 | -1.79 | 9.2 | - | - | 1.53 | - | - | - | - |
| 1028 | Known | 207.15 | -1.77 | 11.1 | - | - | 1.95 | - | - | - | - |
| 1030 | Known | 207.32 | -2.14 | 9.9 | - | - | 2.58 | - | - | - | - |
| 1035 | Known | 207.76 | 0.17 | 3.0 | - | - | 0.03 | - | - | - | - |
| 1037 | Known | 207.91 | 0.30 | 2.7 | 1.70 | 0.03 | 0.08 | 0.10 | 0.01 | 8.60 | 0.03 |
| 1041 | Known | 208.53 | -19.10 | 1.7 | - | - | 0.50 | - | - | - | - |
| 1042 | Known | 208.57 | -1.78 | 2.5 | 1.20 | 0.10 | 0.24 | 0.26 | 0.02 | 8.20 | 0.12 |
| 1045 | Known | 208.66 | -2.96 | 4.9 | - | - | 0.47 | - | - | - | - |
| 1055 | Known | 210.57 | -2.10 | 3.2 | 3.10 | 0.00 | 0.24 | 0.26 | 0.01 | 9.00 | 0.03 |
| 1057 | New | 210.70 | -0.06 | 4.8 | - | - | 0.27 | - | - | - | - |
| 1059 | Known | 210.81 | -0.24 | 2.5 | 1.60 | 0.09 | 0.03 | 0.09 | 0.03 | 8.40 | 0.19 |
| 1060 | Known | 210.83 | -1.03 | 3.4 | - | - | 0.17 | - | - | - | - |
| 1062 | Known | 211.24 | -0.40 | 11.3 | - | - | 1.44 | - | - | - | - |
| 1063 | New | 211.25 | -3.86 | 2.9 | 1.80 | 0.00 | 0.15 | 0.18 | 0.00 | 9.10 | 0.00 |
| 1065 | New | 211.77 | -3.74 | 2.8 | - | - | 0.15 | - | - | - | - |
| 1069 | Known | 212.01 | -1.31 | 4.5 | - | - | 0.25 | - | - | - | - |
| 1070 | Known | 212.16 | -3.43 | 5.5 | 5.30 | 0.00 | 0.39 | 0.30 | 0.02 | 9.00 | 0.09 |
| 1072 | New | 212.45 | -0.86 | 5.5 | - | - | 0.34 | - | - | - | - |
| 1073 | Known | 212.47 | -19.01 | 2.8 | - | - | 1.25 | - | - | - | - |
| 1076 | New | 212.64 | 6.35 | 3.5 | - | - | 0.18 | - | - | - | - |
| 1085 | New | 213.31 | 0.30 | 5.5 | - | - | 0.30 | - | - | - | - |
| 1086 | Known | 213.34 | -12.60 | 5.2 | - | - | 1.25 | - | - | - | - |

Continued on next page

**Table A.1 – continued from previous page**

| **FSR ID** | **Type** | **l** [deg] | **b** [deg] | $D^{meth}$ [kpc] | $D^{iso}$ [kpc] | $\Delta D^{iso}$ [kpc] | $A_H^{HK}$ [mag] | $A_H^{iso}$ [mag] | $\Delta A_H^{iso}$ [mag] | **Age** [log($age/yr$)] | **ΔAge** [log($age/yr$)] |
|---|---|---|---|---|---|---|---|---|---|---|---|
| 1089 | Known | 213.46 | 3.30 | 2.5 | 2.60 | 0.18 | -0.07 | 0.00 | 0.00 | 9.00 | 0.03 |
| 1092 | New | 213.89 | -4.31 | 3.5 | - | - | 0.20 | - | - | - | - |
| 1100 | New | 214.48 | 2.78 | 3.9 | - | - | 0.23 | - | - | - | - |
| 1101 | Known | 214.54 | -0.85 | 3.1 | 2.00 | 0.00 | 0.07 | 0.06 | 0.00 | 9.30 | 0.00 |
| 1104 | Known | 215.31 | -2.27 | 2.8 | 2.00 | 0.17 | 0.11 | 0.12 | 0.02 | 8.60 | 0.09 |
| 1106 | New | 215.71 | -6.16 | 4.6 | - | - | 0.25 | - | - | - | - |
| 1113 | New | 216.30 | 3.25 | 3.3 | - | - | 0.17 | - | - | - | - |
| 1125 | New | 217.67 | -2.70 | 4.0 | - | - | 0.20 | - | - | - | - |
| 1127 | Known | 217.76 | -0.69 | 2.6 | 1.80 | 0.17 | 0.10 | 0.12 | 0.02 | 8.70 | 0.00 |
| 1129 | New | 218.16 | -0.63 | 10.2 | - | - | 1.36 | - | - | - | - |
| 1131 | New | 218.38 | -16.20 | 2.2 | - | - | 0.20 | - | - | - | - |
| 1133 | New | 218.54 | 14.49 | 2.1 | - | - | 0.07 | - | - | - | - |
| 1137 | Known | 219.25 | -8.92 | 6.9 | - | - | 1.18 | - | - | - | - |
| 1143 | Known | 219.49 | -10.56 | 7.7 | - | - | 1.51 | - | - | - | - |
| 1148 | Known | 219.85 | -2.23 | 2.7 | 2.40 | 0.13 | 0.08 | 0.20 | 0.01 | 8.20 | 0.12 |
| 1149 | New | 220.07 | -0.11 | 3.5 | - | - | 0.08 | - | - | - | - |
| 1151 | New | 220.35 | -7.71 | 2.4 | - | - | 0.17 | - | - | - | - |
| 1153 | New | 220.60 | 2.49 | 3.0 | - | - | -0.04 | - | - | - | - |
| 1154 | Known | 220.80 | -1.72 | 11.9 | - | - | 1.53 | - | - | - | - |
| 1158 | New | 221.18 | 1.17 | 3.4 | - | - | 0.11 | - | - | - | - |
| 1165 | Known | 222.04 | -5.31 | 3.1 | 3.00 | 0.00 | 0.18 | 0.14 | 0.01 | 9.10 | 0.03 |
| 1167 | New | 222.18 | -6.07 | 4.0 | - | - | 0.25 | - | - | - | - |

Continued on next page

**Table A.1 – continued from previous page**

| **FSR ID** | **Type** | **l** [deg] | **b** [deg] | $D^{meth}$ [kpc] | $D^{iso}$ [kpc] | $\Delta D^{iso}$ [kpc] | $A_H^{HK}$ [mag] | $A_H^{iso}$ [mag] | $\Delta A_H^{iso}$ [mag] | **Age** [log($age/yr$)] | **ΔAge** [log($age/yr$)] |
|---|---|---|---|---|---|---|---|---|---|---|---|
| 1170 | New | 222.64 | -0.51 | 4.5 | - | - | 0.36 | - | - | - | - |
| 1171 | New | 223.12 | -2.76 | 5.6 | - | - | 0.44 | - | - | - | - |
| 1172 | New | 223.23 | -4.08 | 3.3 | - | - | 0.19 | - | - | - | - |
| 1173 | New | 223.29 | -0.48 | 3.3 | 2.10 | 0.30 | 0.17 | 0.16 | 0.04 | 8.70 | 0.05 |
| 1174 | Known | 223.54 | 10.09 | 2.9 | 2.80 | 0.00 | 0.15 | 0.10 | 0.00 | 10.00 | 0.03 |
| 1179 | New | 224.01 | -9.66 | 2.3 | - | - | 0.03 | - | - | - | - |
| 1180 | New | 224.09 | 1.04 | 2.9 | - | - | 0.12 | - | - | - | - |
| 1183 | New | 224.21 | 0.32 | 3.1 | - | - | 0.13 | - | - | - | - |
| 1186 | Known | 224.53 | -2.39 | 9.7 | - | - | 1.04 | - | - | - | - |
| 1189 | Known | 224.67 | 0.40 | 2.0 | 1.20 | 0.00 | -0.01 | 0.10 | 0.00 | 8.00 | 0.00 |
| 1190 | New | 224.79 | -1.73 | 12.5 | - | - | 1.65 | - | - | - | - |
| 1191 | New | 224.87 | -5.76 | 3.2 | - | - | 0.18 | - | - | - | - |
| 1203 | New | 226.15 | 7.83 | 2.6 | - | - | 0.10 | - | - | - | - |
| 1206 | Known | 226.59 | -2.30 | 2.8 | 2.70 | 0.00 | 0.12 | 0.30 | 0.01 | 7.70 | 0.10 |
| 1214 | Known | 227.49 | -0.56 | 5.7 | 4.10 | 0.00 | 0.47 | 0.36 | 0.00 | 9.40 | 0.00 |
| 1215 | Known | 227.87 | 5.38 | 2.0 | 2.00 | 0.00 | -0.06 | 0.00 | 0.00 | 9.10 | 0.03 |
| 1222 | Known | 228.95 | 4.51 | 2.2 | 1.60 | 0.05 | -0.01 | 0.01 | 0.01 | 9.20 | 0.00 |
| 1228 | New | 229.91 | -1.60 | 4.5 | - | - | 0.21 | - | - | - | - |
| 1230 | Known | 230.58 | 9.95 | 1.7 | 2.50 | 0.00 | 0.00 | 0.02 | 0.00 | 9.20 | 0.00 |
| 1231 | Known | 230.80 | 1.01 | 4.9 | 1.70 | 0.00 | 0.39 | 0.28 | 0.00 | 9.50 | 0.00 |
| 1232 | Known | 231.00 | 3.12 | 2.9 | - | - | 0.11 | - | - | - | - |
| 1234 | New | 231.16 | 1.53 | 2.7 | - | - | 0.13 | - | - | - | - |

Continued on next page

**Table A.1 – continued from previous page**

| **FSR ID** | **Type** | **l** [deg] | **b** [deg] | $D^{meth}$ [kpc] | $D^{iso}$ [kpc] | $\Delta D^{iso}$ [kpc] | $A_H^{HK}$ [mag] | $A_H^{iso}$ [mag] | $\Delta A_H^{iso}$ [mag] | **Age** [log($age/yr$)] | **ΔAge** [log($age/yr$)] |
|---|---|---|---|---|---|---|---|---|---|---|---|
| 1237 | Known | 231.47 | -4.28 | 11.1 | - | - | 0.97 | - | - | - | - |
| 1240 | Known | 231.80 | -0.59 | 3.0 | 2.50 | 0.45 | 0.19 | 0.29 | 0.05 | 8.40 | 0.20 |
| 1243 | New | 232.02 | 1.98 | 3.9 | - | - | 0.24 | - | - | - | - |
| 1245 | New | 232.18 | 6.19 | 2.8 | - | - | 0.07 | - | - | - | - |
| 1246 | Known | 232.35 | -7.30 | 2.1 | 2.10 | 0.03 | 0.10 | 0.17 | 0.01 | 8.80 | 0.00 |
| 1248 | Known | 232.61 | 1.00 | 12.9 | - | - | 1.54 | - | - | - | - |
| 1249 | New | 232.61 | 5.58 | 3.6 | - | - | 0.21 | - | - | - | - |
| 1252 | New | 233.07 | -1.82 | 2.5 | - | - | -0.04 | - | - | - | - |
| 1259 | Known | 234.24 | -0.48 | 4.9 | - | - | 0.36 | - | - | - | - |
| 1260 | New | 234.58 | -1.09 | 4.3 | - | - | 0.24 | - | - | - | - |
| 1266 | Known | 235.38 | 0.15 | 4.2 | - | - | 0.25 | - | - | - | - |
| 1267 | New | 235.48 | 1.80 | 2.4 | 1.90 | 0.20 | -0.01 | 0.05 | 0.01 | 8.90 | 0.00 |
| 1269 | Known | 235.61 | -3.83 | 6.6 | - | - | 0.32 | - | - | - | - |
| 1271 | Known | 235.99 | 5.38 | 2.5 | 1.70 | 0.12 | 0.12 | 0.10 | 0.02 | 8.80 | 0.03 |
| 1272 | Known | 236.06 | -4.62 | 3.2 | 1.60 | 0.00 | 0.04 | 0.06 | 0.00 | 9.20 | 0.00 |
| 1274 | Known | 236.28 | 0.07 | 2.2 | 2.20 | 0.00 | -0.00 | 0.09 | 0.02 | 8.30 | 0.12 |
| 1275 | New | 236.40 | -2.16 | 5.5 | - | - | 0.37 | - | - | - | - |
| 1279 | New | 237.45 | -11.21 | 2.7 | - | - | 0.20 | - | - | - | - |
| 1284 | New | 237.94 | -5.08 | 2.8 | 2.20 | 0.20 | 0.11 | 0.18 | 0.03 | 8.40 | 0.20 |
| 1286 | New | 238.09 | -2.40 | 3.7 | - | - | 0.31 | - | - | - | - |
| 1287 | Known | 238.17 | -5.54 | 6.4 | - | - | 0.33 | - | - | - | - |
| 1288 | Known | 238.22 | -3.34 | 2.9 | 1.40 | 0.12 | 0.02 | 0.08 | 0.01 | 8.10 | 0.10 |

Continued on next page

**Table A.1 – continued from previous page**

| **FSR ID** | **Type** | **l** [deg] | **b** [deg] | $D^{meth}$ [kpc] | $D^{iso}$ [kpc] | $\Delta D^{iso}$ [kpc] | $A_H^{HK}$ [mag] | $A_H^{iso}$ [mag] | $\Delta A_H^{iso}$ [mag] | **Age** [log($age/yr$)] | **ΔAge** [log($age/yr$)] |
|---|---|---|---|---|---|---|---|---|---|---|---|
| 1290 | New | 238.32 | -3.63 | 3.4 | - | - | 0.14 | - | - | - | - |
| 1291 | Known | 238.40 | -6.78 | 2.1 | 1.00 | 0.00 | -0.01 | 0.05 | 0.00 | 9.00 | 0.00 |
| 1299 | Known | 239.93 | -4.94 | 3.3 | 1.70 | 0.15 | 0.24 | 0.34 | 0.00 | 8.30 | 0.06 |
| 1303 | New | 241.33 | -15.25 | 2.3 | - | - | 0.11 | - | - | - | - |
| 1305 | New | 241.57 | -2.51 | 2.9 | 2.10 | 0.03 | 0.02 | 0.17 | 0.01 | 8.50 | 0.07 |
| 1309 | Known | 242.09 | 0.50 | 2.6 | - | - | -0.03 | - | - | - | - |
| 1311 | Known | 242.69 | -6.80 | 3.1 | - | - | 0.11 | - | - | - | - |
| 1318 | Known | 243.78 | 0.35 | 3.2 | - | - | 0.12 | - | - | - | - |
| 1319 | Known | 244.00 | -2.07 | 2.9 | - | - | 0.08 | - | - | - | - |
| 1323 | Known | 245.67 | -4.31 | 4.2 | 4.20 | 0.00 | 0.18 | 0.13 | 0.00 | 9.00 | 0.00 |
| 1325 | Known | 245.91 | -1.74 | 5.2 | 2.90 | 0.00 | 0.49 | 0.40 | 0.00 | 9.20 | 0.00 |
| 1327 | New | 246.35 | -4.75 | 4.9 | - | - | 0.12 | - | - | - | - |
| 1328 | Known | 246.45 | -4.46 | 2.2 | 2.20 | 0.00 | 0.04 | 0.04 | 0.01 | 8.30 | 0.00 |
| 1330 | Known | 246.72 | -0.77 | 2.2 | 1.60 | 0.06 | 0.12 | 0.20 | 0.01 | 8.60 | 0.03 |
| 1333 | Known | 246.79 | 3.37 | 2.4 | 2.20 | 0.00 | 0.09 | 0.08 | 0.00 | 9.10 | 0.00 |
| 1336 | New | 247.64 | -0.53 | 5.2 | - | - | 0.48 | - | - | - | - |
| 1337 | Known | 247.71 | -2.52 | 2.9 | 1.50 | 0.00 | 0.27 | 0.33 | 0.00 | 9.10 | 0.00 |
| 1338 | Known | 247.81 | 1.31 | 2.4 | 2.50 | 0.07 | 0.08 | 0.09 | 0.04 | 8.80 | 0.07 |
| 1339 | New | 247.90 | -0.12 | 3.9 | - | - | 0.15 | - | - | - | - |
| 1340 | Known | 247.95 | -4.15 | 3.1 | 1.90 | 0.09 | 0.27 | 0.32 | 0.01 | 8.60 | 0.03 |
| 1344 | Known | 248.26 | -0.19 | 3.6 | - | - | 0.13 | - | - | - | - |
| 1347 | New | 248.97 | -4.12 | 3.0 | 1.40 | 0.00 | 0.28 | 0.23 | 0.00 | 9.00 | 0.00 |

Continued on next page

**Table A.1 – continued from previous page**

| **FSR ID** | **Type** | **l** [deg] | **b** [deg] | $D^{meth}$ [kpc] | $D^{iso}$ [kpc] | $\Delta D^{iso}$ [kpc] | $A_H^{HK}$ [mag] | $A_H^{iso}$ [mag] | $\Delta A_H^{iso}$ [mag] | **Age** [log(*age*/*yr*)] | **ΔAge** [log(*age*/*yr*)] |
|---|---|---|---|---|---|---|---|---|---|---|---|
| 1349 | Known | 249.12 | -0.64 | 2.8 | - | - | 0.07 | - | - | - | - |
| 1354 | Known | 249.83 | 2.97 | 2.2 | 1.60 | 0.03 | -0.02 | 0.05 | 0.01 | 8.60 | 0.03 |
| 1355 | New | 249.97 | 15.22 | 2.3 | - | - | 0.29 | - | - | - | - |
| 1358 | Known | 250.44 | 1.60 | 2.1 | 2.10 | 0.00 | -0.05 | 0.01 | 0.00 | 8.60 | 0.00 |
| 1359 | Known | 250.98 | -2.85 | 6.7 | - | - | 0.66 | - | - | - | - |
| 1361 | New | 251.56 | -5.00 | 2.8 | 1.80 | 0.15 | 0.18 | 0.23 | 0.00 | 9.00 | 0.05 |
| 1362 | Known | 251.60 | 6.65 | 1.9 | 1.70 | 0.00 | 0.01 | 0.05 | 0.00 | 9.00 | 0.00 |
| 1368 | Known | 253.49 | 2.14 | 2.4 | - | - | 0.15 | - | - | - | - |
| 1373 | Known | 254.57 | 6.08 | 1.3 | 2.80 | 0.09 | -0.01 | 0.02 | 0.01 | 8.90 | 0.03 |
| 1375 | Known | 255.61 | 3.98 | 2.3 | 2.30 | 0.00 | 0.15 | 0.09 | 0.00 | 9.10 | 0.00 |
| 1378 | New | 256.33 | -5.43 | 3.5 | - | - | 0.30 | - | - | - | - |
| 1382 | New | 257.00 | 4.04 | 3.0 | - | - | 0.27 | - | - | - | - |
| 1383 | New | 257.08 | -5.23 | 4.7 | - | - | 0.41 | - | - | - | - |
| 1384 | Known | 257.27 | 4.27 | 2.0 | 2.10 | 0.13 | 0.15 | 0.16 | 0.01 | 9.20 | 0.03 |
| 1386 | Known | 257.99 | -1.00 | 5.5 | 5.70 | 0.00 | 0.78 | 0.69 | 0.03 | 8.90 | 0.07 |
| 1387 | New | 258.12 | -1.33 | 4.6 | 4.70 | 0.00 | 0.69 | 0.63 | 0.00 | 8.80 | 0.00 |
| 1388 | Known | 258.50 | 2.30 | 3.0 | 3.20 | 0.13 | 0.29 | 0.23 | 0.01 | 9.20 | 0.06 |
| 1389 | New | 258.57 | 10.63 | 2.1 | - | - | 0.15 | - | - | - | - |
| 1392 | Known | 258.87 | -3.33 | 6.3 | 2.90 | 0.00 | 0.72 | 0.57 | 0.00 | 9.20 | 0.00 |
| 1393 | Known | 259.06 | 2.00 | 3.5 | 3.80 | 0.00 | 0.38 | 0.27 | 0.00 | 8.90 | 0.00 |
| 1395 | Known | 259.34 | 0.93 | 4.1 | - | - | 0.73 | - | - | - | - |
| 1397 | New | 259.91 | 0.35 | 3.1 | - | - | 0.56 | - | - | - | - |

Continued on next page

**Table A.1 – continued from previous page**

| **FSR ID** | **Type** | **l** [deg] | **b** [deg] | $D^{meth}$ [kpc] | $D^{iso}$ [kpc] | $\Delta D^{iso}$ [kpc] | $A_H^{HK}$ [mag] | $A_H^{iso}$ [mag] | $\Delta A_H^{iso}$ [mag] | **Age** [log($age/yr$)] | **ΔAge** [log($age/yr$)] |
|---|---|---|---|---|---|---|---|---|---|---|---|
| 1399 | New | 259.95 | 2.06 | 2.1 | 2.60 | 0.00 | 0.33 | 0.33 | 0.00 | 9.30 | 0.00 |
| 1401 | New | 261.50 | -0.85 | 4.0 | - | - | 0.62 | - | - | - | - |
| 1404 | Known | 261.53 | 3.76 | 2.6 | 2.70 | 0.00 | 0.26 | 0.22 | 0.01 | 9.20 | 0.00 |
| 1406 | New | 261.63 | -0.65 | 2.6 | - | - | 0.46 | - | - | - | - |
| 1410 | Known | 262.35 | -1.78 | 3.4 | - | - | 0.40 | - | - | - | - |
| 1411 | New | 262.39 | -2.12 | 6.9 | - | - | 0.79 | - | - | - | - |
| 1412 | New | 262.93 | -1.91 | 3.4 | - | - | 0.23 | - | - | - | - |
| 1415 | New | 263.74 | -1.81 | 9.1 | 9.30 | 0.00 | 0.84 | 0.78 | 0.01 | 9.10 | 0.07 |
| 1416 | New | 263.80 | 3.91 | 2.8 | - | - | 0.30 | - | - | - | - |
| 1418 | New | 263.97 | -0.31 | 3.4 | - | - | 0.42 | - | - | - | - |
| 1420 | Known | 264.09 | -5.51 | 2.4 | 3.10 | 0.00 | 0.14 | 0.15 | 0.00 | 9.10 | 0.00 |
| 1424 | New | 264.19 | 0.18 | 2.8 | 1.10 | 0.00 | 0.48 | 0.47 | 0.00 | 7.30 | 0.00 |
| 1426 | Known | 264.41 | -8.48 | 2.4 | - | - | 0.10 | - | - | - | - |
| 1428 | Known | 264.48 | -0.28 | 4.7 | - | - | 0.68 | - | - | - | - |
| 1430 | New | 264.65 | 0.08 | 7.0 | 7.10 | 0.00 | 1.32 | 1.30 | 0.01 | 8.50 | 0.00 |
| 1433 | Known | 264.81 | -2.91 | 3.0 | 1.30 | 0.00 | 0.10 | 0.20 | 0.00 | 7.50 | 0.00 |
| 1436 | New | 264.91 | -2.87 | 3.4 | 2.00 | 0.00 | 0.18 | 0.30 | 0.00 | 7.00 | 0.00 |
| 1437 | Known | 265.09 | -2.58 | 4.9 | - | - | 0.29 | - | - | - | - |
| 1438 | Known | 265.15 | 1.46 | 8.5 | - | - | 2.82 | - | - | - | - |
| 1443 | New | 265.72 | -3.54 | 5.0 | - | - | 0.16 | - | - | - | - |
| 1444 | Known | 265.80 | -5.01 | 3.4 | 2.40 | 0.00 | 0.17 | 0.12 | 0.00 | 9.00 | 0.00 |
| 1445 | Known | 265.94 | -3.00 | 3.8 | - | - | 0.20 | - | - | - | - |

Continued on next page

**Table A.1 – continued from previous page**

| **FSR ID** | **Type** | **l** [deg] | **b** [deg] | $D^{meth}$ [kpc] | $D^{iso}$ [kpc] | $\Delta D^{iso}$ [kpc] | $A_H^{HK}$ [mag] | $A_H^{iso}$ [mag] | $\Delta A_H^{iso}$ [mag] | **Age** [log(*age*/*yr*)] | **ΔAge** [log(*age*/*yr*)] |
|---|---|---|---|---|---|---|---|---|---|---|---|
| 1447 | New | 266.14 | -9.37 | 2.1 | - | - | 0.24 | - | - | - | - |
| 1450 | New | 266.94 | -0.37 | 5.8 | 5.90 | 0.00 | 1.00 | 0.95 | 0.00 | 8.80 | 0.00 |
| 1452 | New | 267.60 | -2.09 | 3.0 | 2.10 | 0.20 | 0.21 | 0.27 | 0.03 | 8.50 | 0.15 |
| 1453 | Known | 267.77 | -1.09 | 9.5 | - | - | 1.37 | - | - | - | - |
| 1454 | New | 267.81 | -2.71 | 3.8 | - | - | 0.22 | - | - | - | - |
| 1458 | Known | 268.65 | 3.21 | 2.1 | 1.50 | 0.00 | 0.16 | 0.19 | 0.00 | 9.20 | 0.00 |
| 1460 | New | 269.13 | -0.19 | 3.7 | 3.50 | 0.15 | 0.83 | 0.94 | 0.01 | 9.00 | 0.00 |
| 1461 | Known | 269.18 | -1.44 | 8.7 | - | - | 1.59 | - | - | - | - |
| 1466 | Known | 269.73 | 0.98 | 6.2 | - | - | 1.35 | - | - | - | - |
| 1469 | Known | 270.27 | 0.84 | 6.7 | - | - | 1.66 | - | - | - | - |
| 1472 | Known | 270.76 | 3.22 | 2.4 | 2.50 | 0.00 | 0.37 | 0.37 | 0.00 | 8.90 | 0.00 |
| 1474 | New | 271.33 | -0.66 | 3.4 | - | - | 0.57 | - | - | - | - |
| 1476 | New | 271.63 | 0.41 | 4.4 | - | - | 0.91 | - | - | - | - |
| 1477 | Known | 271.66 | -0.71 | 2.6 | - | - | 0.37 | - | - | - | - |
| 1478 | New | 271.98 | -4.34 | 6.0 | - | - | 0.37 | - | - | - | - |
| 1480 | Known | 272.50 | 2.87 | 2.1 | 2.00 | 0.00 | 0.13 | 0.15 | 0.00 | 9.30 | 0.00 |
| 1482 | Known | 273.13 | -0.77 | 2.3 | 2.20 | 0.07 | 0.20 | 0.27 | 0.01 | 8.10 | 0.07 |
| 1487 | Known | 273.82 | -15.89 | 1.2 | 0.40 | 0.00 | 0.01 | 0.06 | 0.01 | 7.90 | 0.06 |
| 1489 | New | 274.45 | 0.38 | 4.9 | - | - | 0.77 | - | - | - | - |
| 1493 | Known | 275.37 | -1.16 | 2.4 | - | - | 0.11 | - | - | - | - |
| 1497 | Known | 276.48 | -3.12 | 3.3 | - | - | 0.29 | - | - | - | - |
| 1500 | New | 276.83 | -1.20 | 3.3 | - | - | 0.32 | - | - | - | - |

Continued on next page

**Table A.1 – continued from previous page**

| **FSR ID** | **Type** | **l** [deg] | **b** [deg] | $D^{meth}$ [kpc] | $D^{iso}$ [kpc] | $\Delta D^{iso}$ [kpc] | $A_H^{HK}$ [mag] | $A_H^{iso}$ [mag] | $\Delta A_H^{iso}$ [mag] | **Age** [log(*age*/*yr*)] | **ΔAge** [log(*age*/*yr*)] |
|---|---|---|---|---|---|---|---|---|---|---|---|
| 1502 | Known | 277.11 | -0.81 | 2.3 | 1.50 | 0.00 | 0.09 | 0.12 | 0.00 | 9.00 | 0.00 |
| 1504 | Known | 277.65 | -0.71 | 2.9 | - | - | 0.17 | - | - | - | - |
| 1507 | New | 277.94 | -3.28 | 11.0 | - | - | 0.99 | - | - | - | - |
| 1508 | New | 278.51 | -0.61 | 2.9 | 2.70 | 0.09 | 0.27 | 0.41 | 0.02 | 7.90 | 0.09 |
| 1509 | New | 278.69 | -1.07 | 4.1 | - | - | 0.54 | - | - | - | - |
| 1512 | Known | 279.19 | -2.61 | 3.5 | - | - | 0.29 | - | - | - | - |
| 1513 | New | 279.20 | -1.58 | 4.5 | - | - | 0.45 | - | - | - | - |
| 1515 | Known | 279.48 | 0.15 | 2.6 | 2.80 | 0.07 | 0.12 | 0.14 | 0.01 | 9.20 | 0.00 |
| 1516 | Known | 279.53 | 0.08 | 2.6 | - | - | 0.11 | - | - | - | - |
| 1517 | New | 279.55 | -0.07 | 4.7 | - | - | 0.41 | - | - | - | - |
| 1519 | Known | 279.92 | 0.27 | 2.5 | - | - | 0.29 | - | - | - | - |
| 1520 | New | 280.21 | 0.07 | 2.4 | 1.70 | 0.00 | 0.16 | 0.13 | 0.00 | 9.40 | 0.00 |
| 1521 | New | 280.44 | -1.62 | 5.8 | 5.90 | 0.00 | 0.53 | 0.47 | 0.00 | 9.20 | 0.00 |
| 1522 | New | 280.71 | 0.12 | 2.4 | 1.80 | 0.00 | 0.26 | 0.25 | 0.00 | 8.80 | 0.00 |
| 1524 | New | 281.51 | -1.99 | 9.8 | - | - | 1.09 | - | - | - | - |
| 1525 | Known | 282.02 | -1.16 | 10.0 | - | - | 2.19 | - | - | - | - |
| 1526 | Known | 282.06 | -2.40 | 2.5 | 2.10 | 0.32 | 0.09 | 0.04 | 0.00 | 9.00 | 0.03 |
| 1527 | New | 282.14 | -1.36 | 9.5 | - | - | 1.46 | - | - | - | - |
| 1530 | New | 282.34 | -1.07 | 6.5 | 6.60 | 0.00 | 1.00 | 1.30 | 0.00 | 6.80 | 0.00 |
| 1531 | New | 282.83 | 0.63 | 5.3 | - | - | 0.67 | - | - | - | - |
| 1532 | Known | 282.93 | -3.03 | 3.8 | - | - | 0.24 | - | - | - | - |
| 1533 | Known | 283.01 | 0.44 | 2.1 | 2.10 | 0.10 | 0.18 | 0.16 | 0.03 | 8.50 | 0.15 |

Continued on next page

**Table A.1 – continued from previous page**

| **FSR ID** | **Type** | **l** [deg] | **b** [deg] | $D^{meth}$ [kpc] | $D^{iso}$ [kpc] | $\Delta D^{iso}$ [kpc] | $A_H^{HK}$ [mag] | $A_H^{iso}$ [mag] | $\Delta A_H^{iso}$ [mag] | **Age** [log(*age*/*yr*)] | **ΔAge** [log(*age*/*yr*)] |
|---|---|---|---|---|---|---|---|---|---|---|---|
| 1534 | Known | 283.14 | -1.46 | 2.7 | 2.30 | 0.26 | 0.10 | 0.25 | 0.02 | 8.30 | 0.04 |
| 1535 | New | 283.33 | -2.70 | 3.3 | - | - | 0.26 | - | - | - | - |
| 1537 | Known | 283.85 | -3.69 | 2.7 | 2.70 | 0.00 | 0.01 | 0.02 | 0.01 | 9.00 | 0.00 |
| 1540 | Known | 284.62 | 0.04 | 1.9 | 1.70 | 0.15 | -0.00 | 0.10 | 0.01 | 8.20 | 0.08 |
| 1541 | New | 284.73 | -8.50 | 1.9 | - | - | 0.11 | - | - | - | - |
| 1542 | Known | 285.24 | -0.84 | 3.0 | - | - | 0.32 | - | - | - | - |
| 1544 | Known | 285.34 | -8.82 | 1.4 | 1.30 | 0.06 | -0.01 | 0.03 | 0.02 | 8.70 | 0.06 |
| 1545 | Known | 285.87 | 0.08 | 1.4 | 1.50 | 0.07 | -0.12 | 0.01 | 0.01 | 7.50 | 0.07 |
| 1547 | Known | 286.23 | -0.15 | 5.4 | - | - | 0.91 | - | - | - | - |
| 1549 | Known | 286.80 | -0.49 | 4.2 | - | - | 0.70 | - | - | - | - |
| 1550 | Known | 287.01 | -2.09 | 6.1 | - | - | 0.23 | - | - | - | - |
| 1551 | Known | 287.40 | -0.34 | 1.8 | 1.30 | 0.00 | 0.02 | 0.30 | 0.00 | 7.30 | 0.00 |
| 1552 | Known | 287.42 | -0.58 | 3.6 | - | - | 0.60 | - | - | - | - |
| 1553 | Known | 287.58 | -0.70 | 4.5 | - | - | 0.60 | - | - | - | - |
| 1555 | New | 287.77 | 0.17 | 5.0 | - | - | 0.76 | - | - | - | - |
| 1557 | New | 288.25 | 0.09 | 5.0 | - | - | 0.48 | - | - | - | - |
| 1558 | Known | 288.69 | 0.43 | 2.2 | 2.10 | 0.06 | 0.20 | 0.19 | 0.01 | 8.00 | 0.07 |
| 1559 | Known | 289.16 | 0.31 | 5.6 | 3.30 | 0.00 | 0.54 | 0.40 | 0.00 | 9.40 | 0.00 |
| 1561 | New | 289.37 | 6.62 | 2.2 | - | - | 0.10 | - | - | - | - |
| 1562 | Known | 289.52 | -0.40 | 2.3 | 2.20 | 0.10 | 0.20 | 0.25 | 0.00 | 8.60 | 0.00 |
| 1564 | Known | 289.90 | -5.57 | 2.1 | 1.70 | 0.03 | 0.03 | 0.12 | 0.03 | 8.60 | 0.13 |
| 1565 | Known | 290.19 | 2.88 | 1.9 | 2.00 | 0.00 | -0.02 | 0.00 | 0.00 | 9.70 | 0.03 |

Continued on next page

**Table A.1 – continued from previous page**

| **FSR ID** | **Type** | **l** [deg] | **b** [deg] | $D^{meth}$ [kpc] | $D^{iso}$ [kpc] | $\Delta D^{iso}$ [kpc] | $A_H^{HK}$ [mag] | $A_H^{iso}$ [mag] | $\Delta A_H^{iso}$ [mag] | **Age** [log(*age*/*yr*)] | **ΔAge** [log(*age*/*yr*)] |
|---|---|---|---|---|---|---|---|---|---|---|---|
| 1567 | Known | 290.40 | 1.66 | 7.4 | - | - | 0.66 | - | - | - | - |
| 1568 | New | 290.44 | -9.84 | 1.9 | - | - | 0.11 | - | - | - | - |
| 1570 | Known | 290.70 | -0.33 | 4.0 | - | - | 0.49 | - | - | - | - |
| 1571 | Known | 290.74 | 0.20 | 4.4 | - | - | 0.43 | - | - | - | - |
| 1575 | Known | 291.21 | -0.16 | 2.0 | 1.80 | 0.19 | 0.04 | 0.09 | 0.02 | 7.90 | 0.09 |
| 1576 | Known | 291.64 | -0.51 | 3.5 | 1.00 | 0.00 | 0.66 | 0.90 | 0.00 | 7.70 | 0.00 |
| 1582 | New | 292.38 | -1.82 | 2.0 | 1.80 | 0.15 | 0.15 | 0.26 | 0.03 | 7.90 | 0.20 |
| 1583 | New | 292.40 | 3.61 | 3.8 | - | - | 0.33 | - | - | - | - |
| 1584 | New | 292.42 | -4.28 | 3.2 | - | - | 0.19 | - | - | - | - |
| 1586 | New | 292.84 | -1.20 | 4.4 | 4.10 | 0.25 | 0.61 | 0.64 | 0.02 | 8.90 | 0.10 |
| 1587 | Known | 292.92 | -2.41 | 1.5 | 2.00 | 0.25 | 0.08 | 0.19 | 0.03 | 8.30 | 0.10 |
| 1588 | Known | 293.21 | 0.58 | 3.8 | 4.00 | 0.20 | 0.25 | 0.17 | 0.01 | 8.90 | 0.07 |
| 1589 | Known | 294.11 | -0.03 | 1.1 | 1.60 | 0.17 | -0.10 | 0.04 | 0.03 | 7.70 | 0.20 |
| 1590 | Known | 294.38 | 6.18 | 1.8 | 1.70 | 0.03 | -0.05 | 0.04 | 0.01 | 9.20 | 0.02 |
| 1591 | New | 294.52 | -1.09 | 5.6 | 5.80 | 0.10 | 0.86 | 0.85 | 0.00 | 8.70 | 0.00 |
| 1592 | Known | 294.85 | -1.62 | 4.4 | - | - | 0.54 | - | - | - | - |
| 1594 | New | 295.47 | -7.04 | 2.5 | - | - | 0.15 | - | - | - | - |
| 1595 | New | 295.62 | -0.68 | 6.1 | - | - | 0.83 | - | - | - | - |
| 1596 | Known | 295.79 | -0.21 | 3.2 | 2.20 | 0.00 | 0.46 | 0.47 | 0.00 | 8.90 | 0.00 |
| 1600 | Known | 297.52 | -1.76 | 3.8 | 3.30 | 0.07 | 0.48 | 0.40 | 0.01 | 9.00 | 0.07 |
| 1603 | New | 298.22 | -0.51 | 2.2 | 2.40 | 0.25 | 0.25 | 0.21 | 0.01 | 9.20 | 0.06 |
| 1605 | New | 298.38 | -2.71 | 5.6 | - | - | 0.29 | - | - | - | - |

Continued on next page

**Table A.1 – continued from previous page**

| **FSR ID** | **Type** | **l** [deg] | **b** [deg] | $D^{meth}$ [kpc] | $D^{iso}$ [kpc] | $\Delta D^{iso}$ [kpc] | $A_H^{HK}$ [mag] | $A_H^{iso}$ [mag] | $\Delta A_H^{iso}$ [mag] | **Age** [log($age/yr$)] | **ΔAge** [log($age/yr$)] |
|---|---|---|---|---|---|---|---|---|---|---|---|
| 1608 | New | 298.84 | 5.44 | 3.3 | - | - | 0.37 | - | - | - | - |
| 1611 | Known | 299.32 | 4.56 | 1.8 | 1.90 | 0.07 | 0.11 | 0.13 | 0.02 | 9.30 | 0.07 |
| 1612 | New | 299.39 | 3.05 | 1.9 | - | - | 0.13 | - | - | - | - |
| 1614 | Known | 299.76 | 0.86 | 1.9 | 1.60 | 0.30 | -0.05 | 0.14 | 0.01 | 8.30 | 0.10 |
| 1615 | Known | 300.11 | -0.67 | 3.5 | 3.50 | 0.00 | 0.58 | 0.60 | 0.02 | 9.20 | 0.03 |
| 1616 | New | 300.48 | -0.67 | 5.7 | - | - | 0.87 | - | - | - | - |
| 1622 | New | 301.42 | -0.44 | 7.0 | - | - | 1.31 | - | - | - | - |
| 1624 | Known | 301.50 | 2.20 | 2.9 | 3.40 | 0.00 | 0.27 | 0.18 | 0.00 | 9.00 | 0.00 |
| 1625 | New | 301.51 | 4.42 | 1.6 | - | - | 0.02 | - | - | - | - |
| 1627 | Known | 301.71 | -5.53 | 3.5 | 1.50 | 0.00 | 0.32 | 0.26 | 0.00 | 9.70 | 0.00 |
| 1630 | New | 302.61 | 0.72 | 3.7 | - | - | 0.58 | - | - | - | - |
| 1632 | Known | 303.18 | -4.29 | 7.9 | - | - | 0.50 | - | - | - | - |
| 1633 | Known | 303.22 | 2.47 | 1.4 | 1.40 | 0.00 | -0.00 | 0.10 | 0.01 | 7.50 | 0.03 |
| 1637 | Known | 303.63 | -2.08 | 2.4 | 2.30 | 0.03 | 0.31 | 0.30 | 0.02 | 8.90 | 0.07 |
| 1638 | New | 303.72 | -8.54 | 1.9 | - | - | 0.15 | - | - | - | - |
| 1641 | New | 304.36 | -1.72 | 3.7 | - | - | 0.35 | - | - | - | - |
| 1643 | Known | 305.37 | 0.07 | 5.8 | - | - | 1.18 | - | - | - | - |
| 1644 | New | 305.51 | -4.32 | 2.2 | 1.70 | 0.05 | 0.19 | 0.19 | 0.03 | 8.50 | 0.25 |
| 1645 | New | 306.42 | 0.72 | 7.6 | - | - | 1.38 | - | - | - | - |
| 1650 | New | 307.05 | -5.60 | 3.5 | - | - | 0.38 | - | - | - | - |
| 1651 | New | 307.31 | 3.61 | 3.9 | - | - | 0.33 | - | - | - | - |
| 1653 | New | 307.72 | -0.55 | 2.8 | - | - | 0.44 | - | - | - | - |

Continued on next page

**Table A.1 – continued from previous page**

| **FSR ID** | **Type** | **l** [deg] | **b** [deg] | $D^{meth}$ [kpc] | $D^{iso}$ [kpc] | $\Delta D^{iso}$ [kpc] | $A_H^{HK}$ [mag] | $A_H^{iso}$ [mag] | $\Delta A_H^{iso}$ [mag] | **Age** [log($age/yr$)] | **ΔAge** [log($age/yr$)] |
|---|---|---|---|---|---|---|---|---|---|---|---|
| 1655 | Known | 307.74 | 1.56 | 2.0 | 1.60 | 0.15 | 0.12 | 0.14 | 0.01 | 8.40 | 0.07 |
| 1656 | New | 307.89 | -4.25 | 3.1 | - | - | 0.23 | - | - | - | - |
| 1659 | New | 308.29 | -0.08 | 5.6 | - | - | 1.12 | - | - | - | - |
| 1660 | Known | 308.68 | 0.60 | 6.3 | - | - | 1.36 | - | - | - | - |
| 1661 | New | 308.76 | -7.26 | 2.7 | - | - | 0.21 | - | - | - | - |
| 1663 | New | 309.07 | 2.08 | 5.5 | - | - | 0.73 | - | - | - | - |
| 1666 | New | 309.71 | 0.68 | 5.8 | - | - | 1.29 | - | - | - | - |
| 1668 | New | 310.40 | 0.38 | 2.6 | - | - | 0.28 | - | - | - | - |
| 1670 | Known | 310.84 | 0.16 | 5.1 | 2.50 | 0.00 | 1.11 | 1.19 | 0.00 | 8.50 | 0.00 |
| 1677 | Known | 314.62 | 0.81 | 6.0 | - | - | 1.12 | - | - | - | - |
| 1678 | New | 314.66 | -4.46 | 3.1 | - | - | 0.22 | - | - | - | - |
| 1679 | Known | 314.72 | -0.30 | 4.2 | 3.40 | 0.40 | 0.53 | 0.60 | 0.05 | 8.80 | 0.05 |
| 1681 | New | 314.90 | 0.83 | 5.8 | - | - | 1.04 | - | - | - | - |
| 1682 | New | 315.31 | 1.78 | 7.1 | - | - | 1.04 | - | - | - | - |
| 1686 | New | 316.00 | -0.29 | 5.0 | 1.70 | 0.00 | 0.97 | 0.97 | 0.00 | 9.30 | 0.00 |
| 1688 | New | 317.00 | 3.89 | 3.7 | - | - | 0.41 | - | - | - | - |
| 1689 | New | 317.11 | 0.17 | 5.4 | - | - | 1.26 | - | - | - | - |
| 1692 | New | 318.21 | -17.35 | 1.1 | - | - | 0.07 | - | - | - | - |
| 1693 | New | 318.43 | -6.71 | 2.0 | - | - | 0.18 | - | - | - | - |
| 1694 | New | 318.55 | -4.33 | 11.1 | - | - | 1.85 | - | - | - | - |
| 1696 | New | 319.60 | 0.95 | 5.6 | - | - | 1.16 | - | - | - | - |
| 1698 | New | 320.82 | -2.05 | 6.7 | - | - | 0.71 | - | - | - | - |

Continued on next page

**Table A.1 – continued from previous page**

| **FSR ID** | **Type** | **l** [deg] | **b** [deg] | $D^{meth}$ [kpc] | $D^{iso}$ [kpc] | $\Delta D^{iso}$ [kpc] | $A_H^{HK}$ [mag] | $A_H^{iso}$ [mag] | $\Delta A_H^{iso}$ [mag] | **Age** [log($age/yr$)] | **ΔAge** [log($age/yr$)] |
|---|---|---|---|---|---|---|---|---|---|---|---|
| 1700 | New | 322.91 | -3.04 | 6.0 | - | - | 0.59 | - | - | - | - |
| 1701 | New | 323.08 | -0.42 | 7.7 | - | - | 2.17 | - | - | - | - |
| 1703 | New | 325.79 | 0.12 | 5.7 | - | - | 1.23 | - | - | - | - |
| 1704 | Known | 325.80 | -2.97 | 2.7 | 2.00 | 0.18 | 0.22 | 0.21 | 0.01 | 9.10 | 0.06 |
| 1706 | Known | 326.01 | -1.93 | 1.5 | 1.30 | 0.00 | 0.08 | 0.07 | 0.02 | 8.90 | 0.07 |
| 1709 | New | 327.95 | -0.79 | 5.6 | - | - | 1.42 | - | - | - | - |
| 1710 | Known | 328.40 | 4.33 | 4.3 | - | - | 0.38 | - | - | - | - |
| 1712 | New | 328.83 | 0.90 | 6.8 | - | - | 2.09 | - | - | - | - |
| 1713 | New | 329.37 | -8.55 | 1.8 | - | - | 0.15 | - | - | - | - |
| 1714 | New | 329.39 | 2.88 | 5.9 | - | - | 0.84 | - | - | - | - |
| 1716 | New | 329.79 | -1.59 | 6.4 | 5.40 | 0.00 | 0.89 | 0.79 | 0.03 | 9.10 | 0.07 |
| 1717 | Known | 329.82 | -2.20 | 2.2 | - | - | 0.08 | - | - | - | - |
| 1719 | New | 330.61 | 3.29 | 3.1 | - | - | 0.42 | - | - | - | - |
| 1722 | New | 332.99 | 1.88 | 4.9 | - | - | 1.16 | - | - | - | - |
| 1723 | New | 333.03 | 5.85 | 1.1 | 1.10 | 0.03 | -0.02 | 0.00 | 0.00 | 8.80 | 0.03 |
| 1726 | Known | 334.55 | 1.09 | 3.0 | 2.30 | 0.00 | 0.37 | 0.38 | 0.00 | 9.10 | 0.03 |
| 1727 | New | 334.72 | -0.86 | 5.4 | - | - | 1.59 | - | - | - | - |
| 1730 | Known | 335.47 | -6.24 | 1.4 | 0.90 | 0.00 | 0.05 | 0.08 | 0.00 | 10.00 | 0.00 |
| 1734 | New | 338.86 | 5.81 | 1.8 | - | - | 0.29 | - | - | - | - |
| 1737 | New | 340.10 | 7.25 | 1.6 | - | - | 0.28 | - | - | - | - |
| 1738 | Known | 340.11 | -7.88 | 1.4 | 1.00 | 0.06 | 0.12 | 0.15 | 0.00 | 9.00 | 0.03 |
| 1739 | New | 340.27 | -3.39 | 4.3 | - | - | 0.80 | - | - | - | - |

Continued on next page

**Table A.1 – continued from previous page**

| **FSR ID** | **Type** | **l** [deg] | **b** [deg] | $D^{meth}$ [kpc] | $D^{iso}$ [kpc] | $\Delta D^{iso}$ [kpc] | $A_H^{HK}$ [mag] | $A_H^{iso}$ [mag] | $\Delta A_H^{iso}$ [mag] | **Age** [log($age/yr$)] | **ΔAge** [log($age/yr$)] |
|---|---|---|---|---|---|---|---|---|---|---|---|
| 1744 | New | 342.71 | 1.18 | 6.4 | - | - | 1.76 | - | - | - | - |
| 1746 | New | 345.17 | 3.43 | 2.8 | - | - | 0.38 | - | - | - | - |
| 1748 | New | 346.44 | 8.22 | 2.2 | - | - | 0.37 | - | - | - | - |
| 1749 | New | 346.49 | 13.76 | 1.5 | - | - | 0.25 | - | - | - | - |
| 1750 | New | 346.72 | 1.84 | 3.5 | - | - | 0.59 | - | - | - | - |
| 1751 | New | 346.87 | 12.20 | 1.5 | - | - | 0.28 | - | - | - | - |
| 1754 | New | 348.04 | -0.32 | 5.7 | - | - | 1.47 | - | - | - | - |
| 1763 | New | 350.88 | 5.83 | 3.2 | - | - | 0.33 | - | - | - | - |
| 1766 | New | 352.22 | -2.12 | 4.2 | - | - | 0.83 | - | - | - | - |
| 1767 | New | 352.60 | -2.17 | 3.6 | - | - | 0.66 | - | - | - | - |
| 1769 | New | 353.31 | 6.13 | 3.4 | - | - | 0.28 | - | - | - | - |
| 1775 | New | 354.55 | -5.80 | 4.6 | - | - | 0.42 | - | - | - | - |
| 1776 | New | 354.72 | -5.24 | 3.5 | - | - | 0.23 | - | - | - | - |
| 1778 | New | 356.38 | 9.16 | 1.3 | - | - | 0.07 | - | - | - | - |
| 1785 | New | 358.56 | -14.55 | 2.8 | - | - | 0.33 | - | - | - | - |

# Appendix B

Appendix B contains a summary table of the number of clusters used to measure the extinction per unit distance values, per longitude bin/range. The plots used to measure the extinction per unit distance values are also provided for reference. A discussion of these values is provided in Chapter 9.

**Note:**

- Table B.1 has been presented in graphical form in Figure 9.2.
- Figure B.6 (*Top*) has been published in Buckner and Froebrich (2013).

Table B.1: This table lists the number of clusters used to measure the extinction per unit distance values, per longitude bin/range.

| **Bin** $l(\pm 30)$ [deg] | **No. Clusters** |
|---:|---:|
| 60 | 43 |
| 70 | 55 |
| 80 | 71 |
| 90 | 85 |
| 100 | 99 |
| 110 | 98 |
| 120 | 94 |
| 130 | 81 |
| 140 | 68 |
| 150 | 57 |
| 160 | 42 |
| 170 | 40 |
| 180 | 41 |
| 190 | 47 |
| 200 | 50 |
| 210 | 52 |
| 220 | 56 |
| 230 | 53 |
| 240 | 57 |
| 250 | 66 |
| 260 | 72 |
| 270 | 79 |
| 280 | 76 |
| 290 | 69 |
| 300 | 62 |

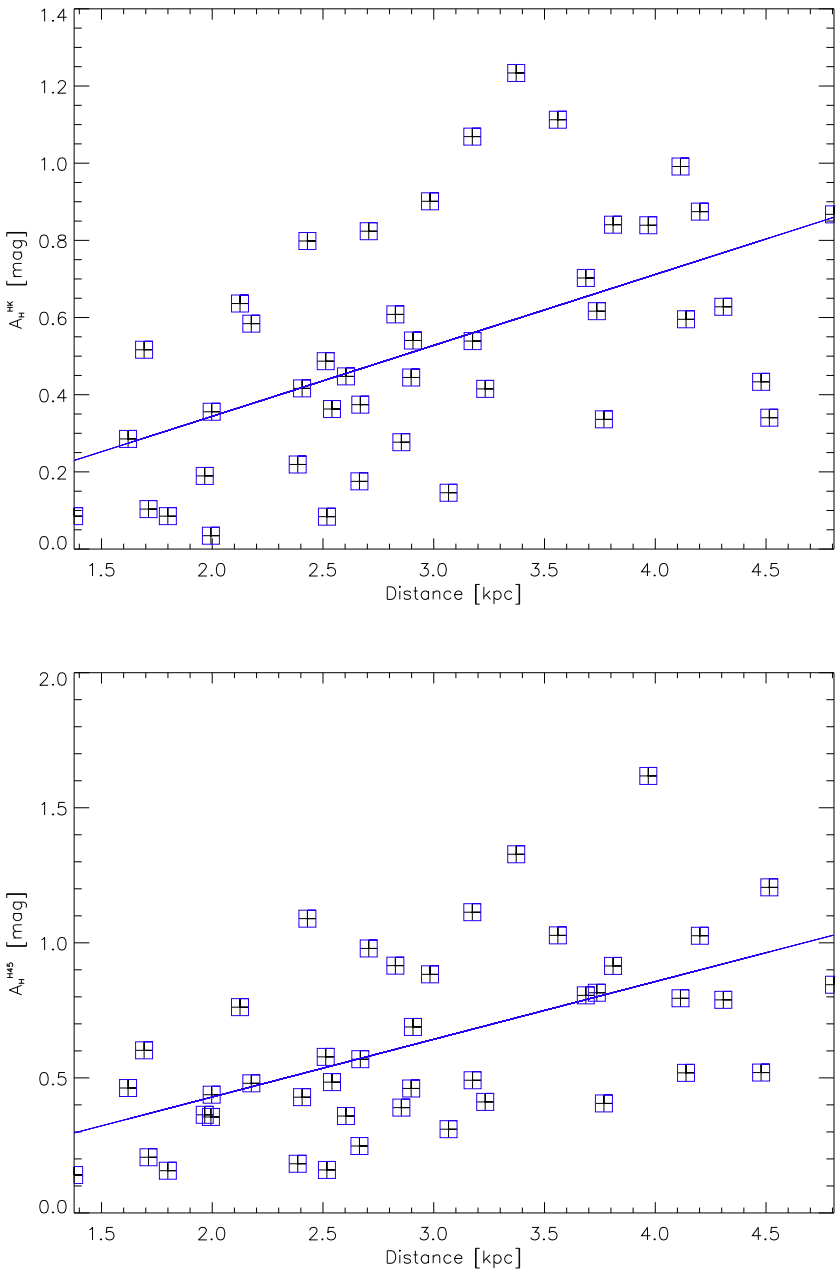


Figure B.1: Plot shows cluster distances against their $H$-band extinctions (*Top*) $A_H^{HK}$ and (*Bottom*) $A_H^{H45}$, for clusters in the region $l = 60° \pm 30°$ (see Sect. 9.2 for details). Black crosses represent clusters in this region, and blue boxed crosses are clusters included in the fit at the $3\sigma$ level.

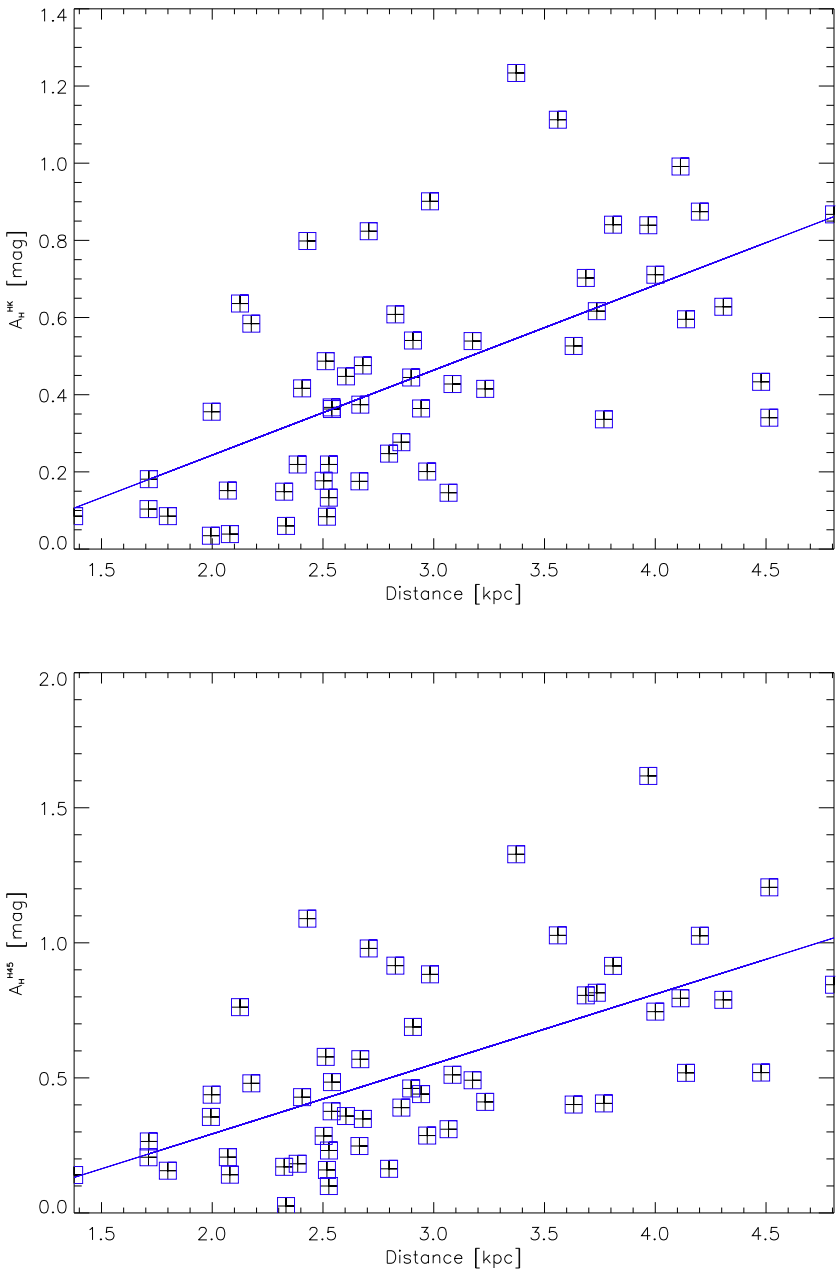


Figure B.2: Plot shows cluster distances against their $H$-band extinctions (*Top*) $A_H^{HK}$ and (*Bottom*) $A_H^{H45}$, for clusters in the region $l = 70° \pm 30°$ (see Sect. 9.2 for details). Black crosses represent clusters in this region, and blue boxed crosses are clusters included in the fit at the $3\sigma$ level.

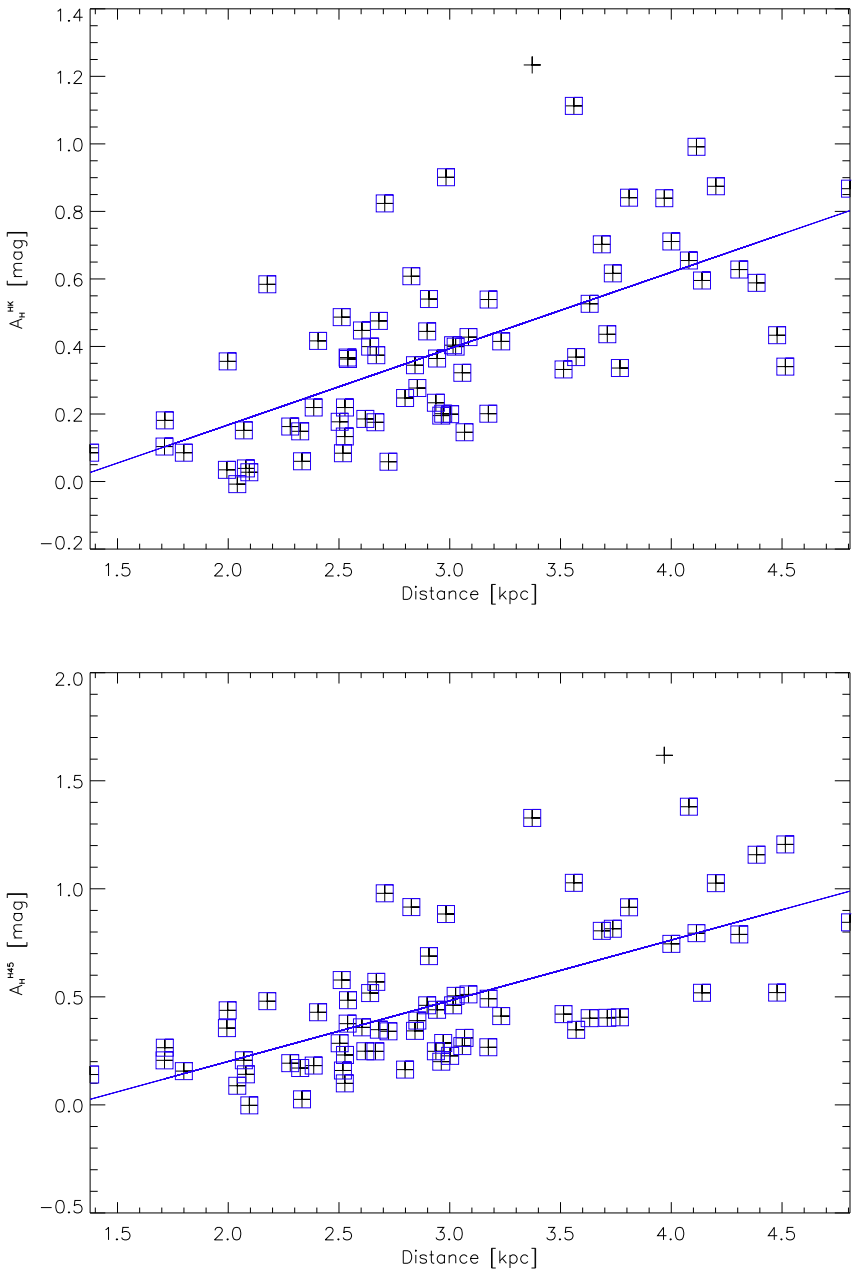


Figure B.3: Plot shows cluster distances against their $H$-band extinctions (*Top*) $A_H^{HK}$ and (*Bottom*) $A_H^{H45}$, for clusters in the region $l = 80° \pm 30°$ (see Sect. 9.2 for details). Black crosses represent clusters in this region, and blue boxed crosses are clusters included in the fit at the $3\sigma$ level.

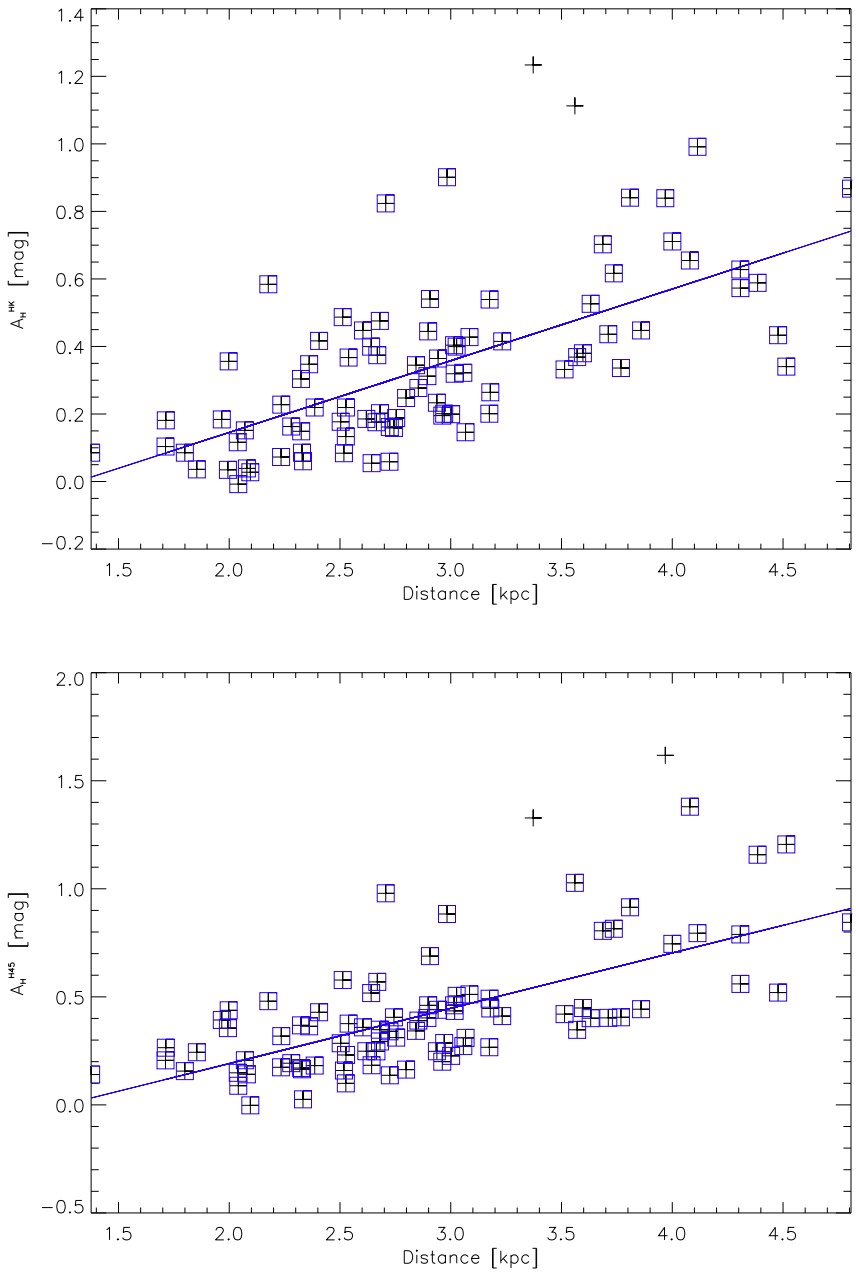


Figure B.4: Plot shows cluster distances against their $H$-band extinctions (*Top*) $A_H^{HK}$ and (*Bottom*) $A_H^{H45}$, for clusters in the region $l = 90° \pm 30°$ (see Sect. 9.2 for details). Black crosses represent clusters in this region, and blue boxed crosses are clusters included in the fit at the $3\sigma$ level.

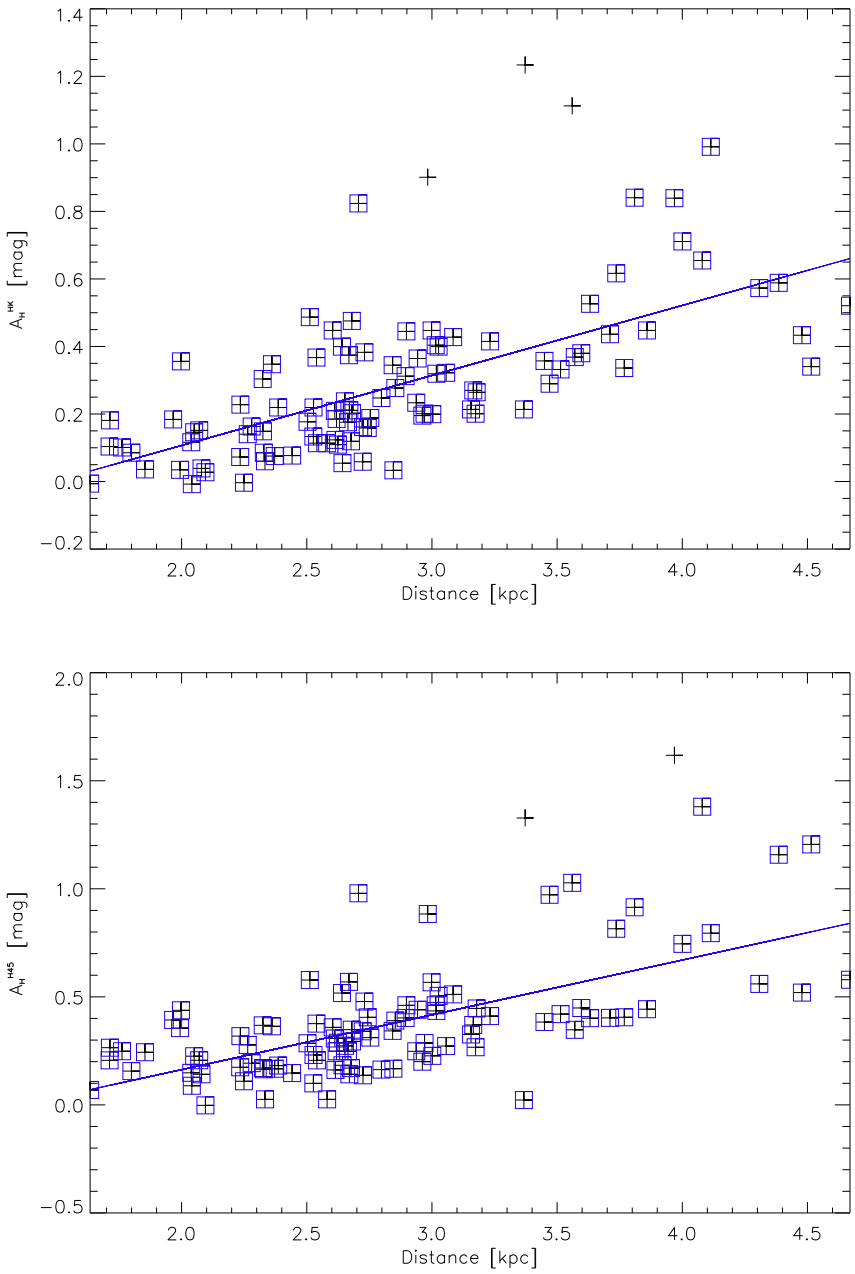


Figure B.5: Plot shows cluster distances against their $H$-band extinctions (*Top*) $A_H^{HK}$ and (*Bottom*) $A_H^{H45}$, for clusters in the region $l = 100° \pm 30°$ (see Sect. 9.2 for details). Black crosses represent clusters in this region, and blue boxed crosses are clusters included in the fit at the $3\sigma$ level.

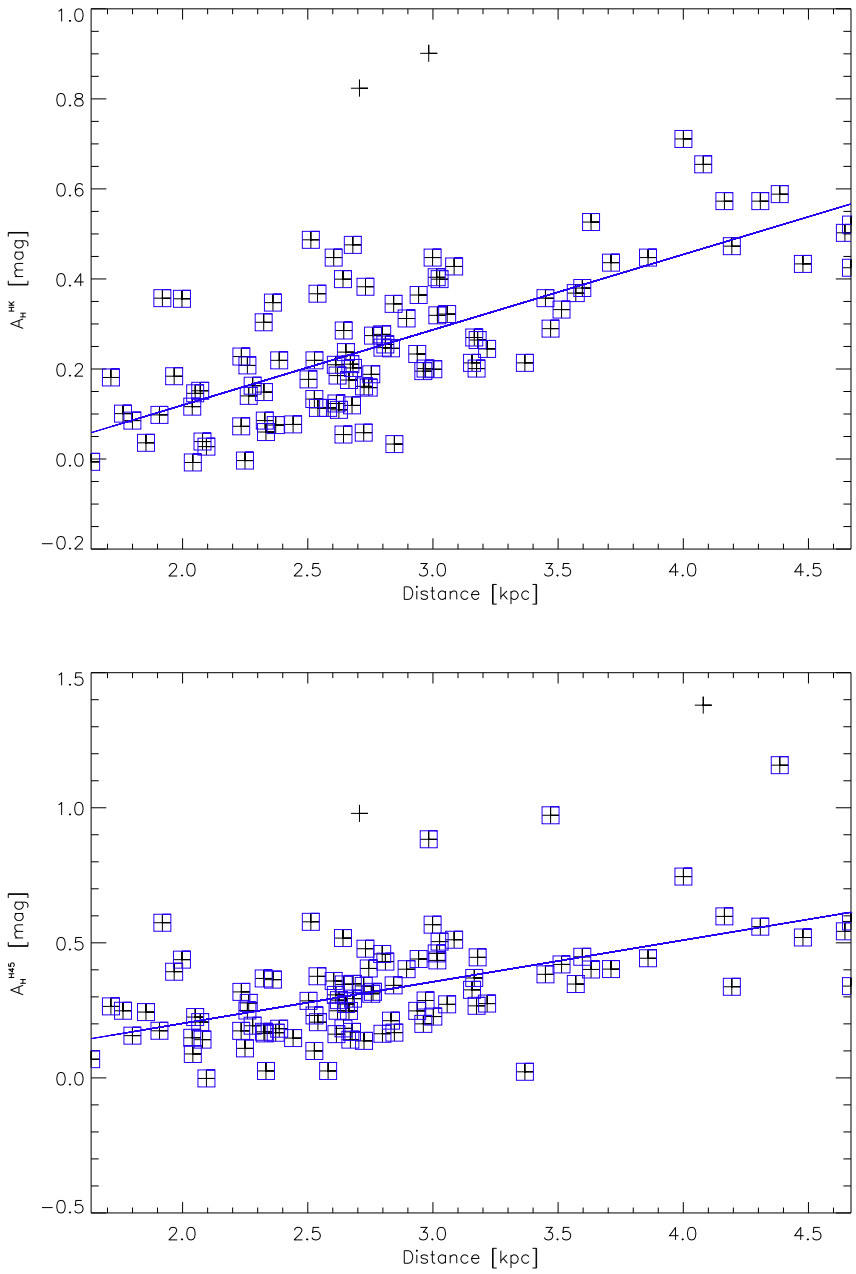


Figure B.6: Plot shows cluster distances against their $H$-band extinctions (*Top*) $A_H^{HK}$ and (*Bottom*) $A_H^{H45}$, for clusters in the region $l = 110° \pm 30°$ (see Sect. 9.2 for details). Black crosses represent clusters in this region, and blue boxed crosses are clusters included in the fit at the $3\sigma$ level.

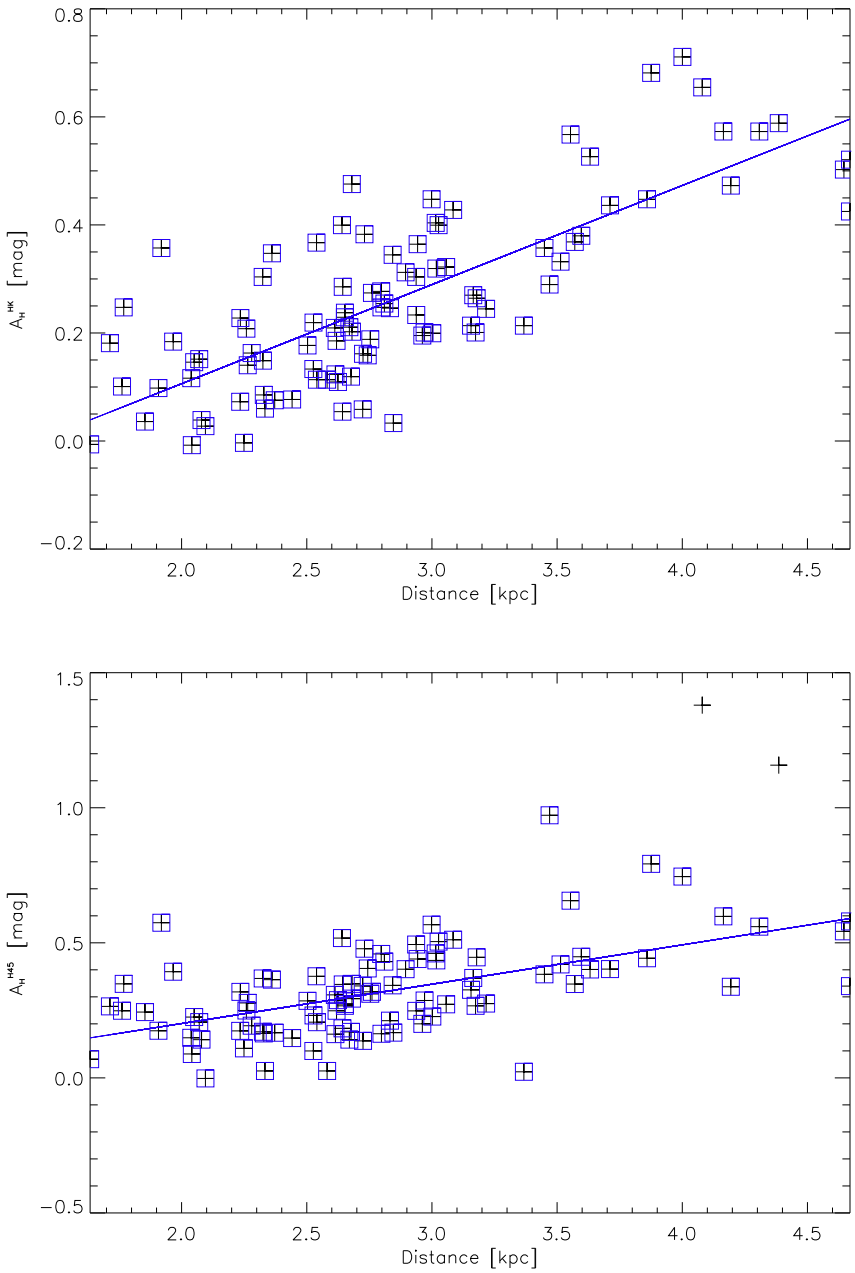


Figure B.7: Plot shows cluster distances against their $H$-band extinctions (*Top*) $A_H^{HK}$ and (*Bottom*) $A_H^{H45}$, for clusters in the region $l = 120° \pm 30°$ (see Sect. 9.2 for details). Black crosses represent clusters in this region, and blue boxed crosses are clusters included in the fit at the $3\sigma$ level.

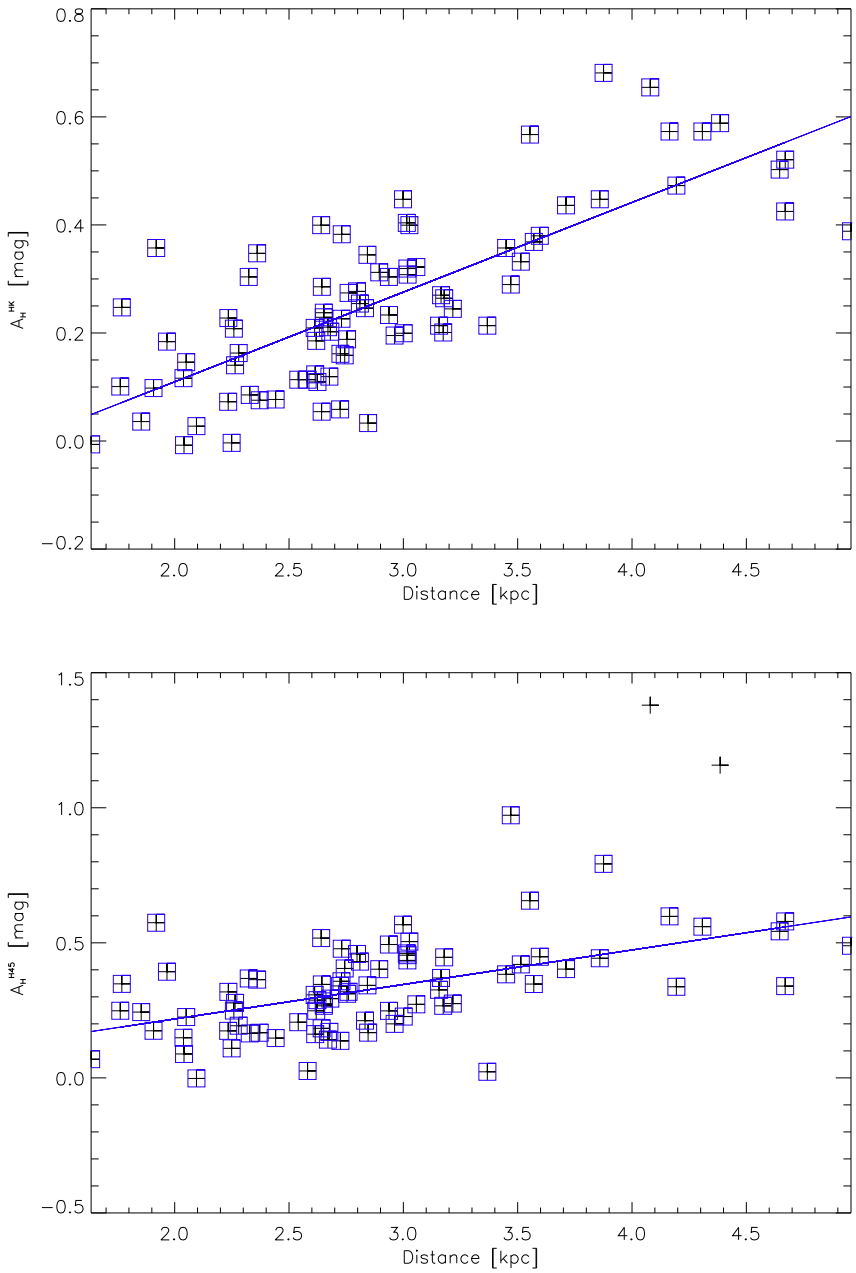


Figure B.8: Plot shows cluster distances against their $H$-band extinctions (*Top*) $A_H^{HK}$ and (*Bottom*) $A_H^{H45}$, for clusters in the region $l = 130° \pm 30°$ (see Sect. 9.2 for details). Black crosses represent clusters in this region, and blue boxed crosses are clusters included in the fit at the $3\sigma$ level.

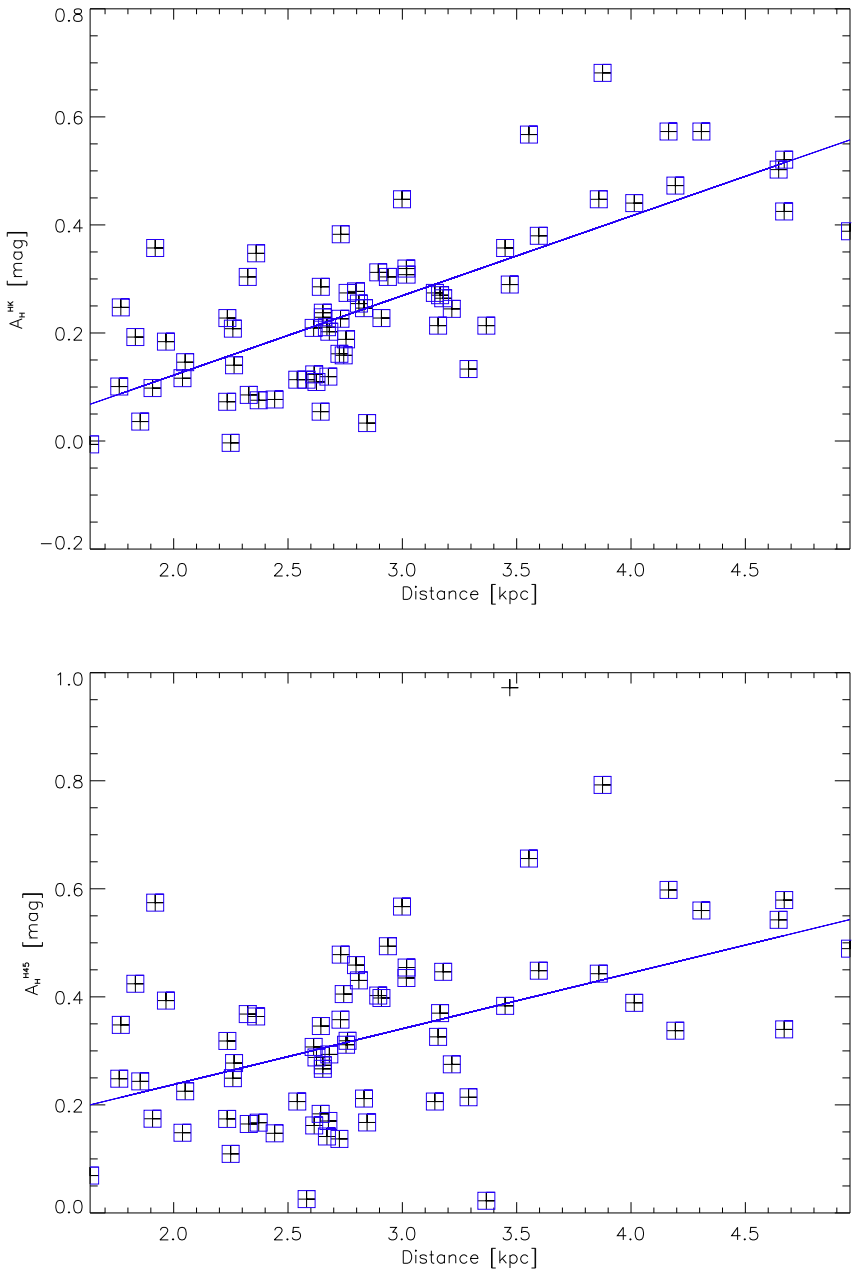


Figure B.9: Plot shows cluster distances against their $H$-band extinctions (*Top*) $A_H^{HK}$ and (*Bottom*) $A_H^{H45}$, for clusters in the region $l = 140° \pm 30°$ (see Sect. 9.2 for details). Black crosses represent clusters in this region, and blue boxed crosses are clusters included in the fit at the $3\sigma$ level.

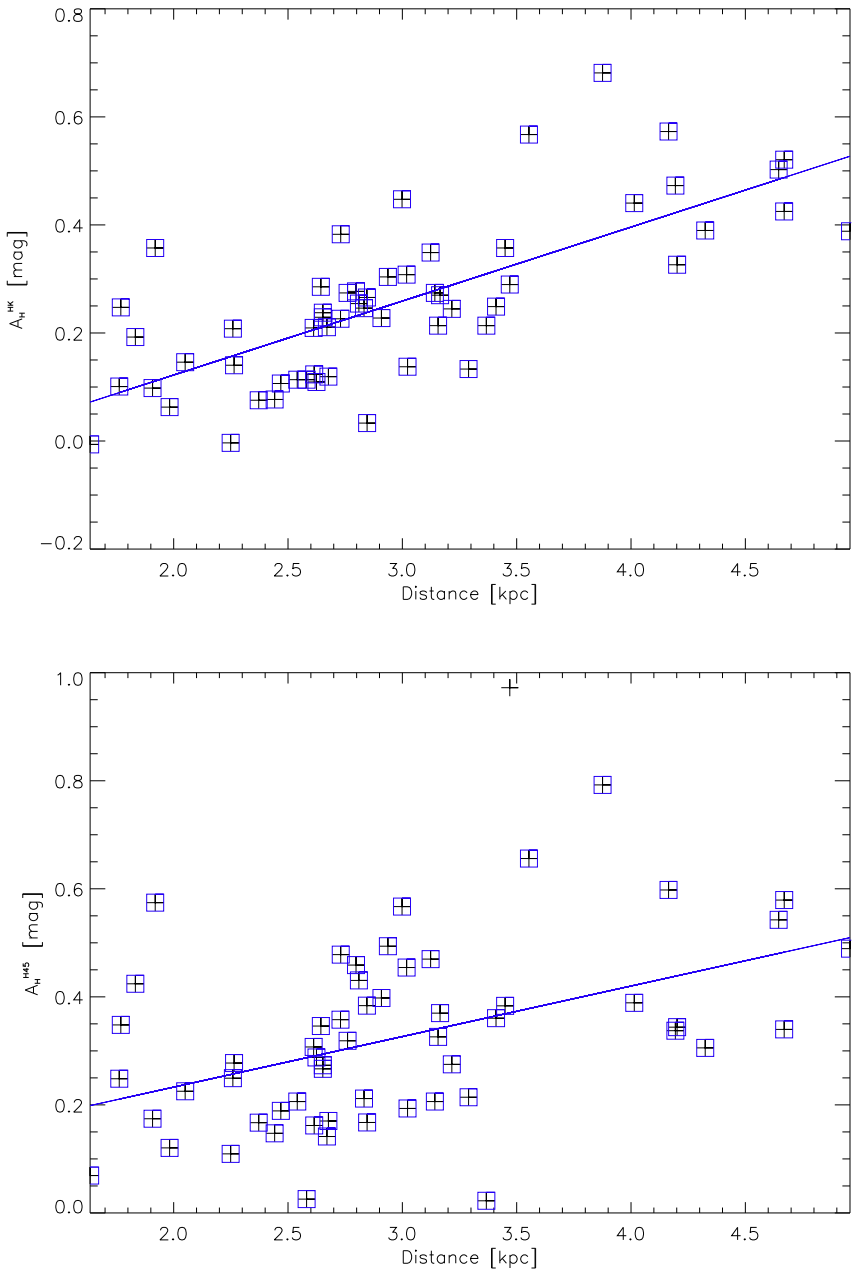


Figure B.10: Plot shows cluster distances against their $H$-band extinctions (*Top*) $A_H^{HK}$ and (*Bottom*) $A_H^{H45}$, for clusters in the region $l = 150° \pm 30°$ (see Sect. 9.2 for details). Black crosses represent clusters in this region, and blue boxed crosses are clusters included in the fit at the $3\sigma$ level.

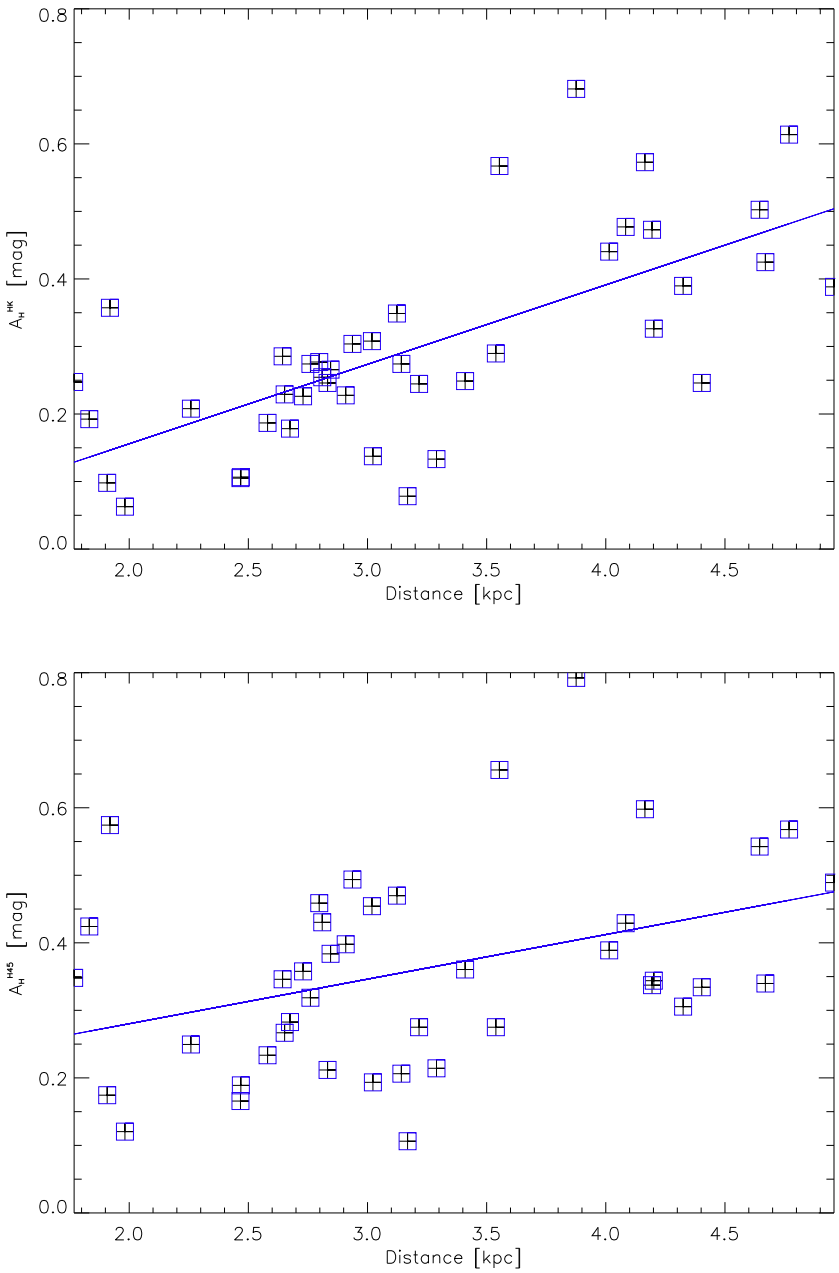


Figure B.11: Plot shows cluster distances against their $H$-band extinctions (*Top*) $A_H^{HK}$ and (*Bottom*) $A_H^{H45}$, for clusters in the region $l = 160° \pm 30°$ (see Sect. 9.2 for details). Black crosses represent clusters in this region, and blue boxed crosses are clusters included in the fit at the $3\sigma$ level.

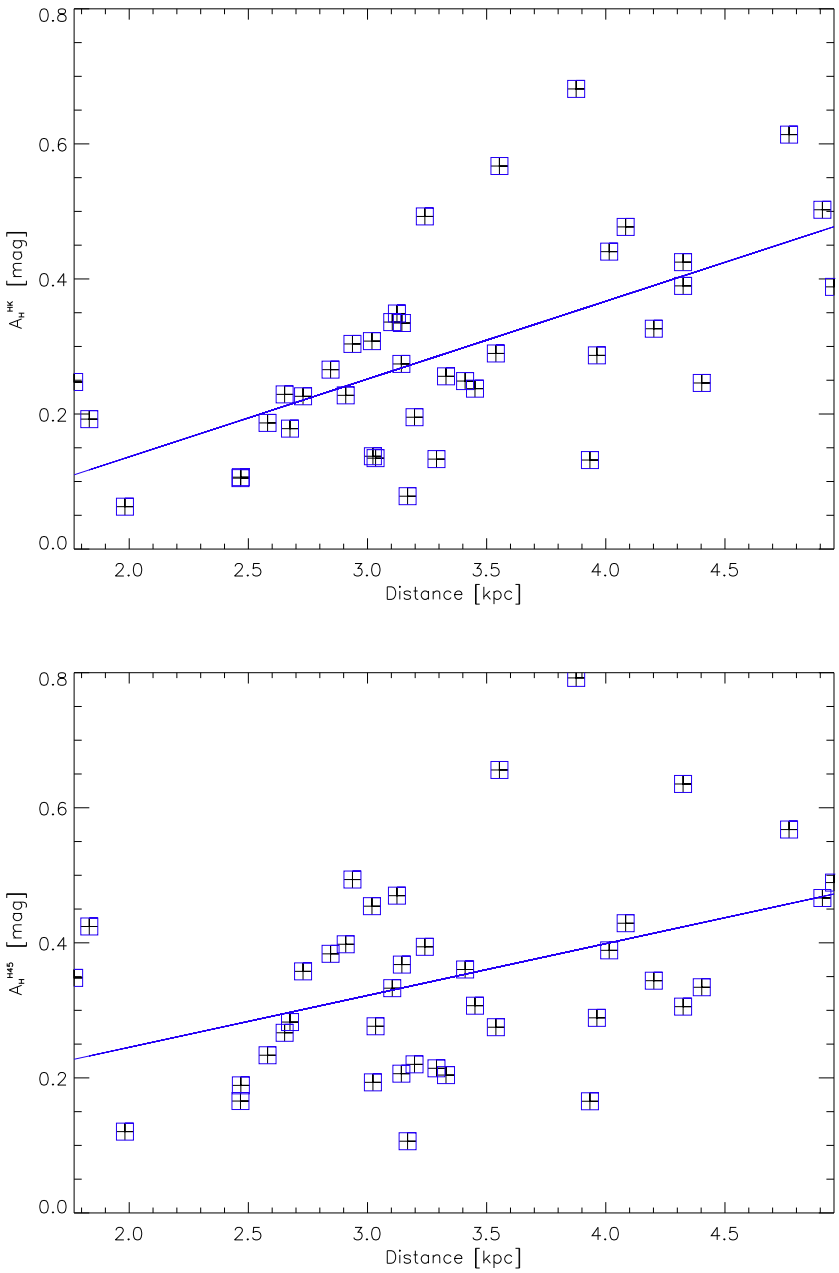


Figure B.12: Plot shows cluster distances against their $H$-band extinctions (*Top*) $A_H^{HK}$ and (*Bottom*) $A_H^{H45}$, for clusters in the region $l = 170° \pm 30°$ (see Sect. 9.2 for details). Black crosses represent clusters in this region, and blue boxed crosses are clusters included in the fit at the $3\sigma$ level.

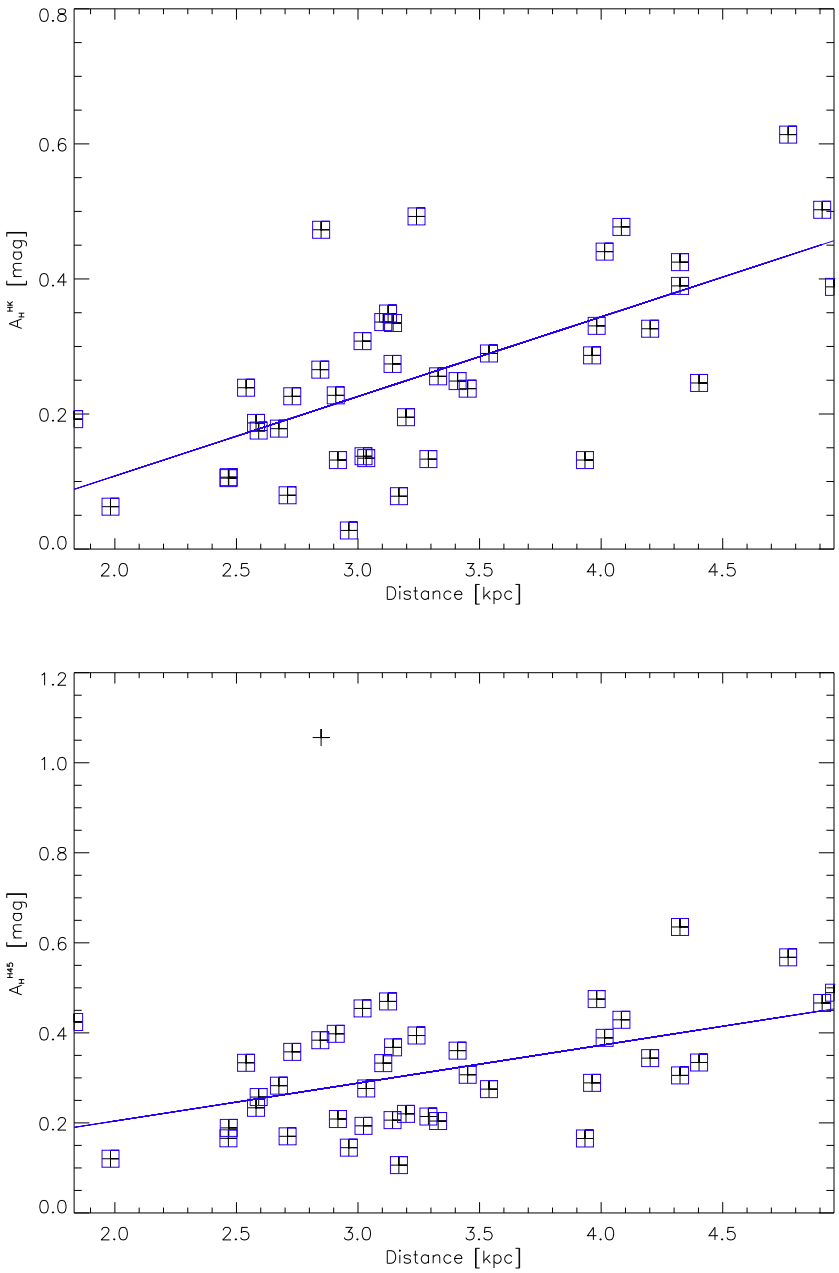


Figure B.13: Plot shows cluster distances against their $H$-band extinctions (*Top*) $A_H^{HK}$ and (*Bottom*) $A_H^{H45}$, for clusters in the region $l = 180° \pm 30°$ (see Sect. 9.2 for details). Black crosses represent clusters in this region, and blue boxed crosses are clusters included in the fit at the $3\sigma$ level.

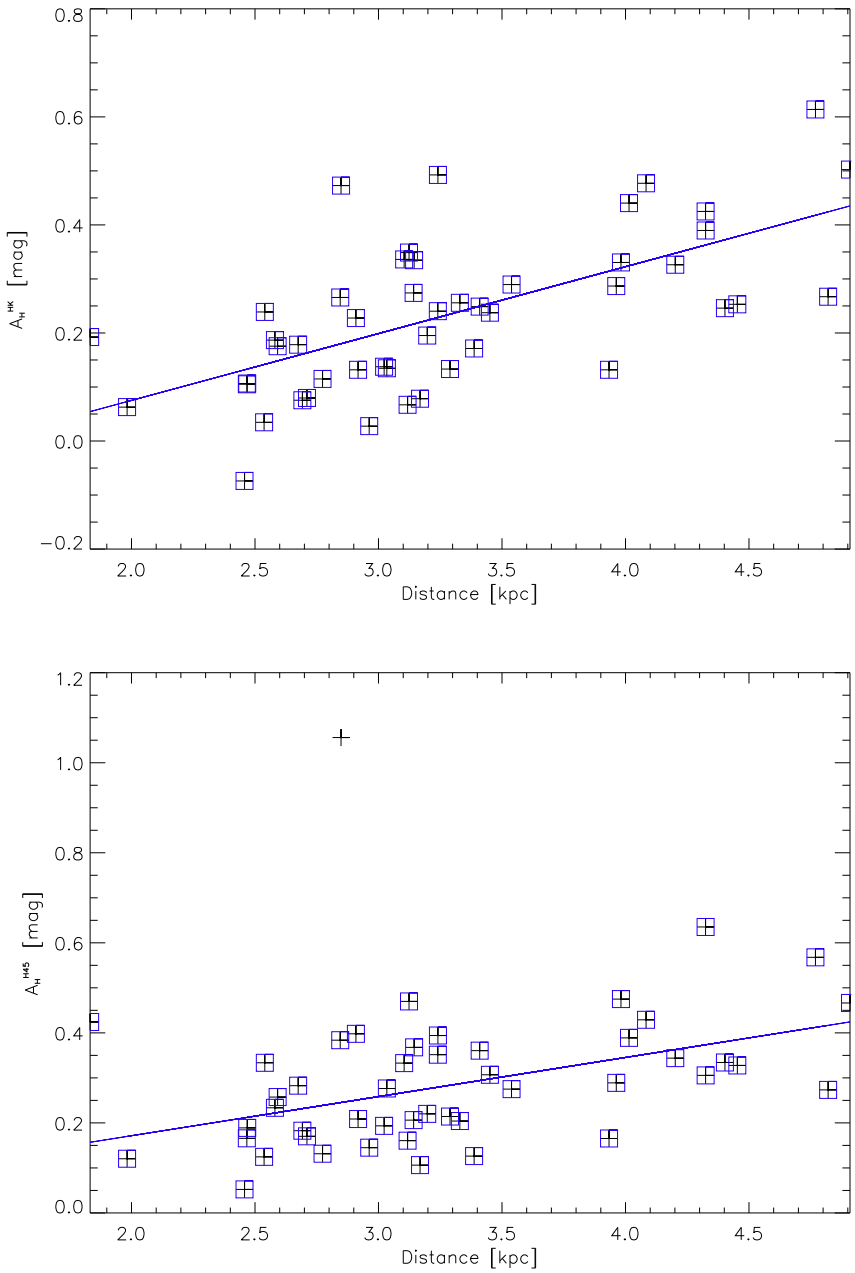


Figure B.14: Plot shows cluster distances against their $H$-band extinctions (*Top*) $A_H^{HK}$ and (*Bottom*) $A_H^{H45}$, for clusters in the region $l = 190° \pm 30°$ (see Sect. 9.2 for details). Black crosses represent clusters in this region, and blue boxed crosses are clusters included in the fit at the $3\sigma$ level.

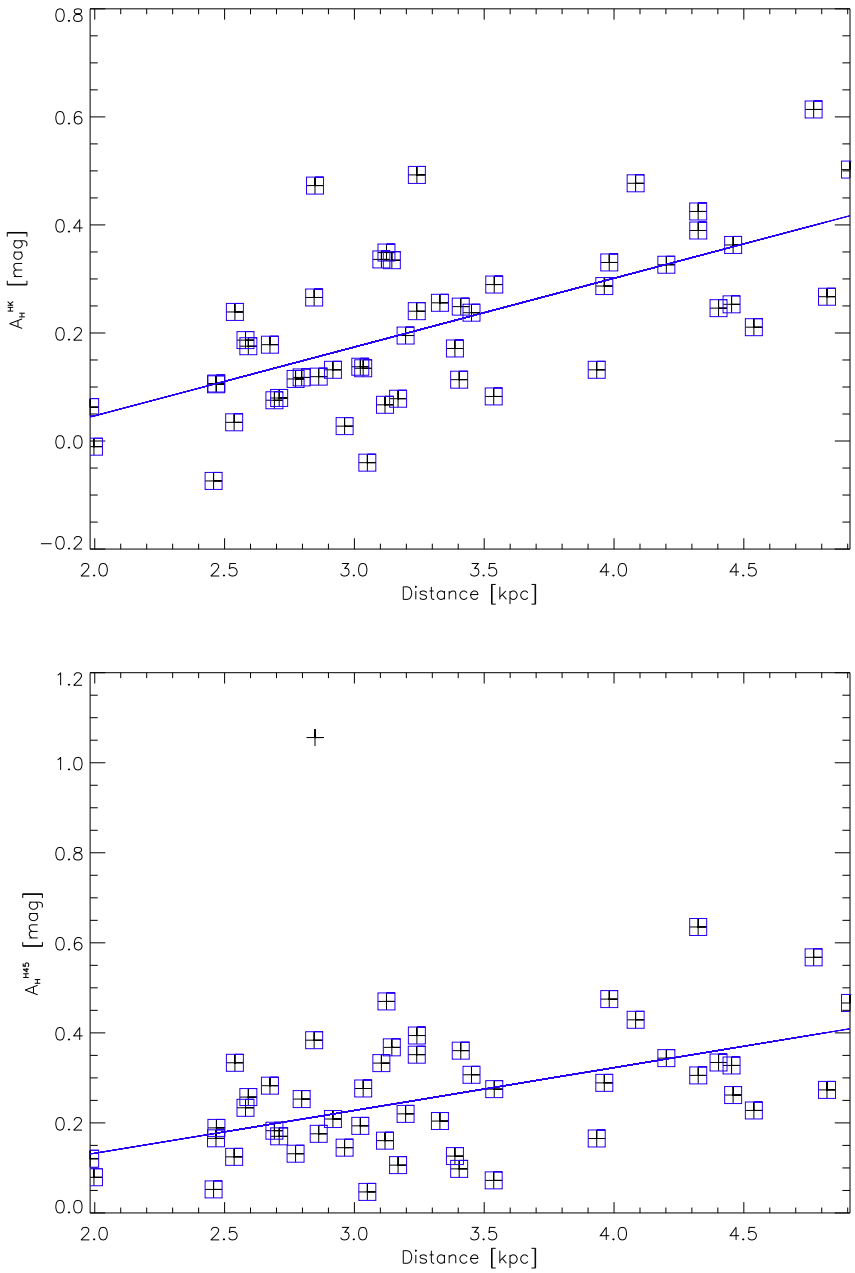


Figure B.15: Plot shows cluster distances against their $H$-band extinctions (*Top*) $A_H^{HK}$ and (*Bottom*) $A_H^{H45}$, for clusters in the region $l = 200° \pm 30°$ (see Sect. 9.2 for details). Black crosses represent clusters in this region, and blue boxed crosses are clusters included in the fit at the $3\sigma$ level.

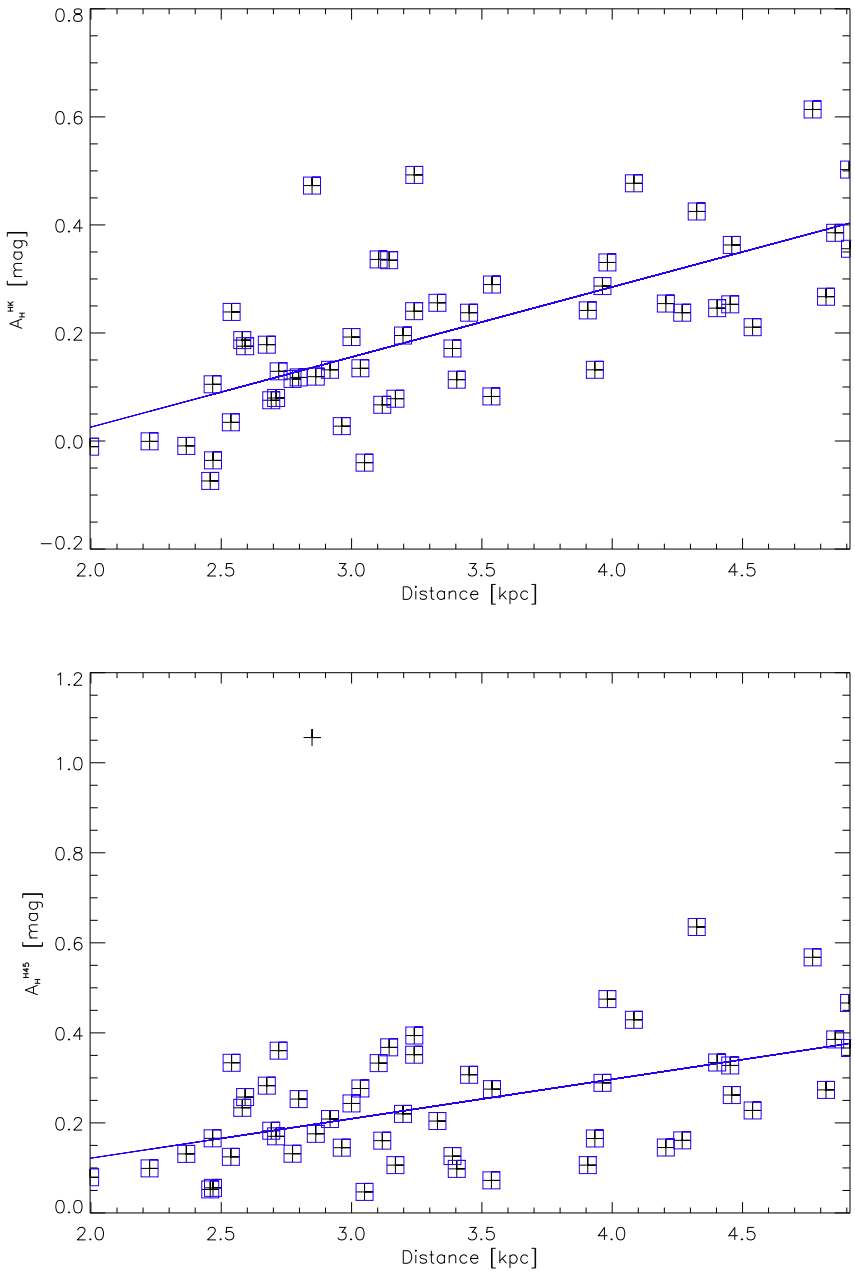


Figure B.16: Plot shows cluster distances against their $H$-band extinctions (*Top*) $A_H^{HK}$ and (*Bottom*) $A_H^{H45}$, for clusters in the region $l = 210° \pm 30°$ (see Sect. 9.2 for details). Black crosses represent clusters in this region, and blue boxed crosses are clusters included in the fit at the $3\sigma$ level.

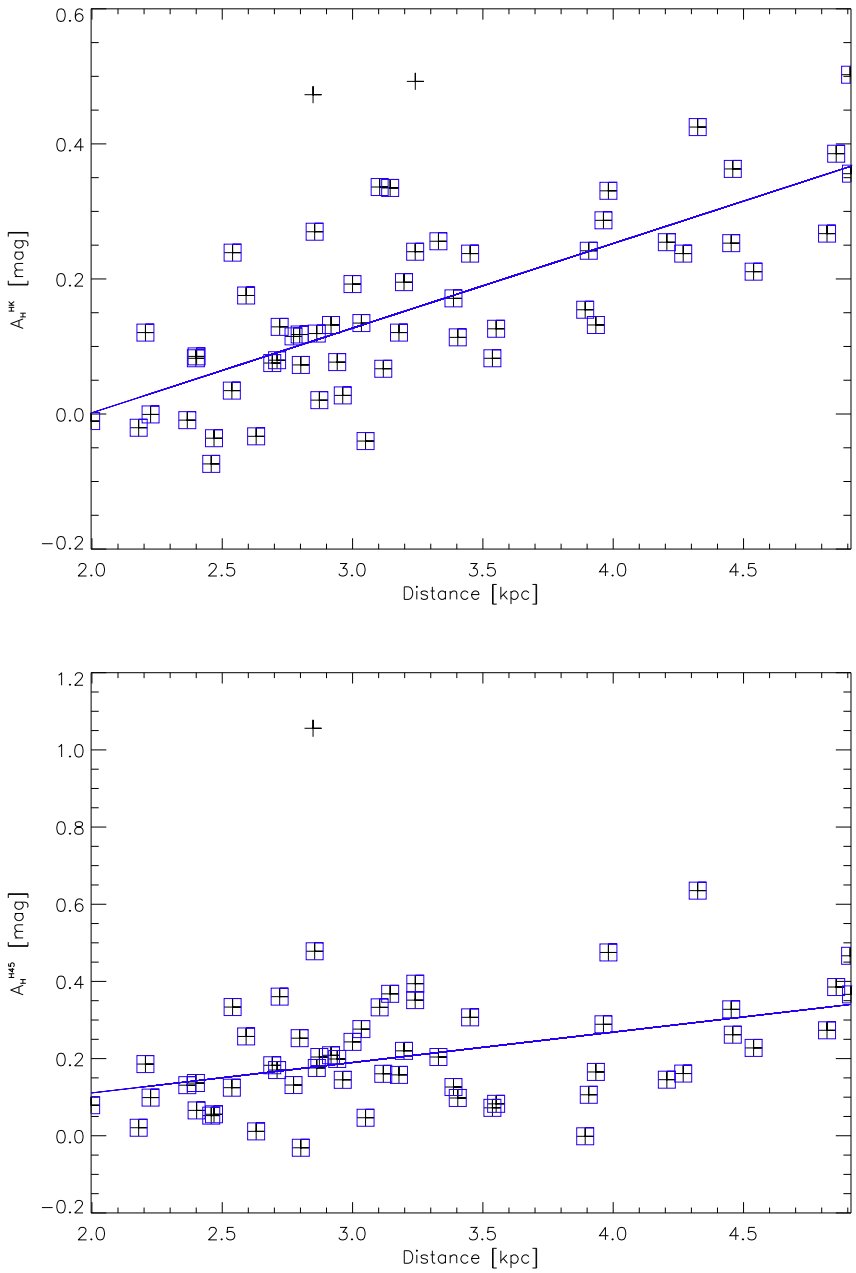


Figure B.17: Plot shows cluster distances against their $H$-band extinctions (*Top*) $A_H^{HK}$ and (*Bottom*) $A_H^{H45}$, for clusters in the region $l = 220° \pm 30°$ (see Sect. 9.2 for details). Black crosses represent clusters in this region, and blue boxed crosses are clusters included in the fit at the $3\sigma$ level.

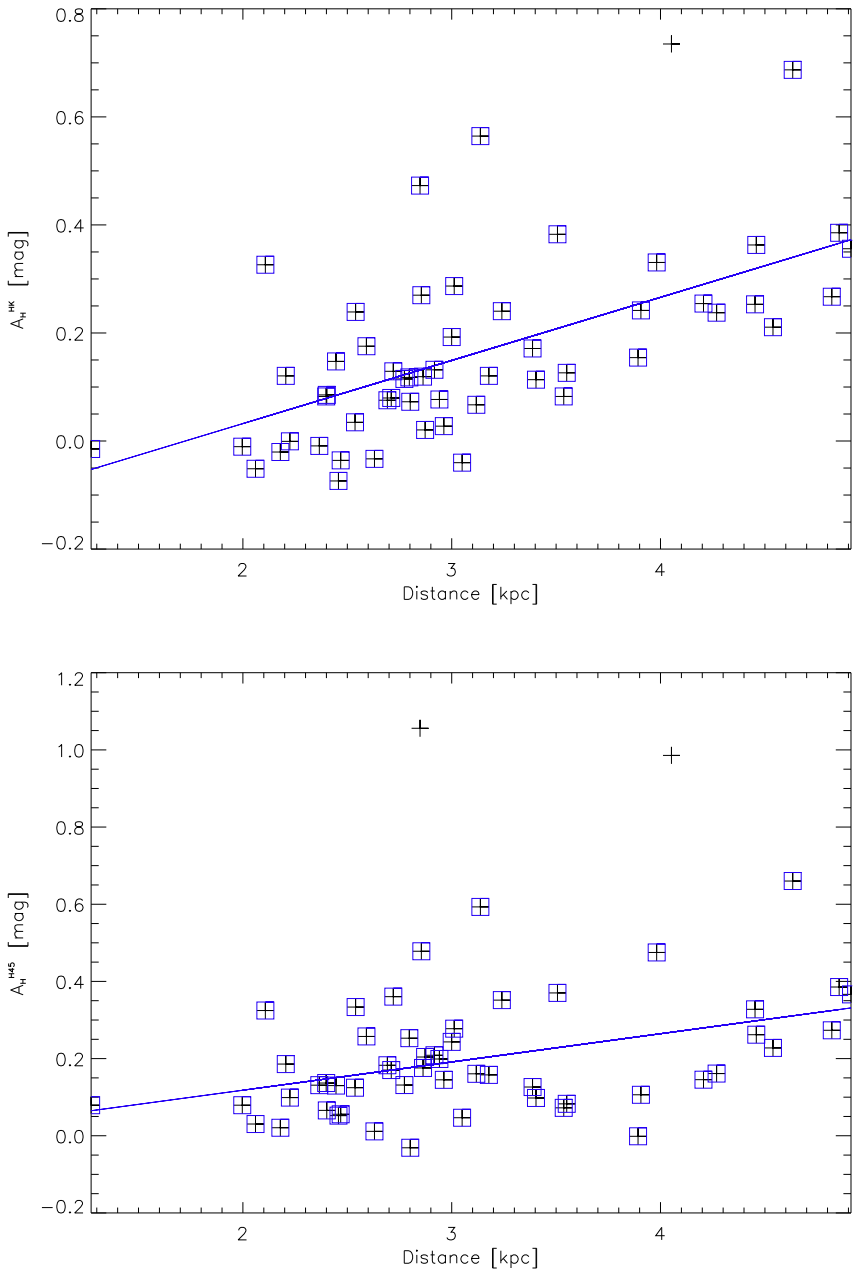


Figure B.18: Plot shows cluster distances against their $H$-band extinctions (*Top*) $A_H^{HK}$ and (*Bottom*) $A_H^{H45}$, for clusters in the region $l = 230° \pm 30°$ (see Sect. 9.2 for details). Black crosses represent clusters in this region, and blue boxed crosses are clusters included in the fit at the $3\sigma$ level.

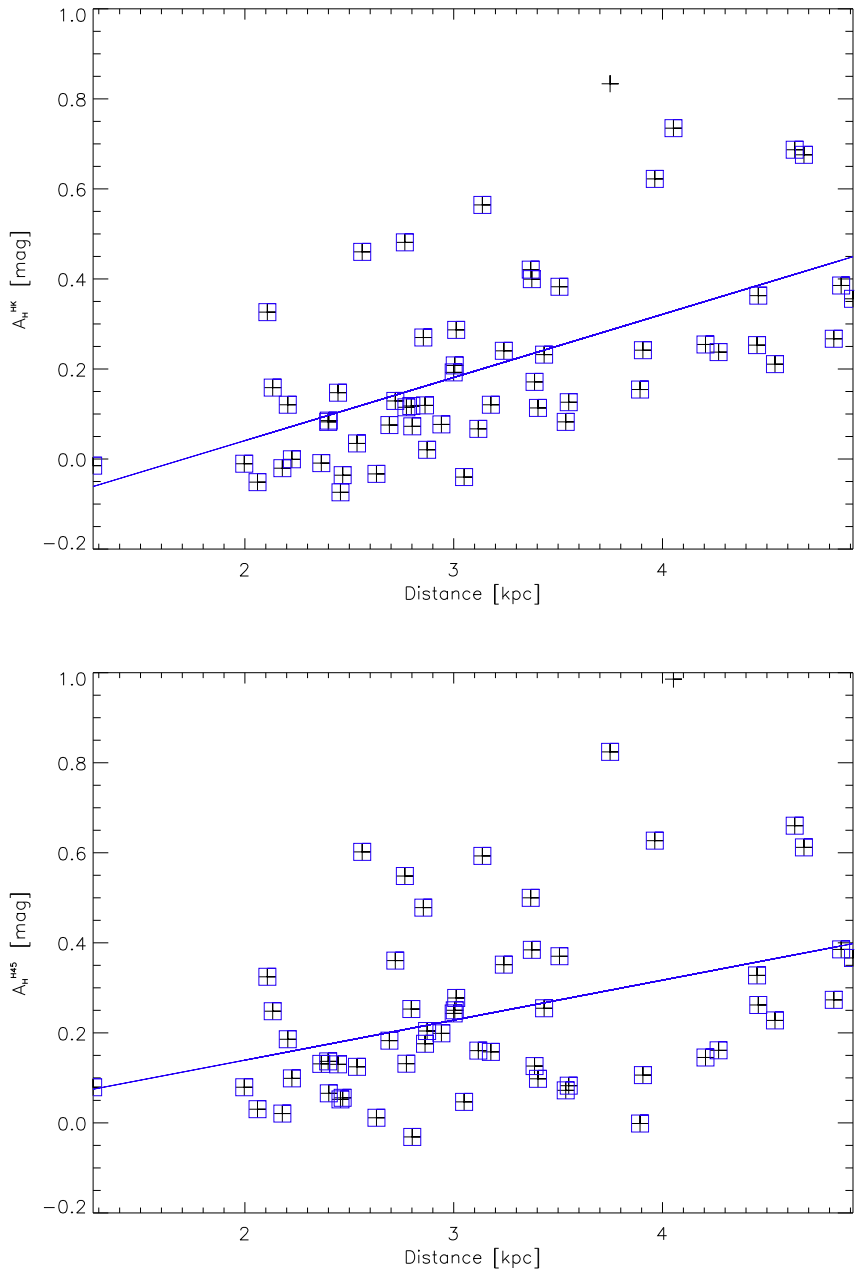


Figure B.19: Plot shows cluster distances against their $H$-band extinctions (*Top*) $A_H^{HK}$ and (*Bottom*) $A_H^{H45}$, for clusters in the region $l = 240° \pm 30°$ (see Sect. 9.2 for details). Black crosses represent clusters in this region, and blue boxed crosses are clusters included in the fit at the $3\sigma$ level.

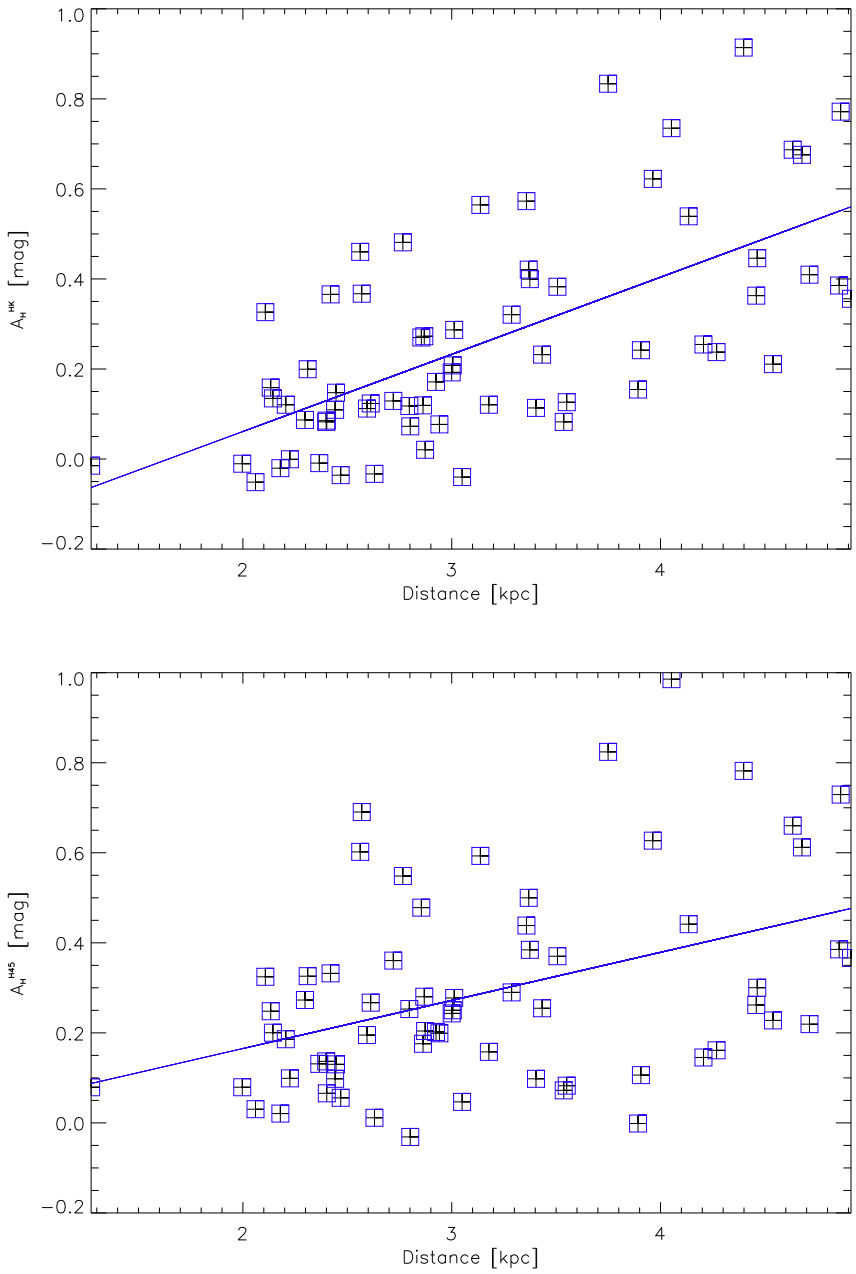


Figure B.20: Plot shows cluster distances against their $H$-band extinctions (*Top*) $A_H^{HK}$ and (*Bottom*) $A_H^{H45}$, for clusters in the region $l = 250° \pm 30°$ (see Sect. 9.2 for details). Black crosses represent clusters in this region, and blue boxed crosses are clusters included in the fit at the $3\sigma$ level.

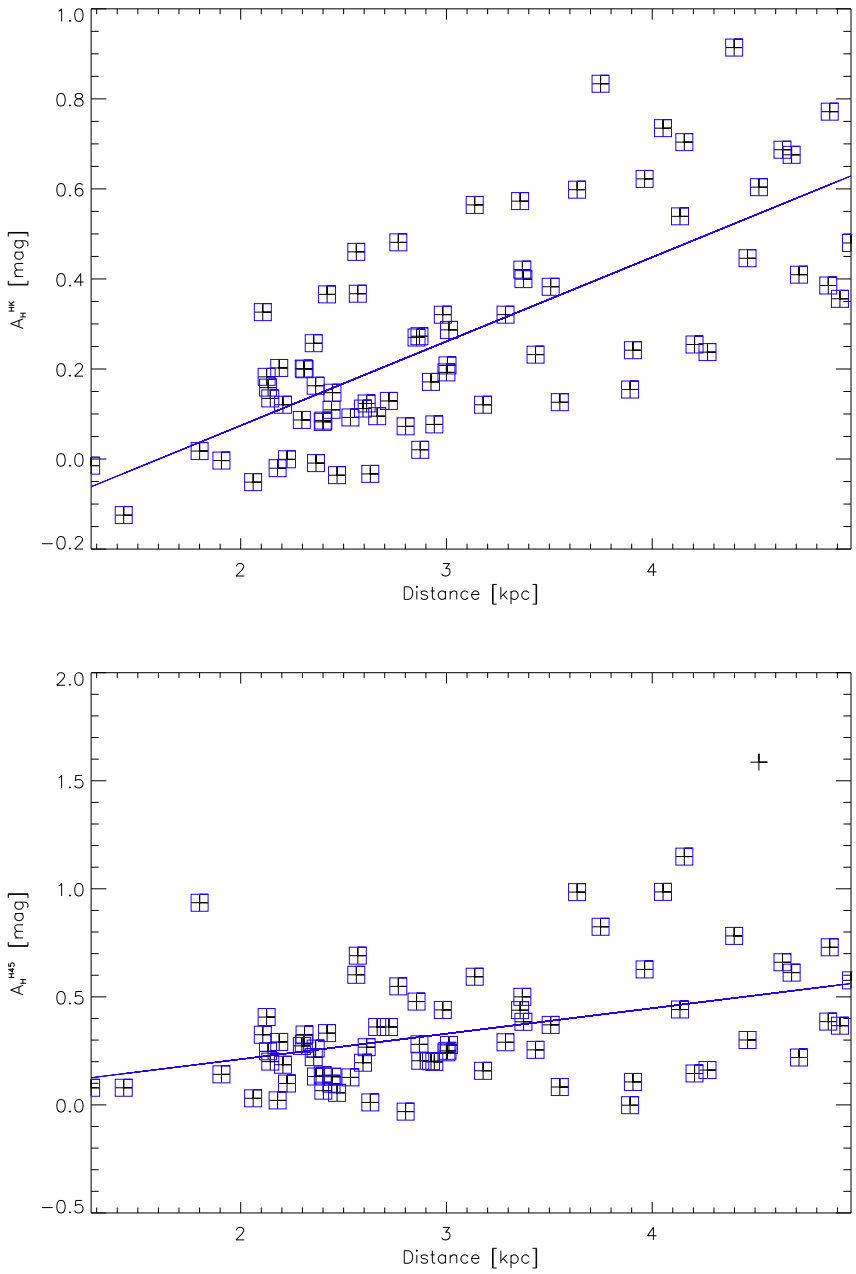


Figure B.21: Plot shows cluster distances against their $H$-band extinctions (*Top*) $A_H^{HK}$ and (*Bottom*) $A_H^{H45}$, for clusters in the region $l = 260° \pm 30°$ (see Sect. 9.2 for details). Black crosses represent clusters in this region, and blue boxed crosses are clusters included in the fit at the $3\sigma$ level.

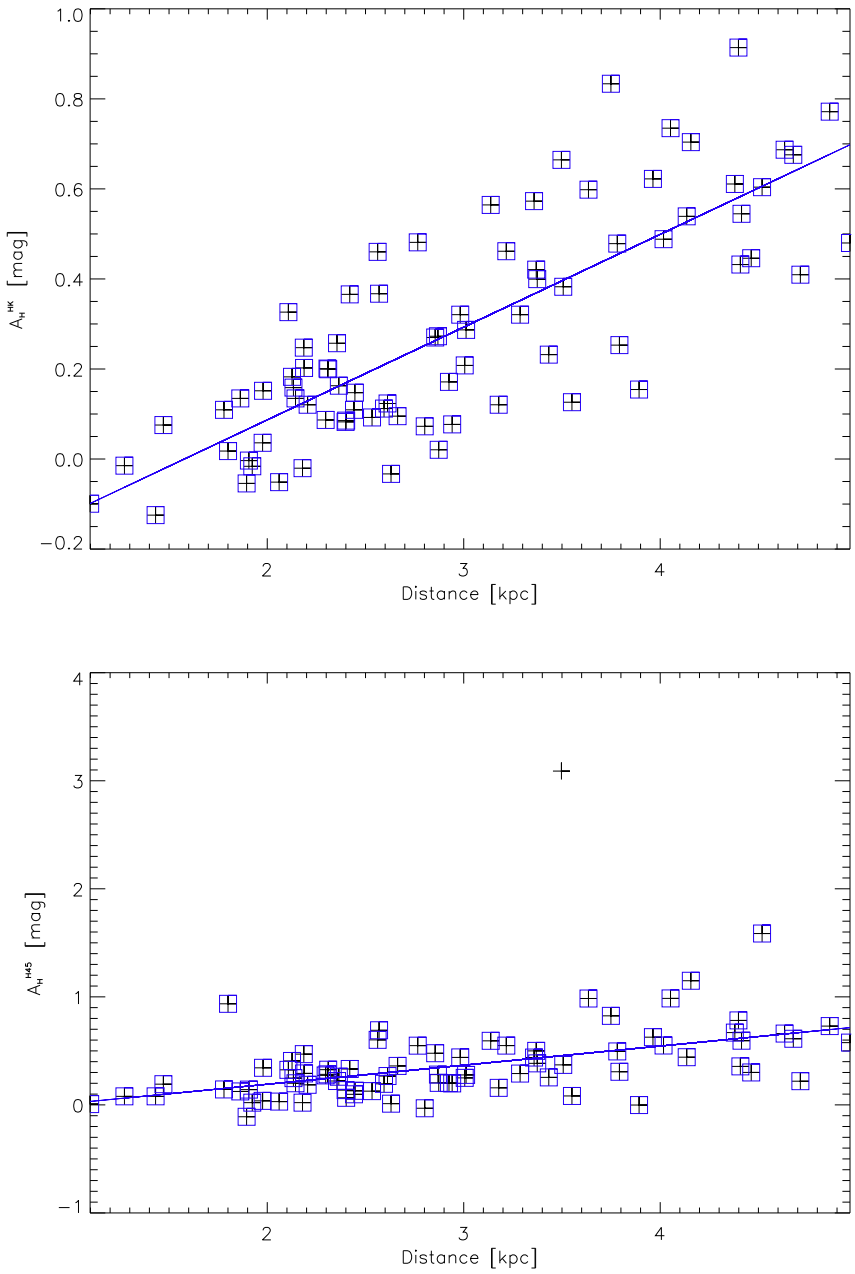


Figure B.22: Plot shows cluster distances against their $H$-band extinctions (*Top*) $A_H^{HK}$ and (*Bottom*) $A_H^{H45}$, for clusters in the region $l = 270° \pm 30°$ (see Sect. 9.2 for details). Black crosses represent clusters in this region, and blue boxed crosses are clusters included in the fit at the $3\sigma$ level.

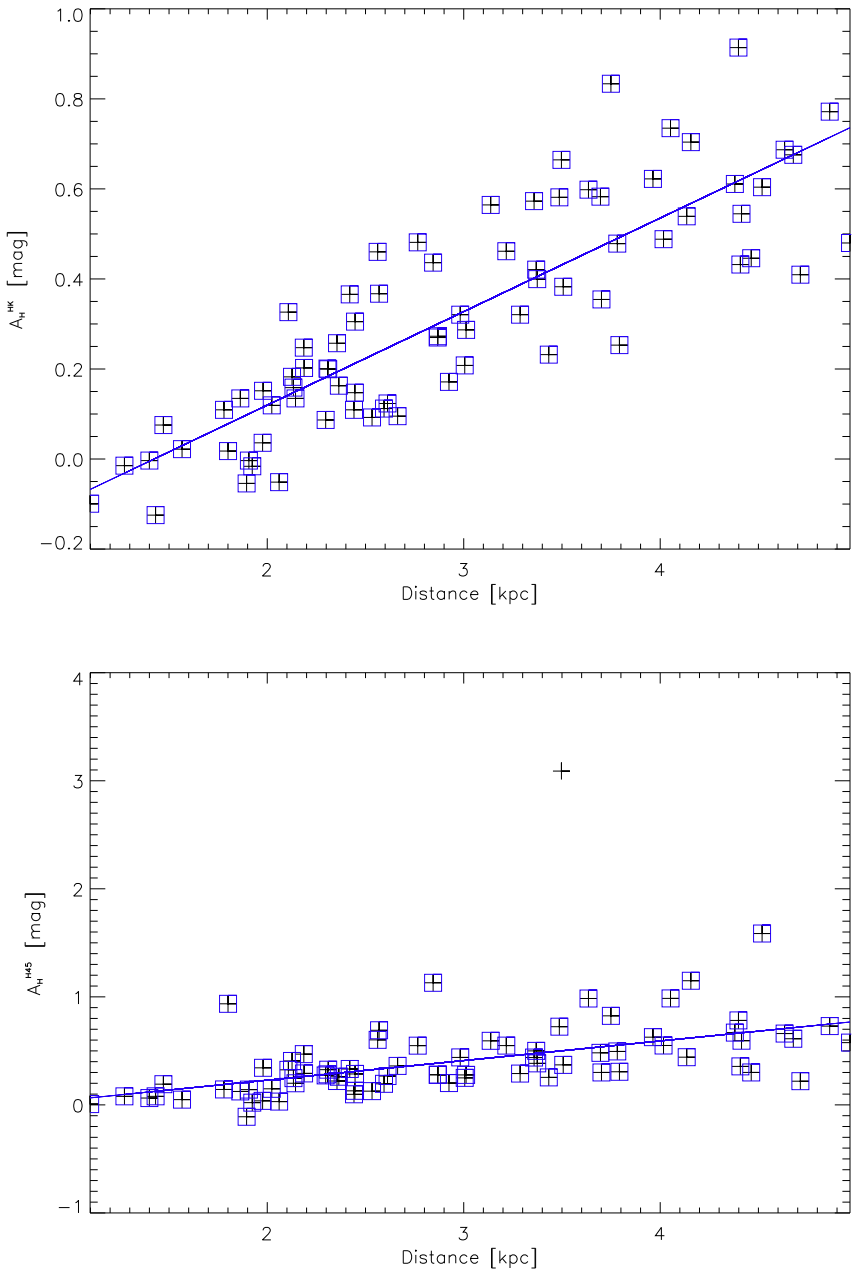


Figure B.23: Plot shows cluster distances against their $H$-band extinctions (*Top*) $A_H^{HK}$ and (*Bottom*) $A_H^{H45}$, for clusters in the region $l = 280° \pm 30°$ (see Sect. 9.2 for details). Black crosses represent clusters in this region, and blue boxed crosses are clusters included in the fit at the $3\sigma$ level.

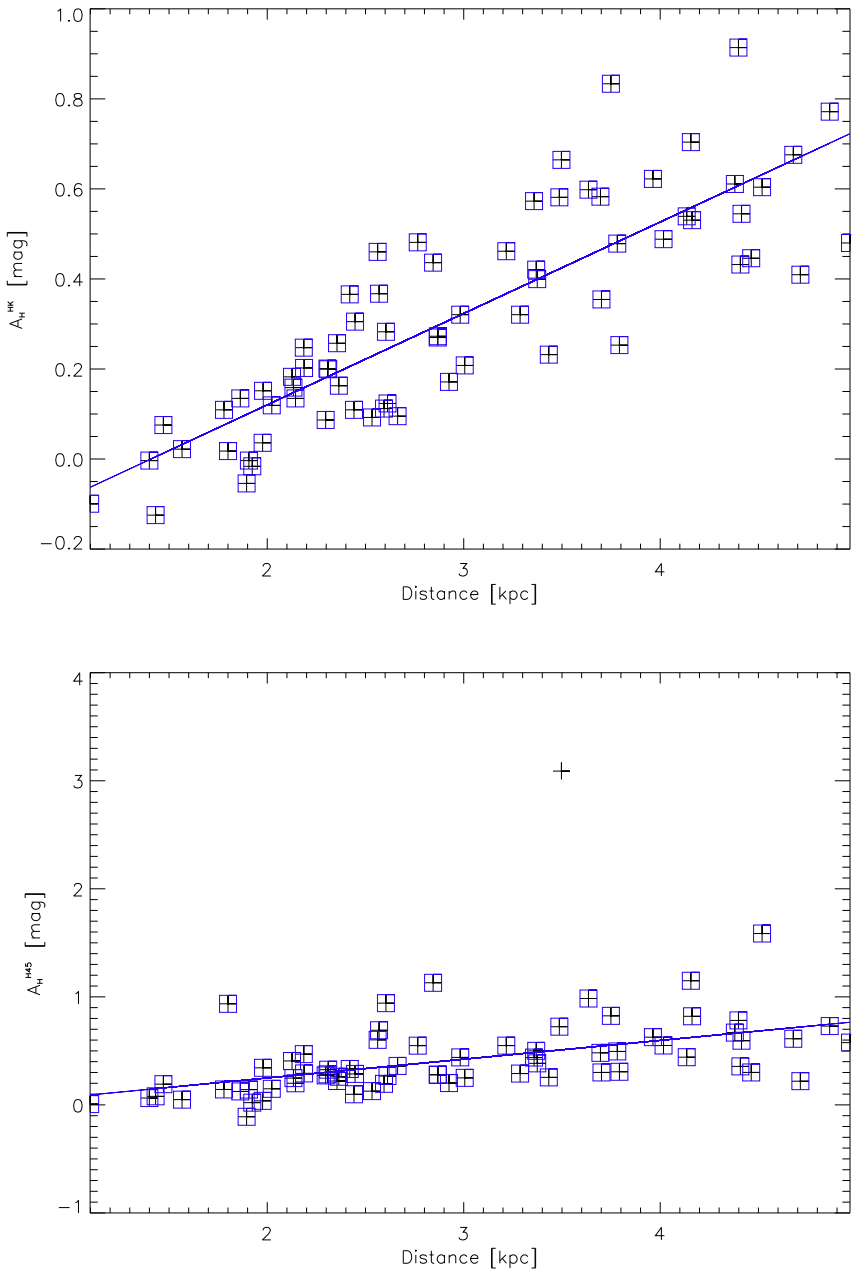


Figure B.24: Plot shows cluster distances against their $H$-band extinctions (*Top*) $A_H^{HK}$ and (*Bottom*) $A_H^{H45}$, for clusters in the region $l = 290° \pm 30°$ (see Sect. 9.2 for details). Black crosses represent clusters in this region, and blue boxed crosses are clusters included in the fit at the $3\sigma$ level.

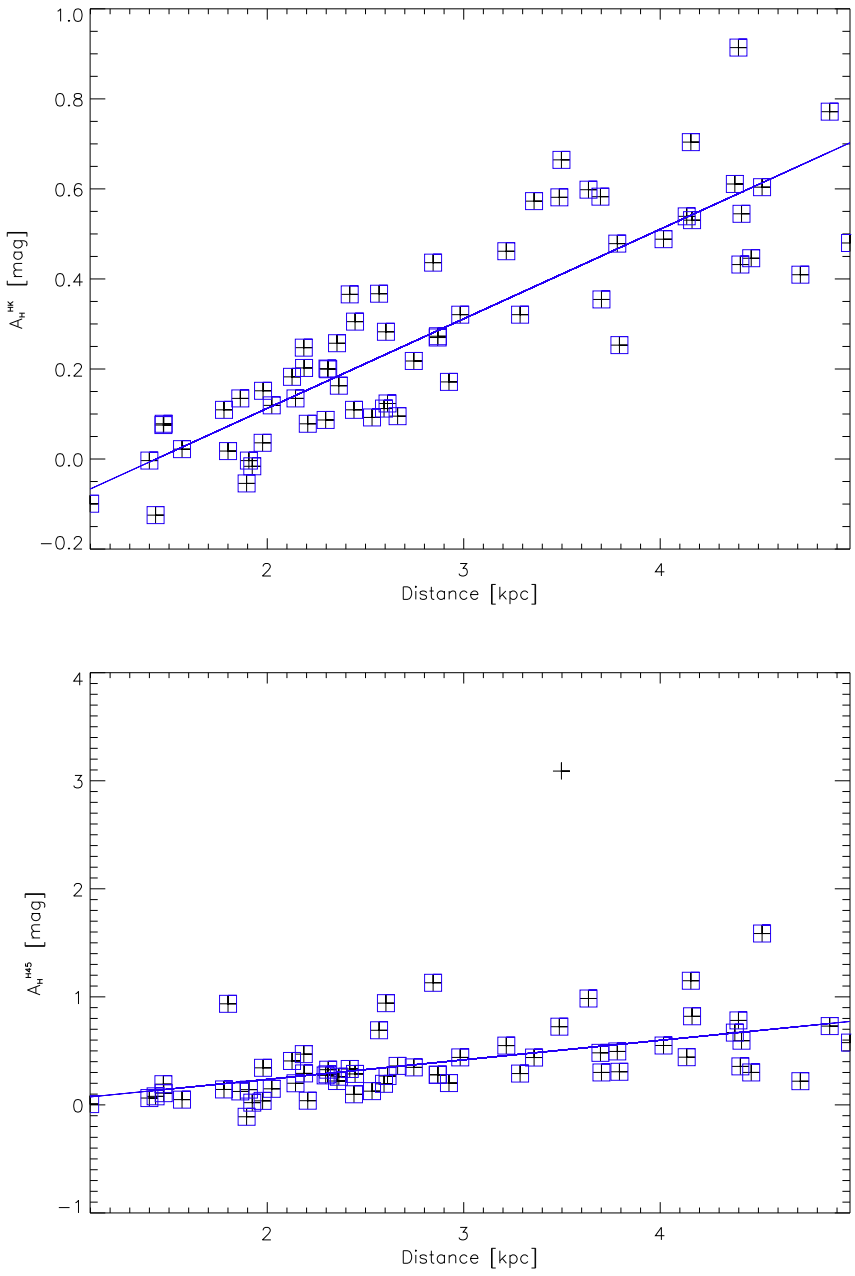


Figure B.25: Plot shows cluster distances against their $H$-band extinctions (*Top*) $A_H^{HK}$ and (*Bottom*) $A_H^{H45}$, for clusters in the region $l = 300° \pm 30°$ (see Sect. 9.2 for details). Black crosses represent clusters in this region, and blue boxed crosses are clusters included in the fit at the $3\sigma$ level.

# Appendix C

Appendix C contains a summary table of the scale height and vertical zero point values that were measured for various sub-samples used in the analysis of the temporal and spatial evolution of cluster scale height. A discussion of these values is provided in Chapter 10.

**Note:**

- Table C.1 has been presented in graphical form in Figures 10.1, 10.6 and 10.6.
- Table C.2 has been presented in graphical form in Figures 10.4, 10.5 and 10.7.
- The data contained in these tables has been published in Buckner and Froebrich (2014).

Table C.1: Data used to investigate the dependence of cluster scale height, vertical zero point and age. This table lists for each sample and age bin: the minimum and maximum cluster age; number of clusters ($N_{\rm cl}$); vertical zero point ($Z_0$) and uncertainty ($\Delta Z_0$); scale height ($h_0$) and uncertainty ($\Delta h_0$).

| Sample | $\rm Age_{min}$ | $\rm Age_{max}$ | $N_{\rm cl}$ | $Z_0$ | $\Delta Z_0$ | $h_0$ | $\Delta h_0$ |
|---|---|---|---|---|---|---|---|
| | [log(age/yr)] | | | [pc] | | [pc] | |
| CS 1 | 6.000 | 6.850 | 40 | -2 | 8 | 36 | 9 |
| CS 1 | 6.850 | 7.200 | 40 | 9 | 8 | 62 | 15 |
| CS 1 | 7.200 | 7.420 | 40 | 6 | 8 | 56 | 14 |
| CS 1 | 7.420 | 7.550 | 40 | -20 | 8 | 47 | 12 |
| CS 1 | 7.550 | 7.755 | 40 | -10 | 8 | 65 | 16 |
| CS 1 | 7.760 | 7.950 | 40 | -6 | 8 | 76 | 19 |
| CS 1 | 7.950 | 8.060 | 40 | -20 | 8 | 72 | 18 |
| CS 1 | 8.060 | 8.150 | 40 | -3 | 8 | 59 | 15 |
| CS 1 | 8.150 | 8.255 | 40 | -1 | 8 | 60 | 15 |
| CS 1 | 8.255 | 8.350 | 40 | -9 | 8 | 58 | 14 |
| CS 1 | 8.350 | 8.445 | 40 | -13 | 8 | 63 | 16 |
| CS 1 | 8.445 | 8.505 | 40 | -22 | 8 | 74 | 18 |
| CS 1 | 8.505 | 8.580 | 40 | -9 | 8 | 73 | 18 |
| CS 1 | 8.585 | 8.632 | 40 | -24 | 8 | 85 | 21 |
| CS 1 | 8.635 | 8.690 | 40 | -29 | 8 | 79 | 20 |
| CS 1 | 8.695 | 8.735 | 40 | -8 | 8 | 68 | 17 |
| CS 1 | 8.735 | 8.800 | 40 | -25 | 8 | 79 | 20 |
| CS 1 | 8.800 | 8.865 | 40 | -12 | 8 | 67 | 16 |
| CS 1 | 8.870 | 8.930 | 40 | -9 | 8 | 87 | 21 |
| CS 1 | 8.935 | 9.005 | 40 | -23 | 8 | 98 | 24 |
| CS 1 | 9.005 | 9.100 | 40 | -39 | 8 | 146 | 36 |
| CS 1 | 9.100 | 9.200 | 40 | 8 | 8 | 263 | 65 |
| CS 1 | 9.200 | 9.400 | 40 | -109 | 8 | 352 | 87 |
| CS 1 | 9.400 | 9.700 | 40 | -56 | 8 | 549 | 135 |
| CS 2 | 6.00 | 7.02 | 29 | -35 | 11 | 58 | 16 |
| CS 2 | 7.03 | 7.50 | 40 | -41 | 8 | 82 | 20 |
| CS 2 | 7.50 | 7.83 | 40 | -25 | 8 | 50 | 12 |
| CS 2 | 7.84 | 8.09 | 40 | -13 | 8 | 53 | 13 |
| CS 2 | 8.09 | 8.30 | 40 | -16 | 8 | 61 | 15 |
| CS 2 | 8.30 | 8.45 | 40 | -13 | 8 | 63 | 16 |
| CS 2 | 8.45 | 8.60 | 40 | 11 | 8 | 59 | 15 |
| CS 2 | 8.60 | 8.78 | 40 | -23 | 8 | 86 | 21 |
| CS 2 | 8.78 | 9.01 | 40 | -13 | 8 | 78 | 19 |
| CS 2 | 9.03 | 9.90 | 40 | -20 | 8 | 340 | 84 |
| CS 3 | 6.00 | 7.17 | 38 | -51 | 9 | 82 | 21 |
| CS 3 | 7.20 | 7.66 | 40 | -25 | 8 | 60 | 15 |
| CS 3 | 7.68 | 8.00 | 40 | -23 | 8 | 58 | 14 |
| CS 3 | 8.00 | 8.23 | 40 | -4 | 8 | 64 | 16 |
| CS 3 | 8.23 | 8.42 | 40 | -26 | 8 | 55 | 14 |
| CS 3 | 8.42 | 8.54 | 40 | 5 | 8 | 56 | 14 |
| CS 3 | 8.55 | 8.69 | 40 | -21 | 8 | 91 | 22 |
| CS 3 | 8.69 | 8.95 | 40 | -34 | 8 | 76 | 19 |
| CS 3 | 8.96 | 10.12 | 40 | -9 | 8 | 76 | 19 |

Table C.2: Data used to investigate the dependence between cluster scale height, vertical zero point and Galactocentric distance. This table lists for each sample: the Age bin (1) <80 Myr, (2) 80 Myr-200 Myr, (3) 200 Myr-1 Gyr, (4) >1 Gyr; Galactocentric distance $R_{GC}$; number of clusters ($N_{\rm cl}$); vertical zero point ($Z_0$) and uncertainty ($\Delta Z_0$); scale height ($h_0$) and uncertainty ($\Delta h_0$).

| Sample | Age bin | $R_{GC}$ [kpc] | $N_{\rm cl}$ | $h_0$ [pc] | $\Delta h_0$ | $Z_0$ [pc] | $\Delta Z_0$ |
|---|---|---|---|---|---|---|---|
| CS 1 | 1 | $6.9 \pm 0.6$ | 90 | 34 | 6 | -13 | 3.4 |
| CS 1 | 1 | $7.9 \pm 0.7$ | 82 | 53 | 10 | 13 | 3.8 |
| CS 1 | 1 | $9.1 \pm 0.7$ | 60 | 71 | 15 | -9 | 5.2 |
| CS 1 | 2 | $6.9 \pm 0.6$ | 60 | 52 | 11 | -4 | 5.2 |
| CS 1 | 2 | $7.9 \pm 0.7$ | 57 | 57 | 12 | -4 | 5.5 |
| CS 1 | 2 | $9.1 \pm 0.7$ | 33 | 119 | 32 | 2 | 9.9 |
| CS 1 | 3 | $6.9 \pm 0.6$ | 121 | 53 | 8 | -8 | 2.6 |
| CS 1 | 3 | $7.9 \pm 0.7$ | 134 | 76 | 11 | -17 | 2.6 |
| CS 1 | 3 | $9.1 \pm 0.7$ | 151 | 83 | 12 | -23 | 2.6 |
| CS 1 | 4 | $6.9 \pm 0.6$ | 57 | 335 | 72 | -25 | 5.5 |
| CS 1 | 4 | $7.9 \pm 0.7$ | 57 | 387 | 83 | -11 | 5.5 |
| CS 1 | 4 | $9.1 \pm 0.7$ | 58 | 232 | 49 | -131 | 5.4 |
| CS 2 | 1 | $7.4 \pm 0.4$ | 23 | 37 | 12 | -37 | 15 |
| CS 2 | 1 | $8.0 \pm 0.3$ | 66 | 52 | 11 | -13 | 4.7 |
| CS 2 | 1 | $8.6 \pm 0.3$ | 33 | 106 | 28 | -49 | 9.9 |
| CS 2 | 2 | $7.4 \pm 0.4$ | 21 | 80 | 26 | -4 | 16 |
| CS 2 | 2 | $8.0 \pm 0.3$ | 32 | 69 | 19 | -21 | 10 |
| CS 2 | 2 | $8.5 \pm 0.3$ | 15 | 64 | 24 | -26 | 23 |
| CS 2 | 3 | $7.4 \pm 0.4$ | 45 | 66 | 16 | -14 | 7.1 |
| CS 2 | 3 | $8.0 \pm 0.3$ | 68 | 52 | 10 | -4 | 4.6 |
| CS 2 | 3 | $8.5 \pm 0.3$ | 38 | 115 | 29 | -17 | 8.5 |
| CS 2 | 4 | $7.4 \pm 0.4$ | 18 | 173 | 59 | -7 | 19.0 |
| CS 2 | 4 | $8.0 \pm 0.3$ | 17 | 245 | 86 | -116 | 20.2 |
| CS 2 | 4 | $8.5 \pm 0.3$ | 13 | - | - | - | - |
| CS 3 | 1 | $7.4 \pm 0.4$ | 23 | 39 | 12 | -41 | 15 |
| CS 3 | 1 | $8.0 \pm 0.3$ | 59 | 54 | 11 | -21 | 5.3 |
| CS 3 | 1 | $8.5 \pm 0.3$ | 24 | 120 | 37 | -72 | 14 |
| CS 3 | 2 | $7.4 \pm 0.4$ | 21 | 80 | 26 | -5 | 16 |
| CS 3 | 2 | $8.0 \pm 0.3$ | 28 | 69 | 20 | -13 | 12 |
| CS 3 | 2 | $8.5 \pm 0.3$ | 16 | 82 | 30 | -36 | 22 |
| CS 3 | 3 | $7.4 \pm 0.4$ | 44 | 68 | 16 | -14 | 7.3 |
| CS 3 | 3 | $8.0 \pm 0.3$ | 64 | 57 | 12 | -17 | 4.9 |
| CS 3 | 3 | $8.5 \pm 0.3$ | 42 | 96 | 23 | -10 | 7.7 |
| CS 3 | 4 | $7.4 \pm 0.4$ | 14 | - | - | - | - |
| CS 3 | 4 | $8.0 \pm 0.3$ | 13 | - | - | - | - |
| CS 3 | 4 | $8.5 \pm 0.3$ | 10 | - | - | - | - |